ISSN 1997-1397 (Print)
ISSN 2313-6022 (Online)

Журнал Сибирского федерального университета

Математика и физика

Journal of Siberian Federal University

Mathematics & Physics

2024 17 (5)

ISSN 1997-1397 (Print)

ISSN 2313-6022 (Online)

ЖУРНАЛ СИБИРСКОГО ФЕДЕРАЛЬНОГО УНИВЕРСИТЕТА
Математика и Физика

2024 17 (5)

JOURNAL OF SIBERIAN FEDERAL UNIVERSITY
Mathematics & Physics

Издание индексируется Scopus (Elsevier), Emerging Sources Citation Index (WoS, Clarivate Analytics), Российским индексом научного цитирования (НЭБ), представлено в международных и российских информационных базах: Ulrich's periodicals directiory, ProQuest, EBSCO (США), Google Scholar, MathNet.ru, КиберЛенинке.

Включено в список Высшей аттестационной комиссии «Рецензируемые научные издания, входящие в международные реферативные базы данных и системы цитирования».

Все статьи представлены в открытом доступе http://journal.sfu-kras.ru/en/series/mathematics_physics.

Журнал Сибирского федерального университета. Математика и физика.
Journal of Siberian Federal University. Mathematics & Physics.

Учредитель: Федеральное государственное автономное образовательное учреждение высшего образования "Сибирский федеральный университет"(СФУ)
Главный редактор: А.М. Кытманов. Редакторы: В.Е. Education Зализняк, А.В. Щуплев.
Компьютерная верстка: Г.В. Хрусталева
№ 5. 26.10.2024. Индекс: 42327. Тираж: 1000 экз. Свободная цена
Адрес редакции и издателя: 660041 г. Красноярск, пр. Свободный, 79, оф. 32-03.
Отпечатано в типографии Издательства БИК СФУ
660041 г. Красноярск, пр. Свободный, 82а.
Свидетельство о регистрации СМИ ПИ № ФС 77-28724 от 29.06.2007 г., выданное Федеральной службой по надзору в сфере массовых коммуникаций, связи и охраны культурного наследия
http://journal.sfu-kras.ru
Подписано в печать 15.10.24. Формат 84×108/16. Усл.печ. л. 12,0.
Уч.-изд. л. 11,8. Бумага тип. Печать офсетная.
Тираж 1000 экз. Заказ 20401
Возрастная маркировка в соответствии с Федеральным законом № 436-ФЗ:16+

CONTENTS

СОДЕРЖАНИЕ

Journal of Siberian Federal University. Mathematics & Physics 2024, 17(5), 559–569

EDN: COUDXV
УДК 541.122: 538.214

Conversion of Cr(III) and Co(III) During the Synthesis of Co/Cr Codoped Bismuth Niobate Pyrochlore According to NEXAFS Data

Ksenia A. Badanina*
Pitirim Sorokin Syktyvkar State University
Syktyvkar, Russian Federation

Sergey V. Nekipelov†
Institute of Physics and Mathematics of the Komi Science Center UB RAS
Syktyvkar, Russian Federation

Alexey M. Lebedev‡
National Research Center – Kurchatov Institute
Moscow, Russian Federation

Nadezhda A. Zhuk§
Pitirim Sorokin Syktyvkar State University
Syktyvkar, Russian Federation

Dmitriy S. Beznosikov¶
Federal State Unitary Enterprise «General Radio Frequency Centre»
Syktyvkar, Russian Federation

Received 10.04.2024, received in revised form 29.05.2024, accepted 04.07.2024

Abstract. Cubic pyrochlore of the composition $Bi_2Co_{0.5}Cr_{0.5}Nb_2O_{9+\Delta}$ (sp. gr. Fd-3m, a = 10.4838(8) Å) was synthesized in several stages using a solid-phase reaction from oxide precursors at a final temperature of 1050 °C. Using NEXAFS spectroscopy data, the electronic state of cobalt and chromium ions during the synthesis process was studied. It has been established that before the formation of phase-pure pyrochlore, Cr(III) ions are converted to Cr(VI), and then again to Cr(III); Cobalt ions Co(III) are reduced to Co(II). NEXAFS Cr2p spectra of ceramics synthesized at 650 °C, according to the main characteristics of the spectrum, coincide with the spectrum of $K_2Cr_2O_7$ and indicate the chromium content in the oxide ceramics in the form of tetrahedral CrO_4^{2-} ions, and according to the nature of the Co2p spectrum, cobalt ions are in the Co(II) state and Co(III). In the composition of pyrochlore $Bi_2Co_{0.5}Cr_{0.5}Nb_2O_{9+\Delta}$, synthesized at 1050 °C, cobalt and chromium appear predominantly in the form of Co(II) and Cr(III) ions. Analysis of phase transformations showed that changes in the oxidation state of transition element ions and the color of ceramics are associated with the formation of intermediate synthesis products.

Keywords: pyrochlore, bismuth niobate, NEXAFS, cobalt.

Citation: K.A. Badanina, S.V. Nekipelov, A.M. Lebedev, N.A. Zhuk, D.S. Beznosikov, Conversion of Cr(III) and Co(III) During the Synthesis of Co/Cr Codoped Bismuth Niobate Pyrochlore According to NEXAFS Data, J. Sib. Fed. Univ. Math. Phys., 2024, 17(5), 559–569. EDN: COUDXV.

*badanina-ksenia@mail.ru
†nekipelovsv@mail.ru
‡lebedev.alex.m@gmail.com
§nzhuck@mail.ru
¶uvn71p3@gmail.com

Introduction

Currently, pyrochlores based on bismuth niobate are being actively studied due to their promising dielectric properties [1, 2]. Exhibiting low values of dielectric losses and high dielectric constant, tunable temperature coefficient of capacitance, chemical inertness with respect to low-melting conductors, materials based on oxide pyrochlores are promising as multilayer ceramic capacitors and tunable microwave dielectric components [3]. The crystal structure of pyrochlores $A_2B_2O_6O'$ is formed by two interpenetrating cationic sublattices A_2O' and B_2O_6 [4]. Octahedral positions B are occupied by relatively small cations (Nb^{+5}), larger ions (Bi^{+3}) are distributed in eight-coordinated positions A. A feature of bismuth-containing pyrochlores is the partial vacancy of the bismuth sublattice and the distribution of dopants - ions of transition 3d elements (Co, Cu, Zn , Mn) in both cation sublattices of bismuth and niobium, causing relaxation processes in ceramics [5,6]. New studies of pyrochlores based on bismuth niobate doped with transition 3d ions (Cr, Mn, Fe, Co, Ni, Cu, Zn) [5–11] have shown that low-porosity ceramics with low dielectric losses and high values of dielectric constant are formed. The possibility of solid-phase synthesis of multielement pyrochlores containing various combinations of atoms of 3d elements was shown in [12]. A study of the phase formation of a representative of mixed pyrochlores $Bi_2Co_{0.5}Cr_{0.5}Nb_2O_{9+\Delta}$ showed [13] that during the synthesis (at 650 °C) the color of the ceramics strikingly and reversibly changes from green to brown, and the synthesis of phase-pure pyrochlore occurs at a temperature not lower than 1050 °C. It has been established that the formation of the pyrochlore phase occurs through the reaction of solid-phase interaction of orthorhombic bismuth niobate (α-$BiNbO_4$) with oxides of transition elements. In the presented work, based on X-ray spectroscopy data, the oxidation states of cobalt and chromium ions in ceramics are analyzed and the reason for the change in the color of ceramics is established. The phase composition of $Bi_2Co_{0.5}Cr_{0.5}Nb_2O_{9+\Delta}$ ceramics at intermediate stages of solid-phase synthesis was studied in detail. The data obtained contribute to a deep understanding of the processes occurring during high-temperature processing of materials.

1. Materials and methods

For the solid-phase synthesis of the $Bi_2Co_{0.5}Cr_{0.5}Nb_2O_{9+\Delta}$ sample, oxides of bismuth (III), niobium (V), chromium (III) and cobalt (II,III) of analytical grade taken in stoichiometric quantities were used. The stoichiometric mixture of oxides was thoroughly homogenized in an agate mortar for one hour, then pressed into disk shapes. The main stages of pyrochlore phase formation were studied using X-ray phase analysis of samples sequentially calcined at temperatures of 650, 850, 950, 1000 and 1050 °C for 15 hours at each stage of heat treatment. After each calcination step, the sample was carefully homogenized and pressed back into disk shape to ensure tight contact of the ceramic grains. X-ray data were obtained using a Shimadzu 6000 X-ray diffractometer (CuKα radiation; $2\theta = 10 - 80°$; scanning speed 2.0 °/min). The study of the microstructure and elemental mapping of the surface of the samples was carried out using scanning electron microscopy and energy-dispersive X-ray spectroscopy (Tescan VEGA 3LMN scanning electron microscope, INCA Energy 450 energy-dispersive spectrometer). The unit cell parameters of pyrochlores were calculated using the CSD software package [14]. Research using NEXAFS spectroscopy was carried out at the NanoFES station of the KISI synchrotron source at the Kurchatov Institute (Moscow). NEXAFS spectra were obtained by recording the total electron yield (TEY) with an energy resolution of 0.5 eV and 0.7 eV in the region of the Cr2p and Co2p absorption edges, respectively.

2. Results and discussion

As a review of the literature shows [12, 13, 15], the solid-phase synthesis of mixed pyrochlores based on bismuth niobate is a multi-step process, which is associated with the low reactivity of niobium (V) oxides and some transition elements, which include CoO, NiO [12, 16]. In addition, the features of the solid-phase synthesis method are the duration of calcination and the multi-stage heat treatment process with intermediate remixing of the reaction mixture, which are necessary to accelerate the reaction and obtain a homogeneous synthesis product [17]. It was previously established that a sample of the composition $Bi_2Co_{0.5}Cr_{0.5}Nb_2O_{9+\Delta}$ during ceramic synthesis reversibly changes its color in the temperature range of 500–650 °C from green to brown. In order to investigate the unusual thermal behavior of the complex oxide, the charge state of transition element ions in ceramics was studied using NEXAFS spectroscopy and the phase composition of samples calcined at 650, 850, 950, 1000 and 1050 °C. According to X-ray phase analysis of a sample calcined at 650 °C, the X-ray diffraction pattern shows reflections of intermediate products of the interaction of bismuth (III) oxide with chromium (III) and niobium (V) oxides - bismuth chromate $Bi_6Cr_2O_{15}$ (sp.gr. *Ccc2*), bismuth niobates $Bi_5Nb_3O_{15}$ (sp.gr. *P4/mmm*) and $BiNbO_4$ (sp.gr. *Pnna*), monoclinic β-Nb_2O_5 (sp.gr. *P2/m*) and pyrochlore (sp.gr. *Fd-3m*) [5, 18–23]. Noteworthy is the formation of bismuth chromate, which has its own intense red-orange color due to electronic transitions with charge transfer [20, 21]. The fact is that chromium (III) oxide does not oxidize under these synthesis conditions; this requires an oxygen atmosphere, a long duration and temperature of calcination. Meanwhile, the formation of chromium (VI) compounds can be indirectly indicated by the orange-brown color of the ceramics (Fig. 2) synthesized at 650 °C.

In order to establish or refute the presence of chromium (VI) ions in the sample, NEXAFS studies of the charge state of the ions were carried out. NEXAFS spectra of chromium ions in the composition of $Bi_2Co_{0.5}Cr_{0.5}Nb_2O_{9+\Delta}$ ceramics synthesized at 650 °C are presented in Fig. 1. As the figure shows, the spectra have a rich structure; in particular, absorption bands at 578, 580.5 and 589 eV can be clearly distinguished in the $Cr2p_{3/2}$ and $Cr2p_{1/2}$ spectra of the sample. Comparison of the spectra of the samples with the spectra of the oxides CrO_3, CrO_2, Cr_2O_3 and potassium dichromate $K_2Cr_2O_7$ [24–27] shows that the low-energy bands in the spectrum coincide in the energy position of the peaks with the spectra of CrO_3 and $K_2Cr_2O_7$, which indicates that chromium ions in the composition of the samples have charge state of Cr(VI) and are in a tetrahedral environment in the form of CrO_4^{2-} ions, similar to $K_2Cr_2O_7$, which is consistent with the results of X-ray phase analysis. It is interesting to note that the spectra of chromium change significantly with increasing temperature: in the low-temperature sample (650 °C) they practically coincide with the NEXAFS Cr2p spectrum of $K_2Cr_2O_7$, and those calcined at high temperature (1050 °C) — with the spectra of Cr_2O_3.

Indeed, signals appear at 577 eV and 578 eV, and in the region of 586-588 eV, characteristic of Cr(III) ions in an octahedral environment [27]. This allows us to assert that the charge state of chromium ions changes with increasing temperature of heat treatment of the sample from Cr(VI) to Cr(III). As X-ray phase analysis shows, the reason for the change in the charge state of chromium ions is the formation of an intermediate synthesis product — bismuth (VI) chromate, which is stable in a given temperature range and gives the ceramic a brown color. Apparently, with an increase in the synthesis temperature, bismuth chromate thermally dissociates with the formation of oxygen and oxide compounds of chromium (III), as evidenced by the disappearance of its reflections in the X-ray diffraction pattern of the sample synthesized at a temperature

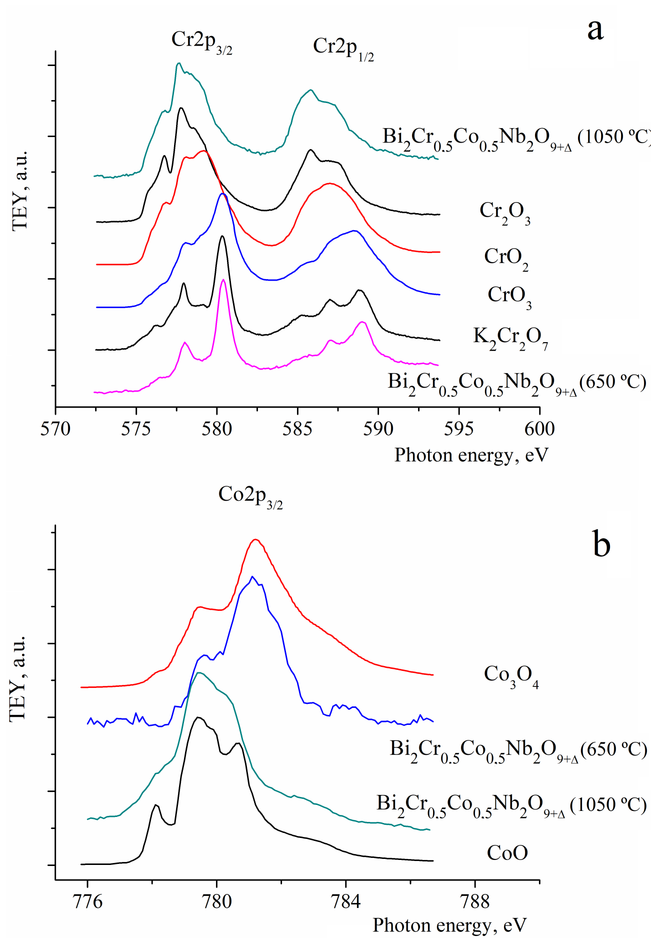

Fig. 1. NEXAFS Cr2p-spectra (a) and Co2p-spectra (b) of the $Bi_2Co_{0.5}Cr_{0.5}Nb_2O_{9+\Delta}$, synthesized at 650 and 1050 °C, oxides Cr_2O_3, CrO_2, CrO_3, CoO, Co_3O_4 and potassium dichromate $K_2Cr_2O_7$

of 850 °C. The dissociation products interact with precursors to form a pyrochlore phase at 1050 °C, in which chromium ions are predominantly in the form of Cr(III) ions, as evidenced by NEXAFS data. According to X-ray diffraction data, active interaction of precursors is detected at temperatures above 650 °C. Reflections of niobium (V) oxide are not detected in the X-ray diffraction patterns of samples synthesized at 850 °C and above; bismuth chromate $Bi_6Cr_2O_{15}$ is practically not detected at 750 °C, and $Bi_5Nb_3O_{15}$ — at 900 °C. The pyrochlore phase appears in noticeable quantities in samples obtained at a temperature of 750 °C. At this temperature, the concentrations of Nb_2O_5 and $Bi_6Cr_2O_{15}$ decrease significantly. Apparently, low-temperature synthesis of pyrochlore is difficult due to the chemical inertness of Nb_2O_5. It is interesting to note that the intermediate phase in the synthesis of pyrochlore is $Bi_5Nb_3O_{15}$, while the analogue in the synthesis of pyrochlores based on bismuth tantalate is Bi_3TaO_7 (sp.gr. *Fm-3m*) [28]. This is partly due to the fact that the compound $Bi_5Ta_3O_{15}$ is unknown.

For other reasons, it can be assumed that the reactivity of chromium (III) oxide is higher than that of niobium (V), so bismuth oxide reacts with Cr_2O_3 first and in significant quantities. Its maximum relative content is recorded at 750 °C, then its share in the sample rapidly decreases.

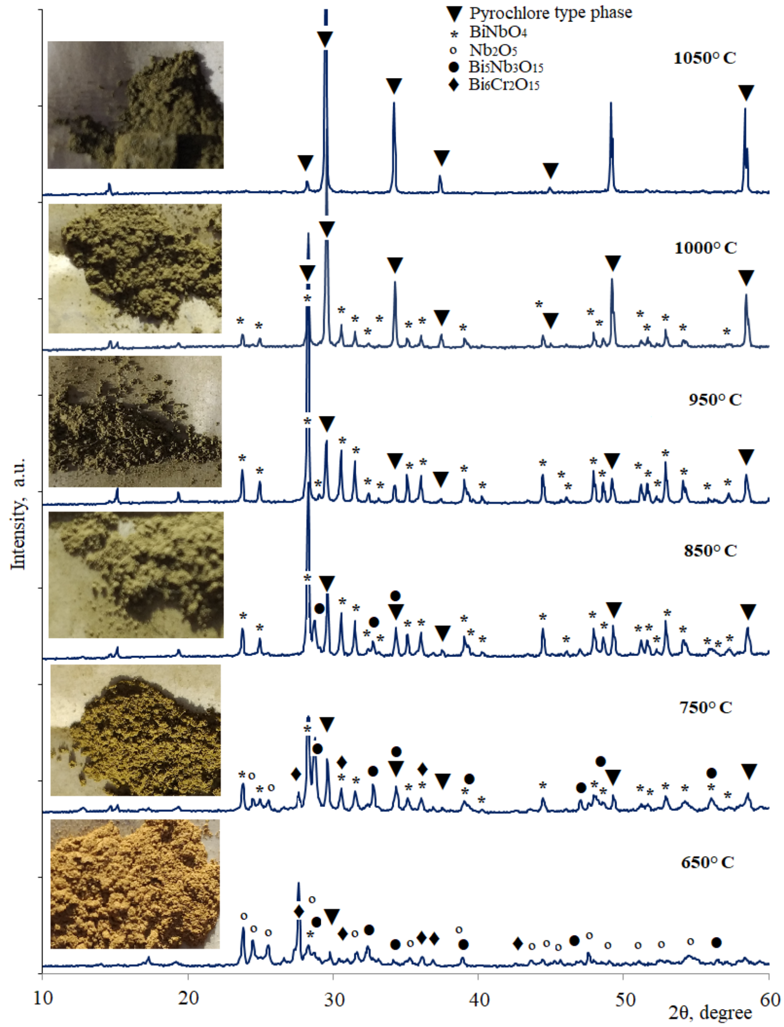

Fig. 2. X-ray diffraction patterns and photographs of $Bi_2Co_{0.5}Cr_{0.5}Nb_2O_{9+\Delta}$ samples sequentially calcined at temperatures of 650, 850, 950, 1000 and 1050 °C

$Bi_5Nb_3O_{15}$ is replaced by α-$BiNbO_4$, which, interacting with oxides of transition elements, forms a pyrochlore phase of a given composition. In the temperature range of 900–1000 °C, reflections of the pyrochlore and α-$BiNbO_4$ phases are clearly observed.

The precursors oxides Cr_2O_3 and Co_3O_4 do not appear on the X-ray diffraction patterns of the samples due to their low content in the initial charge and the high reactivity of chromium (III) oxide. It is interesting to note that, according to NEXAFS spectroscopy, cobalt (II,III) oxide in ceramics synthesized at 650 °C is present as an independent impurity phase. Indeed, as the NEXAFS Co2p spectra of the sample show, the spectrum of the composite in terms of the shape of the spectrum and the energy position of the spectral details is similar to the spectrum of Co_3O_4 oxide, in which cobalt ions are found in the form of octahedrally coordinated Co(II) and Co(III) ions [29]. Meanwhile, as the heat treatment temperature of the sample increases, the charge state of cobalt changes and cobalt ions are detected in ceramics synthesized at 1050 °C, mainly in the form of Co(II) ions. Taking into account that a temperature of 1050 °C corresponds

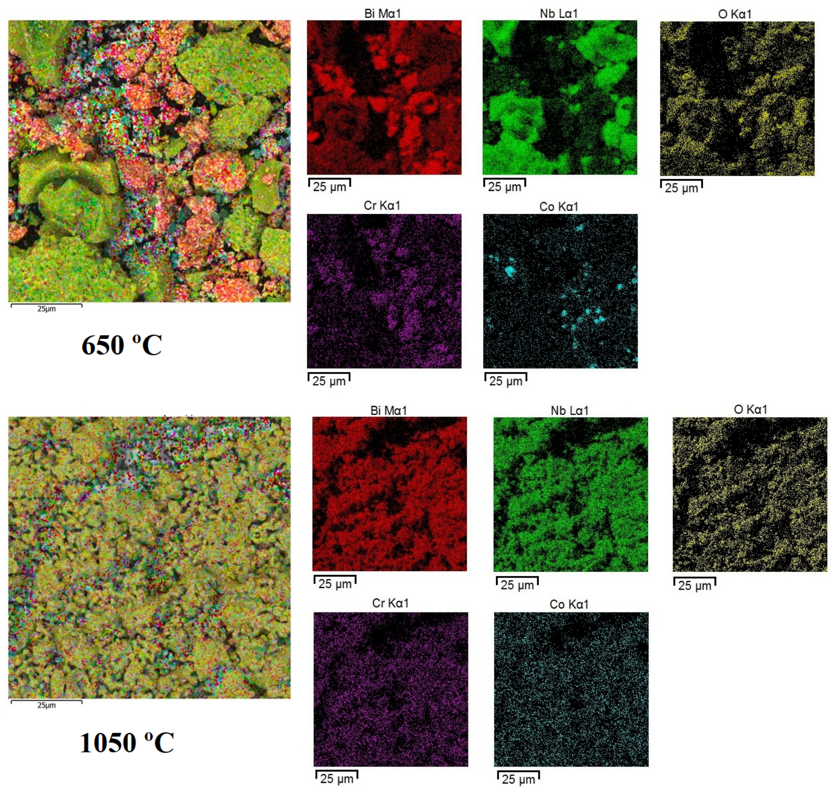

Fig. 3. Element maps of $Bi_2Co_{0.5}Cr_{0.5}Nb_2O_{9+\Delta}$ samples synthesized at 650 °C and 1050 °C

to the production of phase-pure pyrochlore, it can be stated that cobalt ions in the composition of pyrochlore are mainly in the Co(II) state, which is confirmed in the work devoted to the study of cobalt-containing pyrochlores in the ternary system Bi_2O_3-Nb_2O_5-CoO [30]. The change in the oxidation state of cobalt during high-temperature treatment of the sample may be associated with the process of thermal dissociation of Co_3O_4 at a temperature of 920 °C into CoO and oxygen [31].

As shown by elemental mapping of a sample (Fig. 4) synthesized at temperatures below 1050 °C, cobalt atoms are unevenly distributed on the surface of the sample, which indicates that cobalt atoms are not part of the pyrochlore, but represent an impurity phase, which may be Co_3O_4 oxide, which was subsequently subjected to thermal decomposition. Thus, cobalt enters into a high-temperature reaction with bismuth orthoniobate in the form of CoO oxide. This may be the reason that cobalt ions in pyrochlore are predominantly in the Co(II) state.

Microphotographs of the surface of the synthesized samples at temperatures of 650, 850, 950, 1000 and 1050 °C are shown in Fig. 4. A heterogeneous microstructure with heterogeneous grains and inclusions of impurity phases is characteristic of samples calcined at a temperature of 650-1000 °C. A low-porosity, dense microstructure was formed in the sample synthesized at a temperature of 1050 °C. On the surface of the ceramic, both individual small grains and partially fused grains with the formation of large agglomerates are observed, which contributes to the formation of a monolithic microstructure. The average crystallite size determined by X-ray diffraction using the Scherrer formula is ~58 nm (1050 °C), while larger crystallites in the range of 2-10 μm (1050 °C) were determined using a scanning electron microscope (SEM). Apparently, the

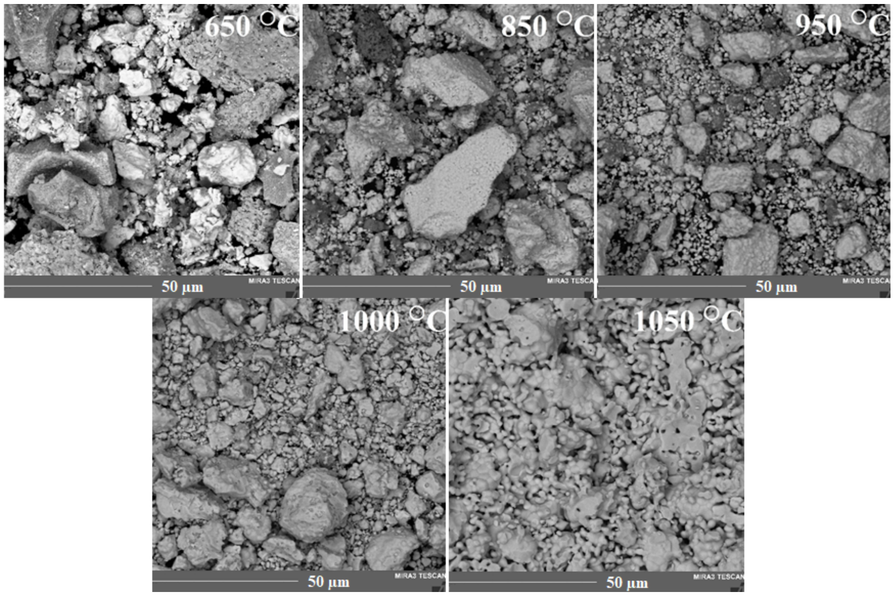

Fig. 4. Microphotographs of the surface of $Bi_2Co_{0.5}Cr_{0.5}Nb_2O_{9+\Delta}$ samples synthesized at temperatures of 650, 850, 950, 1000 and 1050 °C

crystallites in the micrographs are aggregated ceramic grains of much smaller sizes. Full-profile analysis by the Rietveld method showed that the $Bi_2Co_{0.5}Cr_{0.5}Nb_2O_{9+\Delta}$ sample synthesized at 1050 °C is single-phase [13].

The unit cell parameter of the $Bi_2Co_{0.5}Cr_{0.5}Nb_2O_{9+\Delta}$ sample is 10.4838(8) Å and exceeds the cell constant of chromium-containing pyrochlore $Bi_2CrNb_2O_{9+y}$ (a = 10.459(2)) [32], which is explained by the large radius of Co(II) ions compared to Cr(III) ions (R(Cr(III)) = 0.615 Å, R(Co(II))c.n.-6 = 0.745 Å) [33]. Since the radii of Ta(V) and Nb(V) ions (R(Nb(V)/Ta(V))c.n.-6 = 0.064 nm) are equal, the lattice constants for pyrochlores based on bismuth niobate and bismuth tantalate can be comparable. Indeed, the unit cell parameter $Bi_2CrTa_2O_{9+\Delta}$ (a = 10.45523(3) Å) [34] which is due to the closeness of the ionic radii (R(Mg(II)) = 0.72 Å, R(Co(II))c.n.-6 = 0.745 Å). Unit cell parameter for cobalt-containing pyrochlores based on bismuth tantalate $Bi_{1.49}Co_{0.8}Ta_{1.6}O_{7.0}$ a = 10.54051(3) Å and for $Bi_{1.6}Co_{0.8}Ta_{1.6}O_{7\pm\Delta}$ a = 10.5526 (2) Å significantly exceeds the parameter of chromium-cobalt-containing pyrochlore, which is associated with a significant difference in the radii of chromium (III) and cobalt (II) ions (R(Cr(III)) = 0.615 Å, R(Co(II))c.n. 6 = 0.745 Å) [36, 37]. Local chemical analysis using energy-dispersive spectroscopy showed that the chemical composition of the synthesized $Bi_2Co_{0.51}Cr_{0.52}Nb_{2.05}O_{9+\Delta}$ sample is close to the nominal composition. Thus, the atypical thermal behavior of the $Bi_2Co_{0.5}Cr_{0.5}Nb_2O_{9+\Delta}$ sample is associated with the formation of an impurity phase of bismuth chromate, as shown by X-ray phase analysis and NEXAFS spectroscopy.

Conclusions

Using NEXAFS spectroscopy and X-ray phase analysis, it was determined that the change in the oxidation state of cobalt and chromium ions during the synthesis of the $Bi_2Co_{0.5}Cr_{0.5}Nb_2O_{9+\Delta}$ sample is associated with the peculiarities of obtaining pyrochlore by the solid-phase method. It has been established that before the formation of phase-pure pyrochlore, Cr(III) ions are converted to Cr(VI) in the composition of bismuth chromate as an intermediate product of the synthesis, and then again to Cr(III) during the decomposition of bismuth chromate and the formation of pyrochlore; Cobalt ions Co(III) are reduced to Co(II) as a result of thermal dissociation of Co_3O_4. In the composition of pyrochlore $Bi_2Co_{0.5}Cr_{0.5}Nb_2O_{9+\Delta}$, synthesized at 1050 °C, cobalt and chromium appear predominantly in the form of Co(II) and Cr(III) ions. The process of phase formation of pyrochlore is a series of sequential solid-phase reactions involving precursors. A strategically important intermediate product of the synthesis is bismuth orthoniobate α-$BiNbO_4$ due to the fact that doping bismuth orthoniobate with atoms of transition elements leads to the formation of the pyrochlore phase.

The NEXAFS study was carried out within the framework of the topic 122040400069-8, as well as with the financial support of the Ministry of Science and Higher Education of Russia under agreement No. 075-15-2021-1351.

References

[1] C.C.Khaw, K.B.Tan, C.K.Lee, High temperature dielectric properties of cubic bismuth zinc tantalate, *Ceram. Intern.*, **35**(2009), 1473–1480.

[2] G.Giampaoli, T.Siritanon, B.Day, J.Li, M.A.Subramanian, Temperature independent low loss dielectrics based on quaternary pyrochlore oxides, *Prog. Solid State Chem.*, **50**(2018), 16–23.

[3] H.Du, X.Yao, Structural trends and dielectric properties of Bi-based pyrochlores, *J. Mater. Sci. Mater. Electron.*, **15**(2004), 613–616.

[4] M.A.Subramanian, G.Aravamudan, G.V.Subba Rao, Oxide pyrochlores - a review, *Prog. Solid State Chem.*, **15**(1983), 55–143.

[5] S.Kamba, V.Porokhonskyy, A.Pashkin and ets., Anomalous broad dielectric relaxation in $Bi_{1.5}Zn_{1.0}Nb_{1.5}O_7$ pyrochlore, *Phys. Rev. B.*, **66**(2002), 054106.

[6] M.Valant, Dielectric Relaxations in Bi_2O_3-Nb_2O_5-NiO Cubic Pyrochlores, *J. Am. Ceram. Soc.*, **92**(2009), 955–958.

[7] P.Y.Tan, K.B.Tan, C.C.Khaw, Z.Zainal, S.K.Chen, M.P.Chon, Phase equilibria and dielectric properties of $Bi_{3+(5/2)x}Mg_{2-x}Nb_{3-(3/2)x}O_{14-x}$ cubic pyrochlores, *Ceram. Intern.*, **40**(2014), 4237–4246.

[8] M.W.Lufaso, T.A.Vanderah, I.M.Pazos, I.Levin, R.S.Roth, J.C.Nino, V.Provenzano, P.K.Schenck, Phase formation, crystal chemistry, and properties in the system Bi_2O_3-Fe_2O_3-Nb_2O_5, *J. Sol. St. Chem.*, **179**(2006), 3900–3910.

[9] T.A.Vanderah, M.W.Lufaso, A.U.Adler, I.Levin, J.C.Nino, V.Provenzano, P.K.Schenck, Subsolidus phase equilibria and properties in the system Bi_2O_3:Mn_2O_3±x:Nb_2O_5, *J. Sol. St. Chem.*, **179**(2006), 3467–347. DOI: 10.1016/j.jssc.2006.07.014.

[10] I.Levin, T.G.Amos, J.C.Nino, T.A.Vanderah, C.A.Randall, M.T.Lanagan, Structural Study of an Unusual Cubic Pyrochlore $Bi_{1.5}Zn_{0.92}Nb_{1.5}O_{6.92}$., *J. Sol. St. Chem.*, **168**(2002), 69–75.

[11] H.B.Nguyen, L.Noren, Y.Liu, R.L.Withers, X.R.Wei, M.M.Elcombe, The disordered structures and low temperature dielectric relaxation properties of two misplaced-displacive cubic pyrochlores found in the Bi_2O_3-MO-Nb_2O_5 (M = Mg, Ni) systems, *J. Sol. St. Chem.*, **180**(2007), 2558–2565.

[12] E.P.Rylchenko, B.A.Makeev, D.V.Sivkov, R.I.Korolev, N.A.Zhuk, Features of phase formation of pyrochlore-type $Bi_2Cr_{1/6}Mn_{1/6}Fe_{1/6}Co_{1/6}Ni_{1/6}Cu_{1/6}Ta_2O_{9+\Delta}$, *Lett. Mater.*, **12**(2022), 486–492.

[13] N.A.Zhuk, K.A.Badanina, R.I.Korolev, B.A.Makeev, M.G.Krzhizhanovskaya, V.V.Kharton, Phase Formation of Co and Cr Co-Doped Bismuth Niobate with Pyrochlore Structure, *Inorganics*, **11**(2023), 288.

[14] L.G.Akselrud, Yu.N.Grin, P.Yu.Zavalij et al. CSD-universal program package for single crystal or powder structure data treatment, *Thes. Rep. XII Eur. Crystallogr. Meet.*, 1989, 155.

[15] J.C.Nino, M.T.Lanagan, C.A.Randa, Phase formation and reactions in the Bi_2O_3-ZnO-Nb_2O_5-Ag pyrochlore system, *J. Mater. Res.*, **16**(2001), 1460–1464.

[16] N.AZhuk., S.Yu.Kovalenko, R.I.Korolev, B.A.Makeev, M.G.Krzhizhanovskaya, D.V.Sivkov, S.V.Nekipelov, V.N.Sivkov, M.V.Yermolina, Features of Phase Formation of Pyrochlore-type Ceramics $Bi_2Mg(Zn)_{1-x}Ni_xTa_2O_9$, *ACS Omega*, **8**(2023), 11351–11363.

[17] K.N.Parshukova, E.P.Rylchenko, V.A.Muravyev, K.A.Badanina, B.A.Makeev, R.I.Korolev, N.A.Zhuk, Synthesis of multicomponent compounds with a pyrochlore structure, *Glass and ceramics*, **95**(2022), 34–39.

[18] J.A.Da Cruz, E.A.Volnistem, R.F.Ferreira, F D.B.reitas, A.J.M.Sales, L.C.Costa, M.P.F.Graca, Structural characterization of Brazilian niobium pentoxide and treatment to obtain the single phase (H-Nb_2O_5), *Thermal Sci. Engineering Progr.*, **25**(2021), 101015. DOI: 10.1016/j.tsep.2021.101015

[19] J.Gopalakrishnan, R A.amanan, C.N.R.Rao, D.A.Jefferson, J.Smith David, A homologous series of recurrent intergrowth structures of the type $Bi_4A_{m+n-2}B_{m+n}O_{3(m+n)+6}$ formed by oxides of the aurivillius family, *Sol. St. Chem.*, **55**(1984), 101–105.

[20] J.Grins, S.Esmaeilzadeh, S.Hull, Structure and Ionic Conductivity of $Bi_6Cr_2O_{15}$, a New Structure Type Containing $(Bi_{12}O_{14})_{8n+n}$ Columns and CrO_4^{2-} Tetrahedra, *Journal of Solid State Chemistry*, **163**(2002), 144–150.

[21] Y.H.Liu, J.B.Li, J.K.Lianga, J.Luo, L.N.Ji, J.Y.Zhang, G.H.Rao, Phase diagram of the Bi_2O_3-Cr_2O_3 system, *Mater. Chem. Phys.*, **112**(2008), 239–243.

[22] R.S.Roth, J.L.Waring, Synthesis and stability of bismutotantalite, stibiotantalite and chemically similar ABO_4 compounds, *Am. Mineral.*, **48** (1963), 1348–1356.

[23] N.AZhuk., M.G.Krzhizhanovskaya, V.A.Belyy, B.A.Makeev, High-Temperature Crystal Chemistry of α-, β-, and γ-$BiNbO_4$ Polymorphs, *Inorg. Chem.*, **58**(2019), 1518–1526. DOI: 10.1021/acs.inorgchem.8b03024

[24] S.-Y.Jeong, J.-B.Lee, H.Na, T.-Y.Seong, Epitaxial growth of Cr_2O_3 thin film on Al_2O_3 (0001) substrate by radio frequency magnetron sputtering combined with rapid-thermal annealing, *Thin Solid Films*, **518**(2010), 4813–4816.

[25] H.A.Bullen, S.J.Garrett, CrO_2 by XPS: Comparison of CrO_2 Powder to CrO_2 Films on TiO_2 (110) Single Crystal Surfaces, *Surf. Sci. Spectra*, **8**(2001), 225–233.

[26] C.Theil, J.Van Elp, F.Folkmann, Ligand field parameters obtained from and chemical shifts observed at the Cr L2,3 edges, *Physical Review B*, **59**(1999), no. 12, 7931–7936.

[27] Y.Ito, T.Tochio, A.M.Vlaicu and ets., The contribution of the ligands around Cr to the resonant inelastic L X-ray emission spectra, *J. Electron Spectroscopy and Related Phenomena*, **101-103**(1999), 851–858.

[28] M.Struzik, X.Liu, I.Abrahams, F.Krok, M.Malys, J.R.Dygas, Defect structure and electrical conductivity in the pseudo-binary system Bi_3TaO_7-Bi_3NbO_7, *Solid State Ionics*, **218**(2012), 25–30.

[29] T.J.Regan, H.Ohldag, C.Stamm, F.Nolting, J.Luning, J.Stöhr, W R.L.hite, Chemical effects at metal/oxide interfaces studied by x-ray-absorption spectroscopy, *Phys. Rev. B*, **64**(2001), 214422.

[30] T.A.Vanderah, T.Siegrist, M.W.Lufaso, M.C.Yeager, R.S.Roth, J.C.Nino, S.Yates, Phase Formation and Properties in the System Bi_2O_3:$2CoO_{1+x}$:Nb_2O_5, *Eur. J. Inorgan. Chem.*, **2006**(2006), 4908–4914.

[31] B.Bingyang, A.Hamidreza, L.Junhuaб Comparison of the performance for oxidation of formaldehyde on nano-Co_3O_4, 2D-Co_3O_4, and 3D-Co_3O_4 catalysts, *Applied Catalysis B: Environmental*, **142-143**(2013), 677–683.

[32] I.V.Piir, D.A.Prikhodko, S.V.Ignatchenko, A.V.Schukariov, Preparation and structural investigations of the mixed bismuth niobates, containing transition metals, *Sol. St. Ion.*, **101-103**(1997), 1141–1146.

[33] R.D.Shannon, Revised effective ionic radii and systematic studies of interatomic distances in halides and chalcogenides, *Acta Crystallogr. A*, **32**(1976), 751–767.

[34] N.A.Zhuk, N.A.Sekushin, M.G.Krzhizhanovskaya and ets., Cr-doped bismuth tantalate pyrochlore: electrical and thermal properties, crystal structure and ESR, NEXAFS, XPS spectroscopy, *Mater. Res. Bull.*, **158**(2023), 112067.

[35] N.A.Zhuk, M.G.Krzhizhanovskaya, A.V.Koroleva and ets., Cr and Mg codoped bismuth tantalate pyrochlores: Thermal expansion and stability, crystal structure, electrical and optical properties, NEXAFS and XPS study, *J. Sol. St. Chem.*, **323**(2023), 124074.
DOI: 10.1016/j.jssc.2023.124074

[36] N.A.Zhuk, K M.G.rzhizhanovskaya, A.V.Koroleva and ets., Spectroscopic characterization of cobalt doped bismuth tantalate pyrochlore, *Sol. St. Sci.*, **125**(2022), 106820.

[37] N.A.Zhuk, M.G.Krzhizhanovskaya, N.A.Sekushin, D.V.Sivkov, I.EAbdurakhmanov, Crystal structure, dielectric and thermal properties of cobalt doped bismuth tantalate pyrochlore, *J. Mater. Res. Technol.*, **22**(2023), 1791–1799. DOI: 10.1016/j.jmrt.2022.12.059

Конверсия Cr(III) и Co(III) в процессе синтеза кобальт-хромсодержащего пирохлора на основе ниобата висмута по данным NEXAFS

Ксения А. Баданина
Сыктывкарский государственный университет имени Питирима Сорокина
Сыктывкар, Российская Федерация
Сергей В. Некипелов
Физико-математический институт Коми научного центра УрО РАН
Сыктывкар, Российская Федерация
Алексей М. Лебедев
Национальный исследовательский центр – Курчатовский институт
Москва, Российская Федерация
Надежда А. Жук
Сыктывкарский государственный университет имени Питирима Сорокина
Сыктывкар, Российская Федерация
Дмитрий С. Безносиков
Федеральное государственное унитарное предприятие «Главный радиочастотный центр»
Сыктывкар, Российская Федерация

Аннотация. Кубический пирохлор состава $Bi_2Co_{0.5}Cr_{0.5}Nb_2O_{9+\Delta}$ (пр.гр. Fd-3m, a = 10.4838(8) Å) синтезировали в несколько этапов методом твердофазной реакции из оксидных прекурсоров при финальной температуре 1050 °C. По данным NEXAFS-спектроскопии исследовано электронное состояние ионов кобальта и хрома в процессе синтеза. Установлено, что до формирования фазовочистого пирохлора ионы Cr(III) превращаются в Cr(VI), а затем снова в Cr(III); ионы кобальта Co(III) восстанавливаются до Co(II). NEXAFS Cr2p-спектры керамики, синтезированной при 650 °C, по основным характеристикам спектра совпадают со спектром $K_2Cr_2O_7$ и свидетельствуют о содержании хрома в оксидной керамике в виде тетраэдрических ионов CrO_4^{2-}, а по характеру Co2p-спектра ионы кобальта находятся в состоянии Co(II) и Co(III). В составе пирохлора $Bi_2Co_{0.5}Cr_{0.5}Nb_2O_{9+\Delta}$, синтезированного при 1050 °C, кобальт и хром проявляются преимущественно в виде ионов Co(II) и Cr(III). Анализ фазовых превращений показал, что изменение степени окисления ионов переходных элементов и цвета керамики связано с образованием промежуточных продуктов синтеза.

Ключевые слова: пирохлор, ниобат висмута, NEXAFS, кобальт.

EDN: CSWBKZ
УДК 517.95

Symmetries of Linear and Nonlinear Partial Differential Equations

Oleg V. Kaptsov*
Institute of Computational Modelling SB RAS
Krasnoyarsk, Russian Federation

Received 10.03.2024, received in revised form 15.05.2024, accepted 04.07.2024

Abstract. Higher symmetries and operator symmetries of linear partial differential equations are considered The higher symmetries form a Lie algebra, and operator ones form an associative algebra. The relationship between these symmetries is established. New symmetries of two-dimensional stationary equations of gas dynamics are found.

Keywords: higher symmetries, operator symmetries, gas dynamics equations.

Citation: O. V. Kaptsov, Symmetries of Linear and Nonlinear Partial Differential Equations, J. Sib. Fed. Univ. Math. Phys., 2024, 17(5), 570–574. EDN: CSWBKZ.

Introduction

It is well known that symmetries play a crucial role in finding solutions of differential equations. The theory of point symmetries is well described in numerous monographs and textbooks [1–3]. A large number of examples of invariant and partially invariant solutions were presented [4,5]. One can say that theory of point transformations is well developed. Some generalizations of the Lie theory have been proposed.The most successful advances include the theory of higher symmetries of nonlinear equations and operator symmetries of linear equations [2,6–8]. However, the use of higher symmetry operators is complicated because transformations constructed using these operators act in infinite-dimensional spaces and they are represented by formal series [2]. As a result, it is difficult to determine analogs of invariant solutions with respect to such transformations.

Modified definitions of admitted operators and operator symmetries for linear systems of partial differential equations are introduced in this paper. It is easily verified that operator symmetries form an associative algebra with respect to ordinary multiplication and a Lie algebra with commutator multiplication. It is proved that some admitted operator corresponds to each operator symmetry. It turns out that symmetries of linear equations can be transformed into symmetries of nonlinear equations in some cases. Here, as an example, a system of two equations that describes plane, steady, irrotational gas flows is considered [9, 10]. Using hodograph transformation, a linear system is obtained. The admitted operators of this system give rise to an infinite series of symmetries of nonlinear gas dynamics equations.

1. Symmetries

Let us consider the matrix differential operator

$$L = \sum_{|\alpha| \geqslant 0}^{k} A_\alpha(x) \frac{\partial^{|\alpha|}}{\partial x_1^{\alpha_1} \cdots \partial x_n^{\alpha_n}}, \tag{1}$$

*kaptsov@icm.krasn.ru

where $\alpha = (\alpha_1, \dots, \alpha_n)$, A_α are $m \times m$ matrices depending on $x = (x_1, \dots, x_n)$. The operator defines a system of linear partial differential equations

$$Lu = 0, \tag{2}$$

where $u = (u^1, \dots, u^m)$ is a set of unknown with respect to x functions.

Further, the operator of total derivative [1,2] with respect to x_i $(i = 1, \dots, n)$ is denoted by D_{x_i}. The expression D^α means the product of operators $D_{x_1}^{\alpha_1} \cdots D_{x_n}^{\alpha_n}$.

Definition 1. *System (2) admits the operator in canonical form*

$$X = \sum_{j=1}^{m} \eta_j \frac{\partial}{\partial u^j} + \sum_{\substack{1 \leqslant j \leqslant m \\ \alpha \in \mathbb{N}^n}} D^\alpha \eta_j \frac{\partial}{\partial u^j_\alpha}, \tag{3}$$

if there is a matrix differential operator M such that the equality

$$L\eta = MLu, \tag{4}$$

is true, where $u = (u^1, \dots, u^m)$ is a set of arbitrary smooth functions of x, and $\eta = (\eta_1, \dots, \eta_m)$. Relation (4) is called the defining equation.

The above definition differs from the standard one [2,3]. Obviously, condition (4) is sufficient for the classical invariance of system (2). One can shown that it is necessary condition but it is not needed here.

Remark. If system of partial differential equations $L(u) = 0$ is nonlinear system then condition (4) must be replaced by the following condition

$$XL(u) = ML(u)$$

.

It follows from (4) that if u is a solution of system (2) then $\tilde{u} = \eta$ is also solution of this system. Thus the transformation $x \longrightarrow x, \quad u \longrightarrow \eta$ acts on solutions of system (2). Such transformations are called L-symmetries.

Proposition 1. *If $\eta^1, \dots, \eta^p$ are solutions of the defining equations*

$$L\eta^k = M_k Lu, \qquad k = 1, \dots p, \tag{5}$$

then

$$x \longrightarrow x, \quad u \longrightarrow \sum_{k=1}^{p} c_k \eta^k, \qquad c_k \in \mathbb{R} \tag{6}$$

is the L-symmetry of equation (2).

Indeed, since functions η^k satisfy (5) then the equality

$$L(\sum_{k=1}^{p} c_k \eta^k) = (\sum_{k=1}^{p} c_k M_k) Lu.$$

is true due to linearity of the operators. This means that transformation (6) is L-symmetry.

Proposition 2. *The set of L-symmetries of system (2) forms a monoid with the composition operation.*

This immediately follows from the fact that symmetries act on solutions of the system and, therefore, the composition of two L-symmetries of system (2) is an L-symmetry. Moreover, the identity transformation is also a symmetry.

The second method of introducing symmetries of linear equations is described in [7,8]. Some modified versions of definitions are provided below.

Definition 2. *Let differential operator (1) be given. The differential operator S is called the operator symmetry of equation (2) if there is a differential operator $\mathcal{D}$ such that*

$$LS = \mathcal{D}L. \tag{7}$$

It is assumed that S is not a polynomial in L.

Obviously the operator symmetry S acts on solutions of equation (2), i.e., transforms solutions into solutions.

Proposition 3. *Let $\mathcal{S}_1, \mathcal{S}_2$ be two operator symmetries of system (2). Then*

$$b_1\mathcal{S}_1 + b_2\mathcal{S}_2, \quad \mathcal{S}_1\mathcal{S}_2, \quad \mathcal{S}_1\mathcal{S}_2 - \mathcal{S}_2\mathcal{S}_1,$$

also operator symmetries for any $b_1, b_2 \in \mathbb{R}$.

Proof. By condition the equalities

$$L\mathcal{S}_1 = \mathcal{D}_1 L, \qquad L\mathcal{S}_2 = \mathcal{D}_2 L.$$

are true. It follows that

$$L(b_1\mathcal{S}_1 + b_2\mathcal{S}_2) = b_1 L\mathcal{S}_1 + b_2 L\mathcal{S}_2 = b_1\mathcal{D}_1 L + b_2\mathcal{D}_2 L = (b_1\mathcal{D}_1 + b_2\mathcal{D}_2)L,$$

$$L\mathcal{S}_1\mathcal{S}_2 = \mathcal{D}_1 L\mathcal{S}_2 = \mathcal{D}_1\mathcal{D}_2 L,$$

$$L(\mathcal{S}_1\mathcal{S}_2 - \mathcal{S}_2\mathcal{S}_1) = \mathcal{D}_1\mathcal{D}_2 L - \mathcal{D}_2\mathcal{D}_1 L = (\mathcal{D}_1\mathcal{D}_2 - \mathcal{D}_2\mathcal{D}_1)L. \qquad \square$$

Remark. If the commutator of operators $\mathcal{S}_1, \mathcal{S}_2$ is introduced according to the well-known formula $[\mathcal{S}_1, \mathcal{S}_2] = \mathcal{S}_1\mathcal{S}_2 - \mathcal{S}_2\mathcal{S}_1$ then the last expression in the proof is rewritten as

$$L[\mathcal{S}_1, \mathcal{S}_2] = [\mathcal{D}_1, \mathcal{D}_2]L.$$

Corollary. The set of operator symmetries of system (2) forms an associative algebra over $\mathbb{R}$ with respect to ordinary multiplication and a Lie algebra with respect to commutator multiplication.

Proposition 4. *If S is an operator symmetry of equation (2), and $u = (u^1, \dots, u^m)$ is a set of smooth functions then $\eta = Su$ is a solution to the defining equation that generates L-symmetry.*

By assumption, there exists an operator $\mathcal{D}$ that satisfies equality (7). Applying to u the operators on the left and right sides of (7), equality (4) is obtained in which $\eta = Su$ and $M = \mathcal{D}$.

2. Symmetries of stationary gas dynamics equations

The L-symmetries introduced above can be applied to some nonlinear equations. As an example, let us consider the well-known system of stationary equations

$$u_y - v_x = 0, \quad (u^2 - c^2)u_x + 2uvu_y + (v^2 - c^2)v_y = 0, \tag{8}$$

that describes flat steady irrotational flows of compressible fluid [9,10]. Here u, v are components of the velocity vector, c is the speed of sound, expressed from the Bernoulli integral

$$u^2 + v^2 + I(c^2) = const.$$

Writing equations (8) in terms of hodograph variables, system of linear equations [9]

$$x_v - y_u = 0, \quad (u^2 - c^2)y_v - 2uvx_v + (v^2 - c^2)x_u = 0, \tag{9}$$

is obtained for two unknown functions x, y that depend on u, v. It is not difficult to see [9] that both systems admit the following rotation, scaling and translation operators:

$$-v\frac{\partial}{\partial u} + u\frac{\partial}{\partial v} - y\frac{\partial}{\partial x} + x\frac{\partial}{\partial y}\ , \quad x\frac{\partial}{\partial x} + y\frac{\partial}{\partial y}\ , \quad \frac{\partial}{\partial x}\ , \quad \frac{\partial}{\partial y}\ .$$

The rotation operator admitted by the system (9) in canonical form has the form

$$(-y + vx_u - ux_v)\frac{\partial}{\partial x} + (x + vy_u - uy_v)\frac{\partial}{\partial y}\ .$$

Therefore, according to Proposition 1, the transformation

$$\tilde{u} = u\ , \quad \tilde{v} = v\ , \quad \tilde{x} = -y + vx_u - ux_v\ , \quad \tilde{y} = x + vy_u - uy_v$$

acts on solutions of linear system (9) and it is an L-symmetry of this system. Using three other symmetry operators, L-symmetry of the form

$$\tilde{u} = u, \quad \tilde{v} = v \tag{10}$$

$$\tilde{x} = c_1(-y + vx_u - ux_v) + c_2x + c_3, \quad \tilde{y} = c_1(x + vy_u - uy_v) + c_2y + c_4, \tag{11}$$

is obtained, where c_i are arbitrary constants.

In order to obtain symmetries of gas dynamics equations (8), it is necessary to express the derivatives x_u, x_v, y_u, y_v in terms of the derivatives u_x, u_y, v_x, v_y. Using the hodograph transformation, it is easy to find these derivatives [9]

$$x_u = v_y/J, \quad x_v = -u_y/J, \quad y_u = -v_x/J, \quad y_v = u_x/J,$$

where $J = \dfrac{\partial(u,v)}{\partial(x,y)}$ is the Jacobian of functions u, v. Thus, the formulas of transformations (10), (11) have the following form

$$\tilde{u} = u, \quad \tilde{v} = v \tag{12}$$

$$\tilde{x} = c_1\left(-y + \frac{vv_y + uu_y}{J}\right) + c_2x + c_3, \quad \tilde{y} = c_1\left(x - \frac{vv_x + uu_x}{J}\right) + c_2y + c_4. \tag{13}$$

The last expressions determine the transformation of solutions of system (8) back into solutions of this system.

Combination of 10), (11) and

$$\hat{u} = \tilde{u}, \quad \hat{v} = \tilde{v}$$

$$\hat{x} = b_1(-\tilde{y} + \tilde{v}\tilde{x}_u - \tilde{u}\tilde{x}_v) + b_2\tilde{x} + b_3, \quad \hat{y} = c_1(\tilde{x} + \tilde{v}\tilde{y}_u - \tilde{u}\tilde{y}_v) + b_2\tilde{y} + b_4,$$

gives a new second-order symmetry of system (9).

One can obtain symmetries of system (9) of arbitrary order by means of compositions. Thus, an infinite series of symmetries of the system in the hodograph variables arises. An infinite series of symmetries of the gas dynamics equations (8) are obtained by recalculating the corresponding derivatives.

Conclusion

Using the found symmetries, it is possible to construct solutions from known ones. For example, if scale-invariant solutions [9] of system (8) are taken then new solutions can be generated using formulas (12), (13). The first works devoted to new types of symmetries have appeared recently [11, 12]. This approach requires further development and construction of new examples.

This work is supported by the Krasnoyarsk Mathematical Center and financed by the Ministry of Science and Higher Education of the Russian Federation in the framework of the establishment and development of regional Centers for Mathematics Research and Education (Agreement no. 075-02-2024-1378).

References

[1] L.V.Ovsyannikov, Group Analysis of differential equations, Academic Press, NY, 1982.

[2] N.H.Ibragimov, Transformation groups applied to mathematical physics, Reidel, Boston, 1985.

[3] P.Olver, Applications of Lie Groups to Differential Equations, Springer, NY, 1986.

[4] N.H.Ibragimov, (Editor) CRC Handbook of Lie Group Analysis of Differential Equations, Volume I-III, Baton Rouge, CRC Press, 1995.

[5] A.D.Polyanin, V.F.Zaitsev Handbook of Nonlinear Partial Differential Equations Chapman & Hall/CRC Press, 2012.

[6] I.S.Krasil'shchik, A.M.Vinogradov, [et al.], Symmetries and conservation laws for differential equations of mathematical physics, American Mathematical Society, Providence, RI, 1999.

[7] W.Miller, Symmetry and separation of variables, Addison-Wesley Publishing Company, London, 1977.

[8] E.Kalnins, J.Kress, W.Miller, Separation of variables and superintegrability : the symmetry of solvable systems, Bristol: IOP Publishing, 2018.

[9] L.V.Ovsyannikov, Lectures on basic gas dynamics, Institute of Computer Studies, Moscow, Izhevsk, 2003 (in Russian).

[10] L.D.Landau, E.M.Lifshitz, Fluid Mechanics, Elsevier, 2013.

[11] O.V.Kaptsov, Contact Mappings of Jet Spaces, Journal of Siberian Federal University. Mathematics & Physics, 2023, 16(5), 583–590. EDN: DCHWJH

[12] O.V.Kaptsov, Contact germs and partial differential equations, arXiv:2404.01955 ,2024.

Симметрии линейных и нелинейных уравнений с частными производными

Олег В. Капцов
Институт вычислительного моделирования СО РАН
Красноярск, Российская Федерация

Аннотация. Рассматриваются операторы высших и операторных симметрий линейных уравнений с частными производными. Операторы высших симметрий образуют алгебру Ли, а операторные - ассоциативную алгебру. Устанавливается связь между этими симметриями. Найдены новые симметрии двумерных стационарных уравнений газовой динамики.

Ключевые слова: высшие симметрии, операторные симметрии, уравнения газовой динамики.

Journal of Siberian Federal University. Mathematics & Physics 2024, 17(5), 575–585

EDN: EPFRKI
УДК 515

Multivalued Δ-symmetric Covariant Results in Bipolar Metric Spaces

G. N. V. Kishore*
Department of Engineering Mathematics & Humanities
Sagi Rama Krishnam Raju Engineering College
Andhra Pradesh, India

B. Srinuvasa Rao†
Department of Mathematics
Dr.B.R.Ambedkar University
Andhra Pradesh, India

D. Ram Prasad‡
Department of Mathematics
Nalla Malla Reddy Engineering college
Divya nagar, Ghatkesar mandal
Telangana, India

Stojan Radenovic§
Faculty of Mechanical Engineering
University of Belgrade
Beograd, Serbia

Received 10.04.2024, received in revised form 18.05.2024, accepted 02.07.2024

Abstract. In this paper, we proved some coupled fixed point theorems for Hybrid pair of mappings by using Δ-symmetric covariant mappings in bipolar metric spaces. Also we give some examples which supports our results.

Keywords: Δ-symmetric covariant mapping, Hybrid Pair of mappings, Coupled fixed point, bipolar metric spaces.

Citation: G.N.V. Kishore, B.S. Rao, D.R. Prasad, S. Radenovic, Multivalued Δ-symmetric Covariant Results in Bipolar Metric Spaces, J. Sib. Fed. Univ. Math. Phys., 2024, 17(5), 575–585. EDN: EPFRKI.

1. Introduction and preliminaries

In 1922, S. Banach [4] introduced the notion of Banach contraction principle. It was extended by Nadler [13] for multivalued mappings and some results related with generalization of various directions (see [1–18]).

Very recently, in 2016 Mutlu and Gürdal [11] introduced the notion of Bipolar metric spaces, which is one of generalizations metric spaces. Also they investigated some fixed point and coupled fixed point results on this space, see [11, 12].

*gnvkishore@srkrec.ac.in, kishore.apr2@gmail.com
†srinivasabagathi@gmail.com
‡ramprasadmphil09@gmail.com
§radens@beotel.net

In this paper, we proved some coupled fixed point theorems for multivalued maps. Also we provide examples, which supports our main results.

First we recall some basic definitions and results.

Definition 1.1 ([11]). *Let Γ and Θ be a two non-empty sets. Suppose that $d : \Gamma \times \Theta \to [0, +\infty)$ be a mapping satisfying the following properties :*

(π_0) *If $d(\sigma, \tau) = 0$ then $\sigma = \tau$ for all $(\sigma, \tau) \in \Gamma \times \Theta$,*

(π_1) *If $\sigma = \tau$ then $d(\sigma, \tau) = 0$ for all $(\sigma, \tau) \in \Gamma \times \Theta$,*

(π_2) *If $d(\sigma, \tau) = d(\tau, \sigma)$ for all $\sigma, \tau \in \Gamma \cap \Theta$.*

(π_3) *If $d(\sigma_1, \tau_2) \leqslant d(\sigma_1, \tau_1) + d(\sigma_2, \tau_1) + d(\sigma_2, \tau_2)$ for all $\sigma_1, \tau_2 \in \Gamma$, $\tau_1, \tau_2 \in \Theta$.*

Then the mapping d is called a Bipolar-metric on the pair (Γ, Θ) and the triple (Γ, Θ, d) is called a Bipolar-metric space.

Definition 1.2 ([11]). *Assume (Γ_1, Θ_1) and (Γ_2, Θ_2) as two pairs of sets and a function as $\Psi : \Gamma_1 \cup \Theta_1 \rightrightarrows \Gamma_2 \cup \Theta_2$ is said to be a covariant map. If $\Psi(\Gamma_1) \subseteq \Gamma_2$ and $\Psi(\Theta_1) \subseteq \Theta_2$, and denote this with $\Psi : (\Gamma_1, \Theta_1) \rightrightarrows (\Gamma_2, \Theta_2)$. And the mapping $\Psi : \Gamma_1 \cup \Theta_1 \rightrightarrows \Gamma_2 \cup \Theta_2$ is said to be a contravariant map. If $\Psi(\Gamma_1) \subseteq \Theta_2$ and $\Psi(\Theta_1) \subseteq \Gamma_2$, and write $\Psi : (\Gamma_1, \Theta_1) \leftrightarrows (\Gamma_2, \Theta_2)$. In particular, if d_1 and d_2 are bipolar metric on (Γ_1, Θ_1) and (Γ_2, Θ_2), respectively, we some time use the notation $\Psi : (\Gamma_1, \Theta_1, d_1) \rightrightarrows (\Gamma_2, \Theta_2, d_2)$ and $\Psi : (\Gamma_1, \Theta_1, d_1) \leftrightarrows (\Gamma_2, \Theta_2, d_2)$.*

Definition 1.3 ([11]). *Assume (Γ, Θ, d) be a bipolar metric space. A point $\xi \in \Gamma \cup \Theta$ is termed as a left point if $\xi \in \Gamma$, a right point if $\xi \in \Theta$ and a central point if both. Similarly, a sequence $\{\sigma_n\}$ on the set Γ and a sequence $\{\tau_n\}$ on the set Θ are called a left and right sequence respectively. In a bipolar metric space, sequence is the simple term for a left or right sequence. A sequence $\{\xi_n\}$ as considered convergent to a point ξ, if and only if $\{\xi_n\}$ is a left sequence, ξ is a right point and $\lim\limits_{n \to +\infty} d(\xi_n, \xi) = 0$; or $\{\xi_n\}$ is a right sequence, ξ is a left point and $\lim\limits_{n \to +\infty} d(\xi, \xi_n) = 0$. A bisequence $(\{\sigma_n\}, \{\tau_n\})$ on (Γ, Θ, d) is sequence on the set $\Gamma \times \Theta$. If the sequence $\{\sigma_n\}$ and $\{\tau_n\}$ are convergent, then the bisequence $(\{\sigma_n\}, \{\tau_n\})$ is said to be convergent. $(\{\sigma_n\}, \{\tau_n\})$ is Cauchy sequence, if $\lim\limits_{n,m \to +\infty} d(\sigma_n, \tau_m) = 0$. In a bipolar metric space, every convergent Cauchy bisequence is biconvergent. A bipolar metric space is called complete, if every Cauchy bisequence is convergent, hence biconvergent.*

2. Methods / Experimental Section

2.1. Coupled Fixed Point Theorems via Δ-symmetric covariant mapping

Definition 2.1. *Let $\Psi : (\Gamma \times \Theta) \cup (\Theta \times \Gamma) \to CL(\Gamma \cup \Theta)$ be a given covariant mapping. We say that Ψ is a Δ-symmetric covariant mapping if and only if $(\sigma, \tau) \in \Delta$ implies $\Psi(\sigma, \tau) \Re \Psi(\tau, \sigma)$*

Definition 2.2. *Let (Γ, Θ, d) be a bipolar metric spaces, $\sigma \in \Gamma, \tau \in \Theta$ and $\Psi : (\Gamma \times \Theta, \Theta \times \Gamma) \rightrightarrows CL(\Gamma, \Theta)$ be a covariant mapping. An element (σ, τ) is said to be a coupled fixed point of $\Psi : (\Gamma \times \Theta) \cup (\Theta \times \Gamma) \to CL(\Gamma \cup \Theta)$ if $\sigma \in \Psi(\sigma, \tau)$ and $\tau \in \Psi(\tau, \sigma)$.*

Theorem 2.3. *Let (Γ, Θ, d) be an complete bipolar metric space endowed with a partial order $\preceq$. Suppose that Δ is non empty, that is there exists $(\sigma, \rho) \in \Delta$. Let $F : (\Gamma \times \Theta, \Theta \times \Gamma) \rightrightarrows CL(\Gamma, \Theta)$ be a Δ-symmetric covariant mapping and consider that $f : \Gamma \times \Theta \to [0, +\infty)$ as*

$$f(\sigma, \rho) = D(\sigma, F(\varrho, \tau)) + D(F(\tau, \varrho), \rho) \text{ for all } \sigma, \tau \in \Gamma \text{ and } \rho, \varrho \in \Theta \tag{2.1}$$

is lower semi-continuous and there exists a mapping $\psi : [0, +\infty) \to (0, 1)$ *satisfying*

$$\lim_{r \to t^+} \sup \psi(r) < 1 \text{ for each } t \in [0, +\infty). \tag{2.2}$$

Assume that for any $(\sigma, \rho) \in \Delta$ *there exist* $x \in F(\sigma, \rho)$ *and* $y \in F(\rho, \sigma)$ *satisfying*

$$\sqrt{\psi(f(\sigma, \rho))}[d(\sigma, y) + d(x, \rho)] \leqslant f(\sigma, \rho) \tag{2.3}$$

such that

$$f(x, y) \leqslant \psi(f(\sigma, \rho))[d(\sigma, y) + d(x, \rho)]. \tag{2.4}$$

Then $F : (\Gamma \times \Theta) \cup (\Theta \times \Gamma) \to CL(\Gamma \cup \Theta)$ *has a coupled fixed point. That is there exists* $(\alpha, \beta) \in (\Gamma \times \Theta) \cup (\Theta \times \Gamma)$ *such that* $\alpha \in F(\alpha, \beta)$ *and* $\beta \in F(\beta, \alpha)$.

Proof. Since by the definitions of ψ we have $\psi(f(\sigma, \rho)) < 1$ and $\psi(f(\tau, \varrho)) < 1$ for each $\sigma, \tau \in \Gamma$, $\rho, \varrho \in \Theta$, it follows that for any $(\sigma, \rho), (\tau, \varrho) \in \Gamma \times \Theta$, there exist $u \in F(\sigma, \rho)$, $v \in F(\rho, \sigma)$, $l \in F(\tau, \varrho)$ and $m \in F(\varrho, \tau)$ such that

$$\sqrt{\psi(f(\sigma, \rho))} d(\sigma, m) \leqslant D(\sigma, F(\varrho, \tau)) \text{ and } \sqrt{\psi(f(\tau, \varrho))} d(\tau, v) \leqslant D(\tau, F(\rho, \sigma))$$

$$\sqrt{\psi(f(\sigma, \rho))} d(l, \rho) \leqslant D(F(\tau, \varrho), \rho) \text{ and } \sqrt{\psi(f(\tau, \varrho))} d(u, \varrho) \leqslant D(F(\sigma, \rho), \varrho).$$

Therefore, for each $(\sigma, \rho), (\tau, \varrho) \in \Gamma \times \Theta$, there exist $u \in F(\sigma, \rho)$, $v \in F(\rho, \sigma)$, $l \in F(\tau, \varrho)$ and $m \in F(\varrho, \tau)$ satisfying (2.3).
Let $(\sigma_0, \rho_0), (\tau_0, \varrho_0) \in \Delta$ be an arbitrary and fixed. By our assumptions (2.3) and (2.4), choose $\sigma_1 \in F(\sigma_0, \rho_0)$, $\rho_1 \in F(\rho_0, \sigma_0)$ and $\tau_1 \in F(\tau_0, \varrho_0)$, $\varrho_1 \in F(\varrho_0, \tau_0)$ such that

$$\sqrt{\psi(f(\sigma_0, \rho_0))}(d(\sigma_0, \varrho_1) + d(\tau_1, \rho_0)) \leqslant f(\sigma_0, \rho_0) \tag{2.5}$$

$$\sqrt{\psi(f(\tau_0, \varrho_0))}(d(\tau_0, \rho_1) + d(\sigma_1, \varrho_0)) \leqslant f(\tau_0, \varrho_0) \tag{2.6}$$

and

$$f(\sigma_1, \rho_1) \leqslant \psi(f(\sigma_0, \rho_0))(d(\sigma_0, \varrho_1) + d(\tau_1, \rho_0)) \tag{2.7}$$

$$f(\tau_1, \varrho_1) \leqslant \psi(f(\tau_0, \varrho_0))(d(\tau_0, \rho_1) + d(\sigma_1, \varrho_0)). \tag{2.8}$$

From (2.5) and (2.7) we obtain that

$$\begin{aligned} f(\sigma_1, \rho_1) &\leqslant \psi(f(\sigma_0, \rho_0))(d(\sigma_0, \varrho_1) + d(\tau_1, \rho_0)) \leqslant \\ &\leqslant \sqrt{\psi(f(\sigma_0, \rho_0))}\sqrt{\psi(f(\sigma_0, \rho_0))}(d(\sigma_0, \varrho_1) + d(\tau_1, \rho_0)) \leqslant \\ &\leqslant \sqrt{\psi(f(\sigma_0, \rho_0))} f(\sigma_0, \rho_0). \end{aligned} \tag{2.9}$$

From (2.6) and (2.8) we obtain that

$$\begin{aligned} f(\tau_1, \varrho_1) &\leqslant \psi(f(\tau_0, \varrho_0))(d(\tau_0, \rho_1) + d(\sigma_1, \varrho_0)) \leqslant \\ &\leqslant \sqrt{\psi(f(\tau_0, \varrho_0))}\sqrt{\psi(f(\tau_0, \varrho_0))}(d(\tau_0, \rho_1) + d(\sigma_1, \varrho_0)) \leqslant \\ &\leqslant \sqrt{\psi(f(b_0, q_0))} f(b_0, q_0). \end{aligned} \tag{2.10}$$

Since F is a Δ-symmetric covariant mapping and $(\sigma_0, \rho_0), (\tau_0, \varrho_0) \in \Delta$, we have $F(\sigma_0, \rho_0) \Re F(\rho_0, \sigma_0) \Rightarrow (\sigma_1, \rho_1) \in \Delta$ and $F(\tau_0, \varrho_0) \Re F(\varrho_0, \tau_0) \Rightarrow (\tau_1, \varrho_1) \in \Delta$.
By our assumptions (2.3) and (2.4), choose $\sigma_2 \in F(\sigma_1, \rho_1)$, $\rho_2 \in F(\rho_1, \sigma_1)$ and $\tau_2 \in F(\tau_1, \varrho_1)$, $\varrho_2 \in F(\varrho_1, \tau_1)$ such that

$$\sqrt{\psi(f(\sigma_1, \rho_1))}(d(\sigma_1, \varrho_2) + d(\tau_2, \rho_1)) \leqslant f(\sigma_1, \rho_1) \tag{2.11}$$

$$\sqrt{\psi(f(\tau_1,\varrho_1))}(d(\tau_1,\rho_2)+d(\sigma_2,\varrho_1)) \leqslant f(\tau_1,\varrho_1) \tag{2.12}$$

and

$$f(\sigma_2,\rho_2) \leqslant \psi(f(\sigma_1,\rho_1))(d(\sigma_1,\varrho_2)+d(\tau_2,\rho_1)) \tag{2.13}$$

$$f(\tau_2,\varrho_2) \leqslant \psi(f(\tau_1,\varrho_1))(d(\tau_1,\rho_2)+d(\sigma_2,\varrho_1)). \tag{2.14}$$

From (2.11) and (2.13) we obtain that

$$\begin{aligned} f(\sigma_2,\rho_2) &\leqslant \psi(f(\sigma_1,\rho_1))(d(\sigma_1,\varrho_2)+d(\tau_2,\rho_1)) \leqslant \\ &\leqslant \sqrt{\psi(f(\sigma_1,\varrho_1))}\sqrt{\psi(f(\sigma_1,\varrho_1))}(d(\sigma_1,\varrho_2)+d(\tau_2,\rho_1)) \leqslant \\ &\leqslant \sqrt{\psi(f(\sigma_1,\rho_1))}f(\sigma_1,\rho_1). \end{aligned} \tag{2.15}$$

From (2.12) and (2.14) we obtain that

$$\begin{aligned} f(\tau_2,\varrho_2) &\leqslant \psi(f(\tau_1,\varrho_1))(d(\tau_1,\rho_2)+d(\sigma_2,\varrho_1)) \leqslant \\ &\leqslant \sqrt{\psi(f(\tau_1,\varrho_1))}\sqrt{\psi(f(\tau_1,\varrho_1))}(d(\tau_1,\rho_2)+d(\sigma_2,\varrho_1)) \leqslant \\ &\leqslant \sqrt{\psi(f(\tau_1,\varrho_1))}f(\tau_1,\varrho_1) \end{aligned} \tag{2.16}$$

with $(\sigma_2,\rho_2),(\tau_2,\varrho_2) \in \Delta$. Continue in this way, we get bisequence $(\sigma_n,\rho_n),(\tau_n,\varrho_n)$ with $(\sigma_n,\rho_n),(\tau_n,\varrho_n)\in\Delta$, $\sigma_{n+1}\in F(\sigma_n,\rho_n)$, $\rho_{n+1}\in F(\rho_n,\sigma_n)$ and $\tau_{n+1}\in F(\tau_n,\varrho_n)$, $\varrho_{n+1}\in F(\varrho_n,\tau_n)$ such that for all $n\in N$, we have

$$\sqrt{\psi(f(\sigma_n,\rho_n))}(d(\sigma_n,\varrho_{n+1})+d(\tau_{n+1},\rho_n)) \leqslant f(\sigma_n,\rho_n) \tag{2.17}$$

$$\sqrt{\psi(f(\tau_n,\varrho_n))}(d(\tau_n,\rho_{n+1})+d(\sigma_{n+1},\varrho_n)) \leqslant f(\tau_n,\varrho_n) \tag{2.18}$$

and

$$f(\sigma_{n+1},\rho_{n+1}) \leqslant \psi(f(\sigma_n,\rho_n))(d(\sigma_n,\varrho_{n+1})+d(\tau_{n+1},\rho_n)) \tag{2.19}$$

$$f(\tau_{n+1},\varrho_{n+1}) \leqslant \psi(f(\tau_n,\varrho_n))(d(\tau_n,\rho_{n+1})+d(\sigma_{n+1},\varrho_n)). \tag{2.20}$$

From (2.17) and (2.19) we obtain that

$$\begin{aligned} f(\sigma_{n+1},\rho_{n+1}) &\leqslant \psi(f(\sigma_n,\rho_n))(d(\sigma_n,\varrho_{n+1})+d(\tau_{n+1},\rho_n)) \leqslant \\ &\leqslant \sqrt{\psi(f(\sigma_n,\rho_n))}\sqrt{\psi(f(\sigma_n,\rho_n))}(d(\sigma_n,\varrho_{n+1})+d(\tau_{n+1},\rho_n)) \leqslant \\ &\leqslant \sqrt{\psi(f(\sigma_n,\rho_n))}f(\sigma_n,\rho_n). \end{aligned} \tag{2.21}$$

From (2.18) and (2.20) we obtain

$$\begin{aligned} f(\tau_{n+1},\varrho_{n+1}) &\leqslant \psi(f(\tau_n,\varrho_n))(d(\tau_n,\rho_{n+1})+d(\sigma_{n+1},\varrho_n)) \leqslant \\ &\leqslant \sqrt{\psi(f(\tau_n,\varrho_n))}\sqrt{\psi(f(\tau_n,\varrho_n))}(d(\tau_n,\rho_{n+1})+d(\sigma_{n+1},\varrho_n)) \leqslant \\ &\leqslant \sqrt{\psi(f(\tau_n,\varrho_n))}f(\tau_n,\varrho_n). \end{aligned} \tag{2.22}$$

Therefore, we get

$$f(\sigma_{n+1},\rho_{n+1})+f(\tau_{n+1},\varrho_{n+1}) \leqslant \sqrt{\psi(f(\sigma_n,\rho_n))}f(\sigma_n,\rho_n)+\sqrt{\psi(f(\tau_n,\varrho_n))}f(\tau_n,\varrho_n). \tag{2.23}$$

On the other hand

$$f(\sigma_{n+1},\rho_n)+f(\tau_{n+1},\varrho_n) \leqslant \sqrt{\psi(f(\sigma_n,\rho_{n-1}))}f(\sigma_n,\rho_{n-1})+\sqrt{\psi(f(\tau_n,\varrho_{n-1}))}f(\tau_n,\varrho_{n-1}) \tag{2.24}$$

and

$$f(\sigma_n, \rho_{n+1}) + f(\tau_n, \varrho_{n+1}) \leqslant \sqrt{\psi(f(\sigma_{n-1}, \rho_n))} f(\sigma_{n-1}, \rho_n) + \sqrt{\psi(f(\tau_{n-1}, \varrho_n))} f(\tau_{n-1}, \varrho_n). \quad (2.25)$$

Now we prove $f(\sigma_n, \rho_n) + f(\tau_n, \varrho_n) \to 0$ as $n \to +\infty$. Suppose that
$f(\sigma_n, \rho_n) + f(\tau_n, \varrho_n) > 0$ for all $n \in N$, since if $f(\sigma_n, \rho_n) + f(\tau_n, \varrho_n) = 0$ for some $n \in N$. Then we obtain
$(D(\sigma_n, F(\varrho_n, \tau_n)) + D(F(\tau_n, \varrho_n), \rho_n) + (D(\tau_n, F(\rho_n, \sigma_n)) + D(F(\sigma_n, \rho_n), \varrho_n)) = 0$

$$\begin{aligned} D(\sigma_n, F(\varrho_n, \tau_n)) = 0 \quad &\text{implies that} \quad \sigma_n \in \overline{F(\varrho_n, \tau_n)} = F(\varrho_n, \tau_n) \\ D(F(\tau_n, \varrho_n), \rho_n) = 0 \quad &\text{implies that} \quad \rho_n \in \overline{F(\tau_n, \varrho_n)} = F(\tau_n, \varrho_n) \\ D(\tau_n, F(\rho_n, \sigma_n)) = 0 \quad &\text{implies that} \quad \tau_n \in \overline{F(\rho_n, \sigma_n)} = F(\rho_n, \sigma_n) \\ D(F(\sigma_n, \rho_n), \varrho_n) = 0 \quad &\text{implies that} \quad \varrho_n \in \overline{F(\sigma_n, \rho_n)} = F(\sigma_n, \rho_n) \end{aligned}$$

also, we have

$$\begin{aligned} 0 \quad &\leqslant \inf\nolimits_{\varrho_n \in F(\sigma_n, \rho_n)} d(\sigma_n, \varrho_n) = \\ &= D(\sigma_n, F(\sigma_n, \rho_n)) \leqslant \\ &\leqslant D(\sigma_n, F(\varrho_n, \tau_n)) + D(\rho_n, F(\varrho_n, \tau_n)) + D(\rho_n, F(\sigma_n, \rho_n)) \leqslant \\ &\leqslant f(\sigma_n, \rho_n) + \inf\nolimits_{\rho_n \in F(\tau_n, \varrho_n)} d(\rho_n, \rho_n) \leqslant \\ &\leqslant \lim_{n \to +\infty} f(\sigma_n, \rho_n) = 0. \end{aligned}$$

Therefore, $\sigma_n = \varrho_n$ and similarly, we shows that $\tau_n = \rho_n$. Then
$(\sigma_n, \rho_n) \in (\Gamma \times \Theta) \cap (\Theta \times \Gamma)$ is coupled fixed point of F. Hence theorem is proved. □

Using (2.23)–(2.25) and $\psi(t) < 1$, we conclude that $\{f(\sigma_n, \rho_n)\}$ and $\{f(\tau_n, \varrho_n)\}$ are strictly decreasing bisequence of non-negative real numbers. Thus there exist $\delta \geqslant 0$ and $\lambda \geqslant 0$ such that $\lim\limits_{n \to +\infty} f(\sigma_n, \rho_n) = \delta$ and $\lim\limits_{n \to +\infty} f(\tau_n, \varrho_n) = \lambda$.
Now we will prove $\delta = \lambda = 0$. Suppose that $\delta > 0$ and $\lambda > 0$. Letting $n \to +\infty$ in (2.23)–(2.25), we obtain

$$\begin{aligned} \delta + \lambda \quad &\leqslant \lim_{f(\sigma_{n+1}, \rho_{n+1}) \to \delta^+} \sup \sqrt{\psi(f(\sigma_{n+1}, \rho_{n+1})} \delta + \lim_{f(\tau_{n+1}, \varrho_{n+1}) \to \lambda^+} \sup \sqrt{\psi(f(\tau_{n+1}, \varrho_{n+1})} \lambda < \\ &< \delta + \lambda \end{aligned}$$

and

$$\begin{aligned} \delta + \lambda \quad &\leqslant \lim_{f(\sigma_{n+1}, \rho_n) \to \delta^+} \sup \sqrt{\psi(f(\sigma_{n+1}, \rho_n)} \delta + \lim_{f(\tau_{n+1}, \varrho_n) \to \lambda^+} \sup \sqrt{\psi(f(\tau_{n+1}, \varrho_n)} \lambda < \\ &< \delta + \lambda \end{aligned}$$

also

$$\begin{aligned} \delta + \lambda \quad &\leqslant \lim_{f(\sigma_n, \rho_{n+1}) \to \delta^+} \sup \sqrt{\psi(f(\sigma_n, \rho_{n+1})} \delta + \lim_{f(\tau_n, \varrho_{n+1}) \to \lambda^+} \sup \sqrt{\psi(f(\tau_n, \varrho_{n+1})} \lambda < \\ &< \delta + \lambda. \end{aligned}$$

In any case which is contradiction. Hence $\delta = \lambda = 0$, that is
$\lim\limits_{n \to +\infty} f(\sigma_n, \rho_n) = \lim\limits_{n \to +\infty} f(\tau_n, \varrho_n) = 0.$
Now we shows that (σ_n, ρ_n) and (τ_n, ϱ_n) are Cauchy bisequences in (Γ, Θ, d).
Suppose that

$\delta = \lim_{f(\sigma_{n+1},\rho_{n+1})\to 0^+} \sup \sqrt{\psi(f(\sigma_{n+1},\rho_{n+1})}$
and $\lambda = \lim_{f(\tau_{n+1},\varrho_{n+1})\to 0^+} \sup \sqrt{\psi(f(\tau_{n+1},\varrho_{n+1})}$. Then by our assumption (2.2), we have $\delta < 1$, $\lambda < 1$. Let ξ *and* ζ be such that $\delta < \xi < 1$ and $\lambda < \zeta < 1$ then there is some $n_0 \in N$ such that $\sqrt{\psi(f(\sigma_{n+1},\rho_{n+1})} < \xi$, $\sqrt{\psi(f(\tau_{n+1},\varrho_{n+1})} < \zeta$, for each $n \geqslant n_0$. Thus, from (2.23), we obtain

$$\begin{aligned} f(\sigma_{n+1},\rho_{n+1}) + f(\tau_{n+1},\varrho_{n+1}) &\leqslant \xi f(\sigma_n,\rho_n) + \zeta f(\tau_n,\varrho_n) \leqslant \\ &\leqslant \xi^2 f(\sigma_{n-1},\rho_{n-1}) + \zeta^2 f(\tau_{n-1},\varrho_{n-1}) \leqslant \\ &\vdots \\ &\leqslant \xi^{n+1-n_0} f(\sigma_{n_0},\rho_{n_0}) + \zeta^{n+1-n_0} f(\tau_{n_0},\varrho_{n_0}). \end{aligned} \tag{2.26}$$

Since $\psi(t) \geqslant b > 0$ for all $t \geqslant 0$, from (2.17), (2.18) and (2.26), we get

$$\begin{aligned} (d(\sigma_n,\varrho_{n+1}) + d(\tau_{n+1},\rho_n)) + (d(\tau_n,\rho_{n+1}) + d(\sigma_{n+1},\varrho_n)) &\leqslant \\ \leqslant \frac{1}{\sqrt{b}}(\xi^{n-n_0} f(\sigma_{n_0},\rho_{n_0}) + \zeta^{n-n_0} f(\tau_{n_0},\varrho_{n_0})). \end{aligned} \tag{2.27}$$

On the other hands from (2.24) and (2.25)

$$\begin{aligned} f(\sigma_{n+1},\rho_n) + f(\tau_{n+1},\varrho_n) \quad &\leqslant \xi f(\sigma_n,\rho_{n-1}) + \zeta f(\tau_n,\varrho_{n-1}) \leqslant \\ &\leqslant \xi^2 f(\sigma_{n-1},\rho_{n-2}) + \zeta^2 f(\tau_{n-1},\varrho_{n-2}) \\ &\vdots \\ &\leqslant \xi^{n+1} f(\sigma_1,\rho_0) + \zeta^{n+1} f(\tau_1,\varrho_0) \end{aligned} \tag{2.28}$$

and

$$\begin{aligned} (d(\sigma_n,\varrho_n) + d(\tau_{n+1},\rho_{n-1})) + (d(\tau_n,\rho_n) + d(\sigma_{n+1},\varrho_{n-1})) &\leqslant \\ \leqslant \frac{1}{\sqrt{b}}(\xi^{n-n_0} f(\sigma_{n_1},\rho_{n_0}) + \zeta^{n-n_0} f(\tau_{n_1},\varrho_{n_0})) \end{aligned} \tag{2.29}$$

also

$$\begin{aligned} f(\sigma_n,\rho_{n+1}) + f(\tau_n,\varrho_{n+1}) &\leqslant \xi f(\sigma_{n-1},\rho_n) + \zeta f(\tau_{n-1},\varrho_n) \leqslant \\ &\leqslant \xi^2 f(\sigma_{n-2},\rho_{n-1}) + \zeta^2 f(\tau_{n-2},\varrho_{n-1}) \\ &\vdots \\ &\leqslant \xi^{n+1} f(\sigma_0,\rho_1) + \zeta^{n+1} f(\tau_0,\varrho_1) \end{aligned} \tag{2.30}$$

and

$$\begin{aligned} (d(\sigma_{n-1},\varrho_{n+1}) + d(\tau_n,\rho_n)) + (d(\tau_{n-1},\rho_{n+1}) + d(\sigma_n,\varrho_n)) &\leqslant \\ \leqslant \frac{1}{\sqrt{b}}(\xi^{n-n_0} f(\sigma_{n_0},\rho_{n_1}) + \zeta^{n-n_0} f(\tau_{n_0},\varrho_{n_1})). \end{aligned} \tag{2.31}$$

For each $n, m \in N$ with $n < m$, we have (27), (29) and (31)

$$\begin{aligned}
& d(\sigma_n, \varrho_m) + d(\tau_m, \rho_n) + d(\sigma_m, \varrho_n) + d(\tau_n, \rho_m) \leqslant \\
& \leqslant (d(\sigma_n, \varrho_{n+1}) + d(\tau_{n+1}, \rho_n)) + d(\sigma_{n+1}, \varrho_n) + d(\tau_n, \rho_{n+1})) + \\
& \quad +2(d(\sigma_{n+1}, \varrho_{n+1}) + d(\tau_{n+1}, \rho_{n+1})) + \cdots + 2(d(\sigma_{m-1}, \varrho_{m-1}) + d(\tau_{m-1}, \rho_{m-1})) + \\
& \quad +(d(\sigma_{m-1}, \varrho_m) + d(\tau_m, \rho_{m-1})) + (d(\sigma_m, \varrho_{m-1}) + d(\tau_{m-1}, \rho_m)) \leqslant \\
& \leqslant \frac{1}{\sqrt{b}}(\xi^{n-n_0} f(\sigma_{n_0}, \rho_{n_0}) + \zeta^{n-n_0} f(\tau_{n_0}, \varrho_{n_0})) + \frac{2}{\sqrt{b}}(\xi^{n+1-n_0} f(\sigma_{n_1}, \rho_{n_0}) + \\
& \quad +\zeta^{n+1-n_0} f(\tau_{n_1}, \varrho_{n_0})) + \cdots + \frac{2}{\sqrt{b}}(\xi^{m+1-n_0} f(\sigma_{n_1}, \rho_{n_0}) + \\
& \quad +\zeta^{m+1-n_0} f(\tau_{n_1}, \varrho_{n_0})) + \frac{1}{\sqrt{b}}(\xi^{m-n_0} f(\sigma_{n_0}, \rho_{n_1}) + \zeta^{n-n_0} f(\tau_{n_0}, \varrho_{n_1})). \\
& \to 0 \text{ as } n, m \to +\infty.
\end{aligned}$$

Hence, (σ_n, ρ_n) and (τ_n, ϱ_n) are Cauchy bi-sequences in (Γ, Θ, d). Since (Γ, Θ, d) is complete, there exist $\alpha, \beta \in \Gamma$ and $\gamma, \eta \in \Theta$ such that

$$\lim_{n\to+\infty} \sigma_n = \eta, \quad \lim_{n\to+\infty} \tau_n = \gamma, \quad \lim_{n\to+\infty} \rho_n = \beta, \quad \lim_{n\to+\infty} \varrho_n = \alpha. \tag{2.32}$$

By our assumption f is lower semi continuous. Then we have

$$0 \leqslant f(\alpha, \gamma) = D(\alpha, F(\eta, \beta)) + D(F(\beta, \eta), \gamma) \leqslant \lim_{n\to+\infty} \inf f(\tau_n, \varrho_n) = 0.$$

Hence $D(\alpha, F(\eta, \beta)) = 0$ and $D(F(\beta, \eta), \gamma) = 0$ which implies that $\alpha \in F(\eta, \beta)$ and $\gamma \in F(\beta, \eta)$. And similarly we can prove that $\beta \in F(\gamma, \alpha)$ and $\eta \in F(\alpha, \gamma)$.
Again from (2.32), we get

$$d(\alpha, \eta) = d(\lim_{n\to+\infty} \varrho_n, \lim_{n\to+\infty} \sigma_n) = \lim_{n\to+\infty} d(\sigma_n, \varrho_n) = 0$$

and

$$d(\beta, \gamma) = d(\lim_{n\to+\infty} \rho_n, \lim_{n\to+\infty} \tau_n) = \lim_{n\to+\infty} d(\tau_n, \rho_n) = 0.$$

Therefore, $\alpha = \eta$ and $\beta = \gamma$. Then $\alpha \in F(\alpha, \beta)$ and $\beta \in F(\beta, \alpha)$, that is $(\alpha, \beta) \in (\Gamma \times \Theta) \cap (\Theta \times \Gamma)$ is a coupled fixed point of F. Now we prove the uniqueness, let $(\alpha^*, \beta^*) \in (\Gamma \times \Theta) \cup (\Theta \times \Gamma)$ be another coupled fixed point of F. If $(\alpha^*, \beta^*) \in (\Gamma \times \Theta)$, then we obtain

$$0 \leqslant f(\alpha^*, \beta^*) = D(\alpha^*, F(\alpha, \beta)) + D(F(\beta, \alpha), \beta^*) \leqslant \lim_{n\to+\infty} \inf f(\sigma_n, \rho_n) = 0.$$

Therefore, $D(\alpha^*, F(\alpha, \beta)) = 0$ and $D(F(\beta, \alpha), \beta^*) = 0$ implies $\alpha^* \in F(\alpha, \beta)$ and $\beta^* \in F(\beta, \alpha)$. So, we get $\alpha = \alpha^*$ and $\beta = \beta^*$.
Similarly, if $(\alpha^*, \beta^*) \in (\Theta \times \Gamma)$, we have $\alpha = \alpha^*$ and $\beta = \beta^*$.
Then (α, β) is a unique coupled fixed point of F.

Example 2.4. *Let $\Gamma = \{\mathfrak{U}_m(R)/\mathfrak{U}_m(R)$ is upper triangular matrices overR$\}$ and $\Theta = \{\mathfrak{L}_m(R)/\mathfrak{L}_m(R)$ is lower triangular matrices over $R\}$ with the bipolar metric*

$$d(\Phi, \Omega) = \sum_{i,j=1}^{m} |\phi_{ij} - \omega_{ij}|$$

for all $\Phi = (\phi_{ij})_{m\times m} \in \mathfrak{U}_m(R)$ and $\Omega = (\omega_{ij})_{m\times m} \in \mathfrak{L}_m(R)$. On the set (Γ, Θ), we consider the following relation :

$$\Phi, \Omega \in \Gamma \cup \Theta, \Phi \preceq \Omega \Leftrightarrow \phi_{ij} \leqslant \omega_{ij}$$

where $\leqslant$ is usual ordering. Then clearly, (Γ, Θ, d) is a complete bipolar metric space and $(\Gamma, \Theta, \preceq)$ is a partially ordered set. And (Γ, Θ) has the property as in Theorem (2.3). Let $F : (\Gamma \times \Theta, \Theta \times \Gamma) \rightrightarrows CL(\Gamma, \Theta)$ be defined as

$$F(\Phi, \Omega) = (\phi_{ij})_{m\times m} I_{m\times m} \ \ \forall \ (\Phi = (\phi_{ij})_{m\times m}, \quad \Omega = (\omega_{ij})_{m\times m}) \in (\Gamma \times \Theta) \cup (\Theta \times \Gamma).$$

Then

$$\begin{aligned} f(\Phi, \Omega) &= D(\Phi, F(\Omega, \Phi)) + D(F(\Phi, \Omega), \Omega) = \\ &= \inf\{d(\Phi, Y) : Y \in (\omega_{ij})_{m\times m} I_{m\times m}\} + \inf\{d(X, \Omega) : X \in (\phi_{ij})_{m\times m} I_{m\times m}\} = \\ &= d(\Phi, \Omega) + d(\Phi, \Omega) = 2d(\Phi, \Omega) = 2\sum_{i,j=1}^{m} |\phi_{ij} - \omega_{ij}|. \end{aligned}$$

Also, let $\psi : [0, +\infty) \to (0, 1)$ by $\psi(t) = \dfrac{t}{1+t}$ then obviously, $\lim\limits_{r\to t^+} \sup \psi(r) < 1$ for each $t \in [0, +\infty)$ with out loss of generality we may assume that

$$O = (o_{ij})_{m\times m} = Y = (y_{ij})_{m\times m} \preceq \Phi = (\phi_{ij})_{m\times m}$$

and

$$O = (o_{ij})_{m\times m} = X = (x_{ij})_{m\times m} \preceq \Omega = (\omega_{ij})_{m\times m}.$$

It is obviously,

$$\sqrt{\psi(f(\Phi, \Omega))}[d(\Phi, Y) + d(X, \Omega)] \leqslant f(\Phi, \Omega)$$

such that

$$f(X, Y) \leqslant \psi(f(\Phi, \Omega))[d(\Phi, Y) + d(X, \Omega)].$$

Hence all assertions of Theorem (2.3) are satisfied and $(O_{m\times m}, O_{m\times m})$ is the coupled fixed point of F.

Theorem 2.5. *Let (Γ, Θ, d) be an complete bipolar metric space endowed with a partial order $\preceq$. Suppose that Δ is non empty, that is there exists $(\sigma, \rho) \in \Delta$. Let $F : (\Gamma \times \Theta, \Theta \times \Gamma) \rightrightarrows CL(\Gamma, \Theta)$ be a Δ- symmetric covariant mapping and consider that $f : \Gamma \times \Theta \to [0, +\infty)$ as*

$$f(\sigma, \rho) = D(\sigma, F(\varrho, \tau)) + D(F(\tau, \varrho), \rho) \ \ for\ all\ \sigma, \tau \in \Gamma\ and\ \rho, \varrho \in \Theta \tag{2.33}$$

is lower semi-continuous and there exists a mapping $\psi : [0, +\infty) \to (0, 1)$ satisfying

$$\lim_{r\to t^+} \sup \psi(r) < 1 \ for\ each\ t \in [0, +\infty). \tag{2.34}$$

Assume that for any $(\sigma, \rho) \in \Delta$ there exist $x \in F(\sigma, \rho)$ and $y \in F(\rho, \sigma)$ satisfying

$$\sqrt{\psi(d(\sigma, y) + d(x, \rho))}[d(\sigma, y) + d(x, \rho)] \leqslant D(\sigma, F(\varrho, \tau)) + D(F(\tau, \varrho), \rho) \tag{2.35}$$

such that

$$D(x, F(v, u)) + D(F(u, v), y) \leqslant \psi(d(\sigma, y) + d(x, \rho))[d(\sigma, y) + d(x, \rho)] \tag{2.36}$$

for some $v \in F(\varrho, \tau)$ and $u \in F(\tau, \varrho)$. Then $F : (\Gamma \times \Theta) \cup (\Theta \times \Gamma) \to CL(\Gamma \cup \Theta)$ has a coupled fixed point. That is there exists $(\alpha, \beta) \in (\Gamma \times \Theta) \cup (\Theta \times \Gamma)$ such that $\alpha \in F(\alpha, \beta)$ and $\beta \in F(\beta, \alpha)$.

Example 2.6. *Let $\Gamma = \{\mathfrak{U}_m(R)/\mathfrak{U}_m(R)$ is upper triangular matrices over $R\}$ and $\Theta = \{\mathfrak{L}_m(R)/\mathfrak{L}_m(R)$ is lower triangular matrices over $R\}$ with the bipolar metric*

$$d(\Phi, \Omega) = \sum_{i,j=1}^{m} |\phi_{ij} - \omega_{ij}|$$

for all $\Phi = (\phi_{ij})_{m\times m} \in \mathfrak{U}_m(R)$ *and* $\Omega = (\omega_{ij})_{m\times m} \in \mathfrak{L}_m(R)$*. On the set* (Γ, Θ)*, we consider the following relation :*

$$\Phi, \Omega \in \Gamma \cup \Theta,\ \ \Phi \preceq \Omega \Leftrightarrow \phi_{ij} \leqslant \omega_{ij}$$

where $\leqslant$ *is usual ordering. Then clearly,* (Γ, Θ, d) *is a complete bipolar metric space and* $(\Gamma, \Theta, \preceq)$ *is a partially ordered set. Let* $F : (\Gamma\times\Theta, \Theta\times\Gamma) \rightrightarrows CL(\Gamma, \Theta)$ *be defined as*

$$\begin{aligned} F(\Phi, \Omega) \ &= \frac{(\phi_{ij})_{m\times m}}{3} \\ &\forall \ \ (\Phi = (\phi_{ij})_{m\times m},\ \Omega = (\omega_{ij})_{m\times m}) \in (\Gamma\times\Theta) \cup (\Theta\times\Gamma) \end{aligned}$$

define $\psi : [0, +\infty) \to (0, 1)$ *by* $\psi(t) = \frac{1}{5}$*. First we shall prove that* $F(\Phi, \Omega)$ *satisfies all the conditions of Theorem (2.5). In fact it is easy to see that the mapping* $f(\Phi, \Omega) = \frac{4}{15}\sum_{i,j=1}^{m} |\phi_{ij} - \omega_{ij}|$ *is lower semi continuous. Thus for all*
$(\Phi, \Omega) \in (\Gamma\times\Theta) \cup (\Theta\times\Gamma)$*, there exist* $X \in F(\Phi, \Omega) = \frac{(\phi_{ij})_{m\times m}}{3}$ *and*
$Y \in F(\Omega, \Phi) = \frac{(\omega_{ij})_{m\times m}}{3}$ *such that*

$$\begin{aligned} D(\Phi, F(\Omega, \Phi)) + D(F(\Phi, \Omega), Q) &= \frac{4}{15}\left(\sum_{i,j=1}^{m} |\phi_{ij} - \omega_{ij}|\right) = \\ &= \frac{1}{5}\left(\sum_{i,j=1}^{m} |\frac{4}{3}\phi_{ij} - \frac{4}{3}\omega_{ij}|\right) = \\ &= \frac{1}{5}\left(\sum_{i,j=1}^{m} |(\phi_{ij} - \frac{1}{3}\omega_{ij}) + (\frac{1}{3}\phi_{ij} - \omega_{ij})|\right) \leqslant \\ &\leqslant \frac{1}{5}\left(\sum_{i,j=1}^{m} |\phi_{ij} - \frac{1}{3}\omega_{ij}| + \sum_{i,j=1}^{m} |\frac{1}{3}\phi_{ij} - \omega_{ij}|\right) \leqslant \\ &\leqslant \psi(d(\Phi, Y) + d(X, \Omega))[d(\Phi, Y) + d(X, \Omega)]. \end{aligned}$$

It is obviously,

$$\sqrt{\psi(d(\Phi, Y) + d(X, \Omega))}[d(\Phi, Y) + d(X, \Omega)] \leqslant D(\Phi, F(\Omega, \Phi)) + D(F(\Phi, \Omega), \Omega)$$

such that

$$D(X, F(Y, X)) + D(F(X, Y), Y) \leqslant \psi(d(\Phi, Y) + d(X, \Omega))[d(\Phi, Y) + d(X, \Omega)].$$

Hence all assertions of Theorem (2.5) are satisfied and $(O_{m\times m}, O_{m\times m})$ *is the coupled fixed point of* F*.*

3. Declaration

- **Competing Interesting:** The authors declare that they have no competing interest.
- **Funding:** No funding
- **Author contributions :** All authors contributed equally and significantly in writing this article. All authors read and approved the final manuscript.

References

[1] I.Altun, A common fixed point theorem for multivalued Ćirić type mappings with new type compatibility, *An. St. Univ. Ovidius constanta*, **17**(2009), no. 2, 19–26.

[2] H.Aydi, Mohammad Barakat, Abdelbsset Felht, Huseyin Isik, On ϕ-contraction type couplings in partial metric spaces, *Journal of Mathematical Analysis*, **8**(2017), no. 4, 78–89.

[3] D.Bajovic, Z.D.Mitrovir̀c, M.Saha, Remark on contraction principle in conex$_{tvs}$ b-metric spaces, *The Journal of Analysis.* DOI: 10.1007/s41478-020-00261-x

[4] S.Banach, Sur les operations dans les ensembles abstraits etleur applications aux equations integrales, *Fund. Math.*, **3**(1922), 133–181. DOI: 10.4236/ahs.2013.22012

[5] M.Berinde, V.Berinde, On a general class of multivalued weakly picard mappigs, *J. Math. Anal. Appl.*, **326**(2007), 772–782. DOI: 10.1016/J.JMAA.2006.03.016

[6] P.Debnath, N.Konwar, S.Radenovir̀c, Metric Fixed Point Theory: Applications in Science, Engineering and Behavioural Science, Springer Nature Singapore, 2021.

[7] Y.Feng, S.Liu, Fixed point theorems of multi-valued contractive mappings, *J. Math. Anal. Appl.*, **317**(2006), 103–112.

[8] N.Hussain, A.Alotaibi, Coupled coincidences for multi-valued contractions in partially ordered metric spaces, *Fixed point theory and Applications*, **2011**(2011), 82.

[9] G.Mani, A.J.Gnanaprakasam, Z.D.Mitrovic, M.-F.Bota, Solving an Integral Equation via Fuzzy Triple Controlled Bipolar Metric Spaces, *Mathematics*, **9**(2021), 3181. DOI: 10.3390/math9243181

[10] N.Mizoguchi, W.Takahashi, Fixed point theorems for multi-valued mappings on complete metric spaces, *J. Math. Anal. Appl.*, **141**(1989), 177–188.

[11] A.Mutlu, Utku Gürdal, Bipolar metric spaces and some fixed point theorems, *J. Nonlinear Sci. Appl.*, **9**(2016), no. 9, 5362–5373. DOI:1 0.22436/jnsa.009.09.05

[12] A.Mutlu, Kübra Özkan, Utku Gürdal, Coupled fixed point theorems on bipolar metric spaces, *European journal of pure and applied mathematics*, **10**(2017), то. 4, 655–667.

[13] S.B.Nadler. jr, multi-valued contractio mappings, *Pacific. J. Math.*, **30**(1969), 475–488.

[14] K.P.R.Rao, G.N.V.Kishore, P.R.Sobhana Babu, Triple coincidence point theorems for multivalued maps in partially ordered metric spaces, *Universal Journal of Computational Mathematics*, **1**(2013), no. 2, 19–23. DOI: 10.13189/ujcmj.2013.010201

[15] B.E.Rhoades, A fixed point theorems for a multivalued non-self mappigs , *Comment. Math. Univ. Carolin.*, **37**(1996), no. 2, 401–404.

[16] B.Samet, C.Vetro, Coupled fixed point theorems for multi-valued nonlinear contraction mappings in partially ordered metric spaces, *Nonlinear Analysis*, **74**(2011), 4260–4268. DOI: 10.1016/j.na.2011.04.007

[17] B.Samet, Erdal Karapinar, Hassen Aydi and Vesna Cojbasic Rajic, *D iscussion on some coupled fixed point theorems*, *Fixed Point Theory and Applications*, **2013**(2013), 50. DOI: 10.1186/1687-1812-2013-50

[18] V.Todorcevic, Harmonic Quasiconformal Mappings and Hyperbolic Type Metrics, Springer Nature Switzerland AG, 2019.

Многозначные Δ-симметричные ковариантные результаты в биполярных метрических пространствах

Г. Н. В. Кишор
Факультет инженерной математики и гуманитарных наук
Инженерный колледж Саги Рама Кришнам Раджу
Андхра-Прадеш, Индия

Б. Шринуваса Рао
Департамент математики
Амбедкар университет
Андхра-Прадеш, Индия

Д. Рам Прасад
Факультет математики
Инженерный колледж Налла Малла Редди
Дивья нагар, Гхаткесар мандал
Телангана, Индия

Стоян Раденович
Факультет машиностроения
Белградский университет
Белград, Сербия

Аннотация. В этой статье мы докаываем некоторые теоремы о парных фиксированных точках для гибридных пар в отображениях, использующих Δ-симметрические ковариантные отображения в биполярных метрических пространствах. Мы также даем некоторые примеры, которые основаны на наших результатах.

Ключевые слова: Δ-симметричное ковариантное отображение, гибридная пара отображений, связанная неподвижная точка, биполярные метрические пространства.

EDN: JSPTAR
УДК 519.635.1, 519.635.4

On Calculation of Bending of a Thin Orthotropic Plate Using Legendre and Chebyshev Polynomials of the First Kind

Oksana V. Germider*
Vasily N. Popov†
Northern (Arctic) Federal University named after M. V. Lomonosov
Arkhangelsk, Russian Federation

Received 10.04.2024, received in revised form 05.05.2024, accepted 24.06.2024

Abstract. The problem of bending of a thin orthotropic rectangular plate clamped at the edges is considered in the paper. The solution is obtained using the Legendre and Chebyshev polynomials of the first kind. The function that approximates the solution of the biharmonic equation for an orthotropic plate is presented in the form of a double series expansion in these polynomials. Matrix transformations and properties of the Legendre and Chebyshev polynomials are also used. Roots of these polynomials are used as collocation points, and boundary value problem is reduced to a system of linear algebraic equations with respect to coefficients of the expansion. The problem of bending of a plate caused by the action of a distributed transverse load of constant intensity that corresponds to hydrostatic pressure is considered. This boundary value problem has analytical solution. The results of calculations for various ratios of the lengths of sides of the plate are presented. The values of deviation of solutions constructed using Legendre and Chebyshev polynomials from the analytical solution of the problem are presented in terms of the infinite norm and the finite norm in the space of square-integrable functions.

Keywords: bending a thin orthotropic plate, collocation method, Chebyshev polynomials of the first kind, Legendre polynomials.

Citation: O.V. Germider, V.N. Popov, On Calculation of Bending of a Thin Orthotropic Plate Using Legendre and Chebyshev Polynomials of the First Kind, J. Sib. Fed. Univ. Math. Phys., 2024, 17(5), 586–598. EDN: JSPTAR.

Study of bending of a thin rectangular plate is essential in modeling thin-walled spatial structures. Structures made of orthotropic materials unlike structures made of isotropic materials have high load-bearing capacity. Then one can reduce their weight with an increase in their strength. In this regard, the development of methods for modelling of such plates under the action of various types of loads is one of the main tasks of mechanics of thin-walled structures. Solution of the problem of bending the median plane of a square orthotropic plate pinched on all sides is constructed [1]. The method of initial functions using an exponential series with unknown coefficients was employed. Distributions of bending moments and shearing forces were found. The results of calculation of bending of a rectangular plate based on integral transformations under the action of constant intensity load, hydrostatic pressure and point load concentrated in the center of the plate were presented [2], [3]. Bending of the orthotropic plate under various boundary conditions was studied [4]. Numerical solution of the problem of bending of a rectangular plate consisting

*o.germider@narfu.ru https://orcid.org/0000-0002-2112-805X
†v.popov@narfu.ru https://orcid.org/0000-0003-0803-4419

of orthotropic layers arbitrarily oriented in the plane of the plate which are rigidly fixed to each other was obtained by the method of collocation and least residuals [5]. Equilibrium models of plates with rigid inclusions were considered [6]. A dynamic stiffness matrix was constructed for plane vibrations of a free orthotropic plate [7]. The results of analysis of frequencies of these vibrations were presented [8]. Deflections of a structural element representing a plate with a contour attachment the points of which are located on a rigid base when an acceleration pulse is transmitted in the direction perpendicular to the plane of the plate were calculated [9]. Study was conducted on bending of rectangular orthotropic thin plates with rotationally fixed edges under the action of arbitrary transverse loads [10]. The procedure for obtaining the stress distribution over the plate thickness for a strongly orthotropic material for three approximate models was described [11]. The first approximate model is the classical Kirchhoff-Love theory. The second model allows one to find transverse shear deformations and stresses. The third approximation is the Ambartsumian theory. It allows one to find transverse shear and normal stresses. In the presented work, to construct a solution of the problem of bending of a thin rectangular orthotropic plate with pinched edges systems of Legendre and Chebyshev polynomials of the first kind orthogonal on the segment $[-1, 1]$ are used. They play an important role both in the general theory of special functions and in the theory of orthogonal polynomials. Function that approximates the solution of the biharmonic equation for an orthotropic plate is represented as a double series expansion over these polynomials in combination with matrix transformations. In this case, the boundary value problem is written in dimensionless form. To find the coefficients in this decomposition approach proposed in [12] is used. It is based on the properties of Legendre and Chebyshev polynomials. The problem of bending of the plate due to the action of a distributed transverse load of constant intensity that corresponds to hydrostatic pressure is considered. This problem has analytical solution. The results of numerical solution of the problem are presented. Following [13], the obtained values of deviation of the constructed solutions using Legendre and Chebyshev polynomials from the analytical solution of the problem are given in terms of the infinite norm [14] and the finite norm in the space of functions integrable with the square [14, 15]. To discretize the integral norm the decomposition of the integrand function into the Chebyshev series is used. Coefficients of this decomposition can be found using values of this function calculated in the roots of Chebyshev polynomials. The importance of sampling by function values at points is emphasized in [16]. Verification of the obtained values of the integral norm was carried out using algorithm from [17] in the Maple computer algebra system.

1. Derivation of basic equations

Let us consider a thin orthotropic rectangular plate ($0 \leqslant x \leqslant d_1$, $0 \leqslant y \leqslant d_2$, $-h/2 \leqslant z \leqslant h/2$) which is under the action of a transverse load of intensity $q(x, y)$. Let us take the median plane of the undeformed plate for the xy plane, and z axis is directed towards the unloaded outer plane. Volumetric forces are neglected. In this case, the partial differential equation to determine bending of the plate has the form [18]:

$$D_x \frac{\partial^4 \omega}{\partial x^4} + 2H \frac{\partial^4 \omega}{\partial x^2 \partial y^2} + D_y \frac{\partial^4 \omega}{\partial y^4} = q, \tag{1}$$

where $\omega(x, y)$ is the bending of the median surface of the plate, $D_x = E'_x h^3/12$, $D_y = E'_y h^3/12$, $H = D_1 + 2D_{xy}$, $D_1 = E\text{"} h^3/12$, $D_{xy} = Gh^3/12$, G is the shear modulus, h is the thickness of the plate. Bending stiffnesses D_x and D_y are [19]

$$D_x = \frac{E_x h^3}{12(1-\nu_1\nu_2)}, \quad D_y = \frac{E_y h^3}{12(1-\nu_1\nu_2)}, \quad D_1 = \nu_1 D_y = \nu_2 D_x, \tag{2}$$

where E_x and E_y are Young's modules for the main directions of elasticity, ν_1, ν_2 are Poisson's coefficients.

For a plate clamped along the contour, i.e., for $x = 0$, d_1 and $y = 0$, d_2, boundary conditions have the form [18]

$$\omega = 0, \quad \frac{\partial \omega}{\partial x} = 0, \quad x = 0,\, d_1, \tag{3}$$

$$\omega = 0, \quad \frac{\partial \omega}{\partial y} = 0, \quad y = 0,\, d_2. \tag{4}$$

Let us rewrite equation (1) and boundary conditions (3) and (4) in new dimensionless variables $x^* = x/d_1$ and $y^* = y/d_1$:

$$\frac{\partial^4 \omega^*}{\partial x^{*4}} + \frac{2H}{D_x}\frac{\partial^4 \omega^*}{\partial x^{*2}\partial y^{*2}} + \frac{D_y}{D_x}\frac{\partial^4 \omega^*}{\partial y^{*4}} = q^*, \tag{5}$$

$$\omega^* = 0, \quad \frac{\partial \omega^*}{\partial x^*} = 0, \quad x^* = 0,\, 1, \tag{6}$$

$$\omega^* = 0, \quad \frac{\partial \omega^*}{\partial y^*} = 0, \quad y^* = 0,\, d_2^*; \quad d_2^* = \frac{d_2}{d_1}, \tag{7}$$

where $q = q_0 q^*$, $\omega = \dfrac{\omega^* q_0 d_1^4}{D_x}$, q_0 is the intensity of some constant load.

Let us construct a solution of boundary value problem (5)–(7) by the collocation method using Chebyshev polynomials of the first kind and the roots of these polynomials as collocation points.

2. Construction of a solution of boundary value problem using Chebyshev polynomials of the first kind

Let us present function ω^* as a double Chebyshev series. For this purpose, let $x_1 = 2x^* - 1$, $x_2 = 2y^*/d_2^* - 1$, where x_1, $x_2 \in [-1, 1]$ since Chebyshev polynomials of the first kind are defined on the segment $[-1, 1]$. In this case, problem (5)–(7) has the following form in variables x_1 and x_2

$$\kappa_1 \frac{\partial^4 \omega^*}{\partial x_1^4} + \kappa_2 \frac{\partial^4 \omega^*}{\partial x_1^2 \partial x_2^2} + \kappa_3 \frac{\partial^4 \omega^*}{\partial x_2^4} = q^*, \tag{8}$$

$$\omega^* = 0, \quad \kappa_4 \frac{\partial \omega^*}{\partial x_1} = 0, \quad x_1 = -1,\, 1, \tag{9}$$

$$\omega^* = 0, \quad \kappa_5 \frac{\partial \omega^*}{\partial x_2} = 0, \quad x_2 = -1,\, 1, \tag{10}$$

where $\kappa_1 = 16$, $\kappa_2 = \dfrac{32H}{D_x d_2^{*2}}$, $\kappa_3 = \dfrac{16 D_y}{D_x d_2^{*4}}$, $\kappa_4 = 2$, $\kappa_5 = \dfrac{2}{d_2^*}$.

Limiting the expansion of ω^* to the terms of the series with numbers $k_i \leqslant n_i$ for x_i $(i = 1, 2)$, one can write

$$\omega^*(x_1, x_2) = \sum_{\substack{k_i=0\\ i=1,2}}^{n_i} a_{k_1k_2} T_{k_1}(x_1) T_{k_2}(x_2) = \mathbf{T_1}(x_1) \otimes \mathbf{T_2}(x_2)\mathbf{A}, \tag{11}$$

where $\mathbf{T_i}(x_i) = (T_0(x_i)\, T_1(x_i) \ldots T_{n_i-1}(x_i)\, T_{n_i}(x_i))$ is a matrix of size $1\times n_i'$ $(n_i' = n_i+1,\ i = 1,\ 2)$, the elements of which are Chebyshev polynomials of the first kind $T_{j_i}(x_i) = \cos(j_i \arccos x_i)$ $(j_i = \overline{0, n_i},\ i = 1,\ 2)$ [20], $\mathbf{A}$ is the matrix with size $n_1'n_2' \times 1$ with elements $a_{k_1k_2}$: $\mathbf{A} = (a_{00}\, a_{01} \ldots a_{n_1n_2-1}\, a_{n_1n_2})^T$. The sign $\otimes$ in (11) is used to denote the Kronecker tensor product of two matrices [21]. The elements of the matrix are found by collocation. Let us choose the roots of polynomials T_{n_1+1} and T_{n_2+1} as collocation points in (8) for x_1 и x_2:

$$x_{i,k_i} = \cos\left(\frac{\pi(2n_i - 2k_i + 1)}{2(n_i + 1)}\right), \quad k_i = \overline{0, n_i},\ i = 1, 2. \tag{12}$$

Then

$$T_{j_i}(x_{i,k_i}) = \cos\left(\frac{\pi j_i(2n_i - 2k_i + 1)}{2(n_i + 1)}\right), \quad j_i, k_i = \overline{0, n_i},\ i = 1, 2. \tag{13}$$

Moreover, if n_i is odd then $x_{i,m_i} = -x_{i,n_i-m_i}$ and $T_{j_i}(x_{i,m_i}) = (-1)^{j_i} T_{j_i}(x_{i,n_i-m_i})$, $(m_i = \overline{0,\ (n_i-1)/2};\ j_i = \overline{0,\ n_i};\ i = 1, 2)$. If n_i is even then $x_{i,n_i/2} = 0$, $x_{i,m_i} = -x_{i,n_i-m_i}$ and $T_{j_i}(x_{i,m_i}) = (-1)^{j_i} T_{j_i}(x_{i,n_i-m_i})$, $(m_i = \overline{0,\ n_i/2 - 1};\ j_i = \overline{0,\ n_i};\ i = 1, 2)$. The value of $T_{j_i}(0)$ is found using the following representation [20]

$$T_{j_i}(x_i) = \sum_{k=0}^{[j_i/2]} \varsigma_k x_i^{j_i-2k}, \quad \varsigma_k = \frac{(-1)^k 2^{j_i-2k-1} j_i(j_i - k - 1)!}{(j_i - 2k)!k!},$$

where $[j_i/2]$ is the integer part of the number $j_i/2$. If j_i is even then $T_{j_i}(0) = \varsigma_{j_i/2} = (-1)^{j_i/2}$, otherwise $T_{j_i}(0) = 0$ $(i = 1, 2)$.

The derivative of $\mathbf{T_i}(x_i)$ with respect to x_i is represented as a product of $\mathbf{T_i}\mathbf{J_i}$ as follows [22]

$$\frac{\mathrm{d}T_{j_i}}{\mathrm{d}x_i} = j_i \sum_{\substack{k_i=0\\ j_i+k_i-\text{nech.}}}^{j_i-1} c_{k_i} T_{k_i}(x_i), \quad j_i \geqslant 1,$$

where $c_0 = 1$ and $c_{k_i} = 2$ $(k_i > 0)$, and $\mathbf{J_i}$ is an upper-triangular matrix with nonzero elements $J_{i,0\,j_i} = j_i$ (j_i is odd, $j_i = \overline{1,\ n_i}$) and $J_{i,k_i\,j_i} = 2j_i$ ($j_i - k_i > 0$ and $j_i + k_i$ – odd, $j_i,\ k_i = \overline{1,\ n_i}$, $i = 1, 2$). Here and below, numbering of rows and columns in matrices is started from scratch.

For the second and fourth derivatives of $\mathbf{T_i}(x_i)$ with respect to x_i one can write

$$\frac{\mathrm{d}^j\mathbf{T_i}}{\mathrm{d}x_i^j} = \mathbf{T_i}\mathbf{J_i}^j, \quad j = 2, 4;\ i = 1, 2. \tag{14}$$

Substituting collocation points (12) into equation (8), a system of linear algebraic equations is obtained. Then equations at points $x_i = x_{i,0}$ and $x_i = x_{i,n_i}$ are excluded, and equations corresponding to boundary conditions $\omega^*(\pm1, x_{2,k_2}) = 0$ and $\omega^*(x_{1,k_1}, \pm1) = 0$ are introduced:

$$\mathbf{T_1}(-1) \otimes \mathbf{T_2}(x_{2,k_2})\mathbf{A} = 0, \quad \mathbf{T_1}(1) \otimes \mathbf{T_2}(x_{2,k_2})\mathbf{A} = 0, \quad k_2 = \overline{0,\ n_2}, \tag{15}$$

$$\mathbf{T_1}(x_{1,k_1}) \otimes \mathbf{T_2}(-1)\mathbf{A} = 0, \quad \mathbf{T_1}(x_{1,k_1}) \otimes \mathbf{T_2}(1)\mathbf{A} = 0, \quad k_1 = \overline{1,\ n_1 - 1}. \tag{16}$$

At points $x_i = x_{i,1}$ and $x_i = x_{i,n_i-1}$ equations satisfying conditions $\left.\dfrac{\partial \omega^*}{\partial x_i}\right|_{x_i=\pm 1} = 0$ $(i = 1,\, 2)$ are written

$$\mathbf{T_1}(-1)\mathbf{J_1} \otimes \mathbf{T_2}(x_{2,k_2})\mathbf{A} = 0, \quad \mathbf{T_1}(1)\mathbf{J_1} \otimes \mathbf{T_2}(x_{2,k_2})\mathbf{A} = 0, \quad k_2 = \overline{0,\, n_2}, \tag{17}$$

$$\mathbf{T_1}(x_{1,k_1}) \otimes (\mathbf{T_2}(-1)\mathbf{J_2})\,\mathbf{A} = 0, \quad \mathbf{T_1}(x_{1,k_1}) \otimes (\mathbf{T_2}(1)\mathbf{J_2})\,\mathbf{A} = 0, \quad k_1 = \overline{1,\, n_1 - 1}. \tag{18}$$

As a result, using (11), (14)-(18), one can obtain

$$\mathbf{BA} = \mathbf{F}, \quad \mathbf{B} = \sum_{m=1}^{5} \mathbf{B_m}, \tag{19}$$

where $\mathbf{F} = (f_{00}\, f_{01}\, \ldots\, f_{n_1\, n_2})^T$ with elements $f_{k_1\, k_2} = q^*(x_{1,k_1}, x_{2,k_2})$, $(k_i = \overline{2,\, n_i - 2},\, i = 1, 2)$, square matrices $\mathbf{B_m}$ $(m = \overline{1,5})$ of size $n_1' n_2' \times n_1' n_2'$ defined as

$$\mathbf{B_1} = \kappa_1 \mathbf{G_1''}\mathbf{J_1}^4 \otimes \mathbf{G_2''}, \quad \mathbf{B_2} = \kappa_2 \mathbf{G_1''}\mathbf{J_1}^2 \otimes \left(\mathbf{G_2''}\mathbf{J_2}^2\right), \quad \mathbf{B_3} = \kappa_3 \mathbf{G_1''} \otimes \left(\mathbf{G_2''}\mathbf{J_2}^4\right)$$

$$\mathbf{B_4} = \mathbf{G_3} \otimes \mathbf{G_2} + \mathbf{G_1''} \otimes \mathbf{G_4}, \quad \mathbf{B_5} = \kappa_4 \mathbf{G_5}\mathbf{J_1} \otimes \mathbf{G_2} + \kappa_5 \mathbf{G_1''} \otimes (\mathbf{G_6}\mathbf{J_2})\,.$$

Here $\mathbf{G_i}$, $\mathbf{G"_i}$, $\mathbf{G_{3+i}}$ and $\mathbf{G_{4+i}}$ are square matrices with sizes $n_i' \times n_i'$ $(i = 1, 2)$:

$$\mathbf{G_i} = \begin{bmatrix} \mathbf{T_i}(x_{i,0}) \\ \mathbf{T_i}(x_{i,1}) \\ \mathbf{T_i}(x_{i,2}) \\ \ldots \\ \mathbf{T_i}(x_{i,n_i-2}) \\ \mathbf{T_i}(x_{i,n_i-1}) \\ \mathbf{T_i}(x_{i,n_i}) \end{bmatrix}, \; \mathbf{G_i''} = \begin{bmatrix} \mathbf{0} \\ \mathbf{0} \\ \mathbf{T_i}(x_{i,2}) \\ \ldots \\ \mathbf{T_i}(x_{i,n_i-2}) \\ \mathbf{0} \\ \mathbf{0} \end{bmatrix}, \; \mathbf{G_{2+i}} = \begin{bmatrix} \mathbf{T_i}(-1) \\ \mathbf{0} \\ \mathbf{0} \\ \ldots \\ \mathbf{0} \\ \mathbf{0} \\ \mathbf{T_i}(1) \end{bmatrix}, \; \mathbf{G_{4+i}} = \begin{bmatrix} \mathbf{0} \\ \mathbf{T_i}(-1) \\ \mathbf{0} \\ \ldots \\ \mathbf{0} \\ \mathbf{T_i}(1) \\ \mathbf{0} \end{bmatrix}.$$

To find values $\mathbf{T_i}(-1)$ and $\mathbf{T_i}(1)$ relations $T_{i,j_i}(-1) = (-1)^{j_i}$, $T_{i,j_i}(1) = 1$, $(j_i = \overline{0,\, n_i},\, i = 1, 2)$ are used citebibGer3.

The elements of matrix $\mathbf{A}$ are obtained from equation (19). Function ω^* is restored the using (11).

3. Constructing a solution of boundary value problem using Legendre polynomials

Let us represent function ω^* as a finite sum of a double Legendre series:

$$\omega^*(x_1, x_2) = \sum_{\substack{k_i=0 \\ i=1,2}}^{n_i} a_{k_1 k_2} P_{k_1}(x_1) P_{k_2}(x_2) = \mathbf{P_1}(x_1) \otimes \mathbf{P_2}(x_2)\mathbf{A}, \tag{20}$$

where $\mathbf{P_i}(x_i) = (P_0(x_i)\, P_1(x_i) \ldots P_{n_i-1}(x_i)\, P_{n_i}(x_i))$ $(i = 1, 2)$, and Legendre polynomials $P_{j_i}(x_i)$ are defined as follows

$$P_0(x_i) = 1, \quad P_1(x_i) = x_i, \quad (j_i + 1)P_{j_i+1}(x_i) = (2j_i + 1)x_i P_{j_i}(x_i) - j_i P_{j_i-1}(x_i), \quad j \geqslant 1.$$

As collocation points x_{i,k_i} for x_i in equation (8) the roots of polynomial P_{n_i+1} $(i = 1, 2)$ are used. According to [22], these roots x_{i,k_i} are eigenvalues of a symmetric matrix $\mathbf{L_i}$ of size

$n_i' \times n_i'$ with nonzero elements $L_{i,k_i+1\,k_i} = L_{i,k_i\,k_i+1} = (k_i+1)/\sqrt{4(k_i+1)^2-1}$ $(k_i = \overline{0,\, n_i-1}$, $i = 1,2)$. Moreover, if n_i is odd then $x_{i,m_i} = -x_{i,n_i-m_i}$ and $P_{j_i}(x_{i,m_i}) = (-1)^{j_i} P_{j_i}(x_{i,n_i-m_i})$, $(m_i = \overline{0,\, (n_i-1)/2}$; $j_i = \overline{0,\, n_i}$; $i = 1,2)$. If n_i is even then $x_{i,n_i/2} = 0$, $x_{i,m_i} = -x_{i,n_i-m_i}$ and $P_{j_i}(x_{i,m_i}) = (-1)^{j_i} P_{j_i}(x_{i,n_i-m_i})$, $(m_i = \overline{0,\, n_i/2-1}$; $j_i = \overline{0,\, n_i}$; $i = 1,2)$. The value $P_{j_i}(0)$ is found using the following representation [22]

$$P_{j_i}(x_i) = \sum_{k=0}^{[j_i/2]} \varsigma_k x_i^{j_i-2k}, \quad \varsigma_k = \frac{(-1)^k (2j_i-2k)!}{2^{j_i}(j_i-2k)!(j_i-k)!k!}.$$

Thus, if j_i is even then

$$P_{j_i}(0) = \varsigma_{j_i/2} = \frac{(-1)^{j_i/2} j_i!}{2^{j_i}\left(\dfrac{j_i}{2}\right)!^2},$$

otherwise, $P_{j_i}(0) = 0$ $(i = 1,2)$.

The derivative of $\mathbf{P_i}(x_i)$ with respect to x_i is represented as a product of $\mathbf{P_i J_i}$ using [22]

$$\frac{\mathrm{d}P_{j_i}}{\mathrm{d}x_i} = \sum_{\substack{k_i=0 \\ j_i+k_i-\text{nech.}}}^{j_i-1} (2k_i+1) P_{k_i}(x_i), \quad j_i \geqslant 1,$$

where $\mathbf{J_i}$ is an upper-triangular matrix of size $n_i' \times n_i'$ with nonzero elements $J_{i,k_i\,j_i} = 2k_i + 1$ $(j_i - k_i > 0$ and $j_i + k_i$ – odd, $j_i,\, k_i = \overline{0,\, n_i}$, $i = 1,2$ For the second and fourth derivatives of $\mathbf{P_i}(x_i)$ with respect to x_i one can write

$$\frac{\mathrm{d^j}\mathbf{P_i}}{\mathrm{d}x_i^j} = \mathbf{P_i J_i}^j, \quad j = 2,4;\ i = 1,2. \tag{21}$$

Using the selected collocation points for equation (8), equalities (20) and (21)and taking into account boundary conditions (9) and (10), system of equations (19) is obtained, where matrices $\mathbf{G_i}$, $\mathbf{G"_i}$, $\mathbf{G_{3+i}}$, $\mathbf{G_{4+i}}$ and $\mathbf{G"_i}$ are defined by $\mathbf{P_i}$ $(i = 1,2)$. In this case, the values $\mathbf{P_i}(-1)$ and $\mathbf{P_i}(1)$ are found using as follows $P_{i,j_i}(-1) = (-1)^{j_i}$, $P_{i,j_i}(1) = 1$, $(j_i = \overline{0,\, n_i}$, $i = 1,2)$. Restoring elements of matrix $\mathbf{A}$ from (19), one can obtain function $(\omega^*(x_1,x_2)$ from (20).

4. Numerical results and their analysis

As an example, let us consider the problem of bending of a rectangular orthotropic plate under the action of a transverse load which is defined as

$$q^*(x^*,y^*) = \cos(\pi(2x^*-1))\left(1+\cos\left(\pi\left(\frac{2y^*}{d_2^*}-1\right)\right)\right) + \\ + \cos\left(\pi\left(\frac{2y^*}{d_2^*}-1\right)\right)\left(\frac{2H}{D_x d_2^{*2}}\cos(\pi(2x^*-1)) + \frac{\nu_2}{\nu_1 d_2^{*4}}(1+\cos(\pi(2x^*-1)))\right). \tag{22}$$

In this case, the analytical solution of boundary value problem (5)–(7) has the form

$$\omega_a^*(x^*,y^*) = \frac{1}{16\pi^4}(1+\cos(\pi(2x^*-1)))\left(1+\cos\left(\pi\left(\frac{2y^*}{d_2^*}-1\right)\right)\right). \tag{23}$$

The values of the physical parameters from [1] and [18] are used in calculations: $E_x' = 131 \cdot 10^7$ kg/m^2, $E_y' = 42 \cdot 10^7$ kg/m^2, $E' = 5.1 \cdot 10^7$ kg/m^2, $G = 11.1 \cdot 10^7$ kg/m^2. Deviations of constructed solutions (11) and (20) from analytical solution (23) are found by the infinite norm [14]:

$$\|\omega^* - \omega_a^*\|_\infty = \max_{(x^*,y^*)\in\Omega} |\omega^*(x^*,y^*) - \omega_a^*(x^*,y^*)|, \tag{24}$$

where $\Omega = [0,\,1] \times [0,\,d_2^*]$, and the finite norm in the space of square integrable functions [14] and [15]:

$$\|\omega^* - \omega_a^*\|_2 = \left(\int_0^1 \int_0^{d_2^*} (\omega^*(x^*,y^*) - \omega_a^*(x^*,y^*))^2 \mathrm{d}x^* \mathrm{d}y^*\right)^{1/2}. \tag{25}$$

Evaluation of expression (24) is carried out in term of the infinite norm of the difference between vectors $\mathbf{W}$ and $\mathbf{W_a}$ with elements equal to the values of functions ω^* and ω_a^* at uniformly distributed points $(x_{k_1}^*, y_{k_2}^*)$ from Ω domain:

$$e_\infty = \|\mathbf{W} - \mathbf{W_a}\|_\infty = \max_{\substack{0\leqslant k_i\leqslant m_i\\ i=1,2}} |\omega^*(x_{k_1}^*, y_{k_2}^*) - \omega_a^*(x_{k_1}^*, y_{k_2}^*)|,$$

where $\mathbf{W} = (w_{00}\, w_{01}\, \dots\, w_{m_1\, m_2})^T$, $w_{k_1 k_2} = \omega^*(x_{k_1}^*, y_{k_2}^*)$, $\mathbf{W_a} = (w_{a,00}\, w_{a,01}\, \dots\, w_{a,m_1\, m_2})^T$ and $w_{a,k_1 k_2} = \omega_a^*(x_{k_1}^*, y_{k_2}^*)$ $(k_i = \overline{0, m_i},\ i = 1,2)$. The obtained values of the deviation estimate for the infinite norm e_∞ are presented in the Tab. 1 for $n_1 = n_2 = n$ and $m_1 = m_2 = 100$ for $d_2^* = \dfrac{d_2}{d_1}$ from [2,3] and [23]. The notation $e_{T,\infty}$ is used in the case of Chebyshev polynomials, and notation $e_{P,\infty}$ is used for Legendre polynomials. The degree of 10 is indicated in parentheses. For values d_2^* shown in Tab. 1 the maximum deflection value in the center of the plate is $0.002566496\ 10^{-9}$. The third and sixth columns of this table present estimates of the deviations of solutions (11) and (20) between successive iterations of $n-1$ and n according to the infinite norm

$$e_{n,\infty} = \max_{\substack{0\leqslant k_i\leqslant m_i\\ i=1,2}} |\omega_n^*(x_{k_1}^*, y_{k_2}^*) - \omega_{n-1}^*(x_{k_1}^*, y_{k_2}^*)|,$$

where $m_1 = m_2 =$100. The fourth column of Tab. 1 contains the values of the infinite norm $\tilde{e}_{T,\infty}$ of the difference between $\mathbf{W_a}$ and the vector with elements obtained as a result of interpolation of function (23) by Chebyshev polynomials. The corresponding values of the norm $\tilde{e}_{P,\infty}$ in the case of Legendre polynomials are given in the seventh column of this table. It can be seen from the results presented in Tab. 1 that solutions obtained using Legendre and Chebyshev polynomials of the first kind coincide with the analytical solution with high accuracy (23) for relatively small values of n. The obtained values of deviation for the infinite norm $e_{T,\infty}$ and $e_{P,\infty}$ of these solutions approach the corresponding values of deviation norms $\tilde{e}_{T,\infty}$ and $\tilde{e}_{P,\infty}$ for polynomial interpolations of function (23). It indicates good approximation properties of the method. The values of $e_{T,n,\infty}$ and $e_{P,n,\infty}$ can be used as an estimate of the error of the constructed solutions.

To discretize norm (25), integrand function $(\omega^*(x^*,y^*) - \omega_a^*(x^*,y^*))^2$ is represented the in the form of a partial sum of a double series according to Chebyshev polynomials

$$(\omega^*(x_1,x_2) - \omega_a^*(x_1,x_2))^2 = \sum_{\substack{k_i=0\\ i=1,2}}^{q_i} a_{q,k_1k_2} T_{k_1}(x_1) T_{k_2}(x_2) = \mathbf{T_{1,q}}(x_1) \otimes \mathbf{T_{2,q}}(x_2) \mathbf{A_q}, \tag{26}$$

where $\mathbf{T_{q,i}}(x_i) = (T_0(x_i)\, T_1(x_i) \dots T_{q_i-1}(x_i)\, T_{q_i}(x_i))$. Matrix elements $\mathbf{A_q} = (a_{q,00}\, a_{q,01} \dots a_{q,q_1q_2-1}\, a_{q_1q_2})^T$ are determined using roots x_{i,k_i} of polynomials T_{q_i+1} $(i = 1,2)$:

$$\mathbf{A} = \mathbf{G_{1,q}}^{-1} \otimes \mathbf{G_{2,q}}^{-1} \mathbf{S_q}, \tag{27}$$

Table 1. Values of deviations in term of the infinite norm e_∞, $e_{n,\infty}$ and $\tilde{e}_\infty$ versus n for $q^*(x^*, y^*)$ given in (22)

n	$e_{T,\infty}$	$e_{T,n,\infty}$	$\tilde{e}_{T,\infty}$	$e_{P,\infty}$	$e_{P,n,\infty}$	$\tilde{e}_{P,\infty}$
$d_2^* = 0.5$						
9	5.5(−6)	7.2(-6)	1.1(−7)	8.1(−6)	9.1(−6)	1.4(−7)
12	7.9(−9)	1.8(−8)	2.7(−11)	1.3(−8)	2.9(−7)	8.9(−11)
15	5.2(−11)	6.2(−11)	3.0(−13)	9.5(−11)	1.1(−10)	5.1(−13)
18	1.0(−14)	5.7(−13)	2.7(−17)	2.0(−14)	1.1(−12)	6.1(−17)
$d_2^* = 1.0$						
9	5.4(−6)	7.1(−6)	1.1(−7)	7.9(−6)	8.9(−6)	1.4(−7)
12	7.8(−9)	1.8(−8)	2.7(−11)	1.3(−8)	2.9(−7)	8.9(−11)
15	5.1(−11)	6.1(−11)	3.0(−13)	9.3(−11)	1.0(−10)	5.1(−13)
18	1.0(−14)	5.6(−13)	2.7(−17)	2.0(−14)	1.1(−12)	6.1(−17)
$d_2^* = 1.5$						
9	5.8(−6)	7.7(−6)	1.1(−7)	8.6(−6)	9.6(−6)	1.4(−7)
12	8.4(−9)	1.9(−7)	2.7(−11)	1.4(-8)	3.1(-7)	8.9(-11)
15	5.5(−11)	6.5(−11)	3.0(−13)	1.0(−10)	1.1(−10)	5.1(−13)
18	1.0(−14)	6.0(−13)	3.1(−17)	2.2(−14)	1.2(−12)	6.1(−17)

where $\mathbf{S_q} = (s_{00}\, s_{01}\, \dots\, s_{q_1\, q_2})^T$ with elements: $s_{k_1\, k_2} = (\omega^*(x_{1,k_1}, x_{2,k_2}) - \omega_a^*(x_{1,k_1}, x_{2,k_2}))^2$, ($k_i = \overline{0,\, q_i}$, $i = 1, 2$), square matrix $\mathbf{G_{i,q}}$ has size $(q_i + 1) \times (q_i + 1)$ and it is defined similarly to $\mathbf{G_i}$ ($i = 1, 2$). The inverse to $\mathbf{G_{i,q}}$ matrix $\mathbf{G_{i,q}}^{-1}$ is obtained by transposing $\mathbf{G_{i,q}}$ then multiplying $\mathbf{G_{i,q}}^T$ by $2/(q_i + 1)$ and dividing elements of the first row of this matrix by 2 ($i = 1, 2$). It follows from the equality [20]

$$\frac{2}{q_i + 1} \sum_{k_i=0}^{q_i} T_{j_1}(x_{i,k_i}) T_{j_2}(x_{i,k_i}) = \gamma_{T,j_1} \delta_{j_1,j_2},$$

where δ_{j_1,j_2} is the Kronecker symbol, $\gamma_{T,0} = 2$, $\gamma_{T,j_1} = 1$ ($j_1 > 0$, $i = 1, 2$).

Using representation (26), one can obtain for the double integral in (25)

$$e_2^2 = \int_0^1 \int_0^{d_2^*} (\omega^*(x^*, y^*) - \omega_a^*(x^*, y^*))^2 \mathrm{d}x^* \mathrm{d}y^* = \frac{d_2^*}{4} \int_{-1}^1 \int_{-1}^1 (\omega^*(x_1, x_2) - \omega_a^*(x_1, x_2))^2 \mathrm{d}x_1 \mathrm{d}x_2 =$$

$$= \frac{d_2^*}{4} \int_{-1}^1 \mathbf{T_{1,q}}(x_1) \mathrm{d}x_1 \otimes \int_{-1}^1 \mathbf{T_{2,q}}(x_2) \mathrm{d}x_2 \mathbf{A_q}. \quad (28)$$

According to [20], there is the following relation for $j_i = 0$ and even j_i

$$\int_{-1}^1 T_{j_i}(x_i) \mathrm{d}x_i = \frac{2}{1 - j_i^2}, \quad j_i \geqslant 0,\ i = 1, 2,$$

otherwise, the value of the integral is zero.

Then

$$\int_{-1}^1 \mathbf{T_{i,q}}(x_i) \mathrm{d}x_i = \mathbf{R_i}, \quad (29)$$

where $\mathbf{R_i}$ is a matrix of size $1 \times (q_i + 1)$ with elements $R_{i,0\, j_i} = 2/(1 - j_i^2)$ (j_i — even, $j_i = \overline{0,\, q_i}$, $i = 1, 2$).

Substituting (27) and (29) into (28), one can obtain

$$e_2^2 = \frac{d_2^*}{4}\mathbf{R_1} \otimes \mathbf{R_i}\left(\mathbf{G_{1,q}}^{-1} \otimes \mathbf{G_{2,q}}^{-1}\mathbf{S_q}\right). \tag{30}$$

The Tab. 2 shows the values of deviations $e_{T,2}$ and $e_{P,2}$ of constructed solutions (11) and (20) from the analytical solution of problem (23) in term of the norm (25) based on (30) at $q_1 = q_2 = 10$. The degree of 10 is indicated in parentheses.

Table 2. Values of deviations in term of the integral norm e_2, $e_{n,2}$ and $\tilde{e}_2$ versus n for $q^*(x^*, y^*)$ given in (22)

n	$e_{T,2}$	$e_{T,n,2}$	$\tilde{e}_{T,2}$	$e_{P,2}$	$e_{P,n,2}$	$\tilde{e}_{P,2}$
$d_2^* = 0.5$						
9	2.0(–6)	2.5(–6)	2.6(–8)	3.1(–6)	2.8(–6)	2.5(–8)
12	2.9(–9)	6.6(–8)	8.2(–12)	4.7(–9)	1.0(–7)	6.3(–12)
15	1.9(–11)	2.3(–11)	6.4(–14)	3.4(–11)	3.8(–11)	5.4(–14)
18	3.8(–15)	2.1(-13)	7.6(-18)	7.5(–15)	4.1(–13)	8.2(–18)
$d_2^* = 1.0$						
9	2.8(–6)	3.5(–6)	3.7(–8)	4.1(–6)	4.4(–6)	3.6(–8)
12	4.1(–9)	9.2(–8)	1.1(–11)	6.6(–9)	1.5(–7)	8.9(–12)
15	2.7(–11)	6.2(–11)	9.0(–14)	4.9(–11)	5.4(–11)	7.6(–14)
18	5.3(–15)	3.0(–13)	1.1(–17)	1.1(–14)	5.8(–13)	1.1(–17)
$d_2^* = 1.5$						
9	3.5(–6)	4.4(–6)	4.5(–8)	5.1(–6)	5.5(–6)	4.4(–8)
12	5.0(–9)	1.1(–7)	1.4(–11)	8.2(–9)	1.8(–7)	1.1(–11)
15	3.3(–11)	4.0(–11)	1.1(–13)	6.1(–11)	6.7(–11)	9.3(–14)
18	6.7(–15)	3.7(–13)	1.5(–17)	1.3(–14)	7.1(–13)	1.5(–17)

Verification of the obtained values of $e_{T,2}$ and $e_{P,2}$ was carried out using algorithm from [17] in the Maple computer algebra system. The third and sixth columns of Tab. 2 show the values of deviations of obtained solutions (11) and (20) between successive iterations of $n-1$ and n in term of the integral norm calculated similarly to (30). The fourth column of this table shows the values of norm $\tilde{e}_{T,2}$ in the case of interpolation of function (23) by Chebyshev polynomials. The corresponding values of norm $\tilde{e}_{P,2}$ when using Legendre polynomials are given in the seventh column of this table.

Tables 3 and 4 show the values of $\omega^*(x^*, y^*)$ in the center of the plate, as well as the norms $e_{n,\infty}$ and $e_{n,2}$ versus n for $q^*(x^*, y^*) = 1$ and $q^*(x^*, y^*) = x^*$, respectively. For the square orthotropic plate ($d_2^* = 1$) under the action of a load with dimensionless intensity $q^*(x^*, y^*) = 1$, comparison with the results obtained in [1] is presented. The maximum bending value in the center of the plate $\omega^*(x^*, y^*)$ is equal to 0.00225757 for $n = 12$, and the value of 0.002257679 is reached for $n = 44$, where n is the number of members of the exponential series [1]. The results presented in Tables 1–4 show that solutions obtained using Legendre and Chebyshev polynomials of the first kind have sufficiently fast convergence, and the obtained norm estimates can be used as an estimate of the error of the constructed solutions in the corresponding function spaces.

Conclusion

Solution of the bending problem of a thin orthotropic rectangular plate clamped along the contour is constructed using the collocation method in the matrix implementation. Chebyshev

Table 3. Values of $\omega^*(x^*, y^*)$ in the center of the plate and the norms $e_{n,\infty}$ and $e_{n,2}$ versus n for $q^*(x^*, y^*) = 1$

n	$\omega_T^*\left(\frac{1}{2}, \frac{d_2^*}{2}\right)$	$e_{T,n,\infty}$	$\omega_P^*\left(\frac{1}{2}, \frac{d_2^*}{2}\right)$	$e_{P,n,\infty}$	$e_{T,n,2}$	$e_{P,n,2}$
$d_2^* = 0.5$						
9	0.000485168	6.4(–7)	0.000485279	7.2(–7)	1.9(–7)	2.2(–7)
12	0.000484932	4.2(–8)	0.000484931	5.5(–8)	1.1(–8)	1.5(–8)
15	0.000484933	2.1(–9)	0.000484933	2.7(–9)	2.7(–10)	3.6(–10)
18	0.000484933	8.2(-10)	0.000484933	1.1(–9)	6.6(–11)	1.1(–10)
$d_2^* = 1$						
9	0.002258721	1.8(–6)	0.002259184	2.1(–6)	8.5(–7)	9.9(–7)
12	0.002257672	1.5(–7)	0.002257670	2.1(–7)	4.7(–8)	6.6(–8)
15	0.002257679	6.7(–9)	0.002257678	8.2(–9)	1.1(–9)	1.4(–9)
18	0.002257679	2.7(–9)	0.002257679	3.5(–9)	2.8(–10)	4.0(–10)
$d_2^* = 1.5$						
9	0.002710060	7.4(–6)	0.002710432	7.5(–6)	3.0(–6)	3.1(–6)
12	0.002709799	1.2(–6)	0.002709800	1.9(–6)	5.4(–7)	8.1(–7)
15	0.002709801	4.6(–8)	0.002709801	6.3(–8)	1.3(–8)	1.8(–8)
18	0.002709802	1.3(–8)	0.002709803	1.9(–8)	2.7(–9)	4.3(–9)

Table 4. Values of $\omega^*(x^*, y^*)$ in the center of the plate and the norms $e_{n,\infty}$ and $e_{n,2}$ versus n for $q^*(x^*, y^*) = x^*$

n	$\omega_T^*\left(\frac{1}{2}, \frac{d_2^*}{2}\right)$	$e_{T,n,\infty}$	$\omega_P^*\left(\frac{1}{2}, \frac{d_2^*}{2}\right)$	$e_{P,n,\infty}$	$e_{T,n,2}$	$e_{P,n,2}$
$d_2^* = 0.5$						
9	0.000242584	6.0(–7)	0.000242640	6.6(–7)	1.1(–7)	1.3(–7)
12	0.000242466	3.4(–8)	0.000242466	4.3(–8)	5.7(–9)	8.1(–9)
15	0.000242466	3.6(–9)	0.000242466	5.1(–9)	4.5(-10)	6.8(–10)
18	0.000242466	6.1(-10)	0.000242466	8.5(–10)	4.2(–11)	6.6(–11)
$d_2^* = 1$						
9	0.001129361	9.1(-7)	0.001129592	1.1(–6)	4.4(–7)	5.1(–7)
12	0.001128836	1.5(–7)	0.001128835	2.1(–7)	3.6(–8)	5.2(–8)
15	0.001128839	8.9(–9)	0.001128839	1.2(–8)	1.2(-9)	1.7(-9)
18	0.001128840	2.2(–9)	0.001128840	3.2(–9)	2.9(–10)	4.7(–10)
$d_2^* = 1.5$						
9	0.001355030	4.1(–6)	0.001355215	4.2(–6)	1.7(–6)	1.7(–6)
12	0.001354899	7.8(–7)	0.001354900	1.1(–6)	2.9(–7)	4.2(–7)
15	0.001354901	5.0(–8)	0.001354900	6.6(–8)	9.3(–9)	1.3(–8)
18	0.001354901	1.5(–8)	0.001354901	2.3(–8)	2.5(–9)	4.1(–9)

polynomials of the first kind and Legendre polynomials are used as the basic system of functions. The results of modeling the bending of the median plane of the plate under consideration for various ratios of the lengths of the sides of the plate and types of transverse load using the roots of the Chebyshev and Legendre polynomials are presented. It is shown that the constructed solution of the boundary value problem converges quickly enough to the analytical solution given in the work. Estimates of the errors of the constructed solutions for the infinite norm and the finite norm in the space of functions integrable with the square are obtained.

The research was carried out at the expense of a grant from the Russian Science Foundation, project no. 24-21-00381.

References

[1] D.P.Goloskokov, A.V.Matroso, Method of initial functions in analyses of the bending of a thin orthotropic plate clamped along the contour, *Vestnik of Saint Petersburg University. Applied Mathematics. Computer Science. Control Processes*, **17**(2021), no. 4, 330–344 (in Russian). DOI: 10.21638/11701/spbu10.2021.402

[2] R.Li, Y.Zhong, B.Tian, Y.Liu, On the finite integral transform method for exact bending solutions of fully clamped orthotropic rectangular thin plates, *Applied Mathematics Letters*, **22**(2009), 1821–1827. DOI: 10.1016/j.aml.2009.07.003

[3] V.R.Lakshmi Gorty, N.Gupt, Bending of fully clamped orthotropic rectangular thin plates using finite continuous ridgelet transform, *Materials Today: Proceedings*, **47**(2021), 4199–4205. DOI: 10.1016/j.matpr.2021.04.458

[4] Q.Xu, Z.Yang, S.Ullah, Z.Jinghui, Y.Gao, Analytical bending solutions of orthotropic rectangular thin plates with two adjacent edges free and the others clamped or simply supported using finite integral transform method, *Advances in Civil Engineering*, (2020), no. 8848879, 1–11. DOI: 10.1155/2020/8848879

[5] S.K.Golushko, S.V.Idimeshev, V.P.Shapeyev, Razrabotka i primeneniye metoda kollokatsiy i naimen'shikh nevyazok dlya resheniya zadach mekhaniki anizotropnykh sloyev plastin, *Vychislitel'nyye tekhnologii*, **19**(2014), no. 5, 24–36 (in Russian).

[6] P.Lazarev, G.M.Semenova, N.A.Romanova, On a Limiting Passage as the Thickness of a Rigid Inclusions in an Equilibrium Problem for a Kirchhoff-Love Plate with a Crack, *J. Sib. Fed. Univ. Math. Phys.*, **14**(2021), no 1, 28–41. DOI: 10.17516/1997-1397-2021-14-1-1-14

[7] O.Ghorbel, J.B.Casimir, L.Hammami, I.Tawfiq, M.Haddar, In-plane dynamic stiffness matrix for a free orthotropic plate, *Journal of Sound and Vibration*, **364**(2016), 234–246. DOI: 10.1016/j.jsv.2015.11.028

[8] A.Deutsch, M.Eisenberger Benchmark analytic in-plane vibration frequencies of orthotropic rectangular plates, *Journal of Sound and Vibration*, **541**(2022), 117248. DOI: 10.1016/j.jsv.2022.117248

[9] I.V.Shcherbakov, B.A.Lyukshin, Modelirovaniye povedeniya otklika ortotropnoy plastiny pri vozdeystvii dinamicheskoy nagruzki, *Vestnik Tomskogo gosudarstvennogo universiteta. Matematika i mekhanika*, **61**(2019), 111–118. (in Russian). DOI: 10.17223/19988621/61/10

[10] S.Zhang, L.Xu, Bending of rectangular orthotropic thin plates with rotationally restrained edges: A finite integral transform solution, *Applied Mathematical Modelling*, **46**(2017), 48–62. DOI: 10.1016/j.apm.2017.01.053.

[11] S.V.Sheshenin, R.R.Muradkhanov, Asimptoticheskoye issledovaniye izgiba plastiny dlya sil'no ortotropnogo materiala, *Izvestiya Rossiyskoy akademii nauk. Mekhanika tverdogo tela*, **3**(2023), 36–57 (in Russian). DOI: 10.31857/S0572329922600608

[12] O.V.Germider, V.N.Popov, On the calculation of the Poiseuille number in the annular region for non-isothermal gas flow, *Journal of Siberian Federal University Mathematics and Physics*, **16**(2023), no. 3, 330–339. EDN: NHSPJB

[13] X.Hu, Z.Wang, B.Hu, A collocation method based on roots of chebyshev polynomial for solving Volterra integral equations of the second kind, *Applied Mathematics Letters*, **29**(2023), no. 108804. DOI: 10.1016/j.aml.2023.108804

[14] E.Kosov, V.Temlyakov, Sampling discretization of the uniform norm and applications, *J. Math. Anal. Appl.*, (2024), no. 128431. DOI: 10.1016/j.jmaa.2024.128431

[15] S.I.Novikov, Ob odnoy zadache interpolyatsii so znachitel'nym znacheniyem L_2-normy operatora Laplasa, *Tr. IMM UrO RAN*, **28**(2022), no. 4, 143–153 (in Russian). DOI: 10.21538/0134-4889-2022-28-4-143-153

[16] V.N.Temlyakov, Diskretizatsiya integral'nykh norm polinomov s garmonikami iz giperbolicheskogo kresta po znacheniyam v tochkakh, *Trudy MIAN*, **312**(2021), 282–293 (in Russian). DOI: 10.4213/tm4133

[17] J.Berntsen, T.O.Espelid, A.Genz, Algorithm 698: DCUHRE: an adaptive multidemensional integration routine for a vector of integrals, *ACM Trans. Math. Softw*, **17**(1991), no 4, 452–456. DOI: 10.1145/210232.210234

[18] S.P.Timoshenko, S.Woinowsky-Kriege, Theory of plates and shells, New York, McGraw-Hill, 1959.

[19] E.Ventsel, Th.Krauthammer, Thin Plates and Shells. Theory: Analysis and Applications, Boca Raton, CRC Press, 2001.

[20] J.Mason, D.Handscomb, Chebyshev polynomials, Florida. CRC Press, 2003.

[21] S.Liu, G.Trenkler, Hadamard, Khatri-Rao, Kronecker and other matrix products, *International Journal of Information and Systems Sciences*, **4**(2008), no. 1, 160–177.

[22] J.Shen, T.Tang, L.Wang, Spectral Methods, Berlin, Springer Berlin Heidelberg, 2011.

[23] R.W.Laureano, J.L.Mantari, J.Yarasca, A.S.Oktem, J.Monge, X.Zhou, Boundary Discontinuous Fourier analysis of clamped isotropic and cross-ply laminated plates via Unified Formulation, *Composite Structures*, **328**(2024), no. 117736. DOI: 10.1016/j.compstruct.2023.117736

Вычисление изгиба тонкой ортотропной пластины с использованием многочленов Лежандра и Чебышева первого рода

Оксана В. Гермидер
Василий Н. Попов
Северный (Арктический) федеральный университет имени М. В. Ломоносова
Архангельск, Российская Федерация

Аннотация. В работе получено решение задачи об изгибе тонкой ортотропной прямоугольной пластины, защемленной по краям, с использованием многочленов Лежандра и Чебышева первого рода. Функция, аппроксимирующая решение бигармонического уравнения для ортотропной пластины, представлена в виде разложения в двойной ряд по этим многочленам в комбинации с матричными преобразованиями и свойствами многочленов Лежандра и Чебышева. С использованием корней этих многочленов в качестве точек коллокации краевая задача приведена к решению системы линейных алгебраических уравнений относительно коэффициентов в разложении искомой функции по этим многочленам. Представлены результаты вычисления изгиба пластины, обусловленного действием распределенной поперечной нагрузки постоянной интенсивности, нагрузки вида, допускающего аналитическое решение краевой задачи, и с интенсивностью, соответствующей гидростатическому давлению, для различных отношений длин сторон пластины. Полученные значения отклонений построенных решений с использованием многочленов Лежандра и Чебышева от аналитического решения задачи приведены по бесконечной норме и конечной норме в пространстве интегрируемых с квадратом функций.

Ключевые слова: изгиб тонкой ортотропной пластины, метод коллокации, многочлены Чебышева первого рода, многочлены Лежандра.

Journal of Siberian Federal University. Mathematics & Physics 2024, 17(5), 599–608

EDN: HQYJXW
УДК 517

On Generalized Voigt Function and its Associated Properties

Ulfat Ansari[†]
Musharraf Ali[*]
Department of Mathematics, Gandhi Faiz-E-Aam College
Shahjahanpur-242001, India
Affiliated to Mahatma Jyotiba Phule Rohilkhand University
Bareilly-243006, India
Mohd Ghayasuddin[‡]
Department of Mathematics, Integral University
Centre Shahjahanpur-242001, India

Received 10.03.2024, received in revised form 15.04.2024, accepted 26.05.2024

Abstract. In the present manuscript, we aim to present a new type of the generalized Voigt function, and investigate its series representations. By using the series representations of our function, we also point out some generating relations associated with the Kampé de Fériet function, Srivastava's triple hypergeometric series, confluent hypergeometric functions of one and two variables, and generalized hypergeometric function. Furthermore, two interesting recurrence relations of our introduced Voigt function are also indicated.

Keywords: Voigt function, Wright function, Kampé de Fériet function, Srivastava's triple hypergeometric series.

Citation: Ulfat Ansari, Musharraf Ali, Mohd Ghayasuddin, On Generalized Voigt Function and its Associated Properties, J. Sib. Fed. Univ. Math. Phys., 2024, 17(5), 599–608. EDN: HQYJXW.

1. Introduction and preliminaries

The well-known Voigt functions $K(x_1, x_2)$ and $L(x_1, x_2)$ have occurred in a wide variety of problems in physics such as astrophysical spectroscopy, transfer of radiation in heated atmosphere and also in the theory of neutron reactions.

The integral representations of these two functions (due to Reiche [11]) are given as follows:

$$K(x_1, x_2) = \frac{1}{\sqrt{\pi}} \int_0^\infty \exp\left(- x_2 t - \frac{1}{4} t^2 \right) \cos(x_1 t) dt \tag{1.1}$$

and

$$L(x_1, x_2) = \frac{1}{\sqrt{\pi}} \int_0^\infty \exp\left(- x_2 t - \frac{1}{4} t^2 \right) \sin(x_1 t) dt \tag{1.2}$$

$$(x_1 \in \Re; x_2 \in R^+).$$

Afterwards, Srivastava and Miller [13] presented the following interesting extension of these Voigt functions:

$$V_{\mu,\nu}(x_1, x_2) = \sqrt{\frac{x_1}{2}} \int_0^\infty t^\mu \exp\left(- x_2 t - \frac{1}{4} t^2 \right) J_\nu(x_1 t) dt \tag{1.3}$$

[†]ansari.ulfat96@gmail.com http://orcid.org/0009-0006-9977-4285
[*]drmusharrafali@gmail.com http://orcid.org/0000-0001-9791-3217
[‡]ghayas.maths@gmail.com http://orcid.org/0000-0001-8346-4078

$$(x_1, x_2 \in R^+; \Re(\mu+\nu) > -1),$$

where $J_\nu(x_1)$ denotes the familiar Bessel function [12, p.109, eq.(3)].

It is well-known that $J_{-\frac{1}{2}}(x_1) = \sqrt{\frac{2}{\pi x_1}} \cos x_1$ and $J_{\frac{1}{2}}(x_1) = \sqrt{\frac{2}{\pi x_1}} \sin x_1$.

Thus, we have

$$K(x_1, x_2) = V_{\frac{1}{2},-\frac{1}{2}}(x_1, x_2) \text{ and } L(x_1, x_2) = V_{\frac{1}{2},\frac{1}{2}}(x_1, x_2). \tag{1.4}$$

In continuation of this study, Klusch [7] replaced the number $\frac{1}{4}$ before t^2 in (1.3) by a variable to propose the following slightly more generalization of the function in (1.3):

$$\Omega_{\mu,\nu}(x_1, x_2, x_3) = \sqrt{\frac{x_1}{2}} \int_0^\infty t^\mu \exp(-x_2 t - x_3 t^2) J_\nu(x_1 t) dt \tag{1.5}$$

$$(x_1, x_2, x_3 \in R^+; \Re(\mu+\nu) > -1).$$

It is easy to see that

$$\Omega_{\mu,\nu}\left(x_1, x_2, \frac{1}{4}\right) = V_{\mu,\nu}(x_1, x_2). \tag{1.6}$$

Furthermore, various generalizations of the Voigt function have been introduced and investigated by a number of authors (see for details, [15, 3, 9, 4] and the references cited therein).

The classical Wright function $W_{a,b}(x_1)$ is defined by (see [8], see also [6, 10])

$$W_{a,b}(x_1) = \sum_{n \geqslant 0} \frac{1}{\Gamma(b+an)} \frac{(x_1)^n}{n!}, \tag{1.7}$$

$$(b \in \mathbb{C}, a > -1).$$

In 2015, EI-Shahed and Salem [2] introduced the following extension of above Wright function:

$$W_{a,b}^{c,d}(x_1) = \sum_{n \geqslant 0} \frac{(c)_n}{(d)_n \, \Gamma(b+an)} \frac{(x_1)^n}{n!} \tag{1.8}$$

$$(a \in \Re,\ b, c, d \in \mathbb{C}, a > -1, d \neq 0, -1, -2, \cdots, \text{ with } x_1 \in \mathbb{C} \text{ and } |x_1| < 1 \text{ with } a = -1).$$

Clearly, on setting $c = d$ in (1.8), we easily get the function given in (1.7).

Also, we have the following relation between the classical Bessel function and classical Wright function (see [5]):

$$J_\nu(x_1) = \left(\frac{x_1}{2}\right)^\nu W_{1,\nu+1}\left(-\frac{x_1^2}{4}\right)$$

or

$$W_{1,\nu+1}\left(-\frac{x_1^2}{4}\right) = \left(\frac{2}{x_1}\right)^\nu J_\nu(x_1). \tag{1.9}$$

Hence, we can also define here the relation between generalized Wright function and classical Bessel function as follows:

$$W_{1,\nu+1}^{c,c}\left(-\frac{x_1^2}{4}\right) = \left(\frac{2}{x_1}\right)^\nu J_\nu(x_1) \text{ or } W_{1,\nu+1}^{d,d}\left(-\frac{x_1^2}{4}\right) = \left(\frac{2}{x_1}\right)^\nu J_\nu(x_1). \tag{1.10}$$

In this paper, we aim to introduce a new generalization of the Voigt function associated with the generalized Wright function $W_{a,b}^{c,d}(x_1)$ given in (1.8). Also, we investigate several properties of this generalized Voigt function such as series representations, generating relations and recurrence relations.

2. Generalized Voigt function and its series representations

In this section, we introduce a new type of the generalized Voigt function and its series representations by making use of series manipulation and integral transform techniques.

Definition 2.1. *Let $x_1, x_2, x_3 \in R^+$, $a \in \Re$, $b, c, d \in \mathbb{C}$, $a \geqslant 1$, $d \neq 0, -1, -2, \cdots$, and $\Re(\mu+\nu) > -1$. Then the generalized Voigt function $\Upsilon_{\mu,\nu}^{(a,b,c,d)}(x_1, x_2, x_3)$ is defined by*

$$\Upsilon_{\mu,\nu}^{(a,b,c,d)}(x_1, x_2, x_3) = \left(\frac{x_1}{2}\right)^{\nu+\frac{1}{2}} \int_0^\infty t^{\mu+\nu} \exp(-x_2 t - x_3 t^2)\, W_{a,b}^{c,d}\left(-\frac{x_1^2 t^2}{4}\right) dt, \tag{2.1}$$

where $W_{a,b}^{c,d}(z)$ is the generalized Wright function given in (1.8).

Remark 2.2. **(i)** *If we set $a = 1$, $b = \nu + 1$ and $c = d$ in* (2.1)*, and by using* (1.10)*, we easily get*

$$\Upsilon_{\mu,\nu}^{(1,\nu+1,c,c)}(x_1, x_2, x_3) = \Omega_{\mu,\nu}(x_1, x_2, x_3) \text{ or } \Upsilon_{\mu,\nu}^{(1,\nu+1,d,d)}(x_1, x_2, x_3) = \Omega_{\mu,\nu}(x_1, x_2, x_3). \tag{2.2}$$

(ii) *Further, on setting $a = 1$, $b = \nu + 1$, $c = d$ and $x_3 = \dfrac{1}{4}$ in* (2.1)*, and by using* (1.10)*, we find that*

$$\Upsilon_{\mu,\nu}^{(1,\nu+1,c,c)}\left(x_1, x_2, \frac{1}{4}\right) = V_{\mu,\nu}(x_1, x_2) \text{ or } \Upsilon_{\mu,\nu}^{(1,\nu+1,d,d)}\left(x_1, x_2, \frac{1}{4}\right) = V_{\mu,\nu}(x_1, x_2). \tag{2.3}$$

(iii) *It is easy to find from* (2.2) *and* (2.3) *that*

$$\Upsilon_{\frac{1}{2},-\frac{1}{2}}^{\left(1,\frac{1}{2},c,c\right)}\left(x_1, x_2, \frac{1}{4}\right) = K(x_1, x_2) \quad \text{or} \quad \Upsilon_{\frac{1}{2},-\frac{1}{2}}^{\left(1,\frac{1}{2},d,d\right)}\left(x_1, x_2, \frac{1}{4}\right) = K(x_1, x_2), \tag{2.4}$$

and

$$\Upsilon_{\frac{1}{2},\frac{1}{2}}^{\left(1,\frac{3}{2},c,c\right)}\left(x_1, x_2, \frac{1}{4}\right) = L(x_1, x_2) \quad \text{or} \quad \Upsilon_{\frac{1}{2},\frac{1}{2}}^{\left(1,\frac{3}{2},d,d\right)}\left(x_1, x_2, \frac{1}{4}\right) = L(x_1, x_2). \tag{2.5}$$

Theorem 2.3. *Let $x_1, x_2, x_3 \in R^+$; $b, c, d \in \mathbb{C}$, $a(\geqslant 1) \in \Re$, $d \neq 0, -1, -2, \cdots$, and $\Re(\mu+\nu) > -1$. Then the generalized Voigt function in* (2.1) *has the following representation:*

$$\begin{aligned}
&\Upsilon_{\mu,\nu}^{(a,b,c,d)}(x_1, x_2, x_3) = \\
&= \frac{x_1^{\nu+\frac{1}{2}}}{2^{\nu+\frac{3}{2}} x_3^A\, \Gamma(b)} \left\{ \Gamma(A) F_{0:a+1;1}^{1:1;0} \left[\begin{matrix} A: & c; & ; \\ -: & \Delta(a;b),\ d; & \frac{1}{2}; \end{matrix} \; -\frac{x_1^2}{4a^a x_3}, \frac{x_2^2}{4x_3} \right] - \right. \\
&\left. - \frac{x_2}{\sqrt{x_3}} \Gamma\left(A + \frac{1}{2}\right) F_{0:a+1;1}^{1:1;0} \left[\begin{matrix} A + \frac{1}{2}: & c; & -; \\ -: & \Delta(a;b),\ d; & \frac{3}{2}; \end{matrix} \; -\frac{x_1^2}{4a^a x_3}, \frac{x_2^2}{4x_3} \right] \right\},
\end{aligned} \tag{2.6}$$

where $A = \dfrac{\mu+\nu+1}{2}$, $\Delta(a;b)$ abbreviates the array of 'a' parameters $\dfrac{b}{a}, \dfrac{b+1}{a}, \cdots, \dfrac{b+a-1}{a}$, and $F_{g:h;k}^{p:q;r}$ denotes the well-known Kampé de Fériet function (see [14, p.63, eq.(16)]).

Proof. Expressing the exponential function $\exp(-x_2 t)$ and generalized Wright function $W_{a,b}^{c,d}\left(-\frac{x_1^2 t^2}{4}\right)$ in their respective series on the right-hand side of (2.1), and interchanging the order of summations and integration, which is guaranteed under the conditions, we get

$$\Upsilon_{\mu,\nu}^{(a,b,c,d)}(x_1,x_2,x_3) = \\ =\left(\frac{x_1}{2}\right)^{\nu+\frac{1}{2}} \sum_{n\geqslant 0}\sum_{m\geqslant 0} \frac{(c)_n}{(d)_n\ \Gamma(b+an)} \frac{\left(-\frac{x_1^2}{4}\right)^n}{n!} \frac{(-x_2)^m}{m!} \int_0^\infty t^{\mu+\nu+2n+m}\ e^{-x_3 t^2} dt. \tag{2.7}$$

It is easy to see from the Euler's Gamma function that

$$\int_0^\infty t^\lambda\ e^{-x_3 t^2} dt = \frac{1}{2} x_3^{-\left(\frac{\lambda+1}{2}\right)} \Gamma\left(\frac{\lambda+1}{2}\right) \tag{2.8}$$

$$(\Re(x_3) > 0; \Re(\lambda) > -1).$$

Applying (2.8) to the integral in (2.7), we find that

$$\Upsilon_{\mu,\nu}^{(a,b,c,d)}(x_1,x_2,x_3) = \frac{x_1^{\nu+\frac{1}{2}}}{2^{\nu+\frac{3}{2}} x_3^A} \sum_{n\geqslant 0}\sum_{m\geqslant 0} \frac{(c)_n}{(d)_n\ \Gamma(b+an)} \frac{\left(-\frac{x_1^2}{4x_3}\right)^n}{n!} \frac{(-x_2)^m}{m!} \Gamma\left(A+n+\frac{m}{2}\right)(x_3)^{-\frac{m}{2}}.$$

Now separating the m-series into its even and odd terms, and by using the result (see [14])

$$\Gamma(b+an) = \Gamma(b)\ a^{an} \left(\frac{b}{a}\right)_n \left(\frac{b+1}{a}\right)_n \left(\frac{b+2}{a}\right)_n \cdots \left(\frac{b+a-1}{a}\right)_n,$$

we arrive at

$$\Upsilon_{\mu,\nu}^{(a,b,c,d)}(x_1,x_2,x_3) = \frac{x_1^{\nu+\frac{1}{2}}}{2^{\nu+\frac{3}{2}} x_3^A\ \Gamma(b)} \times \\ \times \left\{ \Gamma(A) \sum_{n\geqslant 0}\sum_{m\geqslant 0} \frac{(A)_{n+m}\ (c)_n}{\left(\frac{b}{a}\right)_n \left(\frac{b+1}{a}\right)_n \cdots \left(\frac{b+a-1}{a}\right)_n (d)_n \left(\frac{1}{2}\right)_m} \frac{\left(-\frac{x_1^2}{4a^a x_3}\right)^n}{n!} \frac{\left(\frac{x_2^2}{4x_3}\right)^m}{m!} - \right. \\ \left. - \frac{x_2}{\sqrt{x_3}} \Gamma\left(A+\frac{1}{2}\right) \sum_{n\geqslant 0}\sum_{m\geqslant 0} \frac{\left(A+\frac{1}{2}\right)_{n+m} (c)_n}{\left(\frac{b}{a}\right)_n \left(\frac{b+1}{a}\right)_n \cdots \left(\frac{b+a-1}{a}\right)_n (d)_n \left(\frac{3}{2}\right)_m} \frac{\left(-\frac{x_1^2}{4a^a x_3}\right)^n}{n!} \frac{\left(\frac{x_2^2}{4x_3}\right)^m}{m!} \right\}, \tag{2.9}$$

which, upon using the definition of Kampé de Fériet function [14, p. 63, eq. (16)], yields our claimed representation. □

Theorem 2.4. *Let* q, w, x_3, $x_3 - s - t + \frac{x_1 t}{s} \in R^+$; $b,c,d \in \mathbb{C}$, $a(\geqslant 1) \in \Re$, $d \neq 0,-1,-2,\cdots$, *and* $\Re(\mu+\nu) > -1$. *Then the generalized Voigt function in* (2.1) *with a slightly changed variable has the following representation:*

$$\Upsilon_{\mu,\nu}^{(a,b,c,d)}\left(q,w,x_3-s-t+\frac{x_1 t}{s}\right) = \frac{q^{\nu+\frac{1}{2}}}{2^{\nu+\frac{3}{2}} x_3^A\ \Gamma(b)} \sum_{i=-\infty}^{\infty}\sum_{j=0}^{\infty} \frac{\left(\frac{s}{x_3}\right)^i}{i!} \frac{\left(\frac{t}{x_3}\right)^j}{j!} \left\{ \Gamma(A+i+j) \times \right. \tag{2.10}$$

$$\times F^{(3)}\left[\begin{matrix} A+i+j :: -;\ -;\ - : & c;\ -;\ -j; \\ - :: -;\ -;\ - : & \Delta(a;b),\ d;\ \frac{1}{2};\ i+1; \end{matrix} \ -\frac{q^2}{4a^a x_3}, \frac{w^2}{4x_3}, \frac{x_1}{x_3}\right] - \frac{w}{\sqrt{x_3}} \Gamma\left(A+i+j+\frac{1}{2}\right) \times$$

$$\times F^{(3)}\left[\begin{array}{ccccc} A+i+j+\frac{1}{2} :: -;\ -;\ -: & c;\ -;\ -j; & \\ & & -\frac{q^2}{4a^a x_3},\ \frac{w^2}{4x_3},\ \frac{x_1}{x_3} \\ - \quad :: -;\ -;\ -: & \Delta(a;b),\ d;\ \frac{3}{2};\ i+1; & \end{array}\right]\Bigg\},$$

where $A = \dfrac{\mu+\nu+1}{2}$ *and* $F^{(3)}[x_1,x_2,x_3]$ *denotes the well-known Srivastava's triple hypergeometric series (see [14, p. 69, eq. (39)]).*

Proof. We begin by recalling the following known result given by Srivastava et al. [16, p. 8, eq. (1.3)]:

$$\exp\left(s+t-\frac{x_1 t}{s}\right) = \sum_{i=-\infty}^{\infty}\sum_{j\geqslant 0}\frac{s^i}{i!}\frac{t^j}{j!}\ {}_1F_1[-j;\ i+1;\ x_1], \tag{2.11}$$

where ${}_1F_1[\ \alpha;\ \beta;\ x_1]$ is the confluent hypergeometric function (see [12, p. 123, eq. (1)]).

On replacing s,t and x_1 by $s\eta^2, t\eta^2$ and $x_1\eta^2$, respectively, and multiplying both sides of the resulting identity by $\eta^{\mu+\nu}\ \exp(-w\eta - x_3\eta^2)\ W^{c,d}_{a,b}\left(-\dfrac{q^2\eta^2}{4}\right)$, and integrating both sides of the last resulting identity with respect to η from 0 to ∞, we obtain

$$\begin{aligned}\int_0^\infty \eta^{\mu+\nu}\exp\left[-w\eta-\left(x_3-s-t+\frac{x_1 t}{s}\right)\eta^2\right]\ W^{c,d}_{a,b}\left(-\frac{q^2\eta^2}{4}\right)d\eta = \sum_{i=-\infty}^{\infty}\sum_{j\geqslant 0}\frac{s^i}{i!}\frac{t^j}{j!}\times \\ \times\int_0^\infty \eta^{\mu+\nu+2i+2j}\ \exp(-w\eta-x_3\eta^2)\ W^{c,d}_{a,b}\left(-\frac{q^2\eta^2}{4}\right){}_1F_1[\ -j;\ i+1;\ x_1\eta^2]d\eta.\end{aligned} \tag{2.12}$$

On comparing (2.1) and (2.12), we get

$$\begin{aligned}\Upsilon^{(a,b,c,d)}_{\mu,\nu}\left(q,w,x_3-s-t+\frac{x_1 t}{s}\right) = \left(\frac{q}{2}\right)^{\nu+\frac{1}{2}}\sum_{i=-\infty}^{\infty}\sum_{j\geqslant 0}\frac{s^i}{i!}\frac{t^j}{j!}\times \\ \times\int_0^\infty \eta^{\mu+\nu+2i+2j}\ \exp(-w\eta-x_3\eta^2)\ W^{c,d}_{a,b}\left(-\frac{q^2\eta^2}{4}\right){}_1F_1[\ -j;\ i+1;\ x_1\eta^2]d\eta.\end{aligned} \tag{2.13}$$

Now using the series representations of exponential function $\exp(-w\eta)$ and generalized Wright function $W^{c,d}_{a,b}\left(-\dfrac{q^2\eta^2}{4}\right)$ and then by applying the following known results [1, p. 337, eq. (9)]:

$$\int_0^\infty x_1^{s-1}e^{-\alpha x_1^2}{}_1F_1[a;\ b;\ \beta x_1^2]dx_1 = \frac{1}{2}\ \alpha^{-\frac{s}{2}}\Gamma\left(\frac{s}{2}\right){}_2F_1\left[a,\ \frac{s}{2};\ b;\ \frac{\beta}{\alpha}\right]$$

$$(\Re(s)>0;\Re(\alpha)>\max\{0,\Re(\beta)\}),$$

we arrive at

$$\begin{aligned}\Upsilon^{(a,b,c,d)}_{\mu,\nu}\left(q,w,x_3-s-t+\frac{x_1 t}{s}\right) = \frac{q^{\nu+\frac{1}{2}}}{2^{\nu+\frac{3}{2}}\ x_3^A}\sum_{i=-\infty}^{\infty}\sum_{j\geqslant 0}\frac{\left(\frac{s}{x_3}\right)^i}{i!}\frac{\left(\frac{t}{x_3}\right)^j}{j!}\sum_{k=0}^{\infty}\frac{(-w)^k}{k!}\times \\ \times\sum_{l=0}^{\infty}\frac{(c)_l}{(d)_l\Gamma(b+al)}\frac{\left(-\frac{q^2}{4x_3}\right)^l}{l!}\frac{1}{x_3^{\frac{k}{2}}}\Gamma\left(A+i+j+l+\frac{k}{2}\right){}_2F_1\left[-j,\ A+i+j+l+\frac{k}{2};\ i+1;\frac{x_1}{x_3}\right].\end{aligned} \tag{2.14}$$

Now expanding ${}_2F_1$ in its defining series (see [14, p. 29, eq. (4)]), and separating the resulting series into even and odd terms with respect to the summation index k, and arranging the last resulting multiple series into the Srivastava's triple hypergeometric series $F^{(3)}[x_1,x_2,x_3]$, we arrive at the right-hand side of (2.10). This completes the proof. □

3. Generating relations

Here, by using the results given in the previous section, we derive some interesting generating relations.

Theorem 3.1. *Let $q, w, x_3, x_3 - s - t + \frac{x_1 t}{s} \in R^+$; $b, c, d \in \mathbb{C}$, $a(\geqslant 1) \in \Re$, $d \neq 0, -1, -2, \cdots$, and $\Re(\mu+\nu) > -1$. Then the following generating relation holds true:*

$$\left(\frac{x_3}{Z}\right)^A \left\{\Gamma(A) F^{1:1;0}_{0:a+1;1}\left[\begin{array}{lll} A: & c; & -; \\ -: & \Delta(a;b),\ d; & \frac{1}{2}; \end{array} -\frac{q^2}{4a^a Z}, \frac{w^2}{4Z}\right] - \frac{w}{\sqrt{Z}}\Gamma\left(A+\frac{1}{2}\right) \times \right. \tag{3.1}$$

$$\left. \times F^{1:1;0}_{0:a+1;1}\left[\begin{array}{lll} A+\frac{1}{2}: & c; & -; \\ -: & \Delta(a;b),\ d; & \frac{3}{2}; \end{array} -\frac{q^2}{4a^a Z}, \frac{w^2}{4Z}\right]\right\} = \sum_{i=-\infty}^{\infty}\sum_{j\geqslant 0} \frac{(\frac{s}{x_3})^i}{i!}\frac{(\frac{t}{x_3})^j}{j!} \times$$

$$\times \left\{\Gamma(A+i+j) F^{(3)}\left[\begin{array}{ll} A+i+j :: -;\ -;\ -: & c;\ -;\ -j; \\ - :: -;\ -;\ -: & \Delta(a;b),\ d;\ \frac{1}{2};\ i+1; \end{array} -\frac{q^2}{4a^a x_3}, \frac{w^2}{4x_3}, \frac{x_1}{x_3}\right] - \frac{w}{\sqrt{x_3}} \times \right.$$

$$\left. \times\ \Gamma\left(A+i+j+\frac{1}{2}\right) F^{(3)}\left[\begin{array}{ll} A+i+j+\frac{1}{2} :: -;\ -;\ -: & c;\ -;\ -j; \\ - :: -;\ -;\ -: & \Delta(a;b),\ d;\ \frac{3}{2};\ i+1; \end{array} -\frac{q^2}{4a^a x_3}, \frac{w^2}{4x_3}, \frac{x_1}{x_3}\right]\right\},$$

where $Z = x_3 - s - t + \dfrac{x_1 t}{s}$, $F^{p:q;r}_{g:h;k}$ is the Kampé de Fériet function [14, p. 63, eq. (16)] and $F^{(3)}[x_1, x_2, x_3]$ is the Srivastava's triple hypergeometric series [14, p. 69, eq. (39)].

Proof. Expanding the left-hand side of (2.10) with the aid of (2.6) is seen to prove the result here. □

Corollary 3.2. *Let the conditions of Theorem 3.1 be satisfied. Then the following generating relation holds true:*

$$\left(\frac{x_3}{Z}\right)^A \left\{\Gamma(A)\ {}_1F_1\left[A; \frac{1}{2}; \frac{w^2}{4Z}\right] - \frac{w}{\sqrt{Z}}\Gamma\left(A+\frac{1}{2}\right)\ {}_1F_1\left[A+\frac{1}{2}; \frac{3}{2}; \frac{w^2}{4Z}\right]\right\} =$$

$$= \sum_{i=-\infty}^{\infty}\sum_{j\geqslant 0} \frac{(\frac{s}{x_3})^i}{i!}\frac{(\frac{t}{x_3})^j}{j!}\left\{\Gamma(A+i+j)\ \Psi_1\left[A+i+j,\ -j;\ i+1,\ \frac{1}{2};\ \frac{x_1}{x_3},\ \frac{w^2}{4x_3}\right] - \right. \tag{3.2}$$

$$\left. -\frac{w}{\sqrt{x_3}}\Gamma\left(A+i+j+\frac{1}{2}\right)\ \Psi_1\left[A+i+j+\frac{1}{2},\ -j;\ i+1,\ \frac{3}{2};\ \frac{x_1}{x_3},\ \frac{w^2}{4x_3}\right]\right\},$$

where ${}_1F_1[\alpha;\beta;x_1]$ is the confluent hypergeometric function of one variable [12, p.123, eq.(1)] and $\Psi_1[\alpha,\beta;\gamma,\delta;x_1,x_3]$ is the confluent hypergeometric function of two variables [14, p.59, eq.(41)].

Proof. Taking $q \to 0$ in (3.1) is seen to yield the desired result (3.2). □

Corollary 3.3. *Let the condition of Theorem 3.1 be satisfied. Then the following generating relation holds true:*

$$\left(\frac{x_3}{Z}\right)^A {}_2F_{a+1}\left[\begin{array}{l} A,\ c; \\ \Delta(a;b),\ d; \end{array} -\frac{q^2}{4a^a Z}\right] = \sum_{i=-\infty}^{\infty}\sum_{j\geqslant 0} \frac{(\frac{s}{x_3})^i}{i!}\frac{(\frac{t}{x_3})^j}{j!}(A)_{i+j} \times$$

$$\times\ F^{1:1;1}_{0:a+1;1}\left[\begin{array}{ll} A+i+j: & c;\ -j; \\ -: & \Delta(a;b),\ d;\ i+1; \end{array} -\frac{q^2}{4a^a x_3}, \frac{x_1}{x_3}\right], \tag{3.3}$$

where ${}_2F_{a+1}$ denotes the generalized hypergeometric function [14, p. 42, eq. (1)].

Proof. This corollary can be established with the help of (3.1) by putting $w = 0$. □

Corollary 3.4. *Let the condition of Theorem 3.1 be satisfied. Then we have:*

$$\left(\frac{x_3}{Z}\right)^A {}_2F_{a+1}\left[\begin{matrix} A,\ c; \\ \\ \Delta(a;b),\ d; \end{matrix} \quad -\frac{q^2}{4a^a Z}\right] = \sum_{i=-\infty}^{\infty}\sum_{j\geqslant 0} \frac{(\frac{s}{x_3})^i}{i!}\frac{(\frac{t}{x_3})^j}{j!}(A)_{i+j} \times$$
$$\times\, {}_2F_{a+1}\left[\begin{matrix} A+i+j,\ c; \\ \\ \Delta(a;b),\ d; \end{matrix} \quad -\frac{q^2}{4a^a x_3}\right]. \tag{3.4}$$

Proof. On setting $x_1 = 0$ in (3.3), we easily get our claimed result(3.4). □

4. Recurrence relations

In this section, we establish the following recurrence relations for our introduced Voigt function.

Theorem 4.1. *The following recurrence relations for our generalized Voigt function $\Upsilon_{\mu,\nu}^{(a,b,c,d)}(x_1,x_2,x_3)$ holds true:*

$$\Upsilon_{\mu,\nu}^{(a,b,c,c+2)} + c\ \Upsilon_{\mu,\nu}^{(a,b,c+1,c+1)} - (c+1)\ \Upsilon_{\mu,\nu}^{(a,b,c,c+1)} = 0 \tag{4.1}$$

and

$$\Upsilon_{\mu,\nu}^{(a,b-1,c,d)} + (1-b)\ \Upsilon_{\mu,\nu}^{(a,b,c,d)} + \frac{ac}{4d}x_1^2\ \Upsilon_{\mu+2,\nu}^{(a,a+b,c+1,d+1)} = 0. \tag{4.2}$$

Proof. We have the following recurrence relation of the generalized Wright function (see [2, p. 8, eq. (72)]):

$$W_{a,b}^{c,c+2}(z) + c\ W_{a,b}^{c+1,c+1}(z) = (c+1)\ W_{a,b}^{c,c+1}(z). \tag{4.3}$$

From above relation, we can easily arrive at

$$\left(\frac{x_1}{2}\right)^{\nu+\frac12}\int_0^\infty t^{\mu+\nu}\exp(-x_2t-x_3t^2)\ W_{a,b}^{c,c+2}\left(-\frac{x_1^2t^2}{4}\right)dt +$$
$$+\ c\left(\frac{x_1}{2}\right)^{\nu+\frac12}\int_0^\infty t^{\mu+\nu}\exp(-x_2t-x_3t^2)\times W_{a,b}^{c+1,c+1}\left(-\frac{x_1^2t^2}{4}\right)dt =$$
$$= (c+1)\left(\frac{x_1}{2}\right)^{\nu+\frac12}\int_0^\infty t^{\mu+\nu}\exp(-x_2t-x_3t^2)\ W_{a,b}^{c,c+1}\left(-\frac{x_1^2t^2}{4}\right)dt. \tag{4.4}$$

By applying (2.1) in (4.4), we receive our needed result (4.1).

Similarly, the other recurrence relation (4.2) can be established with the help of the following recurrence relation of $W_{a,b}^{c,d}(z)$ (see [2, p. 9, eq. (74)]):

$$W_{a,b-1}^{c,d}(z) + (1-b)W_{a,b}^{c,d}(z) = \frac{ac}{d}z\ W_{a,a+b}^{c+1,d+1}(z).$$

□

5. Concluding remarks

In the present study, we have defined a new type of the generalized Voigt function by making use of the generalized Wright function. We have also studied various interesting and useful properties (for example, series representations involving Kampé de Fériet function $F^{p:q;r}_{g:h;k}$ and Srivastava's triple hypergeometric series $F^{(3)}[x_1, x_2, x_3]$, generating relations and recurrence relations) of our proposed Voigt function.

In this section, we shortly discuss about two interesting variations in the integral representation of our introduced Voigt function $\Upsilon^{(a,b,c,d)}_{\mu,\nu}$.

The generalized Wright function $W^{c,d}_{a,b}(z)$ have the undermentioned relations with the Fox H-Function $H^{m,n}_{r,s}$ and Fox Wright hypergeometric function ${}_p\Psi_q$ (see [2, p.4])):

$$W^{c,d}_{a,b}(z) = \frac{\Gamma(d)}{\Gamma(c)} H^{1,1}_{1,3}\left[-z \Big/ \begin{array}{c} (1-c,1) \\ (0,1),\ (1-b,a),\ (1-d,1) \end{array} \right] \tag{5.1}$$

and

$$W^{c,d}_{a,b}(z) = \frac{\Gamma(d)}{\Gamma(c)} {}_1\Psi_2\left[\begin{array}{c} (c,1); \\ (d,1),\ (b,a); \end{array} \ z \right]. \tag{5.2}$$

Therefore, by using (5.1) and (5.2), we can propose two interesting variations in the integral representation of our generalized Voigt function $\Upsilon^{(a,b,c,d)}_{\mu,\nu}$ as follows:

$$\Upsilon^{(a,b,c,d)}_{\mu,\nu}(x_1, x_2, x_3) = \frac{\Gamma(d)}{\Gamma(c)} \left(\frac{x_1}{2}\right)^{\nu+\frac{1}{2}} \times$$
$$\times \int_0^\infty t^{\mu+\nu} \exp(-x_2 t - x_3 t^2) H^{1,1}_{1,3}\left[\frac{x_1^2 t^2}{4} \Big/ \begin{array}{c} (1-c,1) \\ (0,1),\ (1-b,a),\ (1-d,1) \end{array} \right] dt \tag{5.3}$$

and

$$\Upsilon^{(a,b,c,d)}_{\mu,\nu}(x_1, x_2, x_3) =$$
$$= \frac{\Gamma(d)}{\Gamma(c)} \left(\frac{x_1}{2}\right)^{\nu+\frac{1}{2}} \int_0^\infty t^{\mu+\nu} \exp(-x_2 t - x_3 t^2) {}_1\Psi_2\left[\begin{array}{c} (c,1); \\ (d,1),\ (b,a); \end{array} \ -\frac{x_1^2 t^2}{4} \right] dt. \tag{5.4}$$

The authors declare that there is no conflict of interest.
All authors contributed equally to this paper. They read and approved the final manuscript.

References

[1] A.Erdélyi, W.Magnus, F.Oberhettinger, F.G.Tricomi, Table of integral transforms, Vol. 1, McGraw-Hill, New York, 1954.

[2] M.El-Shahed, A.Salem, An extension of Wright function and its properties, *J. Math.*, **2015**(2015). DOI: 10.1155/2015/950728

[3] K.Gupta, A.Gupta, On the study of unified representations of the generalized Voigt functions, *Palestine J. Math.*, **2**(2013), no. 1, 32–37.

[4] M.Ghayasuddin, J.Choi, N.U.Khan, A multiindex and multivariable generalization of the Voigt functions, *Far East J. Math. Sci.*, **101**(2017), no. 6, 1167–1181.

[5] S.B.Joshi, S.S.Joshi, H.H.Pawar, D.Ritelli, Connections between normalized Wright functions with families of analytic functions with negative coefficients, *Analysis* **42**(2022), no. 2, 111–119. DOI: 10.1515/anly-2021-1027

[6] V.Kiryakova, Some special functions related to fractional calculus and fractional (non-integer) order control systems and equations, *Facta Univ. Ser. Autom. Control Robot.*, **7**(2008), no. 1, 79–98.

[7] D.Klusch, Astrophysical Spectroscopy and neutron reactions, integral transforms and Voigt functions, *Astrophys. Space Sci.*, **175**(1991), 229–240.

[8] N.U.Khan, T.Usman, M.Aman, Some properties concerning the analysis of generalized Wright function, *J. Compu. Appl. Math.*, **376**(2020). DOI: 10.1016/j.cam.2020.112840

[9] N.U.Khan, M.Kamarujjama, M.Ghayasuddin, A generalization of Voigt function involving generalized Whittaker and Bessel functions, *Palestine J. Math.*, **4**(2015), no. 2, 313–318.

[10] I.Podlubny, Fractional differential equations, Academic Press, New York, USA, 1999.

[11] F.Reiche, Uber die Emission, Absorption und Intesitatsverteilung von Spektrallinien, *Ber. Deutsch. Phys. Ges.*, **15**(1913), 3–21.

[12] E.D.Rainville, Special functions, Macmillan Company, New York, 1960. Reprinted by Chelsea Publishing Company, Bronx, New York, 1971.

[13] H.M.Srivastava, E.A.Miller, A unified presentation of the Voigt functions, *Astrophys. Space Sci.*, **135**(1987), 111–118.

[14] H.M.Srivastava, H.L.Manocha, A treatise on generating functions, Halsted Press (Ellis Horwood Limited, Chichester), John Wiley and Sons, New York, Chichester, Brisbane and Toronto, 1984.

[15] H.M.Srivastava, M.A.Pathan, M. Kamarujjama, Some unified presentations of the generalized Voigt functions, *Comm. Appl. Anal.*, **2**(1998), 49–64.

[16] H.M.Srivastava, M.G.Bin-Saad, M.A.Pathan, A new theorem on multidimensional generating relations and its applications, *Proc. Jangjeon Math. Soc.*, **10**(2007), no. 1, 7–22.

Об обобщенной функции Фойгта и связанных с ней свойствах

Ульфат Ансари
Мушарраф Али
Факультет математики, колледж Ганди Фаиз-И-Аам
Шахджаханпур-242001, Индия
Университет Махатмы Джотибы Пхуле Рохилкханда
Барейли-243006, Индия
Мохд Гаясуддин
Факультет математики, Интегральный университет
Центр Шахджаханпур-242001, Индия

Аннотация. В настоящей статье мы стремимся представить новый тип обобщенной функции Фойгта и исследовать ее рядовые представления. Используя рядовые представления нашей функции, мы также указываем некоторые порождающие соотношения, связанные с функцией Кампе де Ферието, тройным гипергеометрическим рядом Шриваставы, конфлюэнтными гипергеометрическими функциями одной и двух переменных и обобщенной гипергеометрической функцией. Кроме того, также указаны два интересных рекуррентных соотношения нашей введенной функции Фойгта.

Ключевые слова: функция Фойгта, функция Райта, функция Кампе де Ферье, тройной гипергеометрический ряд Шриваставы.

Journal of Siberian Federal University. Mathematics & Physics 2024, 17(5), 609–612

EDN: MAGLZV
УДК 512.6

On a New Identity for Double Sum Related to Bernoulli Numbers

Brahim Mittou*
Department of Mathematics
University Kasdi Merbah Ouargla, Algeria
EDPNL & HM Laboratory of ENS Kouba, Algeria

Received 10.04.2024, received in revised form 24.05.2024, accepted 14.07.2024

Abstract. Let m, n and l be integers with $0 \leqslant l \leqslant m+n$. It is the main purpose of this paper to give an identity for the sum:

$$\sum_{\substack{a=0 \\ a+b \geqslant m+n-l}}^{m} \sum_{b=0}^{n} B_{m-a} B_{n-b} \frac{\binom{m}{a}\binom{n}{b}}{a+b+1} \binom{a+b+1}{m+n-l},$$

where B_m $(m = 0, 1, 2, \dots)$ is the Bernoulli number. As corollary we prove that the above sum equal to $\frac{1}{2}$ when $l = 0$.

Keywords: Bernoulli polynomial, Bernoulli number, generating function.

Citation: B. Mittou, On a New Identity for Double Sum Related to Bernoulli Numbers, J. Sib. Fed. Univ. Math. Phys., 2024, 17(5), 609–612. EDN: MAGLZV.

1. Introduction and main results

As the years have gone by, Bernoulli polynomials and numbers have consistently affirmed their significance as crucial mathematical entities. Since their introduction in the 17th century, they have continuously piqued the curiosity of numerous mathematicians and have found applications across a multitude of mathematical disciplines. Bernoulli polynomials $B_m(x)$ $(m = 0, 1, 2, \dots)$ are defined by using the generating function (see e.g., [2–4]):

$$\frac{ze^{xz}}{e^z - 1} = \sum_{m=0}^{\infty} B_m(x) \frac{z^m}{m!}, \quad |z| < 2\pi.$$

The Bernoulli numbers B_m $(m = 0, 1, 2, \dots)$ are the values of the Bernoulli polynomials $B_m(x)$ at $x = 0$ or, equivalently, they are the coefficients in the power series expansion (see e.g., [2, 4]):

$$\frac{z}{e^z - 1} = \sum_{m=0}^{\infty} B_m \frac{z^m}{m!}, \quad |z| < 2\pi.$$

There are numerous properties associated with Bernoulli numbers and polynomials, which readers interested in this topic can explore, for instance, in the following references [3, 4]. In the forthcoming discussion, we will confine ourselves to enumerating the properties upon which we will rely for the demonstration of our results.

*mathmittou@gmail.com, mittou.brahim@univ-ouargla.dz https://orcid.org/0000-0002-5712-9011

The expression of the Bernoulli polynomials in terms of the Bernoulli numbers is given by (see e.g., [2–4]):

$$B_m(x) = \sum_{j=0}^{m} \binom{m}{j} B_{m-j} x^j. \tag{1}$$

The Bernoulli polynomials satisfy the well-known relation (see e.g., [2–4]):

$$\frac{d}{dx} B_m(x) = m B_{m-1}(x) \quad (n \geqslant 1). \tag{2}$$

The Bernoulli polynomials satisfy the difirence equation (see e.g., [4]):

$$B_m(x+1) - B_m(x) = m x^{n-1} \quad (n \geqslant 1),$$

from which

$$B_m(0) = B_m(1) \quad (n \geqslant 2), \tag{3}$$

Many mathematicians, over the course of time, has been deeply intrigued by the pursuit of identifying and rigorously establishing mathematical identities related to Bernoulli numbers. For example, in the work by Vassilev and Missana [4], an interesting identity was established for all positive integers m and n:

$$(-1)^m \sum_{a=0}^{m-1} \binom{m}{a} B_{m+a} = (-1)^n \sum_{a=0}^{n-1} \binom{n}{a} B_{n+a}.$$

In another research, Agoh and Dilcher [1, Lemma 1], for all $m, n \geqslant 0$, proved the following identity:

$$\sum_{a=0}^{m} (-1)^a \binom{m+n+1}{m-a} B_{m-a} B_{n+a+1} - \sum_{a=0}^{n} (-1)^a \binom{n+m+1}{n-a} B_{n-a} B_{m+a+1} =$$

$$= (-1)^n (m+n) B_{m+n+1}.$$

One can also find several identities in [4, Corollary 19.1.18].

The aim of this paper is to establish an identity for the sum associated with the Bernoulli numbers, which is presented as follows:

Let m, n and l be integers with $0 \leqslant l \leqslant m+n$. Set

$$S(m,n,l) := \sum_{\substack{a=0 \\ a+b \geqslant m+n-l}}^{m} \sum_{b=0}^{n} B_{m-a} B_{n-b} \frac{\binom{m}{a}\binom{n}{b}}{a+b+1} \binom{a+b+1}{m+n-l}.$$

Our main identity is the following:

Theorem 1.1. *Let $n < m$ be non-negative integers such that $m+n \geqslant 3$. If $0 \leqslant l \leqslant m+n-3$, then*

$$S(m,n,l) = \sum_{r=0}^{\lfloor \frac{m}{2} \rfloor} \left\{ n\binom{m}{2r} + m\binom{n}{2r} \right\} \frac{(m+n-2r-1)\cdots(l+2-2r)}{(m+n-l)!} B_{2r} B_{l+1-2r}, \tag{4}$$

where it understood that the sum is extended over those r such that $l+1-2r \geqslant 0$.

Remark 1.2. *When relying on the right-hand side of Formula (4), we opt for $B_1 = \frac{1}{2}$ rather than $-\frac{1}{2}$, and this selection is quite common, as many researchers adopt it (see e.g., [3, Remark 1.2]).*

In the special case, when $l = 0$, the sum in Formula (4) becomes restricted to only one term (for $r = 0$), and then we have:

$$(m+n)\frac{(m+n-1)(m+n-2)\cdots(2)}{(m+n)!}B_0B_1 = B_1,$$

which proves the following corollary:

Corollary 1.3. *Let $n < m$ be non-negative integers such that $m+n \geqslant 3$. Then $S(m,n,0) = \frac{1}{2}$.*

2. Proof of Theorem 1.1

The subsequent lemma will assume a pivotal role in establishing the proof for Theorem 1.1.

Lemma 2.1. *Let m and n be positive integers. Then*

$$B_m(x)B_n(x) = \sum_{r=0}^{M_{m,n}} \left\{ n\binom{m}{2r} + m\binom{n}{2r} \right\} \frac{B_{2r}B_{m+n-2r}(x)}{m+n-2r} + (-1)^{m+1}\frac{m!n!}{(m+n)!}B_{m+n},$$

where $M_{m,n} = \max\left\{\lfloor \frac{m}{2} \rfloor, \lfloor \frac{n}{2} \rfloor\right\}$

Proof. See e.g., [2, Ex. 19 p. 276]. □

Now, we are ready to prove Theorem 1.1.

Proof of Theorem 1.1. Suppose that $n < m$ and l be non-negative integers such that $m+n \geqslant 3$ and $0 \leqslant l \leqslant m+n-3$. Then according to Formula (1) we have

$$\sum_{a=0}^{m}\sum_{b=0}^{n}\binom{m}{a}\binom{n}{b}B_{m-a}B_{n-a}\ x^{a+b} = B_m(x)B_n(x). \tag{5}$$

Differentiating $(m+n-l-1)$ times both sides of Formula (5) with respect to x, then dividing by $(m+n-l)!$ gives

$$\sum_{a=0}^{m}\sum_{b=0}^{n}\binom{m}{a}\binom{n}{b}B_{m-a}B_{n-a}\frac{1}{m+n-l}\binom{a+b}{m+n-l-1}\ x^{a+b-m-n+l+1} =$$

$$= \frac{1}{(m+n-l)!}\Big(B_m(x)B_n(x)\Big)^{(m+n-l-1)}. \tag{6}$$

By using the following elementary identity:

$$\frac{1}{m+n-l}\binom{a+b}{m+n-l-1} = \frac{1}{a+b+1}\binom{a+b+1}{m+n-l}$$

we can rewrite Formula (6) as:

$$\sum_{a=0}^{m}\sum_{b=0}^{n}B_{m-a}B_{n-a}\frac{\binom{m}{a}\binom{n}{b}}{a+b+1}\binom{a+b+1}{m+n-l}\ x^{a+b-m-n+l+1} =$$

$$= \frac{1}{(m+n-l)!}\Big(B_m(x)B_n(x)\Big)^{(m+n-l-1)}.$$

Taking $x = 1$ gives

$$S(m,n,l) = \frac{1}{(m+n-l)!}\Big(B_m(x)B_n(x)\Big)^{(m+n-l-1)}(1). \tag{7}$$

Now, taking into consideration Formulas (2) and (3), Lemma 2.1 allows us to get

$$\Big(B_m(x)B_n(x)\Big)^{(m+n-l-1)}(1) = \sum_{r=0}^{\lfloor \frac{m}{2} \rfloor} \left\{ n\binom{m}{2r} + m\binom{n}{2r} \right\} \times$$
$$\times (m+n-2r-1)(m+n-2r-2)\cdots(l+2-2r)B_{2r}B_{l+1-2r}. \tag{8}$$

Consequently, one can show that Formulas (7) and (8) imply Formula (4). This completes the proof. □

The author wishes to express gratitude to the referees and the editor-in-chief for their valuable comments and suggestions. Also, the author is thankful to Bakir Farhi for his help.

References

[1] T.Agoh, K.Dilcher, Integrals of products of Bernoulli polynomials, *J. Math. Anal. Appl.*, **381**(2011), 10–16. DOI: 10.1016/j.jmaa.2011.03.061

[2] T.M.Apostol, Introduction to Analytic Number Theory, Springer-Verlag, New York, 1976.

[3] T.Arakawa, T.Ibukiyama, M.Kaneko, Bernoulli Numbers and Zeta Functions, Springer Japan, 2014.

[4] H.Cohen, Number Theory, Volume II: Analytic and Modern Tools, Springer-Verlag, Berlin, 2007. DOI: 10.1007/978-0-387-49894-2

[5] P.Vassilev, M.V.Missana, On one remarkable identity involving Bernoulli numbers, *Notes on Number Theory and Discrete Mathematics*, **11**(2005), 22–24.

О новом тождестве для двойной суммы, связанной с числами Бернулли

Брахим Митту
Университет Касди Мербах Уаргла, Алжир
EDPNL & HM Laboratory of ENS Kouba, Алжир

Аннотация. Пусть m, n и l — целые числа с $0 \leqslant l \leqslant m+n$. Основной целью данной статьи является дать тождество для суммы:

$$\sum_{\substack{a=0 \\ a+b\geqslant m+n-l}}^{m}\sum_{b=0}^{n} B_{m-a}B_{n-}\frac{\binom{m}{a}\binom{n}{b}}{a+b+1}\binom{a+b+1}{m+n-l},$$

где B_m $(m = 0, 1, 2, \dots)$ — число Бернулли. В качестве следствия мы доказываем, что указанная выше сумма равна $\frac{1}{2}$ при $l = 0$.

Ключевые слова: многочлен Бернулли, число Бернулли, производящая функция.

Journal of Siberian Federal University. Mathematics & Physics 2024, 17(5), 613–621

EDN: NDRKSA
УДК 517.55

The Dirichlet Problem in the Class of $\mathbf{sh_m}$-functions on a Stein Manifold X

Sevdiyar A. Imomkulov*
Sukrotbek I. Kurbonboev†
National University of Uzbekistan
Tashkent, Uzbekistan

Received 10.03.2024, received in revised form 27.04.2024, accepted 14.06.2024

Abstract. The purpose of this paper is to introduce and study strongly m-subharmonic (sh_m) functions on complex manifolds $X \subset \mathbb{C}^N$, $dim X = n,\ n \leqslant N$. There are different ways to define sh_m-functions on complex manifolds: using local coordinates, using retraction $\pi :\ \mathbb{C}^N \to X$ or using Jensen measures (see for example [1, 8, 13]). In this paper we use the local coordinates. In Section 1 we present the definition and simplest properties of sh_m-functions in $\mathbb{C}^n$. In Section 2, we provide the definition of sh_m-functions in the domains $D \subset X$ of the complex manifold X and prove several of their potential properties. Section 3 introduces maximal functions and their properties, while Section 4 presents the main result of the work (Theorem 4.1) concerning the solvability of the Dirichlet problem in regular domains.

Keywords: sh_m-functions, plurisubharmonic functions, Stein manifolds, Dirichlet problem.

Citation: S.A. Imomkulov, S.I. Kurbonboev, The Dirichlet Problem in the Class of sh_m-functions on a Stein Manifold X, J. Sib. Fed. Univ. Math. Phys., 2024, 17(5), 613–621. EDN: NDRKSA.

The theory of strongly m-subharmonic (sh_m) functions plays an important role in the potential theory. It expands and develops the well-known pluripotential theory, introduced at the end of the last century, which at present is the main subject for studying analytic functions of several complex variables and plurisubharmonic functions.

The pluripotential theory is based on plurisubharmonic (psh) functions and is related to the Monge-Ampère operator $(dd^c u)^n$. Here, as usual $d = \partial + \overline{\partial}$ and $d^c = \dfrac{\partial - \overline{\partial}}{4i}$. This theory is based on research in numerous fundamental works of E. Bedford, A. Taylor, J. Siciak, A. Sadullaev and others (see, for example, [2, 10, 14]). sh_m-functions are related to the operator

$$(dd^c u)^m \wedge \beta^{n-m}, \quad 1 \leqslant m \leqslant n, \tag{1}$$

where $\beta = dd^c|z|^2$ is the standard volume form in the complex space $\mathbb{C}^n$.

Since $dd^c u \wedge \beta^{n-1} = \Delta u \beta^n$, operator (1) for $m = 1$ gives the Laplace operator, and for $m = n$ the Monge–Ampère operator. The operator (1) is called the complex operator in Hessians, because it is easy to calculate

$$(dd^c u)^m \wedge \beta^{n-m} = m!(n-m)! H_m(u)\beta^n,$$

where $H_m(u) = \sum\limits_{1 \leqslant j_1 < \ldots < j_m \leqslant n} \lambda_{j_1} \ldots \lambda_{j_m}$ is the Hessian of the eigenvalue vector $\lambda = (\lambda_1, \lambda_2, \ldots, \lambda_n)$ of the matrix $(u_{j,\bar{k}})$.

*sevdi@rambler.ru
†suqrot.qurbonboyev.93@mail.ru

With the help of Hessians, a class of sh_m-functions was defined (see Definition 2.1. below) in the works of Z. Blocki, S. Dinew, S.-Y. Li, H. Lu and others (see, for example, [3, 4, 6, 7]). Moreover, in their works sh_m-functions are also defined in the class $L^1_{loc}(D)$ and a number of their fundamental properties are proven. The potential theory in the class of sh_m-functions is developed in the work of A. Sadullaev and B. Abdullaev [9].

1. Hessians

Let $u \in C^2(D)$ be a twice differentiable function given in a domain $D \subset \mathbb{C}^n$. The second-order differential $dd^c u = \frac{i}{2}\sum_{j,k} u_{j,\bar{k}} dz_j \wedge d\bar{z}_k$ represents a Hermitian quadratic form, where $u_{j,\bar{k}} = \frac{\partial^2 u}{\partial z_j \partial \bar{z}_k}$. Therefore, through an appropriate unitary transformation of coordinates, it can be reduced to a diagonal form $dd^c u = \frac{i}{2}[\lambda_1 dz_1 \wedge d\bar{z}_1 + \cdots + \lambda_n dz_n \wedge d\bar{z}_n]$, where $\lambda_1, \ldots, \lambda_n$ are the eigenvalues of the Hermitian matrix $(u_{j,\bar{k}})$.

It is clear that

$$(dd^c u)^k \wedge \beta^{n-k} = k!(n-k)! H_k(u)\beta^n, \quad k = 1, \ldots, n,$$

where $H_k(u) = \sum_{1 \leqslant j_1 < \cdots < j_k \leqslant n} \lambda_{j_1} \ldots \lambda_{j_k}$ is the Hessian of dimension k of the vector $\lambda = \lambda(u) \in \mathbb{R}^n$.

Definition 1.1 (see [9])**.** *A function $u \in C^2(D)$ is called sh_m in domain $D \subset \mathbb{C}^n$, if it satisfies the following condition*

$$(dd^c u)^k \wedge \beta^{n-k} \geqslant 0 \quad \forall\, k = 1, 2, \ldots, n-m+1.$$

It is known that for all twice differentiable sh_m-functions $u, v_1, \ldots, v_{n-m}$ the following inequality holds

$$dd^c u \wedge dd^c v_1 \wedge \cdots \wedge dd^c v_{n-m} \wedge \beta^{m-1} \geqslant 0. \tag{2}$$

Moreover, if a twice differentiable function u satisfies (2) for all twice differentiable sh_m-functions $v_1, \ldots, v_{n-m}$, then u is a sh_m-function. Using this, we can define sh_m-functions in the class L^1_{loc}.

Definition 1.2 (see [9])**.** *An upper semicontinuous function u in the domain $D \subset \mathbb{C}^n$ is called sh_m in D, if for any twice differentiable sh_m-functions $v_1, \ldots, v_{n-m}$ the current $dd^c u \wedge dd^c v_1 \wedge \cdots \wedge dd^c v_{n-m} \wedge \beta^{m-1}$ defined as*

$$[dd^c u \wedge dd^c v_1 \wedge \cdots \wedge dd^c v_{n-m} \wedge \beta^{m-1}](\omega) =$$
$$= \int u dd^c v_1 \wedge \cdots \wedge dd^c v_{n-m} \wedge \beta^{m-1} \wedge dd^c \omega, \quad \omega \in F^{(0,0)}(D)$$

is positive, where $F^{(0,0)}(D)$ is a space of test functions in D.

The set of sh_m-functions in D is denoted by $sh_m(D)$. It is clear that $psh = sh_1 \subset sh_2 \subset \cdots \subset sh_n = sh$ and we have the following important property.

Theorem 1.1. *If $u \in sh_m(D)$, then for any complex hyperplane $\Pi \subset \mathbb{C}^n$ restriction $u|_\Pi$ is a sh_m-function in $D \bigcap \Pi$, i.e.*

$$u|_\Pi \in sh_m(D \cap \Pi).$$

2. $\mathrm{sh_m}$-functions on a Stein manifold X.

Let us recall the definition of a Stein manifold. Let X be a complex manifold of complex dimension n and denote by $\mathcal{O}(X)$ the ring of holomorphic functions on X.

Definition 2.1 (see [16]). *A complex analytic manifold X of dimension n is called Stein manifold if*

1) X is holomorphic convex, i.e.

$$\hat{K} = \{z: \ z \in X, \ |f(z)| \leqslant \sup_K |f| \ \textit{for all} \ f \in \mathcal{O}(X)\}$$

is a compact subset of X for every compact subset $K \subset X$;

2) If z_1 and z_2 are different points in X, then $f(z_1) \neq f(z_2)$ for some $f \in \mathcal{O}(X)$;

3) For every $z \in X$, one can find functions $f_1, \ldots, f_n \in \mathcal{O}(X)$ which form a coordinate system at z.

It is well-known that the Stein manifold X can always be embedded in some space of higher dimension, $X \subset \mathbb{C}^N, \ N \geqslant n$.

We define sh_m-functions on a Stein manifold $X \subset \mathbb{C}^N$, $\dim X = n$, for $1 \leqslant m \leqslant n$ by restricting $\beta = dd^c||z||^2$, $z = (z_1, \ldots, z_N)$ to X. In local coordinates $\phi(\xi): \ B \to U, \ B \subset \mathbb{C}^n, \ U \subset X, \ \xi = (\xi_1, \ldots, \xi_n)$ the differential form $\beta|_X$ has the following form

$$\beta|_X = \beta|_U = \alpha(\xi) = \frac{i}{2}[d\phi_1(\xi) \wedge d\bar{\phi}_1(\xi) + \cdots + d\phi_N(\xi) \wedge d\bar{\phi}_N(\xi)].$$

Definition 2.2 (see [15]). *A function $u \in C^2(D)$ is called sh_m-function in the domain $D \subset X$ if*

$$[(dd^c u)|_X]^k \wedge [\beta|_X]^{n-k} \geqslant 0, \ \ k = 1, 2, \ldots, n-m+1,$$

or, equivalently, in local coordinates of D the following holds

$$(dd^c u(\varphi(\xi)))^k \wedge \alpha^{n-k}(\xi) \geqslant 0, \ \ k = 1, 2, \ldots, n-m+1. \tag{3}$$

It is clear that if $U_1 \bigcap U_2 \neq \varnothing$ are two open sets on X, then from $\beta|_{U_j} = \beta|_{U_k} \circ \phi_k^{-1} \circ \phi_j$ it is easy to obtain that the positivity of the forms in (3) does not depend on the choice of the local coordinates, i.e. Definition 2.2 is correct.

From the definition of sh_m-function, it obviously follows that if $u, v_1, \ldots, v_{n-m} \in sh_m(D) \bigcap C^2(D)$, then

$$dd^c u \wedge dd^c v_1 \wedge \cdots \wedge dd^c v_{n-m} \wedge [\beta|_X]^{m-1} \geqslant 0. \tag{4}$$

Conversely, if a twice differentiable function u satisfies (4) for all $v_1, \ldots, v_{n-m} \in sh_m(D) \bigcap C^2(D)$, then u is a sh_m-function in D. This conclusion can be proved in the same way as in the case $X = \mathbb{C}^n$ since the differential forms $\beta|_X$ in local coordinates is a strictly positive $(1,1)$ form and by using suitable linear mapping it can be reduced to a diagonal form $\lambda_1 d\xi_1 \wedge d\bar{\xi}_1 + \cdots + \lambda_n d\xi_n \wedge d\bar{\xi}_n$.

As above, we can define sh_m-functions in the class of functions L^1_{loc}.

Definition 2.3 (see [5]). *A function $u \in L^1_{loc}(D)$ is called sh_m in a domain $D \subset X$ if it is upper semicontinuous and for any twice differentiable sh_m-functions $v_1, \ldots, v_{n-m}$ the current $dd^c u \wedge dd^c v_1 \wedge \cdots \wedge dd^c v_{n-m} \wedge [\beta|_X]^{m-1}$ which is defined as*

$$\begin{gathered}\left[dd^c u \wedge dd^c v_1 \wedge \cdots \wedge dd^c v_{n-m} \wedge (\beta|_X)^{m-1}\right](\omega) = \\ = \int u \, dd^c v_1 \wedge \cdots \wedge dd^c v_{n-m} \wedge (\beta|_X)^{m-1} \wedge dd^c \omega, \quad \omega \in F^{0,0}(D)\end{gathered} \tag{5}$$

is positive.

The class of sh_m-functions in a domain D is denoted by $sh_m(D)$. Usually a trivial function $u(z) \equiv -\infty$ is also included in $sh_m(D)$.

The following properties of $sh_m(D)$ follow easily from definitions of sh_m-function.

1) *A linear combination of sh_m-functions with non-negative coefficients also is a sh_m-function, i.e.*

$$u_k(z) \in sh_m(D), \ \ a_k \in \mathbb{R}^+ \ (k = 1, 2, \dots, p) \quad \Rightarrow \quad a_1 u_1(z) + a_2 u_2(z) + \dots + a_p u_p(z) \in sh_m(D);$$

2) *We have the following relation*

$$sh_1(D) \subset \dots \subset sh_m(D) \subset \dots \subset sh_n(D).$$

3) *The limit of a uniformly converging or monotonically decreasing sequence of sh_m-functions is also sh_m-function:*

$$u_j(z) \in sh_m(D), \ \ u_j(z) \rightrightarrows u(z) \quad \Rightarrow \quad u(z) \in sh_m(D);$$

$$u_j(z) \geqslant u_{j+1}(z) \ \ (j = 1, 2, \dots) \ \Rightarrow \ \lim_{j \to \infty} u_j(z) \in sh_m(D).$$

The above properties 1)–3) follow directly from Definition 2.3 and from the Lebesgue–Levi theorem on monotone convergence.

Let us now state properties whose proofs are more complicated.

4) *The maximum of a finite number of sh_m-functions is also a sh_m-function, i.e.,*

$$u_1(z), u_2(z), \dots, u_p(z) \in sh_m(D) \quad \Rightarrow \quad \max\{u_1(z), u_2(z), \dots, u_p(z)\} \in sh_m(D).$$

Proof. We fix $v_1, \dots, v_{m-1} \in sh_m(D) \bigcap C^2(D)$ and put $\alpha = dd^c v_1 \wedge \dots \wedge dd^c v_{n-m} \wedge [\beta|_X]^{m-1}$. According to (4), the differential form α is positive. For small positive number $\varepsilon > 0$, considering the differential form $\alpha + \varepsilon (dd^c \beta|_X)^{n-1}$, without loss of generality, we can assume that it is strictly positive. Then the operator

$$dd^c u \wedge \alpha = dd^c u \wedge dd^c v_1 \wedge \dots \wedge dd^c v_{n-m} \wedge [\beta|_X]^{m-1}$$

is an elliptic operator. If the function $u(z)$ is sh_m-function in D, then from the positivity in the generalized sense of the form $dd^c u \wedge dd^c v_1 \wedge \dots \wedge dd^c v_{n-m} \wedge [\beta|_X]^{m-1}$ we have the positivity of the form $dd^c u \wedge \alpha$, which means α-subharmonicity (see, for example, [11, 12]) of function u in local coordinates, defined by formula (3).

Let us take functions $u_1(z), u_2(z), \dots, u_p(z) \in sh_m(D)$. Since they are α-subharmonic in the local coordinate, the maximum function $u = \max\{u_1(z), u_2(z), \dots, u_p(z)\}$ is also α-subharmonic. This means that $dd^c u \wedge \alpha \geqslant 0$ in the generalized sense. So, we have $dd^c u \wedge \alpha \geqslant 0$ for every $v_1, \dots, v_{m-1} \in sh_m(D) \bigcap C^2(D)$ and $\alpha = dd^c v_1 \wedge \dots \wedge dd^c v_{n-m} \wedge [\beta|_X]^{m-1}$, i.e.

$$\left[dd^c u \wedge dd^c v_1 \wedge \dots \wedge dd^c v_{n-m} \wedge (\beta|_X)^{m-1}\right](\omega) =$$

$$= \int u \, dd^c v_1 \wedge \dots \wedge dd^c v_{n-m} \wedge (\beta|_X)^{m-1} \wedge dd^c \omega \geqslant 0, \quad \forall \omega \in F^{0,0}(D), \ \omega \geqslant 0.$$

According to Definition 2.3, u is a sh_m-function. The proof is complete. □

5) *For any locally uniformly bounded family* $u_t(z) \in sh_m(D)$, $t \in T$, *we have*

$$\left[\sup_t u_t(z)\right]^* \in sh_m(D).$$

Similarly, the regularization of the upper limit of locally uniformly bounded sequence $u_j(z) \in sh_m(D)$ *is a* sh_m*-function, i.e.,* $\left[\varlimsup_{j\to\infty} u_j(z)\right]^* \in sh_m(D)$. *In particular, the regularization of the limit of a monotonically increasing, locally uniformly bounded sequence of* sh_m*-functions is again* sh_m*-function.*

Proof. Let us deal with the supremum, assuming without loss of generality that there exists $M > 0 : \ u_t(z) \leqslant M$. We fix $v_1, \dots, v_{m-1} \in sh_m(D) \bigcap C^2(D)$ and put it as above $\alpha = dd^c v_1 \wedge \dots \wedge dd^c v_{n-m} \wedge [\beta|_X]^{m-1}$, assuming without loss of generality that α is a strictly positive $(n-1, n-1)$-form. Since $dd^c u_j \wedge \alpha \geqslant 0$, then u_j are α-subharmonic functions for the elliptic operator $dd^c u_j \wedge \alpha$. Then, just as for the Laplace operator $dd^c u_j \wedge \beta^{n-1}$ in $\mathbb{C}^n$ (see [14]), we can show that $\left[\sup_t u_t(z)\right]^* \wedge \alpha \geqslant 0$. *The proof is complete.* □

6) *Let* $u_j(z) \in sh_m(D)$ *be a sequence of* sh_m*-functions satisfying* $u_j(z) \leqslant M_j (j = 1, 2, \dots)$ *where* $\sum_{j=1}^{\infty} M_j$ *converges. Then* $\sum_{j=1}^{\infty} u_j(z)$ *is a* sh_m*-function.*

Proof. The functions $u_j(z) - M_j \ (j = 1, 2, \dots)$ are not positive. Therefore, the sequence $v_k(z) = \sum_{j=1}^{k} [u_j(z) - M_j]$ is monotonically decreasing. By property 3) we have $\sum_{j=1}^{\infty} (u_j(z) - M_j) \in sh_m(D)$. Since the series $\sum_{j=1}^{\infty} M_j$ converges, then $\sum_{j=1}^{\infty} u_j(z) \in sh_m(D)$. The proof is complete. □

7) *Let* $\gamma(t) : \mathbb{R} \to \mathbb{R}$ *be a convex and non-decreasing function, and* $u(z) \in sh_m(D)$. *Then* $\gamma \circ u \in sh_m(D)$.

3. Maximal functions.

Maximal functions are analogous of harmonic functions in the class of sh_m-functions, they are studied by the A. Sadullaev, B. Abdullaev [9] in $\mathbb{C}^n$. Let us give the definition of a maximal sh_m-function on a Stein manifold X.

Definition 3.1. *A function* $u(z) \in sh_m(D)$, $D \subset X$ *is called maximal in the domain* $D \subset X$ *if for any function* $v(z) \in sh_m(D)$ *for which* $\varliminf_{z\to\partial D} (u(z) - v(z)) \geqslant 0$ *holds* $u(z) \geqslant v(z)$ *in* D.

The condition $\varliminf_{z\to\partial D} (u(z) - v(z)) \geqslant 0$ for arbitrary sh_m-functions $u(z), v(z)$ can be understood as follows: for any $\varepsilon > 0$ there exists a compact subset $F \subset D$ outside of which $v(z) \leqslant u(z) + \varepsilon$. In particular, $v(z) = -\infty$ if $u(z) = -\infty$.

Let us formulate the following theorem, which allows us to define maximal functions in convenient forms

Theorem 3.1. *The following statements are equivalent*

1) $u(z)$ *is a maximal function in* D;

2) for any subdomain $G \subset\subset D$ *the inequality* $u(z) \geqslant v(z)$, $\forall z \in G$ *holds for all functions* $v(z) \in sh_m(G)$ *satisfying* $\varliminf_{z\to\partial G} (u(z) - v(z)) \geqslant 0$;

3) for any subdomain $G \subset\subset D$ the inequality $u(z) \geqslant v(z)$, $\forall z \in G$ holds for all functions $v(z) \in sh_m(D)$ for which

$$u|_{\partial G} \geqslant v|_{\partial G}.$$

4. The Dirichlet problem in the class of $\mathbf{sh_m}$-functions on a Stein manifold X.

In this section we will discuss the solvability of the Dirichlet problem in the class of sh_m-functions on a Stein manifold $X \subset \mathbb{C}^N, \dim X = n$.

Definition 4.1. *A domain $D \subset X$ is called strictly m-convex if $D = \{\rho(z) < 0\}$ for some strictly sh_m-function $\rho(z)$ in some neighborhood D^+ of $\bar{D}$. Strictly of the sh_m-function $\rho(z)$ means that there is a $\delta > 0$ such that $\rho(z) - \delta \cdot \left(\|z\|^2\right)_X$ is a sh_m-function in D^+.*

Remark 4.1. *If the domain $D \subset X$ is a strictly m-convex, then any point $\zeta_0 \in \partial D$ is a peak point, i.e. there is a peak function $q(z) \in sh_m(D) \bigcap C\left(\overline{D}\right)$: $q\left(\zeta^0\right) = 0$, $q|_{\bar{D}\setminus\{\zeta^0\}} < 0$.*

In fact, by Definition 4.1, there is $\delta > 0$ such that the function

$$q(z) = \rho(z) - \delta \cdot \left(\left\|z - \zeta^0\right\|^2\right)_X$$

is a sh_m-function in D, which will be continuous on $\overline{D}$ and $q\left(\zeta^0\right) = 0$, $q|_{\bar{D}\setminus\zeta^0} < 0$.

Let $D \subset X$ be a strictly m-convex domain and given a continuous function $\varphi(\zeta) \in C(\partial D)$. We consider the following Dirichlet problem: find a function satisfying the following conditions

a) $u \in sh_m(D)$;

b) $\lim\limits_{z \to \zeta} u(z) = \varphi(\zeta)$, $\forall \zeta \in \partial D$;

c) u *is maximal function in* D.

In order to solve the Dirichlet problem, we will use the Perron method. Let us define the following class

$$\mathcal{U}(\varphi, D) = \left\{v \in sh_m(D) : \varlimsup_{z \to \partial D} v(z) \leqslant \varphi(\zeta)\right\}$$

and put

$$\omega(z) = \sup_{v \in U(\varphi, D)} v(z).$$

Theorem 4.1. *The upper regularization $\omega^*(z)$ of $\omega(z)$ is a solution to the Dirichlet problem, i.e. $\omega^*(z)$ satisfies the conditions a), b) and c).*

Proof. First we prove that $\omega^*(z)$ is a sh_m-function in D. Since φ is continuous and by the maximum principle we deduce that the class of functions of $\mathcal{U}(\varphi, D)$ is uniformly bounded from above. By property 5 of Section 2 its regularization is a sh_mf-unction in D.

Now we prove the continuity of the function $\omega^*(z)$ on ∂D. First, we show that $\varliminf\limits_{z \to \zeta^0} \omega(z) \geqslant \varphi(\zeta^0)$ for any fixed point $\zeta^0 \in \partial D$. Set $M = \|\varphi\|_{\partial D}$ and fix $\varepsilon > 0$. Then from the continuity of the function $\varphi(\zeta) \in C(\partial D)$ there is $r > 0$ such that

$$\left|\varphi(\zeta) - \varphi\left(\zeta^0\right)\right| < \varepsilon \quad \forall \zeta \in \partial D \bigcap B\left(\zeta^0, r\right),$$

where $B\left(\zeta^0, r\right) \subset \mathbb{C}^N$.

Since the point ζ^0 is a peak point, then there is a peak function $q(z) \in sh_m(D)$ such that

$$q\left(\zeta^0\right) = 0, \quad \sup_{\|z-\zeta^0\| \geqslant \varepsilon,\ z \in D} q(z) = q_\varepsilon < 0.$$

Let us estimate the boundary values of the following function

$$v_\varepsilon(z) = -\varepsilon + \varphi\left(\zeta^0\right) + \frac{q(z)}{|q_\varepsilon|}\left(M + \varphi\left(\zeta^0\right)\right).$$

If $\zeta \in \partial D \bigcap B\left(\zeta^0, r\right)$, then

$$\overline{\lim_{z\to\zeta}}\, v_\varepsilon \leqslant -\varepsilon + \varphi\left(\zeta^0\right) \leqslant \varphi(\zeta);$$

if $\zeta \in \partial D \backslash B\left(\zeta^0, r\right)$, then

$$\overline{\lim_{z\to\zeta}}\, v_\varepsilon \leqslant -\varepsilon + \varphi\left(\zeta^0\right) - M - \varphi\left(\zeta^0\right) \leqslant \varphi(\zeta).$$

Hence, $\overline{\lim\limits_{z\to\zeta}}\, v_\varepsilon \leqslant \varphi(\zeta)$ for all $\zeta \in \partial D$ and $v_\varepsilon \in \mathcal{U}(\varphi, D)$. Consequently, we get that $v_\varepsilon(z) \leqslant \omega(z)$ and $\underline{\lim\limits_{z\to\zeta^0}}\, \omega(z) \geqslant \underline{\lim\limits_{z\to\zeta^0}}\, v_\varepsilon(z) = -\varepsilon + \varphi\left(\zeta^0\right)$. Since $\varepsilon > 0$ is arbitrary, we have

$$\underline{\lim_{z\to\zeta^0}}\, \omega(z) \geqslant \varphi\left(\zeta^0\right).$$

Now we will show that $\overline{\lim\limits_{z\to\zeta^0}}\, \omega(z) \leqslant \varphi\left(\zeta^0\right)$. To prove this inequality we fix the function $u(z) \in \mathcal{U}(\varphi, D)$ and consider the sum $u(z) + g_\varepsilon(z)$, where

$$g_\varepsilon(z) = -\varepsilon - \varphi\left(\zeta^0\right) + \frac{q(z)}{|q_\varepsilon|}\left(M - \varphi\left(\zeta^0\right)\right).$$

It's clear that $u(z) + g_\varepsilon(z) \in sh_m(D)$. Now let's estimate the boundary values of the function $g_\varepsilon(z)$: If $\zeta \in \partial D \bigcap B\left(\zeta^0, r\right)$, then

$$\overline{\lim_{z\to\zeta}}\, g_\varepsilon(z) \leqslant -\varepsilon - \varphi\left(\zeta^0\right) \leqslant \varphi(\zeta).$$

Similarly, if $\zeta \in \partial D \backslash B\left(\zeta^0, r\right)$, then

$$\overline{\lim_{z\to\zeta}}\, g_\varepsilon(z) \leqslant -\varepsilon - \varphi\left(\zeta^0\right) + \overline{\lim_{z\to\zeta}}\, \frac{q(z)}{|q_\varepsilon|}\left(M - \varphi\left(\zeta^0\right)\right) =$$
$$= -\varepsilon - \varphi\left(\zeta^0\right) + \frac{q(\varepsilon)}{|q_\varepsilon|}\left(M - \varphi\left(\zeta^0\right)\right) = -\varepsilon - M \leqslant -\varphi(\zeta).$$

Consequently, we have

$$\overline{\lim_{z\to\zeta}}\, \left[u(z) + g_\varepsilon(z)\right] \leqslant \overline{\lim_{z\to\zeta}}\, u(z) + \overline{\lim_{z\to\xi}}\, g_\varepsilon(z) \leqslant \overline{\lim_{z\to\zeta}}\, u(z) - \varphi(\zeta) \leqslant 0$$

for any $\zeta \in \partial D$. Thus thanks to the maximum principle, $u(z) + g_\varepsilon(z) \leqslant 0$ in D, i.e. $u(z) \leqslant -g_\varepsilon(z)$, $\forall z \in D$. Since the function $u(z) \in \mathcal{U}(\varphi, D)$ is arbitrary, we get $\omega(z) \leqslant -g_\varepsilon(z)$, $z \in D$. As a consequence we deduce that

$$\overline{\lim_{z\to\zeta^0}}\, \omega(z) \leqslant \overline{\lim_{z\to\zeta^0}}\, \left(-g_\varepsilon(z)\right) = -\varepsilon + \varphi\left(\zeta^0\right).$$

Since $\varepsilon > 0$ is arbitrary, by letting $\varepsilon \to 0$ we get $\overline{\lim\limits_{z\to\zeta^0}}\,\omega(z) \leqslant \varphi(\zeta^0)$.

Combining $\underline{\lim\limits_{z\to\zeta^0}}\,\omega(z) \geqslant \varphi(\zeta^0)$ with $\overline{\lim\limits_{z\to\zeta^0}}\,\omega(z) \leqslant \varphi(\zeta^0)$ we get the continuity $\lim\limits_{z\to\zeta^0}\omega(z) = \varphi(\zeta^0)$ at every point $\zeta^0 \in \partial D$. This means that $\lim\limits_{z\to\zeta}\omega(z) = \varphi(\zeta)$ is true in ∂D, i.e. $\omega(z)$ is continuous on ∂D. It is not difficult to see that the regularization $\omega^*(z)$ is continuous at the boundary i.e., $\lim\limits_{z\to\zeta}\omega^*(z) = \varphi(\zeta)$, $\forall\zeta \in \partial D$.

Let us now prove that the function $\omega^*(z)$ is maximal in D. We will prove this by contrary, assume there is a domain $G \subset\subset D$ and a function $\vartheta(z) \in sh_m(D)$: $\vartheta|_{\partial G} \leqslant \omega|_{\partial G}$, but $\vartheta(z^0) > \omega(z^0)$ at some point $z^o \in G$. It's easy to see that function

$$v(z) = \begin{cases} \max\{\vartheta(z), \omega(z)\}, & z \in G \\ \omega(z), & z \in D\backslash G \end{cases}$$

is a sh_m-function and $v|_{\partial D} = \omega|_{\partial D} = \varphi$. Therefore, $v(z) \leqslant \omega(z)$ and hence $\vartheta(z^o) \leqslant \omega(z^o)$. This leads to contradiction. The proof is complete. □

References

[1] P.Ahag, C.Rafal, H.Lisa, Extension and approximation of m-subharmonic functions, *Complex Variables and Elliptic Equations*, (2017), 1–19.

[2] E.Bedford, B.A.Taylor, The Dirichlet problem for a complex Monge-Ampère equation, *Inventiones Math.*, **37**(1976), 1–44.

[3] Z.Blocki, Weak solutions to the complex Hessian equation, *Ann.Inst.Fourier, Grenoble*, **55**(2005), no. 5, 1735–1756 DOI: 10.5802/aif.2137

[4] S.Dinew, S.Kolodziej, A priori estimates for complex Hessian equations, *Analysis and PDE*, **7**(2014), no. 1, 227–244. DOI: 10.2140/apde.2014.7.227

[5] S.I.Kurbonboev, Strongly m-subharmonic functions on complex manifolds, *Bulletin of NUUz: Mathematics and Natural Sciences*, **5**(2022), no. 2, 91–100.

[6] S.-Y.Li, On the Dirichlet problems for symmetric function equations of the eigenvalues of the complex Hessian, *Asian J. Math.*, **8**(2004), no. 1, 87–10.

[7] H.Lu, A variational Approach to complex Hessian equations in $\mathbb{C}^n$, *Journal of Mathematical Analysis and Applications*, **431**(2015), no. 1, 228–259.

[8] E.A.Poletsky, R.Sigurdsson, Dirichlet problems for plurisubharmonic functions on compact sets, *Math. Z.*, **271**(2012), no. 3-4, 877–892.

[9] A.Sadullaev, B.Abdullaev, Potential theory in the class of m-subharmonic functions, *Trudy Mat. Inst. Steklova*, **279**(2012), 166–192.

[10] J.Siciak, Extreme plurisubharmonic functions in $\mathbb{C}^n$, *Ann. Polon. Math.*, **39**(1981), 175–211.

[11] B.I.Abdullaev, S.A.Imomkulov, R.A.Sharipov, α-subharmonic functions, *Contemporary mathematics. Fundamental directions*, **67**(2021), no. 4, 620–633 (in Russian).

[12] B.I.Abdullaev, R.A.Sharipov, Locally and globally α-polar sets, *Bulletin of the Institute of Mathematics, Tashkent*, (2019), no. 5, 4–8 (in Russian).

[13] J.Garnett, Bounded Analytic Functions, Moscow, Mir, 1984 (in Russian).

[14] A.Sadullaev, Theory of pluripotential. Applications, Saarbrucken. Germany, 2012 (in Russian).

[15] A.Sadullaev, Approximation of sh_m-function on Stein manifold, (preprint), 2024 (in Russian).

[16] L.Hörmander, Introduction to the Theory of Functions of Several Complex Variables, Moscow, Mir, 1968 (in Russian).

Задача Дирихле в классе $\mathbf{sh_m}$-функций на многообразии Штейна X

Севдияр А. Имомкулов
Сукротбек И. Курбонбоев
Национальный университет Узбекистана
Ташкент, Узбекистан

Аннотация. Целью данной работы является введение и изучение sh_m-функций на комплексных многообразиях $X \subset \mathbb{C}^N$, $dimX = n$, $n \leqslant N$. Имеются разные способы определения sh_m-функций на комплексных многообразиях: при помощи локальных координат, при помощи ретракции $\pi : \mathbb{C}^N \to X$, при помощи мер Иенсена (см. [1, 8, 13]). Для определения sh_m-функций на комплексном многообразии X мы пользуемся локальными координатами. В разделе 1 мы приводим определение и простейшие свойства sh_m-функций в пространстве $\mathbb{C}^n$. В разделе 2 дается определение sh_m-функций в областях $D \subset X$ комплексного многообразия X и доказывается ряд их потенциальных свойств. В разделе 3 определяются максимальные функции и их свойства, и в разделе 4 мы докажем основной результат работы (Теорема 4.1.) о разрешимости задачи Дирихле в регулярных областях.

Ключевые слова: sh_m-функции, плюрисубгармонические функции, многообразие Штейна, задача Дирихле.

EDN: OJGPTH
УДК 519.6

Computer Modeling of Temperature Fields in the Soil and the Bearing Capacity of Pile Foundations of Buildings on Permafrost

Mikhail Yu. Filimonov*
Nataliia A. Vaganova†
Krasovskii Institute of Mathematics and Mechanics
Yekaterinburg, Russian Federation
Ural Federal University
Yekaterinburg, Russian Federation
David Zh. Shamugia‡
Irina M. Filimonova§
Ural Federal University
Yekaterinburg, Russian Federation

Received 07.04.2024, received in revised form 27.05.2024, accepted 14.07.2024

Abstract. Global climate warming challenges the permafrost areas losing the frozen state and stability. Industrial development and human activity in these regions also contributes to the degradation of permafrost. The construction of residential buildings and their operation in these territories mainly involves maintaining the soil under these structures in a frozen state throughout the entire period of their operation. For these purposes, pile foundations and ventilated crawl spaces are used. The basements may also include the devices aiding stabilize the soil. For example, it could be hundreds of the seasonally operating cooling devices. An urgent task is long-term forecasting of the dynamics of changes in the bearing capacity of a pile foundation of a building, considering climatic and technogenic impacts on the surrounding soil. A new model and numerical algorithm were developed to study the dynamics of changes in the bearing capacity of piles during the operation of the building, considering temperature monitoring data from temperature sensors located in thermometric wells. Validation of the developed software package was carried out based on the existing and constantly arriving data on soil temperature monitoring to a depth of 10 meters on the server. A comparison of the obtained monitoring data and the calculated data in thermometric wells showed a significant improvement compared to the previously used model and calculation program for this residential building.

Keywords: mathematical modelling, heat and mass transfer, permafrost.

Citation: M.Yu. Filimonov, N.A. Vaganova, D.Zh. Shamugia, I.M. Filimonova, Computer Modeling of Temperature Fields in the Soil and the Bearing Capacity of Pile Foundations of Buildings on Permafrost, J. Sib. Fed. Univ. Math. Phys., 2024, 17(5), 622–631. EDN: OJGPTH.

Introduction

The territories of Western Siberia and the northern latitudes of Russia, which are covered by permafrost, are extremely important for the Russian economy. These regions are rich in various minerals and have great oil and gas fields. In the development strategy of the northern territories

*fmy@imm.uran.ru https://orcid.org/0000-0002-9561-5416
†vna@imm.uran.ru https://orcid.org/0000-0001-6966-9050
‡dawid.shamugia@yandex.ru https://orcid.org/0009-0006-8715-1873
§irina.filimonova4@mail.ru https://orcid.org/0009-0002-2800-9237

of Russia, a significant place is given to the balanced development of the economy, industry, and social infrastructure with the preservation of natural ecosystems. Sustainability of engineering infrastructure in regions occupied by permafrost [1] needs for extra attention due to observed climate warming [2–4]. Experiencing significant changes and degradation of permafrost [5–8] may lead to possible technogenic accidents [9, 10].

In accordance with the Russian Building Code [1], the capital structures and residential buildings require special rules for construction and operation in such territories. In accordance with these rules, the construction should be carried out following two principles. The first principle of construction means the construction and operation of capital structures must keep the foundation soils in a frozen state. The second principle of construction means the permafrost foundation soils should be used in a thawed or thawing state. So, before the construction the thawing layers should be achieved to the expected depth or under the assumption the thawing during the operation. In Russia, more than 75% of all buildings and engineering structures in the permafrost zone were built and operated according to the first principle. Thawing of ice-saturated rocks due to climate change or various technogenic impacts will be accompanied by subsidence of the earth's surface [11] and the development of dangerous frozen geological processes leading to accidents, the possible consequences of which may be the destruction of pile foundations of capital structures and residential buildings [12]. To predict these processes, various methods of monitoring the condition of the foundations of structures are used [13]. The bearing capacity of building foundation piles also depends on the temperature of the surrounding soil, therefore, in the city of Salekhard, employees of the Arctic Research Center of the Yamal-Nenets autonomous district have built and are developing an automatic temperature monitoring (ATM) system for the soil surrounding the pile foundations residential buildings [14, 15]. For this purpose, thermometric wells equipped with temperature sensors were drilled in the ventilated crawl spaces of buildings. Analysis of the temperature data obtained from this system allows us to draw conclusions about the condition of the soil under buildings. However, to model unsteady thermal fields throughout the entire area of a pile foundation, it is necessary to investigate mathematical models based on ATM data. The presence of thermometric wells makes it possible to determine the lithology of the soil and to validate the constructed numerical methods [16]. In accordance with the first principle of construction, it is also necessary to maintain the foundation soils of residential buildings in a frozen state.

Therefore, in the northern regions the pile foundations, ventilated crawl spaces, and various devices for cooling the soil may be used side by side under buildings [17, 18]. The seasonal cooling devices (SCDs) may be mentioned as the most common. The SCD operational principle is based on the physical laws of cooling due to the temperature difference in the soil and in the ventilated crawl space. So, the SCDs are in process only on winter. SCD operation makes significant changes in the surrounding soil and has to be accounted in the mathematical model and is required extra calibration with data from temperature sensors in thermometric wells.

In this study the new algorithm and software were calibrated for a specific residential building (Building I) in the city of Salekhard. In contrast to [16], the climatic and technogenic factors influencing the temperature fields at the base of the pile foundation of this building were studied in detail. Numerical calculations were performed for the dynamics of changes in the bearing capacity of piles in 2021–2023. The presented data verifies the model and the developed numerical algorithm using data from temperature sensors located in thermometric wells. Additional data is obtained from temperature sensors of four thermometric wells. When carrying out numerical calculations, the concept of average bearing capacity of piles was introduced and the dynamics of its changes until January 2024 are shown. Based on the numerical calculations, the further research direction related to improving and increasing the accuracy of the mathematical models, algorithms and software are discussed.

1. Statement of the problem and pethods

Object of study

The object of study is the pile foundation of a nine-story residential building in the city of Salekhard, which, in accordance with the first principle of construction on permafrost, has a ventilated crawl spaces 1.8 meters high, and 186 SCDs are used to cool the soil around 229 piles. Fig. 1 shows a plan of the pile foundation for Building I.

Each automatic monitoring station (SAM station) collects data from four thermometric wells (SAM wells) equipped with temperature sensors that measure soil temperature to a depth of 10 meters with an accuracy of 0.1°C. The triangles in the Fig. 1 are the SAM wells, the squares are the SAM stations, the dots are the piles. Data from all temperature measurements are transmitted to the server every 3 hours using GSM modules. 186 SCDs are not shown in the Fig. 1, but their exact location coordinates in the ventilated crawl space are used in the model and in computer simulations. These devices are vertical cooling devices, which are two-phase closed thermosiphons with a diameter of 38 mm. The aluminum cooling fins of these devices are of 95 cm and the underground depths are of 10 m. To carry out automatic temperature monitoring of the soil in a ventilated crawl space, 6 stations were equipped.

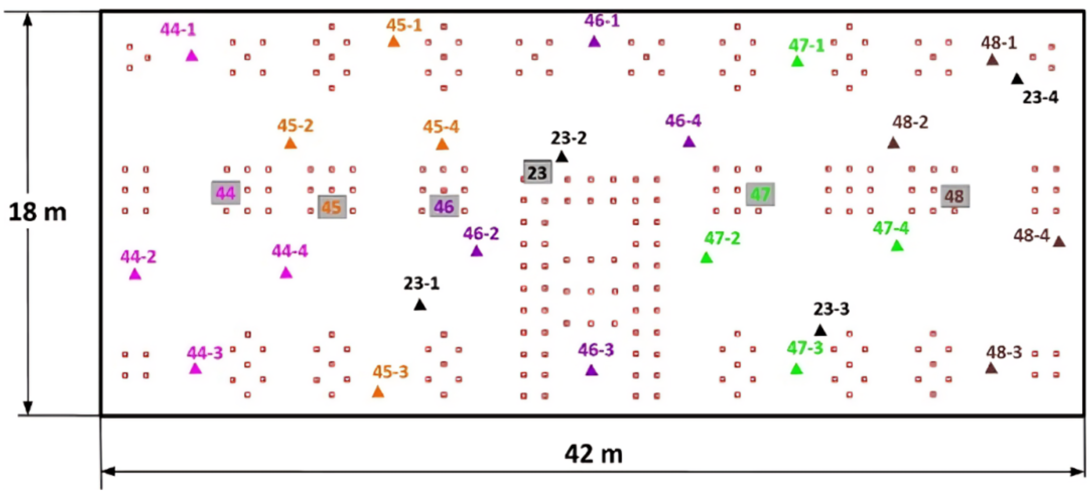

Fig. 1. Scheme of the location of thermometric equipment of the SAMs and the pile foundations under the Building I

Mathematical model

Let $T = T(t, x, y, z)$ be the soil temperature at point (x, y, z) for the time t and at the initial time t_0 has a temperature $T_0(x, y, z)$. Following [16, 19], to describe the temperature regime of the soil under the building, we will use the equation taking into account the localized heat of the phase transition:

$$\rho\big(c_\nu(T) + k\delta(T - T^*)\big)\frac{\partial T}{\partial t} = \nabla\,(\lambda(T)\Delta T), \tag{1}$$

where ρ is density [kg/m^3], T^* is temperature of phase transition $[K]$,

$$c_\nu(T) = \begin{cases} c_1(x,y,z), & T < T^*, \\ c_2(x,y,z), & T > T^* \end{cases} \text{ is specific heat } [\mathrm{J/(kg\cdot K)}],$$

$$\lambda(T) = \begin{cases} \lambda_1(x,y,z), & T < T^*, \\ \lambda_2(x,y,z), & T > T^* \end{cases} \text{ is thermal conductivity coefficient [W/(m} \cdot \text{ K)]},$$

$k = k(x, y, z)$ is specific heat of phase transition, δ is Dirac delta function.

This equation allows to solve the problem of Stefan type without the explicit separation of the phase transition [19]. The heat of phase transition is introduced with using Dirac δ-function in the specific heat ratio. The parameters $c(T)$ and $\lambda(T)$ inserted in (1) were determined during laboratory studies of soil from SAM wells drilled in ventilated crawl space. As the initial time moment we take t_0, corresponding to the moment in time 2 years ago and the reconstructed initial distribution of soil temperature at this moment in time $T_0(x, y, z)$ based on ATM data. As studies based on numerical calculations have shown, such a choice is necessary to take into account the operation of all SCDs and their impact on the soil temperature regime for 2 years. Particular attention was paid to modeling the operation of SCDs considering the ATM data. The calculation of the bearing capacity is carried out based on the condition:

$$F \leqslant F_u/\gamma_n,$$

where F is the design load on the foundation, γ_n is the reliability coefficient for the responsibility of the structure, F_u is the bearing capacity of the foundation, determined in accordance with the Russian Building Code and soil temperature data determined during numerical calculations.

Of course, moisture and migration of water should be mentioned in the problem of temperature distribution in soil. When the soil freezes, migration of water contained in the soil is observed [20–23]. This process has a significant impact on the temperature regime of the soil. Indeed, unfrozen water in the soil will migrate from bottom to top into the freezing zone, and latent heat will affect the temperature distribution of frozen soil due to the freezing of replenished water. In the proposed model, SCDs will also be sources of cold in the ground in winter, from which soil freezing will spread in the horizontal direction, and lateral migration above the groundwater level in the case under consideration will be minimal. This study takes into account the latent heat of the initial water content and assumes that the soils in the basements are generally low-moisture, and the soil surface in a ventilated crawl space is insulated with a concrete slab that protects from evaporation and filtration of rain and melted snow water into the soil.

Validation of numerical algorithms

To find the thermal fields in the soil described by (1) in the area of the pile foundation, the finite difference method with splitting into spatial variables is used [19]. The initial equation for each of the spatial directions is approximated by an implicit central-difference three-point scheme, and a system of difference linear algebraic equations having a tridiagonal form is solved by the sweep method. Since thermal fields in the soil have a significant impact on the physical and mechanical properties of frozen soil and the bearing capacity, an important task is to determine the temperature on the surfaces of piles with sufficient accuracy. In order to test the accuracy of the developed algorithm, the numerical results were compared with data from temperature sensors in SAM wells. Figure 2 compares data for SAM well 44–1 during 2023 for various months. In these Figures, the dashed lines correspond to the data of numerical calculations obtained on the basis of the proposed model, and the solid lines indicate ATM data. In general, the agreement of these data is acceptable for engineering calculations.

2. Results of numerical calculation

A large number of works are devoted to development of numerical methods for solving boundary value problems of heat conduction. Basics of finite difference methods are detailed in the

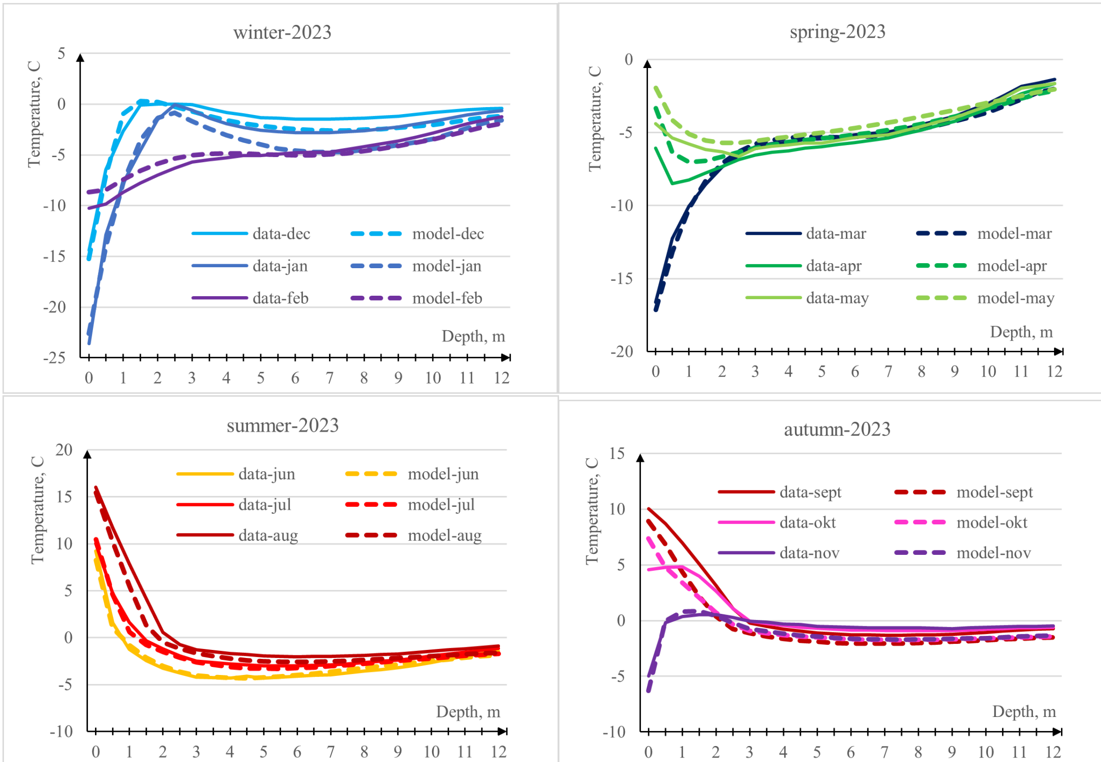

Fig. 2. Comparison of temperature sensor data in well 44–1 with numerical calculation data in the seasons 2023

works [24, 25]. To solve the Stefan problem for the equation (1), the finite difference method using the method of splitting in spatial variables has proven itself well [19].

In numerical calculations, an orthogonal condensed mesh is used. In the $\{x, y\}$-plane, the computational grid is condensed around the elements of the pile foundation (piles and SCDs) and thermometric wells, which are used to set the initial temperature distribution in the three-dimensional computational domain, as well as to test the developed software.

Calculations show that we can use as a computational grid consisting of $331 \times 154 \times 39 = 1987986$ nodes. The calculations were carried out on the supercomputer Uran in N. N. Krasovskii Institute of Mathematics and Mechanics (Yekaterinburg). The time step during the numerical experiments was chosen to be 1 day.

Let us consider the dynamics of changes in the bearing capacity of the pile foundation from 2021 to 2023. To do this, using the developed software, we will determine the bearing capacity of each of the 229 piles. Let us introduce the concept of the average bearing capacity of all piles, equal to the sum of the bearing capacities of all piles on the first day of each month, divided by the number of piles. Fig. 3 shows the change in this characteristic from November 2021 to October 2023. The bearing capacity of all piles is measured in tf. Note that $1tf = 9806,65N$.

To study the bearing capacity of piles, it is also useful to consider the minimum annual average bearing capacity, the average annual average bearing capacity, and the maximum annual average bearing capacity. Fig. 3(b) shows these characteristics. It can be noted that in 2022 there was a noticeable decrease in the maximum average annual bearing capacity, which is explained by a warmer winter period compared to the winter period in 2021 (Fig. 4). In 2023, the winter period became colder than in 2021. In 2022 the maximum average annual bearing capacity increased.

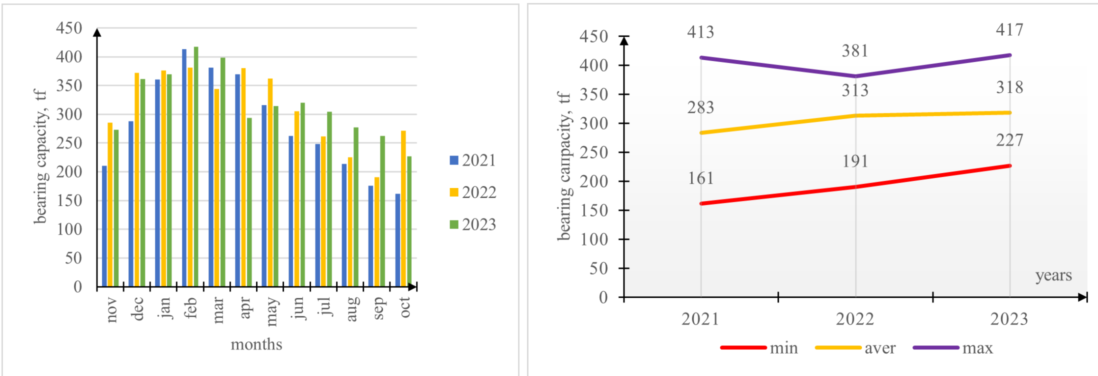

(a) (b)

Fig. 3. Average bearing capacity (a) and minimum, average and maximum bearing capacities (b) in 2021, 2022, 2023

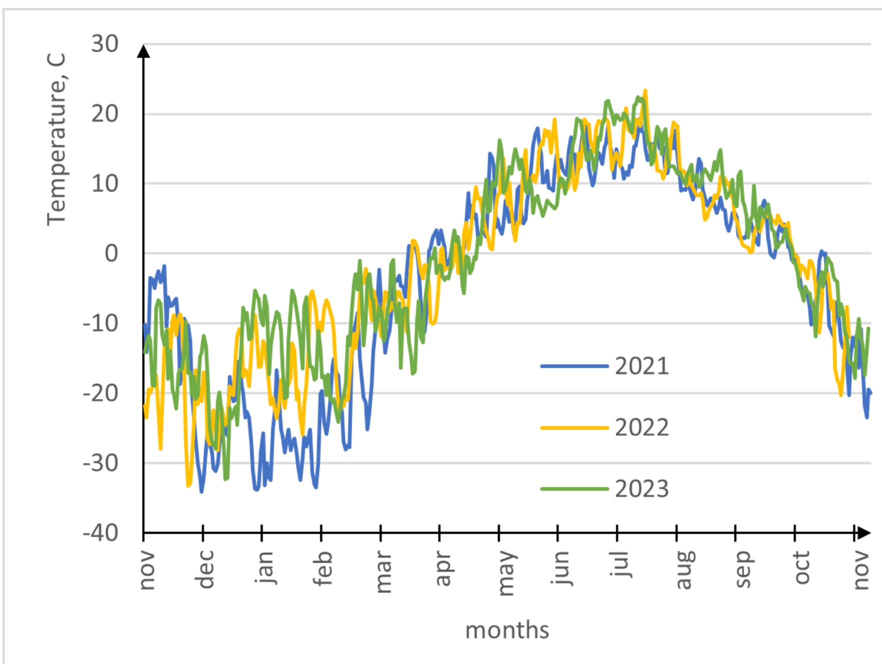

Fig. 4. Air temperature in a ventilated crawl space in 2021, 2022, 2023

For the practical use of the obtained average characteristics, the minimum annual average characteristic is of particular interest, which must be considered when designing and operating residential buildings in regions with permafrost. Numerical calculations did not record a critical change in the bearing capacity of the piles for Building I.

3. Discussions and conclusions

To assess the bearing capacity of piles for residential buildings in permafrost regions, a new model was developed that considers the accumulated ATM data, and a new method for simulating the operation of SCDs, which made it possible to evaluate the various characteristics of the bearing capacity of a specific pile foundation of a residential building. An important point of this study was the detailed validation of the developed numerical methodology on data obtained from temperature sensors placed in SAM wells.

Fig. 5 shows the air temperature in a ventilated crawl space in January 2024 from the temperature sensors at SAM station 44 (orange). If the air temperatures in different parts of the ventilated crawl space generally differ little from each other, then the temperatures on the surface $z = 0$, which is a concrete covering, can already differ significantly. For example, a comparison of surface temperatures at SAM well 44–1 (blue) and at the surface at SAM well 48–2 (yellow) shows that the difference on some days can reach 15°C (Fig. 5).

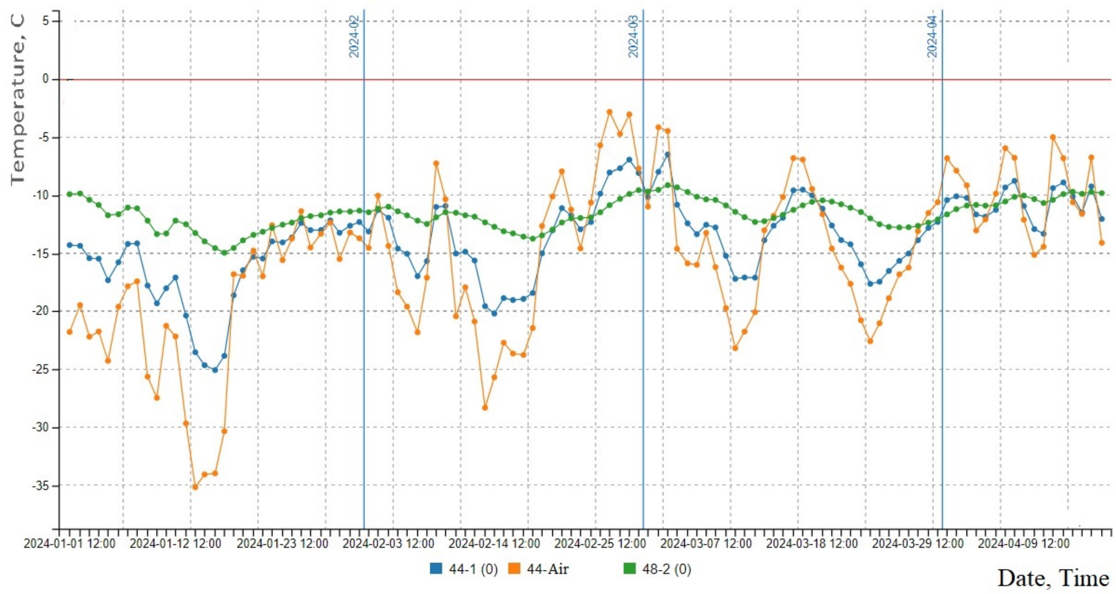

Fig. 5. Air temperature in a ventilated crawl space and surface temperature $z = 0$ at two points in January 2024

A similar situation with a significant difference in temperature on the surface $z = 0$ exists at other points. Fig. 6 shows changes in surface temperature in January 2024 near SAM well 45–1, which has a minimum average temperature at point 45–1(0), and near well 48–2, which has a maximum average temperature at point 48–2(0).

Such differences in surface temperatures can be associated with several factors: utility failures, snow falling into the ventilated crawl space from outside, different operating efficiency of the SCDs, and the presence of utilities, which, despite the necessary thermal insulation, can be additional sources of heat. In any case, to more adequately describe the dynamics of changes in the temperature regime of the soil around the foundation piles, it is advisable to use a two-dimensional approximation of surface temperatures, taking into account the accumulated ATM data and the correct setting of the SCD operation. This approach will also make it possible to carry out numerical calculations in the event of utility accidents, when the surface temperature can increase significantly in winter, first due to the influx of water, and then due to its freezing and the formation of additional thermal insulation of the surface, when a local thermal anomaly occurs that changes the bearing capacity of the soil. Based on a new algorithm for taking into account the influence of SCDs and ATM data on the temperature regime of the soil around foundation piles, software was developed, the validation of which was tested on the available

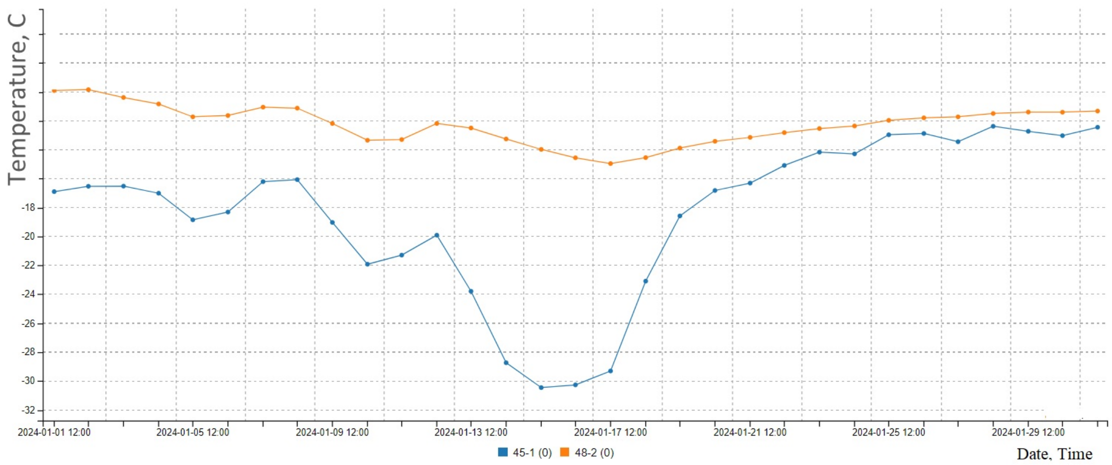

Fig. 6. Surface temperature in a ventilated crawl space of Building I in January 2024

data from temperature sensors from SAM wells. A good agreement between the ATM data and the obtained numerical calculation data was obtained. The greatest difference between the calculated data and the ATM temperature data was observed in the winter months when the bearing capacity of the piles is maximum. This difference may be associated with the need to use the above-described method for setting the temperature on the surface, as well as with the Gibbs-Thomson effect, which is associated with the presence of unfrozen water in the soil, which leads to a change in the shape of the interphase boundary and a decrease in the freezing point of the soil. It was noted in [26] that the deviation of the calculation results from the experimental data gradually increases with decreasing temperature. In our case, comparison of numerical calculations and ATM data in September and October (Fig. 2) showed good agreement. During these months, the soil is the warmest after the summer season, and therefore has a minimum bearing capacity, which is most often used when assessing the reliability of a pile foundation.

The authors thank State Scientific Center of Arctic Research, A. N. Shein and S. A. Kurakov for the development and maintenance of an automatic monitoring system and thermometric equipment in the city of Salekhard (Yamal-Nenetz Autonomous District, Russia).

The work was supported by the Russian Science Foundation grant number 24–21–00160.

References

[1] N.I.Shiklomanov et al., Climate change and stability of urban infrastructure in Russian permafrost regions: prognostic assessment based on GCM climate projections, *Geographical review*, **107**(2017), no. 1, 125–142. DOI: 10.1111/gere.12214

[2] S.J.Hassol et al., Impacts of a warming Arctic: Arctic climate impact assessment, *Cambridge University Press*, 2004, 28–44.

[3] S.E.Chadburn et al., An observation-based constraint on permafrost loss as a function of global warming, *Nat. Clim. Change*, **7**(2017), 340–344. DOI: 10.1038/nclimate3262

[4] F.E.Nelson, O.A.Anisimov, N.I.Shiklomanov, Climate change and hazard zonation in the circum-Arctic permafrost regions, *Nat. Haz.*, **26**(2002), 203–225.

[5] A.A.Vasiliev et al., Permafrost degradation in the Western Russian Arctic, *Environmental Research Letters*, **15**(2020), 045001. DOI: 10.1088/1748-9326/ab6f12

[6] N. Vaganova, M.Y.Filimonov Different shapes of constructions and their effects on permafrost *AIP Conference Proceedings*, **1789**(2016), 020019. DOI: 10.1063/1.4968440

[7] M.Yu.Filimonov, N.A.Vaganova, Thawing of permafrost during the operation of wells of North-Mukerkamyl oil and gas field, *J. Sib. Fed. Univ. Math. Phys.*, **14**(2021), no. 6, 795–804. DOI: 10.17516/1997-1397-2021-14-6-795-804

[8] V.E.Romanovsky et al., Thermal state of permafrost in Russia, *Permafr. Periglac. Process.*, **21**(2010), 136–155. DOI: 10.1002/ppp.683

[9] R.P.Daanen et al., Permafrost degradation risk zone assessment using simulation models, *The Cryosphere*, bf 5(2011), 1043-1056. DOI: 10.5194/tc-5-1043-2011

[10] J. Hjort et al., Degrading permafrost puts Arctic infrastructure at risk by mid-century, *Nat. Commun.*, **9**(2018), 5147. DOI: 10.1038/s41467-018-07557-4

[11] L.Suter, D.Streletskiy, N.Shiklomanov, Assessment of the cost of climate change impacts on critical infrastructure in the circumpolar Arctic *Polar Geography*, **42**(2019). no. 12, 1–20. DOI: 10.1080/1088937X.2019.1686082

[12] Z.Sun et al., Effects of ground subsidence on permafrost simulation related to climate warming, *Atmosphere*, **15**(2023), no. 1, 12. DOI: 10.3390/atmos15010012

[13] T. J.Bouffard et al., Scientific cooperation: supporting circumpolar permafrost monitoring and data sharing, *Land*, **10**(2021), no. 6, 590. DOI: 10.3390/land10060590

[14] A.N.Gromadsky, S.V.Arefiev, N.G.Volkov, Y.K.Kamnev, A.I.Sinitsky, Remote monitoring of the temperature regime of permafrost soils under the buildings of Salekhard, *Sci. bull. of the Yamalo-Nenets Autonomous Okrug*, **3**(2019), 17–21 (in Russian).
DOI: 10.26110/ARCTIC.2019.104.3.003

[15] Ya. K.Kamnev, M. Yu.Filimonov, A.N.Shein, N.A.Vaganova, Automated monitoring the temperature under buildings with pile foundations in Salekhard, *Geography, Environment, Sustainability*, **14**(2021), no. 4, 75–82. DOI: 10.24057/2071-9388-2021-021

[16] M.Y.Filimonov, Y.K.Kamnev, A.N.Shein, N.A.Vaganova, Modeling the temperature field in frozen soil under buildings in the city of Salekhard taking into account temperature monitoring, *Land*,**11**(2022), no. 7, 1102. DOI: 10.3390/land11071102

[17] L.M.Baisheva, P.P.Permyakov, A.M.Bolshakov, Heat and mass transfer of a coolant in horizontal seasonal cooling devices, *IOP Conference Series: Materials Science and Engineering*, **753**(2020), no. 4, 042092 ḊOI: 10.1088/1757-899X/753/4/042092

[18] G. P. Pustovoit, On the potential of seasonal in-ground cooling devices, *Soil Mechanics and Foundation Engineering*, **42**(2005), no. 4, 142–146. DOI: 10.1007/s11204-005-0040-9

[19] A.A.Samarsky, P.N.Vabishchevich, Computational Heat Transfer, Volume 2, The Finite Difference Methodology, New York, Chichester, Wiley, 1995.

[20] P.Lamontagne-Halle, J.M.McKenzie, B.L.Kurylyk et al., Guidelines for cold-regions groundwater numerical modeling, *WIREs Water*, **7**(2020), 1467. DOI: 10.1002/wat2.1467

[21] X.Yang, J.Hu, R Ma, Z.Sun, Integrated hydrologic modelling of groundwater-surface water interactions in cold regions, *Front. Earth. Sci.*, **9**(2021). DOI: 10.3389/feart.2021.721009

[22] B.L.Kurylyk et al., Influence of vertical and lateral heat transfer on permafrost thaw, peatland landscape transition, and groundwater flow, *Water Resour. Res.***52**(2016), 1286–1305. DOI: 10.1002/2015WR018057

[23] S.C.Zipper, P. Lamontagne-Halle, J.M. McKenzie, A.V.Rocha, Groundwater controls on postfire permafrost thaw: water and energy balance effects, *Journal of Geophysical Research: Earth Surface*, **123**(2018), 2677–2694. DOI:10.1029/2018JF004611

[24] N.N.Yanenko, The method of fractional steps (The solution of problems of mathematical physics in several variables), Berlin, Springer-Verl., 1971.

[25] S.V.Patankar, Numerical Heat Transfer and Fluid Flow, New York, Hemisphere, 1980.

[26] Q.Li et al., Dynamic response of a large-diameter end-bearing pile in permafrost, *Sci. Rep.*, **14**(2024), 582. DOI: 10.1038/s41598-023-46639-2

Компьютерное моделирование температурных полей в грунте и несущей способности свайных фундаментов зданий на вечной мерзлоте

Михаил Ю. Филимонов
Наталия А. Ваганова
Институт математики и механики им. Н. Н. Красовского
Екатеринбург, Российская Федерация
Уральский федеральный университет
Екатеринбург, Российская Федерация
Давид Ж. Шамугия
Ирина М. Филимонова
Уральский федеральный университет
Екатеринбург, Российская Федерация

Аннотация. Освоение обширных регионов, занятых вечной мерзлотой, сталкивается с проблемами, связанными с потеплением климата, которое способствует деградации вечной мерзлоты. Строительство жилых домов и их эксплуатация на этих территориях в основном предполагает поддержание грунта под этими сооружениями в мерзлом состоянии на протяжении всего периода их эксплуатации. Для этих целей используются свайные фундаменты и вентилируемые подполья. Сложность компьютерного моделирования возникает из-за учета сезонно действующих охлаждающих устройств, количество которых в конструкции современного здания определяется его размерами и в среднем может достигать 200 штук. Актуальной задачей является долгосрочное прогнозирование динамики изменения несущей способности свайного фундамента здания с учетом климатических и техногенных воздействий на окружающий грунт. Для этих целей были разработаны новая модель и численный алгоритм исследования динамики изменения несущей способности свай в процессе эксплуатации здания с учетом данных температурного мониторинга с датчиков температуры, расположенных в термометрических скважинах. Валидация разработанного программного комплекса проводилась на основе существующих и постоянно поступающих данных мониторинга температуры грунта до глубины до 10 метров. Сравнение полученных данных мониторинга и расчетных данных в термометрических скважинах показало значительное улучшение по сравнению с ранее использованной моделью и программой расчета для данного жилого дома.

Ключевые слова: математическое моделирование, тепломассоперенос, вечная мерзлота.

Journal of Siberian Federal University. Mathematics & Physics 2024, 17(5), 632–643

EDN: RAQXIG
УДК 517.95

Recovering Surface Fluxes on the Boundary of the Domain from Pointwise Measurements

Egor I. Safonov*
Sergey G. Pyatkov†
Daniil A. Parunov‡
Yugra State University
Khanty-Mansiysk, Russian Federation

Received 30.03.2024, received in revised form 29.05.2024, accepted 04.07.2024

Abstract. Inverse problems of recovering surface fluxes on the boundary of a domain from pointwise observations are considered. The prolbem is not well-posed in the Hadamard sense. Sharp conditions on the data ensuring existence and uniqueness of solutions in Sobolev classes are exposed and the numerical method relying on the finite element method in the space variables and a finite difference method in time is constructed. The results of numerical experiments are quite satisfactory and the procedure is stable under small perturbations.

Keywords: inverse problem, surface flux, convection-diffusion, pointwise measurement, Tikhonov's regularization.

Citation: E.I. Safonov, S.G. Pyatkov, D.A. Parunov, Recovering Surface Fluxes on the Boundary of the Domain from Pointwise Measurements, J. Sib. Fed. Univ. Math. Phys., 2024, 17(5), 632–643. EDN: RAQXIG.

Introduction

Under consideration is the parabolic equation

$$Mu = u_t - Lu = u_t - div(c(x,t)\nabla u) + \vec{a}(x,t)\nabla u + a_0(x,t)u = f, \tag{1}$$

where $c = diag(c_1(t,x), \ldots, c_n(t,x))$ is a diagonal matrix with strictly positive continuous entries, $(t,x) \in Q = (0,T) \times G$, $\vec{a}(x,t) = (a_1(x,t), \ldots, a_n(x,t))^T$, $\nabla u = \left(\frac{\partial u}{\partial x_1}, \ldots, \frac{\partial u}{\partial x_n}\right)^T$, $n = 2, 3$, and G is a domain in $\mathbb{R}^n$ with boundary Γ. The equation (1) is furnished with the initial-boundary conditions

$$Bu|_S = g(t,x) \ \ (S = (0,T) \times \Gamma), \quad u|_{t=0} = u_0(x), \tag{2}$$

where $Bu = \sum_{i=1}^{n} \nu_i c_i u_{x_i} + \sigma(t,x)u$, with ν being the outward unit normal to Γ, and with the overdetermination conditions

$$u(t, b_i) = \psi_i(t) \ (i = 1, 2, \ldots, r), \tag{3}$$

*c.gerz.hd@gmail.com
†s_pyatkov@ugrasu.ru
‡daniil19056@yandex.ru

where $\{b_i\}_{i=1}^r$ is a collection of points lying in G. It is possible that $\Gamma = \overline{\Gamma_0 \cup \Gamma_1}$ with $\Gamma_0 \cap \Gamma_1 = \emptyset$, Γ_0, Γ_1 are open subsets of Γ, and the condition (2) is given in the form

$$Bu|_{S_0} = g(t,x),\ u|_{S_1} = g_1(t,x)\ \ (S_i = (0,T) \times \Gamma_i,\ i = 0,1),\quad u|_{t=0} = u_0(x). \tag{4}$$

Assume that $g(t,x) = \sum_{i=1}^{r} \alpha_i(t)\Phi_i(x)$ for some known functions Φ_j, the problem consists in recovering both a solution to (1) satisfying (2), (3) (or (4), (3)) and functions α_j, $j = 1, 2, \ldots, r$. Note that any function g can be approximated by the sums of this form for a suitable choice of basis functions Φ_i.

Inverse problems of recovering the boundary regimes are classical. They arise in many different problems of mathematical physics, in particular, in the heat and mass transfer theory, diffusion, filtration (see [1–3]), and ecology [4–9].

A particular attention is payed to numerical solution of the problems (1)–(3) and close to them. Most of the methods are based on reducing the problems to optimal control ones and minimization of the corresponding quadratic functionals (see, for instance, [10–16]). However, it is possible that these functionals can have several local minima (see Section 3.3 in [17]) and the problem is not always well-posed. Describe some articles, where pointwise measurements are employed as additional data. Numerical determination of constant fluxes in the case of $n = 2$ is described in [11]. Similar results are presented in [18] for $n = 1$. The three-dimensional problem of recovering constant fluxes of green house gases is discussed in [4], but numerical results are presented only in the one-dimensional case. In [5] (see also [6]) the method of recovering a constant surface flux relying on the approach developed in [19] is described, where special solutions to the adjoint problem are employed (see also [7,8]). The surface fluxes depending on t are recovered in [3,14,20,21] in the case of $n = 1$, and in [13,23–25] in the case of $n > 1$. The flux depending on time and spatial variables is reconstructed in [16,26]. The case of flux depending on space variables is discussed in [25]. In this article the flux is sought a finite segment of a series with the use of piecewise linear basis of the finite element method. In literature, there are results in the case in which additional Dirichlet data are given on a part of the boundary and the flux is reconstructed with the use of these data on another part of the boundary (see [27]). The article [15] is devoted to the recovering of the flux $h(t,x)f(x)$ (the function $f(x)$ is unknown) with the use of final or integral overdetermination data. There is a limited number of theoretical results devoted to the problem (1)–(3). If the points $\{b_i\}_{i=1}^r$ are interior points of G then the problem is ill-posed and this fact was observed in many articles (see [28]).

In this article we describe some new theoretical results (see [29]) as applied to this problem, expose a new algorithm of calculating the flux based on our theoretical arguments and describe the results of numerical experiments. The method relies on the finite element method in the space variables and the finite difference method in time. The number of summands in the reprentatation of the function g depends on the number of measurements. The results of numerical experiments are quite satisfactory and the procedure is stable under small perturbations.

1. Preliminaries

The notations of the Sobolev spaces $W_p^s(G)$ and $W_p^s(Q)$ are conventional (see [30, 31]). Given an interval $J = (0,T)$, put $W_p^{s,r}(Q) = W_p^s(J; L_p(G)) \cap L_p\big(J; W_p^r(G)\big)$ and $W_p^{s,r}(S) = W_p^s(J; L_p(\Gamma)) \cap L_p\big(J; W_p^r(\Gamma)\big)$ [30]. By the norm of a vector, we mean the sum of the norms of its coordinates. Denote by $B_\delta(b)$ the ball of radius δ centered at b. The symbol $\rho(X,Y)$ stands for the distance between the sets X,Y.

The definition of the inclusion $\Gamma \in C^s$, $s \geqslant 1$, can be found in [31, Chapter 1]. The coefficients of the equation (1) are assumed to be real. We consider an elliptic operator L, i.e., there exists a constant $\eta_0 > 0$ such that $c_i(t,x) \geqslant \eta_0$ for all $(t,x) \in Q$ and $i = 1,\ldots,n$.

2. Recovering of the heat flux

Under consideration is the conventional heat and mass transfer model (1). We take $G = \Omega \times (0,Z)$, with $\Omega = (0,X)$ for $n = 2$ and Ω is a bounded domain with smooth boundary ($\partial\Omega \in C^2$) for $n = 3$. Let $\Gamma_0 = \{x \in \Gamma : \ x_n = 0\} = \{(0,x') : \ x' \in \Omega\}$ ($x' = (x_1,\ldots,x_{n-1})$) and let $S_0 = (0,T) \times \Gamma_0$. The problem is to find a solution to the equation (1) and the function $g = \sum\limits_{i=1}^{r} \alpha_i(t)\Phi_i(x)$ such that

$$u(b_i,t) = \psi_i(t), \ i = 1,2,\ldots,r, \ b_i \in G, \tag{5}$$

$$u|_{t=0} = u_0(x), \quad c_n u_{x_n}|_{S_0} = g(t,x), \quad u|_{S\setminus S_0} = 0. \tag{6}$$

One or more boundary conditions on $S \setminus S_0$ can be changed. This inverse problem arises in the problem of evaluation of the greenhouse gases emission from wetlands (see [4]).

We now expose some consequences of the results in [29]. Despite the fact that they refer to the model case when c is the identity matrix and the remaining coefficients are independent of t, they are rather sharp and we think that they are valid in more general situation as well. Moreover, the conditions on the data below are actually used in the numerical algorithm. We consider the model problem

$$u_t + Lu = f(t,x), \quad Lu = -\Delta u + \sum_{i=1}^{n} a_i(x) u_{x_i} + a_0(x)u, \tag{7}$$

$$u|_{t=0} = u_0(x), \quad u_{x_n}|_{S_0} = g(t,x), \quad u|_{S\setminus S_0} = 0, \tag{8}$$

$$u(t,b_i) = \psi_i(t) \ (i = 1,2,\ldots,r). \tag{9}$$

As before, the problem consists in recovering both a solution to (7) satisfying (8) and (9) and functions α_i, $i = 1,2,\ldots,r$, characterizing the function $g = \sum\limits_{i=1}^{r} \alpha_i(t)\Phi_i(x)$. We assume that

$$b_i \in K = \{x \ \in G : \ x_n < \rho(x, \Gamma \setminus \Gamma_0)\}. \tag{10}$$

Let $b_i' = (b_{i\,1},\ldots,b_{i\,n-1},0)$, where b_{ij} is the j-th coordinate of the point b_i. It is naturally to assume that $b_i' \neq b_j'$ for $i \neq j$. Let G_δ be the δ-neighborhood about the points b_i' ($i = 1,2,\ldots,r$). Denote $\Gamma_\delta = G_\delta \cap \Gamma_0$. Our conditions for the data have the form

$$a_i \in W_\infty^2(G) \ (i = 1,\ldots,n), \ a_0 \in L_\infty(G), \tag{11}$$

$$u_0(x) \in W_2^1(G), \ f \in L_2(Q), \tag{12}$$

$$\Phi_i(x') \in W_2^{1/2}(\Gamma_0), \ \mathit{supp}\,\Phi_i \subset \Omega, \tag{13}$$

there exists $\delta_0 > 0$, $\delta_0 < \min_i \rho(b_i, \Gamma \setminus \Gamma_0)$ such that

$$\Phi_i(x) \in W_2^1(\Gamma_{\delta_0}) \text{ for } \ n = 2, \quad \Phi_i(x) \in W_2^2(\Gamma_{\delta_0}) \text{ for } \ n = 3, \ i = 1,\ldots,r, \tag{14}$$

$$a_0 \in W^1_\infty(G_{\delta_0} \cap G). \tag{15}$$

Under the conditions (11), (12), there exists a unique solution w_0 to the problem (7), (8), where $g = 0$, such that $w_0 \in W_2^{1,2}(Q)$ (see [33]). Changing the variables $w = u - w_0$, we obtain the simpler problem

$$w_t + Lw = 0, \quad w_{x_n}|_{S_0} = g(t, x), \quad w|_{S\setminus S_0} = 0, \quad w|_{t=0} = 0, \tag{16}$$

$$w(b_i, t) = \psi_i(t) - w_0(t, b_i) = \tilde{\psi}_i(t), \ i = 1, 2, \ldots, r. \tag{17}$$

We assume that the functions $\tilde{\psi}_i(t)$ admit the representations

$$\tilde{\psi}_i(t) = \int_0^t V_{\delta_i}(t-\tau)\psi_{0i}(\tau)d\tau, \quad \psi_{0i} \in \tilde{W}_2^{n/4}(0,T) \ (n = 2, 3), \tag{18}$$

where $V_\gamma(t) = \dfrac{e^{-\gamma^2/4t}}{4\pi t}$ for $n = 2$ and $V_\gamma = \dfrac{\gamma e^{-\gamma^2/4t}}{2\sqrt{\pi}t^{3/2}}$ for $n = 3$. Denote by Ψ the matrix with the entries $\Psi_{ij} = \Phi_j(b'_i)$ $(i, j = 1, 2, \ldots, r)$ and assume that

$$det\, \Psi \neq 0. \tag{19}$$

Theorem 1. *Assume that the conditions* (10)–(14)*,* (18)*,* (19)*, and* (15) *for* $n = 3$ *hold. Then there exists a unique solution to the problem* (7)–(9) *such that* $u \in W_2^{1,2}(Q)$*,* $\alpha_i(t) \in W_2^{1/4}(0,T)$ $(i = 1, 2, \ldots, r)$*.*

Proof. The claim results from Theorem 5 in [29]. First of all, we note that in [29] $\Gamma \in C^2$. Nevertheless, the arguments of the proof remain valid since $W_2^{1,2}(Q)$-solvability of the boundary value problem (7), (8) holds. The well-posedness condition from [29] is reduced to the condition (19). The condition (10) ensures that the sets $\{b \in \Gamma : \ \rho(b_j, \Gamma) = |b_j - b|\}$ consist of one point $b'_j \in \Gamma_0$ and the conditions (10), (13), (14), (18), (19) guarantee the fulfillment of other conditions of Theorem 5 in [29].

Note that the condition (18) is sharp and cannot be weakened. □

3. Numerical algorithm

Describe the numerical algorithm. Consider the case of $n = 2$. We employ FEM (the finite element method). We need to find the functions $\{\alpha_i(t)\}$. As for the functions Φ_i, we can use the piecewise linear basis of FEM, in this case we obtain a piecewise linear approximation of g. Sometimes, it is better to use smoother function. We use some analog of the FEM basis. Define a collection of numbers $x_1^1 < x_1^2 < \ldots, x_1^r$. Let $x_1^0 = \varepsilon > 0$, $x_1^{r+1} = X - \varepsilon$, with ε a sufficiently small parameter. Let $\delta_i = (x_1^{i+1} - x_1^{i-1})/2$, $i = 1, 2, \ldots, r$. Assign

$$\Phi_i(x_1) = \begin{cases} \dfrac{1}{2}\left(1 + \cos\left(\dfrac{\pi}{\delta_i}\left(x_1 - \dfrac{x_1^{i-1} + x_1^{i+1}}{2}\right)\right)\right), \ x_1 \in \left[x_1^{i-1}, x_1^{i+1}\right] \\ 0, \ x_1 \notin \left[x_1^{i-1}, x_1^{i+1}\right] \end{cases} \in W^2_\infty(0, X) \tag{20}$$

for $i = 1, 2, \ldots, r$. Make an additional change of variables

$$v = u - \Phi, \quad \Phi = \sum_{i=1}^{r} \psi_i(t) \frac{x_1^2(x_1 - X)^2 \prod_{j\neq i}(x_1 - x_1^j)}{(x_1^i)^2(x_1^i - X)^2 \prod_{j\neq i}(x_1^i - x_1^j)} \frac{(Z - x_2)}{(Z - x_2^i)}. \tag{21}$$

The function v is a solution to the problem

$$Mv = f - M\Phi = f_0, \quad v(b_i,t) = 0, \ i = 1,2,\ldots,r, \ v|_{t=0} = u_0(x) - \Phi(0,x), \tag{22}$$

$$c_2 v_{x_2}|_{S_0} = g(t,x_1) - g_0(t,x_1) = \tilde{g}, \quad v|_{S\setminus S_0} = 0, \ g_0 = c_2(t,x_1,0)\Phi_{x_2}(t,x_1,0). \tag{23}$$

Describe the method. Construct a triangulation of the domain G and the corresponding basis $\{\varphi_i\}_{i=1}^N$ of FEM. Denote the nodes by $\{y_i\}$. We look for an approximate solution in the form $v = \sum\limits_{i=1}^{N} C_i(t)\varphi_i$. For convenience, we assume that the points $b_i = (b_1^i, b_2^i)$ $(i = 1,2,\ldots,r)$ agree with the nodes $y_{N-r+1},\ldots,y_N$. The functions $C_i(t)$, $i = 1,2,\ldots,N$, are a solution to the system

$$M\vec{C}_t + K\vec{C} = -\vec{F} + \vec{f_0}, \quad \vec{C} = (C_1,C_2,\ldots,C_N)^T, \tag{24}$$

where

$$\vec{F} = \left(\int_0^X g(t,x_1)\varphi_1(x_1,0)\,dx_1,\ldots,\int_0^X g(t,x_1)\varphi_N(x_1,0)\,dx_1\right)^T,$$

and the coordinates of the vector $\vec{f_0}$ are of the form

$$f_i = (f_0(t,x),\varphi_i) + \int_0^X g_0(t,x_1)\varphi_i(x_1,0)\,dx_1, \quad (f_0(t,x),\varphi_i) = \int_G f_0(t,x)\varphi_i\,dx.$$

The matrices M and K have the entries $M_{ij} = (\varphi_i,\varphi_j) = \int\limits_G \varphi_i(x)\varphi_j(x)\,dx$ and

$$K_{jk} = (c_1(t,x)\varphi_{kx_1},\varphi_{jx_1}) + (c_2(t,x)\varphi_{kx_2},\varphi_{jx_2}) + (a(t,x)\nabla\varphi_k,\varphi_j) + (a_0(t,x)\varphi_k,\varphi_j),$$

respectively. We have that $\vec{C}(0) = v_0$. A solution to the system (24) is defined by the finite difference method. Define the step in time $\tau = T/m$ and replace (24) with the system

$$M\frac{\vec{C}_{i+1} - \vec{C}_i}{\tau} + K_{i+1}\vec{C}_{i+1} = -\vec{F}_{i+1} + \vec{f}_{i+1}, \quad \vec{C}_i = (C_i^1,\ldots,C_i^N)^T, \ i = 0,1,2,\ldots,m-1, \tag{25}$$

where $C_i^k \approx C_k(\tau i)$, $\vec{F_i} \approx \vec{F}(\tau i)$, $\vec{f_i} = \vec{f_0}(\tau i)$, $K_i = K(\tau i)$. The system (25) can be written as follows:

$$R_{i+1}\vec{C}_{i+1} = -\tau\vec{F}_{i+1} + \tau\vec{f}_{i+1} + M\vec{C}_i, \ C_i^k = C_k(\tau i), \ \vec{C}_i = (C_i^1,\ldots,C_i^N)^T, \ i = 0,1,2,\ldots,m-1, \tag{26}$$

where $R_{i+1} = M + \tau K_{i+1}$. Assign $\vec{\alpha}_i = (\alpha_i^1,\ldots,\alpha_i^r)^T$, $\vec{\alpha}_i \approx \vec{\tilde{\alpha}}(\tau i)$, $\alpha_i^k \approx \tilde{\alpha}_k(i\tau)$.

In view of (22), we must have $C_k^{N-r+i} = 0$ $(i = 1,2,,\ldots,r)$. Assign $C_0^k = v_0(b_k)$ $(k = 1,\ldots,N)$. The numbers α_0^k are solutions to the system

$$\sum_{i=1}^{r} \alpha_0^i \Phi_i(x_1^k) = c_2(0,x_1,0)u_{0x_2}(b_k'). \tag{27}$$

In dependence of smoothness of a solution we can require the consistency conditions

$$\sum_{i=1}^{r} \alpha_0^i \Phi_i(x_1) = c_2(0,x_1,0)u_{0x_2}(x_1,0), \ \forall x_1 \in (0,X),$$

with α_0^i a solution to the system (27). But they are not necessary, for example, for solutions $u \in W_2^{1,2}(Q)$. We also assume that

$$\det\{\Phi_i(b_1^k)\}_{k,i=1}^r \neq 0, \ \psi_i(t) \neq 0 \ \forall t, i. \tag{28}$$

Assume that we have found the vectors $\vec{\alpha}_i$, $\vec{C}_i$. We seek the quantity $\vec{C}_{i+1}$ as a solution to the system

$$R_{i+1}\vec{C}_{i+1} = -\tau B\vec{\alpha}_{i+1} + \tau\vec{f}_{i+1} + M\vec{C}_i, \tag{29}$$

where $N\times r$-matrix B has the entries $b_{kj} = \int\limits_0^X \Phi_j(x_1)\varphi_k(x_1,0)\,dx_1$ $(j = 1,2,\ldots,r,\ k = 1,\ldots,N)$. The vector $\vec{\alpha}_{i+1}$ is determined from the system

$$\tau B_{i+1}\vec{\alpha}_{i+1} = \tau\Phi_0 R_{i+1}^{-1}\vec{f}_{i+1} + \Phi_0 R_{i+1}^{-1}M\vec{C}_i \tag{30}$$

where the matrix $B_{i+1} = \Phi_0 R_{i+1}^{-1} B^{i+1}$ of dimension $r\times r$, where Φ_0 is a $r\times N$-matrix whose first $N-r$ columns are occupied by zeros and and the last r columns is the identity matrix of dimension $r\times r$. The matrix B_i can be singular (with small elements). To improve the convergence, we employ the Tikhonov regularization. So we replace the system (29) with the system

$$\tau(B_{i+1}^* B_{i+1} + \varepsilon)\vec{\alpha}_{i+1} = \tau B_{i+1}^*\Phi_0 R_{i+1}^{-1}\vec{f}_{i+1} + B_{i+1}^*\Phi_0 R_{i+1}^{-1}M\vec{C}_i,\ \varepsilon > 0, \tag{31}$$

where B_{i+1}^* is the adjoint matrix.

4. Program implementation and results of numerical experiments

In this section, we analyze the results of numerical experiments for several groups of input data. We will consider the dependence of accuracy of determining the coefficients α_i and the function u on the number N of points of the triangulation grid, the number of the overdetermination points b_i and the distance l between them. The coefficients in (1) are defined as follows: $a_0 = 1/(t+1)$, $a_1 = x$, $a_2 = y$, $c_1 = x+2$, $c_2 = y+2$. Characteristics of the computer: Processor: Intel(R) Xeon(R) CPU E5-2678 v3 @ 2.50GHz (2 processors); RAM: 64.0 GB; System type: Windows 10 Pro 64-bit operating system.

First of all, we construct some test data. To define test functions, we construct a solution u to the direct problem (1), (6) with the known boundary condition (6) and the function g depending on the known functions Φ_i and α_i. Next, we take a collection of points b_i and determine the data (5). Solving the inverse problem (1), (5), (6), we find a solution u and the functions $\{\alpha_i\}$. Comparing given function $\{\alpha_i\}$ and obtained after calculations, we can estimate the convergence of the algorithm. To abbreviate the exposition, only graphs of the functions constructed and the results of calculating the parameters α_i will be presented.

Each experiment includes sequential steps:

- Setting the number and coordinates of overdetermination points and the functions α_i;
- Initialization of the domain for constructing a solution to the direct and inverse problems;
- Definition of service arrays of points;
- Solving the direct problem (1), (6);
- Construction of the functions Φ_i and the auxiliary function Φ;
- Solving the inverse problem (22)–(23), restoring the solution u and the function α_i.

Present the software implementation for the first group of data, for the rest we will present only pivot tables.

For the first group of experiments, we take $r = 3$. The overdetermination points b_i have the coordinates: $(0.2; 0.2)$, $(1; 0.5)$, and $(1.8; 0.8)$. We take $\alpha_1 = t+2$, $\alpha_2 = (t-2)^2$, and $\alpha_3 = (t+1)^3$.

Experimentally, it was found that the change in the number of grid points in time m practically does not affect the accuracy of the calculations, so we take it equal to 100. It was also found that with an increase in the number of time points m, it is necessary to decrease the regularization parameter ε, for example, for $m = 200$, you need to take $\varepsilon \leqslant 10^{-10}$, otherwise the algorithm will diverge. For all groups of experiments, we take the parameter $\varepsilon = 10^{-7}$.

1) As the domain of constructing the solution to the problem (1), (5), (6), we take a rectangle with sides $A = 2$ and $B = 1$ located along the axes x_1 and x_2, respectively. The lower left corner of the rectangle is at the point $(0; 0)$, we will use this domain for all groups of experiments. Let's add to the domain r circles with radii $R = 0.1$ and centered at the points b_i.

Using Delaunay triangulation, we get the first mesh Z_0 with 214 nodes. The new grids are obtained by dividing each triangle of the previous grid into 4 parts, we get $Z_1 = 812$ and $Z_2 = 3163$, the Fig. 1.

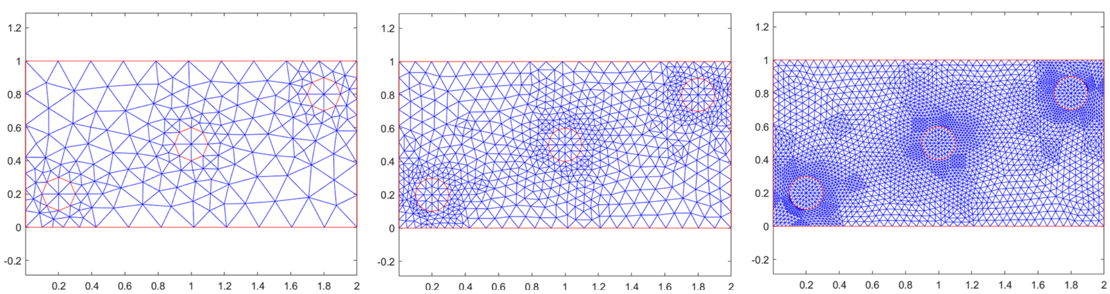

a) b) c)

Fig. 1. Zone with nodes a) $Z_0 = 214$; b) $Z_1 = 812$; c) $Z_2 = 3163$

2) Further, after constructing the triangulation mesh, it is necessary to determine the collections of indices of points, including the points b_i.

3) The time step is defined as $\tau = T/m$. To solve the direct problem (1), (6), we define the right-hand side $f = 1$ (see (1)), the initial condition $u_0 = 1$ and boundary function g assuming that α_i are known. The functions Φ, Φ_i, and the respective function g are constructed in accord with the formulas from the previous section (see (21), (20)). Note that with these almost arbitrary initial data, the consistency conditions at $t = 0, x_2 = 0$ are not fulfilled. This gives rise a large oscillation of a solution at $t = 0$. So, it is necessary to cut off a part of the solution that has a large error at the initial time points which arise in the calculations. One more variant which was used is to define the time shift variable as $\tau_s = 20 \cdot T/m$. It is necessary to extend the time line by changing the start point to $-\tau_s \cdot T/m$. With the shift in time, we get $m + \tau_s + 1$ time points. This stage is not obligatory.

4) A solution to the direct problem (1), (6) is defined by the formulas of the previous section, except for the equation (26) which is replaced with

$$\vec{C}_{i+1} = (M_{i+1} + \tau K_{i+1})^{-1} \cdot (-\tau \vec{G}_{i+1} + \tau \vec{F}_{i+1} + M_{i+1}\vec{C}_i), \ C_i^k = C_k(\tau i), \tag{32}$$

where $\vec{C}_j = (C_j^1, \ldots, C_j^{N-lp-tp-rp})^T, \ j = 0, 1, 2, \ldots, m + \tau_s$.

5) We calculate the functions $M\Phi$, f_0 (see (22)), and the first time derivative of the data $\psi_t^i = (\psi_i((j+1)\tau) - \psi_i(j\tau))/\tau$.

6) For further analysis of the results of solving the problem (22)–(23) and restoring the solution u, we introduce the following quantities that describe the calculation errors: the parameter

$\varepsilon_\alpha = \max_i(\max_j |\alpha^j(i\tau) - \alpha_i^j|)$, where the numbers α_i^j are the results of calculations, $j = 1, \dots, r$; $\varepsilon_u = \max_{i,j} |u_{i,j} - u(y_i, \tau j)|$ is the error in calculating the concentration of a pollutant, where $i = 1, 2, \dots, N$ and $j = 1, 2, \dots, m$. Let T_τ be the total running time of the algorithm, including the time to solve the direct problem, in seconds. The calculation results for three previously defined grids are presented on the Fig. 2.

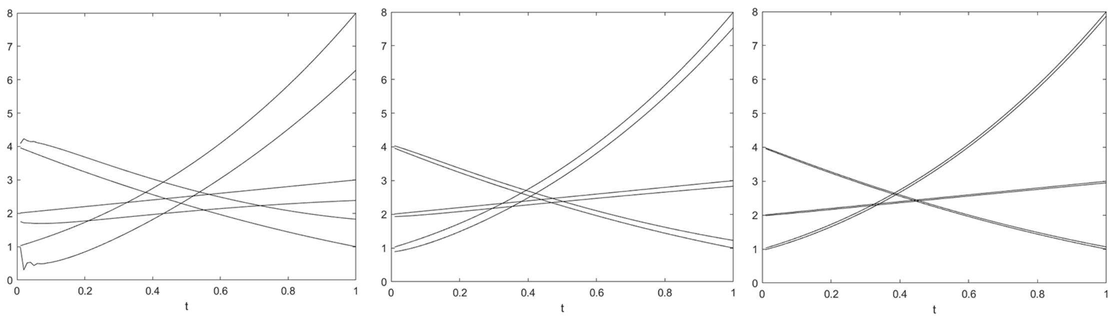

a) b) c)

Fig. 2. The results of calculations of functions α_i on the grids a) Z_0; b) Z_1; c) Z_2

It is quite natural that an increase in the number of nodes leads to an increase in the accuracy of calculations. In this case, the calculation error ε_α, ε_u and the calculation time T_τ for three grids, respectively, are equal to $(1.7116, 0.0996, 74)$, $(0.4589, 0.0285, 238)$, $(0.1306, 0.0082, 1052)$. As is easily seen, the error is inversely proportional to the number of nodes.

Even in the case of the grids Z_0 and Z_1, solutions obtained repeat the profile of the desired solution. In this case, taking into account the increasing computation time, in subsequent experiments we will use Z_0.

For the second group of experiments, we take one overdetermination point and the function $\alpha_1 = \log(t+1)$. The other data are the same.

We present a summary table indicating a different number and coordinates of overdetermination points, the functions α_i, received errors, and calculation time, Tab. 1.

Table 1. Summary table

No	b_i	ε_α	ε_u	τ_s
1	(0.5;0.3)	0.0303	0.0037	35.7
2	(0.5;0.5)	0.0384	0.0044	35.8
3	(0.5;0.7)	0.0572	0.0056	35.4
4	(1;0.3)	0.0248	0.0041	38.1
5	(1;0.5)	0.0315	0.0053	39.2
6	(1;0.7)	0.0475	0.0065	37.9
7	(1.5;0.3)	0.0374	0.0059	37.6
8	(1.5;0.5)	0.0443	0.0078	36
9	(1.5;0.7)	0.0679	0.0098	36.7

According to the results obtained, it can be seen that, despite the use of the grid Z_0, the solutions are quite accurate. The error increases as the distance from the lower bound increases, which corresponds to the theoretical results (Theorem 1).

For the next part of the experiments, we will add random noise to each point of the array of the right-hand side vector, the noise value will be denoted by $n_z(i,j)$. Thus we get $f(i,j) = f(i,j) \cdot (1 + n_z(i,j))$, with $f(i,j)$ the right-hand side in the system, the results are presented in Fig. 3. The coordinates of overdetermination point (0.5; 0.3) and all other parameters are the same.

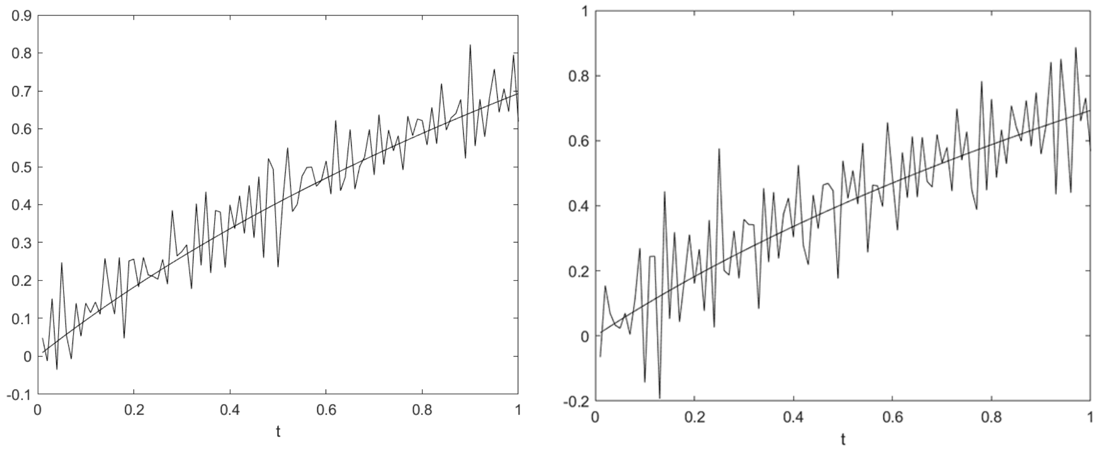

a) b)

Fig. 3. Result of calculations of the function α_1 on a grid with noise a) $n_z = 25\%$; b) $n_z = 50\%$

Despite the introduced noise, the algorithm still shows good convergence, the calculation errors are ε_α, ε_u: (0.19, 0.009) and (0.35, 0.017), respectively.

For the third experimental group, form a table with data for two points with the required functions $\alpha_1 = (t-2)^2$ and $\alpha_2 = \log(t+1)$. The remaining data are the same.

Table 2. Summary table

No	b_i	ε_α	ε_u	τ_s
1	(0.5; 0.3), (1; 0.3)	0.074	0.0067	48.6
2	(0.5; 0.3), (1; 0.5)	0.094	0.0087	50.8
3	(0.5; 0.3), (1; 0.7)	0.149	0.0154	51.7
4	(0.5; 0.3), (1.5; 0.3)	0.058	0.005	52.4
5	(0.5; 0.3), (1.5; 0.5)	0.083	0.0063	53.1
6	(0.5; 0.3), (1.5; 0.7)	0.145	0.011	52.5
7	(0.5; 0.5), (1; 0.3)	0.048	0.0047	50.6
8	(0.5; 0.5), (1; 0.5)	0.077	0.0069	50.7
9	(0.5; 0.5), (1; 0.7)	0.129	0.0097	49.7
10	(0.5; 0.5), (1.5; 0.3)	0.038	0.0046	54.5
11	(0.5; 0.5), (1.5; 0.5)	0.069	0.0052	53.6
12	(0.5; 0.5), (1.5; 0.7)	0.12	0.0083	52.5
13	(0.5; 0.7), (1; 0.3)	0.097	0.0086	49.9
14	(0.5; 0.7), (1; 0.5)	0.072	0.0057	50.1
15	(0.5; 0.7), (1; 0.7)	0.067	0.005	49.5
16	(0.5; 0.7), (1.5; 0.3)	0.054	0.0037	49.9

According to the data obtained, it is possible to confirm the conclusion made earlier that the distance between the points does not affect the accuracy of the calculation. Also, an increase in the number of overdetermination points and the unknown functions α_i increases the calculation error.

This work was supported by the Russian Science Foundation and the Government of the Khanty-Mansiysk Autonomous Okrug-YUGRA (Grant no. 22-11-20031).

References

[1] O.M.Alifanov, E.A.Artyukhin, A.V.Nenarokomov, Inverse Problems in the Study of Complex Heat Transfer, Janus-K, Moscow, Russia, 2009.

[2] V.N.Tkachenko, Mathematical Modeling, Identification and Control of Technological Processes of Heat Treatment of Materials, Naukova Dumka, Kiev, Ukraine, 2008.

[3] O.M.Alianov, M.A.Kukushkin, Control of heat exchange parameters on the aircraft surface, *Ideas and Innpovations*, **10**(2022), no. 1-2, 69–73 (in Russian). DOI: 10.48023/2411-7943_2022_10_1-2_69

[4] M.V.Glagolev, A.F.Sabrekov, Determination of gas exchange on the border between ecosystem and atmosphere, Inverse modeling, *Math. Biol. Bioinform,* (2012), no. 7, 81–101 (in Russian). DOI: 10.17537/2012.7.81

[5] M.V.Glagolev, Inverse modelling method for the determination of the gas flux from the soil, *Environ. Dyn. Glob. Clim. Chang.*, (2010), no. 1, 17–36 (in Russian). DOI:10.17816/edgcc1117-36

[6] A.F.Sabrekov, M.V.Glagolev, I.E.Terentyeva, Determination of the specific flux of methane from soil using inverse modeling based on conjugate equations, In: Reports of the International Conference Mathematical Biology and Bioinformatics, Ed. V.D.Lakhno, IMPB: Pushchino, Russia, 2018, Vol, 7, Article No. e94.

[7] M.V.Glagolev, O.R.Kotsyurbenko, A.F.Sabrekov, Y.V.Litti, I.E.Terentieva, Methodologies for Measuring Microbial Methane Production and Emission from Soils — A Review, *Microbiology*, **90**(2021), 1–19. DOI: 10.1134/S0026261721010057

[8] A.I.Borodulin, B.D.Desyatkov, G.A.Makhov, S.R.Sarmanaev, Determination of the emission of bog methane from the measured values of its concentration in the surface layer of the atmosphere, *Meteorol. Hydrol.*, (1997), no. 1, 66–74.

[9] P.P.Permyakov, Recovering of boundary conditions for heat exchange modeling on the ground surface. Arctic XXI Century, Humanitarian Sciences, **17**(2019), no. 1, 27-35.

[10] S.Wang, L.Zhang, X.Sun, H.Jia, Solution to Two-Dimensional Steady Inverse Heat Transfer Problems with Interior Heat Source Based on the Conjugate Gradient Method, *Math. Prob. Eng.*, **2017**(2017), 2861342. DOI: 10.1155/2017/2861342

[11] S.A.Kolesnik, V.F.Formalev, E.L.Kuznetsova, On inverse boundary thermal conductivity problem of recovery of heat fluxes to the boundaries of anisotropic bodies, *High Temp.*, **53**(2015), 68–72. DOI: 10.7868/S0040364415010111

[12] M.J.Colaco, H.R.B.Orlande, Inverse natural convection problem of simultaneous estimation of two boundary heat fluxes in irregular cavities, *Int. J. Heat Mass Transf.*, **47**(2004), 1201–1215. DOI: 10.1016/j.ijheatmasstransfer.2003.09.007

[13] A.S.A.Alghamdi, Inverse Estimation of Boundary Heat Flux for Heat Conduction Model, *JKAU Eng. Sci.*, **21**(2010), 73–95. DOI: 10.4197/Eng.21-1.5

[14] S.D.Farahani, A.R.Naja, F.Kowsary, M.Ashjaee, Experimental estimation heat ux and heat transfer coefficient by using inverse methods, *Sci. Iran. B*, **23**(2016), 1777–1786. DOI: 10.24200/sci.2016.3925

[15] D.N.Hao, P.X.Thanh, D.Lesnic, Determination of the heat transfer coefficients in transient heat conduction, *Inverse Probl.*, **29**(2013), 095020. DOI: 10.1088/0266-5611/29/9/095020

[16] H.Egger, Y.Heng, W.Marquardt, A.Mhamdi, Efficient Solution of a Three-Dimensional Inverse Heat Conduction Problem in Pool Boiling, AICES-2009-4, Aachen Institute for Advanced Study in Computational Engineering Science, Aachen, Germany, 2009, Preprint.

[17] M.V.Glagolev, I.V.Fillipov, Measuments of Green Gases Flows in Bog Ecossystems, Yugra State University, Khanty-Mansiysk, Russia, 2014.

[18] K.A.Woodbury, J.V.Beck, H.Najafi, Filter solution of inverse heat conduction problem using measured temperature history as remote boundary condition, *Int. J. Heat Mass Transf.*, **72**(2014), 139–147. DOI: 10.1016/j.ijheatmasstransfer.2013.12.073

[19] G.I.Marchuk, Mathematical Models in Environmental Problems, Studies in Mathematics and Its Applications, vol. 16, Elsevier Science Publishers: Amsterdam, The Netherlands, 1986.

[20] Y.M.Matsevity, N.A.Safonov, V.V.Ganchin, On the solution of nonlinear inverse boundary value problems of heat conduction, *J. Mech. Eng.*, **19**(2016), 28–36. DOI: 10.15407/PMACH2016.01.028

[21] T.M.Onyango, D.B.Ingham, D.Lesnic, Restoring boundary conditions in heat conduction, *J. Eng. Math.*, **62**(2008), 85–101. DOI: 10.1007/s10665-007-9192-0

[22] S.Y.Shadrin, A.V.Zhirov, T.S.Smirnova, Reconstruction of the unsteady boundary condition on the heated surface during anodic heating, *Bull. Kostroma State Univ.,* **18**(2012), 22–25.

[23] A.Fernandes, P.Priscila, F.B.Sousa, V.L.Borges, G.Guimaraes, Use of 3D-transient analytical solution based on Green's function to reduce computational time in inverse heat conduction problems, *Appl. Math. Model.*, **34**(2010), 4040–4049.

[24] V.Norouzifard, M.Hamedi, A three-dimensional heat conduction inverse procedure to investigate tool-chip thermal interaction in machining process, *Int. J. Adv. Manuf. Technol.*, **74**(2014), 1637–1648. DOI: 10.1007/s00170-014-6119-6

[25] S.A.Kolesnik, V.F.Formalev, E.L.Kuznetsova, The inverse boundary thermal conductivity problem of recovery of heat fluxes to the boundries of anisotropic bodies, *High Temperature*, **53**(2015), no. 1, 68–72. DOI: 10.1134/S0018151X15010113

[26] S.Abboudi, E.Artioukhine, Simultaneous estimation of two boundary conditions in a two-dimensional heat conduction problem, In: Proceeding of the 5th International Conference on Inverse Problems in Engineering: Theory and Practice, 2004, CRC Press: London, UK, 2019.

[27] D.C.Knupp, L.A.S.Abreu, Explicit boundary heat flux reconstruction employing temperature measurements regularized via truncated eigenfunction expansions, *Int. Commun. Heat Mass Transf.*, **78**(2016), 241–252. DOI:10.1016/j.icheatmasstransfer.2016.09.012

[28] J.V.Beck, B.Blackell, St. C.R.Clair, Inverse Heat Conduction, A Wiley-Interscience Publication, New York, NY, USA, 1985.

[29] S.G.Pyatkov, D.V.Shilenkov, Existence and uniqueness theorems in the inverse problem of recovering surface fluxes from pointwise measurements, *Mathematics*, **10**(2022), 1549. DOI: 10.3390/math10091549

[30] R.Denk, M.Hieber, J.Prüss, Optimal Lp-Lq-estimates for parabolic boundary value problems with inhomogeneous data, *Math. Z.*, **257**(2007), 193–224. DOI: 10.1007/s00209-007-0120-9

[31] O.A.Ladyzhenskaya, V.A.Solonnikov, N.N.Uraltseva, Linear and Quasilinear Equations of Parabolic Type, American Mathematical Society: Providence, RI, USA, 1968.

[32] R.Denk, M.Hieber, J.Prüss, R-boundedness, Fourier multipliers and problems of elliptic and parabolic type, Mem. Am. Math. Soc., 2003.

[33] V.A.Belonogov, S.G.Pyatkov, On solvability of some classes of transmission problems in a cylindrical space domain. *Siber. Electr. Math. Reports*, **18**(2021), no. 1, 176-206. DOI: 10.33048/semi.2021.18.015

Восстановление потока на границе области по точечным замерам

Егор И. Сафонов
Сергей Г. Пятков
Даниил А. Парунов
Югорский государственный университет
Ханты-Мансийск, Российская Федерация

Аннотация. Мы рассматриваем обратные задачи восстановления поверхностных потоков на границе области по точечным замерам. Задача некорректна по Адамару. Мы описываем точные условия, гарантирующие существование и единственность решений в пространствах Соболева и строим численный метод, основанный на методе конечных элементов и методе конечных разностей по времени. Представлены результаты численных экспериментов, которые вполне удовлетворительны и процедура устойчива по отношению к малым возмущениям.

Ключевые слова: поверхностный поток, регуляризация Тихонова, обратная задача, точечное переопределение, конвекция-диффузия.

EDN: VXURMY
УДК 533.951; 550.385

Nonlinear Effect for Anisotropy of Charged Particle Pitch Angle Distribution at Geostationary Orbit

Sergei V. Smolin*
Siberian Federal University
Krasnoyarsk, Russian Federation

Received 10.04.2024, received in revised form 29.05.2024, accepted 14.07.2024

Abstract. The new phenomenological model of a prediction of perpendicular anisotropy index of charged particle pitch angle distribution at geostationary (geosynchronous) orbit (GEO) in the Earth's magnetosphere, and also in any circular orbit depending from the local time LT in an orbit and the geomagnetic activity index Kp is offered. Comparison of model with the numerous experimental data is lead. It is proved, that the general analytical dependence of perpendicular anisotropy index of charged particle pitch angle distribution on GEO received as a first approximation can be used for conditions of magnetically quiet time for quantitative forecasts and comparisons with experimental data on GEO. The nonlinear effect is theoretically predicted for a difference between the maximal value of perpendicular anisotropy index of charged particle pitch angle distribution and the minimal value of perpendicular anisotropy index (in local midnight LT = 0 h) on GEO from the Kp-index of geomagnetic activity. The nonlinear effect for anisotropy of charged particle pitch angle distribution will be, possibly, to some extent and on other radial distances from the Earth.

Keywords: geostationary orbit, new model, anisotropy dynamics of charged particles, data of the CRRES satellite, nonlinear effect.

Citation: S.V. Smolin, Nonlinear Effect for Anisotropy of Charged Particle Pitch Angle Distribution at Geostationary Orbit, J. Sib. Fed. Univ. Math. Phys., 2024, 17(5), 644–653. EDN: VXURMY.

Introduction

The charged particle pitch angle distribution is dependence a differential flux of particles j from a local pitch angle of particles α in the range from 0° up to 180°. It is the important characteristic for the charged particles in velocity space in the Earth's magnetosphere.

In the monography [1] for the description different meeting in the magnetosphere of pitch angle distributions was offered following distribution

$$j(\alpha) = j_\perp \sin^{\gamma(\alpha)} \alpha, \tag{1}$$

where $j_\perp$ is the perpendicular ($\alpha = 90°$) differential flux of charged particles.

The equation (1) differs from standard by that an anisotropy index (or a parameter) of pitch angle distribution not is a constant ($\gamma = const$), and it is function from α ($\gamma = \gamma(\alpha)$).

For the range of pitch angles $0° < \alpha < 90°$ $\gamma(\alpha)$ it is possible to find under the formula

$$\gamma(\alpha) = \frac{\ln j(\alpha) - \ln j_\perp}{\ln \sin \alpha}. \tag{2}$$

*smolinsv@inbox.ru

For $\alpha = 90°$ the equation (2) gives the relation $0/0$, therefore we find a limit for γ at $\alpha \to 90°$, using the rule of Lopitalya and considering, that $\left(\dfrac{dj}{d\alpha}\right)_\perp = 0$

$$\gamma_\perp = -\frac{1}{j_\perp}\left(\frac{d^2 j}{d\alpha^2}\right)_\perp . \tag{3}$$

The perpendicular anisotropy index (parameter) of pitch angle distribution $\gamma_\perp$, presented to a general view the formula (3), is the exact indicator of type of pitch angle distribution and in this its great value. Particularly, if pitch angle distributions are normal or type "head and shoulders" — $\gamma_\perp > 0$. If $\gamma_\perp = 0$, it will already correspond isotropic or "flattop" pitch angle distribution. And at last, pitch angle distributions of type "butterfly". In this case — $\gamma_\perp < 0$. Such representation (3) is exact at definition of the moment of occurrence of butterfly pitch angle distribution.

The literature on pitch angle distributions of the charged particles and anisotropy of pitch angle distributions is extensive, for example [1–13]. From the review for last years it is visible, that statistical and empirical models of anisotropy of charged particles pitch angle distributions are, and the analytical mathematical models based on the physics and describing a perpendicular anisotropy index of charged particles pitch angle distribution, possibly, no.

Therefore the purpose of the given work is mathematical modeling an anisotropy index of charged particles pitch angle distribution at geostationary (geosynchronous) orbit (GEO) in the Earth's magnetosphere in the form of: 1) the new mathematical model based on the physics and describing a perpendicular anisotropy index of charged particles pitch angle distribution on GEO depending from the local time LT on GEO and the Kp-index of geomagnetic activity, 2) the analysis of consequences of the offered analytical model and 3) nonlinear effect for anisotropy of charged particle pitch angle distribution.

1. Mathematical model

As a first approximation dependence of a perpendicular anisotropy index of charged particles pitch angle distribution from time $\gamma_\perp(t)$ we shall find from the equation

$$\frac{d\gamma_\perp}{dt} = \frac{d\gamma_\perp}{dL}\frac{dL}{dt}. \tag{4}$$

At carrying out of numerical calculations we shall assume in the equation (4), that $dL/dt \approx \langle dL/dt \rangle$. Then, the bounce-averaged radial drift velocity of charged particle motion in the Earth's magnetosphere can be determined, for example, for the Earth's dipole magnetic field, so [1]:

$$\left\langle \frac{dL}{dt} \right\rangle = -\Omega \frac{\phi_2}{\phi_0} L^4 \cos\phi, \tag{5}$$

where L is the dimensionless McIlwain parameter; t is the time; ϕ is the azimuth angle (the local time LT $= 0$ h at midnight) or the geomagnetic east longitude in the magnetic equator plane; $\Omega = \dfrac{2\pi}{24}$ is the angular velocity of the Earth's rotation in 1/h; $\phi_0 = 92$ kV; and the dependence ϕ_2, measured in kV, from the index of geomagnetic activity $Kp \equiv Kp(t)$, is determined by the formula [14]

$$\phi_2 = \frac{0.045}{\left(1 - 0.16Kp + 0.01Kp^2\right)^3}. \tag{6}$$

Then the equation (4), taking (5) into account, is written as follows

$$\frac{d\gamma_\perp}{dt} + \frac{d\gamma_\perp}{dL}\frac{\Omega\phi_2(t)L^4(t)\cos\phi(t)}{\phi_0} = 0. \tag{7}$$

Now, we can add equations that describe the trajectory of the spacecraft (SC) in the gravitational field of the Earth to equation (7). It will be easier if one specifies the trajectory (SC) in a parametric form. In this case, for a GEO (for a circular orbit) we get

$$L(t) = 6.6; \quad \phi(t) = \Omega t + \varphi_m, \tag{8}$$

where $\varphi_m = \text{const}$ will be determined from a comparison with experimental data in a GEO and t is already the local time LT along the GEO in hours.

In the future for a spacecraft with any circular orbit or with an elliptical orbit, such a replacement in (7) can be done similarly to (8).

The equations (7), (8) represent the general formulation of new phenomenological model of a prediction of perpendicular anisotropy index dynamics of charged particle pitch angle distribution on GEO in the Earth's magnetosphere.

As a result, using (6)–(8), we receive for $E = \text{const}$, $Kp = \text{const}$, $L = \text{const}$

$$\frac{d\gamma_\perp}{dt} = -C\Omega\cos(\Omega t + \varphi_m), \tag{9}$$

where

$$C = \left|\frac{d\gamma_\perp}{dL}\right| \frac{\phi_2}{\phi_0} L^4 \tag{10}$$

and at such definition (10) $C > 0$ always.

If in (10) $\dfrac{d\gamma_\perp}{dL} < 0$, the equation (9) will be transformed to the equation

$$\frac{d\gamma_\perp}{dt} = C\Omega\cos(\Omega t + \varphi_m^-). \tag{11}$$

Then the analytical solution of the differential equation (11), (10) will look like

$$\gamma_\perp(t) = C[\sin(\Omega t + \varphi_m^-) - \sin\varphi_m^-] + \gamma_{\perp 0}, \tag{12}$$

where $\gamma_{\perp 0}$ is the perpendicular anisotropy index of charged particle pitch angle distribution at $t = 0$, i.e., when the local time along the GEO is $\text{LT} = 0$ h at midnight.

If in (10) $\dfrac{d\gamma_\perp}{dL} > 0$ then the analytical solution of the differential equation (9), (10) looks like

$$\gamma_\perp(t) = -C[\sin(\Omega t + \varphi_m^+) - \sin\varphi_m^+] + \gamma_{\perp 0}. \tag{13}$$

If $Kp(t) \neq \text{const}$ and (6) $\phi_2(t) \neq \text{const}$ (a dependence from time t can be complex), we shall receive, using (10), value C^*

$$C^* = \frac{L^4}{\phi_0} \tag{14}$$

and the following general formula for modeling (predicting) calculations $\gamma_\perp(t)$ on GEO and in any circular orbit SC

$$\gamma_\perp(t) = \pm C^*\Omega \int_0^t \frac{d\gamma_\perp}{dL}\phi_2(t)\cos(\Omega t + \varphi_m^{\mp})dt + \gamma_{\perp 0}, \tag{15}$$

as generally a gradient $\dfrac{d\gamma_\perp}{dL} = f(L, LT, E, Kp, t)$.

2. Experimental data and calculations

For definition at geostationary (geosynchronous) orbit of concrete value $\varphi_m^+ = \text{const}$ we use comparison with the numerous experimental data [5], received on GEO. For $\dfrac{d\gamma_\perp}{dL} > 0$ on these experimental data the maximum of perpendicular anisotropy index of charged particle pitch angle distribution $\gamma_\perp(t_m)$ (13), when $t_m = 13$ h LT on GEO. Thus, in the further t_m will designate the moment of time in hours LT, when the perpendicular anisotropy index of charged particle pitch angle distribution on GEO has the maximal value.

Further in a point of a maximum the first derivative (9) $\dfrac{d\gamma_\perp}{dt}(t = t_m) = 0$, therefore the condition should be satisfied

$$\cos(\Omega t_m + \varphi_m^+) = 0. \tag{16}$$

Considering, that $t_m = 13$ h, the condition (16) is carried out, when $\Omega t_m + \varphi_m^+ = 3\pi/2$. Whence follows, that

$$\varphi_m^+ = \frac{\pi(18 - t_m)}{12}. \tag{17}$$

Under the formula (17) for experimental data [5] value $\varphi_m^+ = 5\pi/12$ rad, $\gamma_{\perp 0} = 0.1860$, $\gamma_\perp(t_m) = 1.5059$ for $Kp = 0$ (Fig. 1), and for $Kp = 3$ $\gamma_{\perp 0} = 0.0$, $\gamma_\perp(t_m) = 1.8353$ (Fig. 2).

For the moment of time $t = t_m$ following analytical dependence turns out $\gamma_\perp(t_m)$ (13) for perpendicular anisotropy index of charged particle pitch angle distribution on GEO, when $Kp \approx \text{const}$, for example, within one day

$$\gamma_\perp(t_m) = -C[\sin(\Omega t_m + \varphi_m^+) - \sin\varphi_m^+] + \gamma_{\perp 0} = C[1 + \sin\varphi_m^+] + \gamma_{\perp 0}, \tag{18}$$

and for the intermediate moment of time $t = t_p$ it is received following dependence $\gamma_\perp(t_p)$

$$\gamma_\perp(t_p) = -C[\sin(\Omega t_p + \varphi_m^+) - \sin\varphi_m^+] + \gamma_{\perp 0}. \tag{19}$$

Further we shall find the useful formula in the form of a difference of two equations (18) and (19)

$$\gamma_\perp(t_m) - \gamma_\perp(t_p) = C[1 + \sin(\Omega t_p + \varphi_m^+)]. \tag{20}$$

The formula (20) is useful to a finding of a constant C, when at $t = 0$ value $\gamma_{\perp 0}$ unknown, and other values in (20) known from experimental data. Then knowing C, value $\gamma_{\perp 0}$ can find from the equation (18). On the other hand at $t_p = 0$ equation (20) passes in the equation (18) as it and should be. If value $\gamma_{\perp 0}$ known, the constant C can be found at once from the equation (18).

Thus, determining φ_m^+ (17), $\gamma_{\perp 0}$ and C, for $\dfrac{d\gamma_\perp}{dL} > 0$ final analytical dependence turns out (13) for perpendicular anisotropy index of charged particle pitch angle distribution on GEO, when $Kp \approx$ const, for example, within one day.

To compare dependence from local time $\gamma_\perp(t)$ (13), (17) with averaged on LT and energy E experimental data for electrons [5] on GEO, let's make modeling calculations (as a first approximation) for Kp=0 and Kp=3. Results of calculations are presented on Fig. 1 and Fig. 2.

For the index of geomagnetic activity $Kp = 0$ (Fig. 1) at comparison (13) with experimental data good conformity is received, as on numerous data [5] the averaged values of an anisotropy index $\gamma_\perp(t)$ for $0 \leqslant Kp \leqslant 1$ have the maximal values approximately in the moment of time $t_m = 13$ h LT on GEO and they rather are not sensitive to value of kinetic energy E. For the geomagnetic activity index $Kp = 3$ (Fig. 2) at comparison more good conformity with numerous data [5] of the averaged values of an anisotropy index $\gamma_\perp(t)$ for $2 \leqslant Kp \leqslant 4$ is received.

The divergence is connected with experiment by that dependence $\gamma_\perp(t)$ (13) while is certain only as a first approximation. Thus, the general analytical dependence of perpendicular anisotropy index of charged particle pitch angle distribution on GEO $\gamma_\perp(t)$ (13), (17), received

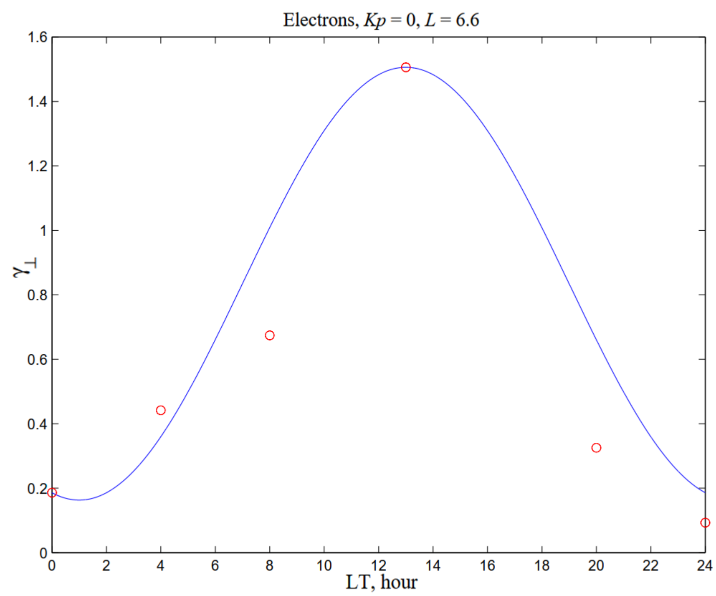

Fig. 1. The continuous line is modeling analytical dependence of perpendicular anisotropy index of electron pitch angle distribution on GEO $\gamma_{\perp}(t)$ (13) from the local time LT for the index of geomagnetic activity $Kp = 0$. Circles are designated the averaged experimental data [5]

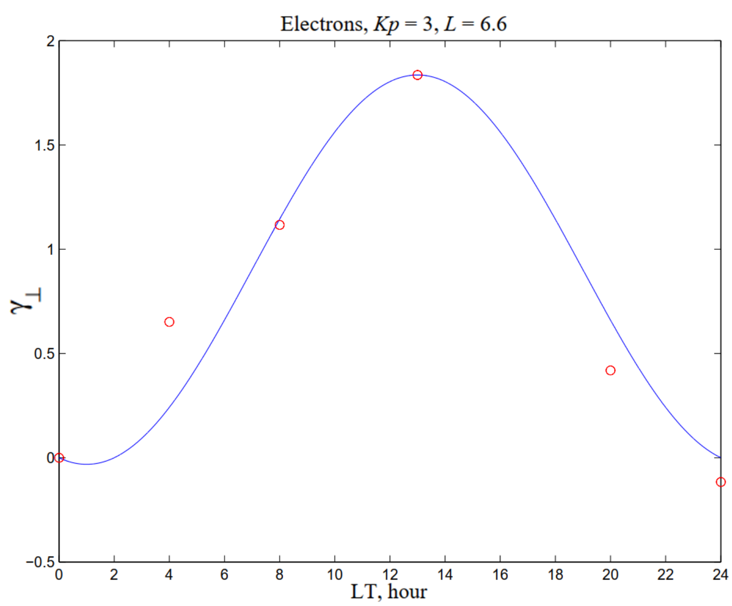

Fig. 2. The continuous line is modeling analytical dependence of perpendicular anisotropy index of electron pitch angle distribution on GEO $\gamma_{\perp}(t)$ (13) from the local time LT for the index of geomagnetic activity $Kp = 3$. Circles are designated the averaged experimental data [5]

as a first approximation, can be used for conditions of magnetically quiet time for quantitative forecasts and comparisons with experimental data on GEO.

Further, for $\dfrac{d\gamma_\perp}{dL} > 0$ and GEO we shall find a modeling (predicted) difference between the maximal value $\gamma_\perp(t_m)$ and the minimal value $\gamma_\perp(0) \equiv \gamma_{\perp 0}$ (at midnight) depending on Kp-index of geomagnetic activity, using for this purpose (18), (17), (10), (6). As a result the following simple equation turns out

$$\gamma_\perp(t_m) - \gamma_{\perp 0} = C[1 + \sin\varphi_m^+]. \tag{21}$$

The right part of the equation (21) should be more zero since on experimental data the difference between the maximal value $\gamma_\perp(t_m)$ and the minimal value $\gamma_{\perp 0}$ always is more than zero.

For an example we shall lead a modeling calculation for electrons on GEO. Thus, interesting nonlinear dependence (21), if approximately within one day Kp = const or $Kp \approx$ const, which is presented on Fig. 3 turns out.

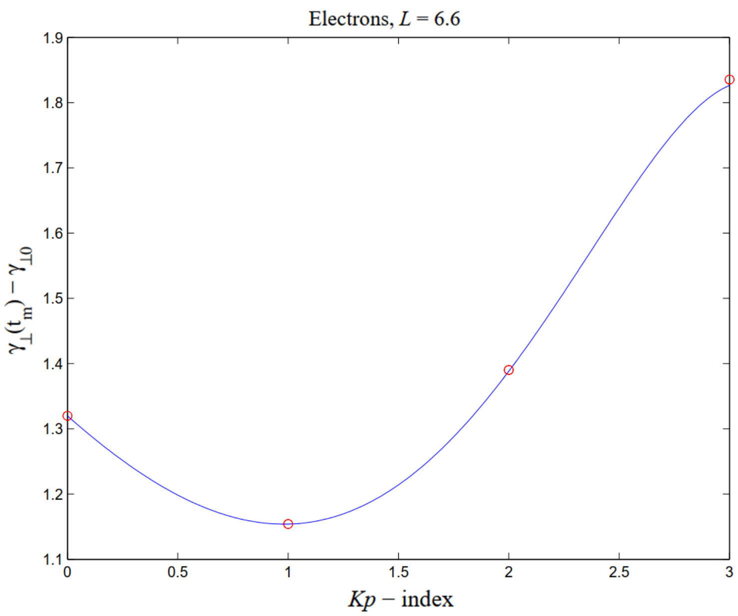

Fig. 3. A continuous line is modeling analytical dependence of a difference of perpendicular anisotropy indexes of electron pitch angle distribution on GEO $\gamma_\perp(t_m) - \gamma_{\perp 0}$ (21) from Kp-index of geomagnetic activity. Circles are designated the averaged experimental data [5]

Thus it is necessary to notice, that the right part of the equation (21), namely C (10), depends in this case as well from a gradient $\dfrac{d\gamma_\perp}{dL}(Kp)$. Therefore, to receive the best consent (21) with the averaged experimental data on GEO [5], we shall make the following. First, we shall believe dependence ϕ_2 from Kp-index of geomagnetic activity under the formula (6) [14] fair. Secondly, using the method of the least squares, we shall find dependence of a gradient $\dfrac{d\gamma_\perp}{dL}$ from Kp-index of geomagnetic activity for conditions of magnetically quiet time ($0 \leqslant Kp \leqslant 3$) in the following form

$$\frac{d\gamma_\perp}{dL}(L = 6.6, Kp) = 0.7234 - 0.5113Kp + 0.2068Kp^2 - 0.0305Kp^3. \tag{22}$$

From here follows, that the offered technique allows to predict (to forecast) very important dependence of a gradient $\dfrac{d\gamma_\perp}{dL}$ from Kp-index of geomagnetic activity. With dependence (22) very good consent (21) with the averaged experimental data [5] has turned out, that evidently proves to be true Fig. 3. Still it is necessary to add, that concrete dependence (22) on GEO is received (forecast) for the first time. The received dependence (22) also shows, that on GEO for a range ($0 \leqslant Kp \leqslant 3$) the gradient $\dfrac{d\gamma_\perp}{dL}(L = 6.6, Kp)$ is more than zero that corresponds to a prospective condition on a gradient prior to the beginning of calculations. And for other distances ($1 < L \leqslant 6.1$) dependence of a gradient $\dfrac{d\gamma_\perp}{dL}$ from Kp-index is visually presented, for example in [11].

Such theoretical prediction (21), in general, it is necessary to check in the further on corresponding experimental data. And still, in the equation (21) value C (10) is certain while as a first approximation, but in the future C can specify on experimental data, using the equation (21).

Thus, the received nonlinear dependence (21) can be considered as a theoretical prediction of nonlinear effect for a difference between the maximal value of a perpendicular anisotropy index of charged particle pitch angle distribution $\gamma_\perp(t_m)$ and the minimal value of a perpendicular anisotropy index $\gamma_\perp(0) \equiv \gamma_{\perp 0}$ (at midnight) on GEO ($L = 6.6$) from Kp-index of geomagnetic activity.

The presented nonlinear effect for anisotropy of charged particle pitch angle distribution (21) will be, possibly, to some extent and on other radial distances from the Earth, i.e. at other values of the McIlwain parameter L.

For some experimental data when a gradient $\dfrac{d\gamma_\perp}{dL} < 0$, the following (similar previous) formulas and the equations are received. In this case for $t_m = 13$ h the condition (16) is carried out, when $\Omega t_m + \varphi_m^- = 5\pi/2$. Whence follows, that

$$\varphi_m^- = \frac{\pi(30 - t_m)}{12}. \tag{23}$$

Under the formula (23) value $\varphi_m^- = 17\pi/12$ rad. For the moment of time $t = t_m$ following analytical dependence $\gamma_\perp(t_m)$ (12) turns out for perpendicular anisotropy index of charged particle pitch angle distribution on GEO, when $Kp \approx$ const, for example, within one day

$$\gamma_\perp(t_m) = C[\sin(\Omega t_m + \varphi_m^-) - \sin\varphi_m^-] + \gamma_{\perp 0} = C[1 - \sin\varphi_m^-] + \gamma_{\perp 0}. \tag{24}$$

The first composant in the right part of the equation (24) should be more zero since on experimental data the difference between the maximal value $\gamma_\perp(t_m)$ and the minimal value $\gamma_{\perp 0}$ always is more than zero.

For the intermediate moment of time $t = t_p$ it is received following dependence $\gamma_\perp(t_p)$

$$\gamma_\perp(t_p) = C[\sin(\Omega t_p + \varphi_m^-) - \sin\varphi_m^-] + \gamma_{\perp 0}. \tag{25}$$

Further we find the useful formula in the form of a difference of two equations (24) and (25)

$$\gamma_\perp(t_m) - \gamma_\perp(t_p) = C[1 - \sin(\Omega t_p + \varphi_m^-)]. \tag{26}$$

The formula (26) is useful for a finding of a constant C, when at $t = 0$ value $\gamma_{\perp 0}$ unknown, and other values in (26) known from experimental data. Then knowing C, the value $\gamma_{\perp 0}$ can be found from the equation (24). On the other hand at $t_p = 0$ the equation (26) passes in the equation (24) as it and should be. If value $\gamma_{\perp 0}$ known the constant C can be found at once from the equation (24).

Thus, determining φ_m^- (23), $\gamma_{\perp 0}$ and C, for $\dfrac{d\gamma_\perp}{dL} < 0$ final analytical dependence turns out (12) for perpendicular anisotropy index of charged particle pitch angle distribution on GEO, when $Kp \approx$ const, for example, within one day.

Formulas and the equations for gradients $\frac{d\gamma_\perp}{dL} < 0$ and $\frac{d\gamma_\perp}{dL} > 0$ are interconnected. In particular, the equation (23) can be presented so

$$\varphi_m^- = \frac{\pi(30 - t_m)}{12} = \frac{\pi(12 + 18 - t_m)}{12} = \pi + \frac{\pi(18 - t_m)}{12} = \pi + \varphi_m^+. \tag{27}$$

Then, using (27) and the reduction formulas in the trigonometry, it is possible to make following transitions of the equations: (24) in (18), (25) in (19), and (26) in (20) and thus to prove interrelation of the equations.

For an example when $\frac{d\gamma_\perp}{dL} < 0$, and $t_m = 12$ LT, in work [13] for the first time have been used special cases of the formulas and the equations (12), (23)–(26) for comparison to numerous experimental data, received with 1999 on 2007 on GEO. Comparison was made only at a qualitative physical level. As in [8] the pitch angle anisotropy (in the form of the relation of two average values) of the Earth's external radiation belt in the field of GEO in another way was quantitatively determined, but for very plenty of experimental data. In this work [13] it has been found, that at $t_m = 12$ LT the value $\varphi_m^- = 3\pi/2$ (23). Thus following final analytical dependence (the special case (12)) has been received for perpendicular anisotropy index of charged particle pitch angle distribution on GEO, when $Kp \approx \text{const}$, for example, within one day

$$\gamma_\perp(t) = C\left[\sin\left(\Omega t + \frac{3\pi}{2}\right) + 1\right] + \gamma_{\perp 0} \equiv 2C\sin^2\left(\frac{\Omega}{2}t\right) + \gamma_{\perp 0}. \tag{28}$$

And for a modeling (predicted) difference between the maximal value $\gamma_\perp(12)$ and the minimal value $\gamma_\perp(0) \equiv \gamma_{\perp 0}$ (at midnight) depending on Kp-index of geomagnetic activity more simple equation (the special case (24)) has been received at $\varphi_m^- = 3\pi/2$

$$\gamma_\perp(12) - \gamma_{\perp 0} = 2C. \tag{29}$$

To compare dependence from local time $\gamma_\perp(t)$ (28) with experimental data [8], test (modeling) calculations have been made [13], for example, for protons with energy $E = 120$ keV on GEO for $Kp = 3$- и $Kp = 5$.

In the same work [13] for the first time nonlinear effect (29) has been theoretically predicted for a difference between the maximal value of perpendicular anisotropy index of charged particle pitch angle distribution (in local midday LT $= 12$ h) and the minimal value of perpendicular anisotropy index (at midnight LT $= 0$ h) on GEO depending on Kp-index of geomagnetic activity.

On the whole, results of all calculations for $\frac{d\gamma_\perp}{dL} < 0$ are very in detail presented in [13].

3. Conclusion

1. The new phenomenological model of a prediction of perpendicular anisotropy index of charged particle pitch angle distribution at geostationary (geosynchronous) orbit (GEO) in the Earth's magnetosphere, and also in any circular orbit depending from the local time LT in an orbit and the geomagnetic activity index Kp is offered.

2. Comparison of model with the numerous experimental data is lead. It is proved, that the general analytical dependence of perpendicular anisotropy index of charged particle pitch angle distribution on GEO received as a first approximation can be used for conditions of magnetically quiet time for quantitative forecasts and comparisons with experimental data on GEO.

3. The nonlinear effect is theoretically predicted for a difference between the maximal value of perpendicular anisotropy index of charged particle pitch angle distribution and the minimal value of perpendicular anisotropy index (in local midnight LT = 0 h) on GEO from Kp-index of geomagnetic activity.

4. The technique is offered which allows to predict (to forecast) very important dependence of a gradient $\dfrac{d\gamma_\perp}{dL}$ from Kp-index of geomagnetic activity. For the first time concrete dependence of a gradient $\dfrac{d\gamma_\perp}{dL}$ from Kp-index on GEO for conditions of magnetically quiet time is received (forecast).

5. The nonlinear effect for anisotropy of charged particle pitch angle distribution will be, possibly, to some extent and on other radial distances from the Earth.

References

[1] S.V.Smolin, Modeling of pitch angle diffusion in the Earth's magnetosphere, Libra, Krasnoyarsk, 1996 (in Russian).

[2] S.V.Smolin, Modeling of pitch angle distribution on the dayside of the Earth's magnetosphere, *Journal of Siberian Federal University. Mathematics & Physics,* **5**(2012), no. 2, 269–275 (in Russian).

[3] S.V.Smolin, Modeling the pitch angle distribution on the nightside of the Earth's magnetosphere, *Geomagnetism and Aeronomy,* **55**(2015), no. 2, 166–173. DOI: 10.1134/S0016793215020152

[4] S.V.Smolin, Two-dimensional phenomenological model of ring current dynamics in the Earth's magnetosphere, *Geomagnetism and Aeronomy,* **59**(2019), no. 1, 27–34. DOI:10.1134/S0016793218040175

[5] X.Gu, Z.Zhao, B.Ni, Y.Shprits, C.Zhou, Statistical analysis of pitch angle distribution of radiation belt energetic electrons near the geostationary orbit: CRRES observations, *J. Geophys. Res.,* **116**(2011), A01208. DOI: 10.1029/2010JA016052

[6] J.E.Borovsky, M.H.Denton, A survey of the anisotropy of the outer electron radiation belt during high-speed-stream-driven storms, *J. Geophys. Res.,* **116**(2011), A05201. DOI: 10.1029/2010JA016151

[7] Y.Chen, R.H.W.Friedel, M.G.Henderson, S.G.Claudepierre, S.K.Morley, H.Spence, REPAD: An empirical model of pitch angle distributions for energetic electrons in the Earth's outer radiation belt, *J. Geophys. Res.,* **119**(2014), 1693–1708. DOI: 10.1002/2013JA019431

[8] J.E.Borovsky, R.H.W.Friedel, M.H.Denton, Statistically measuring the amount of pitch angle scattering that energetic electrons undergo as they drift across the plasmaspheric drainage plume at geosynchronous orbit, *J. Geophys. Res.,* **119**(2014), 1814–1826. DOI: 10.1002/2013JA019310

[9] J.E.Borovsky, T.E.Cayton, M.H.Denton, R.D.Belian, R.A.Christensen , J.C.Ingraham, The proton and electron radiation belts at geosynchronous orbit: Statistics and behavior during high-speed stream-driven storms, *J. Geophys. Res.,* **121**(2016), 5449–5488. DOI: 10.1002/2016JA022520

[10] L.M.Kistler, C.G.Mouikis, The inner magnetosphere ion composition and local time distribution over a solar cycle, *J. Geophys. Res.,* **121**(2016), 2009–2032. DOI: 10.1002/2015JA021883

[11] R.Shi, D.Summers, B.Ni, J.F.Fennell, J.B.Blake, H.E.Spence, G.D.Reeves, Survey of radiation belt energetic electron pitch angle distributions based on the Van Allen Probes MagEIS measurements, *J. Geophys. Res.,* **121**(2016), 1078–1090. DOI: 10.1002/2015JA021724

[12] H.Zhao, R.H.W.Friedel, Y.Chen, G.D.Reeves, D.N.Baker, X.Li, et al, An empirical model of radiation belt electron pitch angle distributions based on Van Allen probes measurements, *J. Geophys. Res.,* **123**(2018), 3493–3511. DOI: 10.1029/2018JA025277

[13] S.V.Smolin, Prediction of nonlinear effect for anisotropy of charged particle pitch angle distribution at geostationary orbit, *Space, Time and Fundamental Interactions,* (2019), no. 3, 88–97. DOI: 10.17238/issn2226-8812.2019.3.88-97

[14] A.Nishida, Geomagnetic diagnosis of the magnetosphere, Springer-Verlag, New York, 1978.

Нелинейный эффект для анизотропии питч-углового распределения заряженных частиц на геостационарной орбите

Сергей В. Смолин
Сибирский федеральный университет
Красноярск, Российская Федерация

Аннотация. Предложена новая феноменологическая модель предсказания перпендикулярного индекса анизотропии питч-углового распределения заряженных частиц на геостационарной (геосинхронной) орбите (ГСО) в магнитосфере Земли, а также на любой круговой орбите в зависимости от местного времени LT на орбите и Kp–индекса геомагнитной активности. Проведено сравнение модели с многочисленными экспериментальными данными. Доказано, что общая аналитическая зависимость перпендикулярного индекса анизотропии питч-углового распределения заряженных частиц на ГСО, полученная в первом приближении, может быть использована для магнитоспокойных условий для количественных прогнозов и сравнений с экспериментальными данными на ГСО. Теоретически предсказан нелинейный эффект для разности между максимальным значением перпендикулярного индекса анизотропии питч-углового распределения заряженных частиц и минимальным значением перпендикулярного индекса анизотропии (в местную полночь LT = 0 ч) на ГСО от Kp–индекса геомагнитной активности. Нелинейный эффект для анизотропии питч-углового распределения заряженных частиц будет, вероятно, в той или иной степени и на других радиальных расстояниях от Земли.

Ключевые слова: геостационарная орбита, новая модель, динамика анизотропии заряженных частиц, данные спутника CRRES, нелинейный эффект.

EDN: STKJDD
УДК 532.6

Secondary Destruction of Organic Coal-water Slurry Drops at Different Temperatures in a Gas Flow

Anna A. Shebeleva*
Alexander V. Shebelev†
Andrey V. Minakov‡
Anastasia K. Okrugina§
Siberian Federal University
Krasnoyarsk, Russian Federation

Received 29.05.2024, received in revised form 04.06.2024, accepted 14.07.2024

Abstract. A computational study of the secondary destruction of a drop of organic water-coal fuel (OCWS) in a gas flow was carried out. For the first time, the influence of the temperature of an OCWF drop, which has non-Newtonian properties, on deformation and its further destruction was studied. The computational study was carried out using a numerical technique based on the VOF method, the LES model was used to take into account turbulence, and the technology of adapted dynamic meshes was used to describe the behavior of the interface on the main turbulent scales, which made it possible to resolve secondary liquid droplets up to 20 μm in size. During the work, the shape of the surface of an OCWF drop during the destruction process, as well as the structure of the flow near and in the wake of the drop, were studied. As a result of the calculations, the dependences of the rate of transverse deformation of the midsection of an OCWF drop for different temperatures were obtained. Judging by the results, with increasing temperature, the destruction time of an OCWF drop decreases, which has a beneficial effect on the mixing of OCWF with air.

Keywords: OCWS fuel, secondary destruction of a drop, deformation rate, mathematical modeling, dynamic mesh adaptation technology.

Citation: A.A. Shebeleva, A.V. Shebelev, A.V. Minakov, A.K. Okrugina, Secondary Destruction of Organic Coal-water Slurry Drops at Different Temperatures in a Gas Flow, J. Sib. Fed. Univ. Math. Phys., 2024, 17(5), 654–664. EDN: STKJDD.

Introduction

Currently, special attention is paid to the socio-economic development of the northern and Arctic regions. This is due to the presence in these regions of large reserves of natural resources, such as non-ferrous metal ores, gas, oil and coal. Since coal production has been increasing recently, coal fuel will remain one of the main energy sources in the near future. However, we should not forget about environmental problems that arise when burning coal, such as emissions of nitrogen oxides and carbon dioxide into the atmosphere. To reduce harmful effects on atmosphere and environment during energy production, it is proposed to use alternative fuels, such

*an_riv@mail.ru https://orcid.org/ 0000-0001-6126-9757
†Ashebelev@sfu-kras.ru
‡Aminakov@sfu-kras.ru
§okrugina_a02@mail.ru

as coal-water fuel (CWF), consisting of water and coal dust, or organic water-coal fuel (OCWF), consisting of water, crushed coal (or combustible waste from its processing), a small amount of chemical additives (for example, surfactants, plasticizers) and a petroleum combustible component (waste oil) [1]. To burn liquid waste of petroleum origin in its original state, large resources are needed; according to data [2], waste of petroleum origin and waste oils form masses amounting to millions of tons per year and require further disposal. However, as part of OCWF, these wastes can be used to intensify ignition and improve rheological characteristics of fuel [3]. Use of by-products from coal mining and oil refining industries as part of OCWF can help eliminate waste from these industries and reduce the harmful impact of energy sector on nature. Also, the advantages of using OCWF include the absence of dust and contamination during storage, transportation and use of fuel. Today, there are technologies for industrial preparation and combustion of CWF in furnaces of power boilers, experimental methods and numerical modeling algorithms have been developed, and practical recommendations have been formulated for the combustion of CWF droplets [4–7]. China and Japan are already using CFC combustion on an industrial scale. The works [3, 8–10] describe stages of preparation and ignition of OCWF droplets. To date, data on the maximum ignition and combustion temperatures are presented for a narrow composition of OCWF, which also complicates the process of studying these types of fuels. The problem of ignition and combustion of OCWF is not simple, this is due to fact that OCWF is multicomponent, contains solid particles, and this fuel most often has non-Newtonian properties. To increase the efficiency of fuel combustion, its preliminary atomization in combustion chamber is required; the technical task in this case is to optimize the process of destruction of the jet, which includes changing the shape of the surface of the drop and its secondary destruction. The development of an effective method for burning OCWF will allow low-quality fossil fuels to be included in the fuel balance and solve the problem of recycling industrial waste that pollutes the environment, thereby improving the environmental situation by reducing harmful emissions into the atmosphere.

One of first experimental works on study of secondary crushing of OCWF droplets was work [11]. The authors, in work [12], conducted a detailed experimental study of OCWF spray for a coaxial nozzle, obtained quantitative information on characteristics of OCWF atomization (average droplet size, shape and spray angle) with and without fuel treatment for purposes of application in design of combustion chambers gas turbines burning OCWF. Also, a semi-empirical correlation was developed to determine average spray particle sizes as a function of various parameters, including Weber number, Reynolds number, and air-to-fuel mass flow ratio. Heating of OCWF (flash atomization) has been found to be very effective in reducing droplet size not only at atmospheric pressure but also at elevated pressure. A detailed experimental study of fragmentation of individual OCWF droplets was carried out for the first time in the work [13]. The authors studied the morphology of droplets at various Weber numbers, $We = \dfrac{\rho_g u_g^2 d_0}{\sigma}$ and Ohnesorge numbers, $Oh = \dfrac{\eta}{\sqrt{\sigma \rho L}}$. Later, in the work [7] a numerical study of behavior of an OCWF drop during secondary crushing was carried out. The results obtained were compared with experimental data on droplet crushing modes considered in the experimental work [7]. Despite the seemingly sufficient number of works in the field of studying OCWF, at the moment there are practically no works related to the numerical study and establishment of the dependence of the shape of the drop surface, deformation, and destruction time on the rheological properties of OCWF [14, 15].

1. Numerical technique for destruction of OCWF droplets

Since one of ways to obtain data on secondary destruction of a fuel droplet is numerical modeling, in our works [16, 17] we proposed and verified a numerical method for the destruction of OCWF droplets. This technique showed good agreement between calculated and experimental data on the destruction of OCWF droplets and the rate of deformation of the droplet. When developing numerical methodology, information about flow structure and physical properties of gas-droplet flows was taken into account. It was also taken into account that fluid under consideration can be either a viscous Newtonian or a non-Newtonian viscoplastic fluid, behaviour of which can be described by one of common rheological models, such as the power-law, Bingham or Herschel-Bulkley model [17] a numerical model was proposed and verified method of destruction of OCWF droplets. To simulate destruction of an OCWF drop, the Ansys Fluent software package was used; the VOF method was used to describe free surface; a detailed description is presented in work [18]. According to this method, the OCWF and air flow are considered as a single two-component medium, and phase distribution within computational domain is determined using marker function F(x,y,z,t). The volume fraction of liquid phase in calculation cell is taken equal to F(x,y,z,t) = 0 if cell is empty, F(x,y,z,t) = 1 if cell is completely filled with liquid, 0 < F(x,y ,z,t) < 1 if interphase boundary passes through the cell. Tracking movement of interface is performed by solving the equation for transfer of volume fraction of liquid phase in cell:

$$\frac{\partial F}{\partial t} + u_i \frac{\partial}{\partial x_i} F = 0, \tag{1}$$

where: u_i is the velocity vector of a two-phase medium, found from solving a system of hydrodynamic equations: the mass conservation equation or the continuity equation:

$$\frac{\partial \rho}{\partial t} + \frac{\partial}{\partial x_i}\left(\rho u_i\right) = 0, \tag{2}$$

and equations of motion or the law of conservation of momentum:

$$\frac{\partial}{\partial t}\left(\rho u_i\right) + \frac{\partial}{\partial x_j}\left(\rho u_i u_j\right) = \frac{\partial \sigma_{ij}}{\partial x_j} - \frac{\partial p}{\partial x_i} - \frac{\partial \tau_{ij}}{\partial x_j} + F_{s_i}, \tag{3}$$

here τ_{ij} is the subgrid stress tensor, F_s is vector of body forces, p is static pressure, ρ is density of two-phase medium. Components of viscous stress tensor σ_{ij}:

$$\sigma_{ij} \equiv \left[\mu\left(\frac{\partial u_i}{\partial x_j} + \frac{\partial u_j}{\partial x_i}\right)\right] - \frac{2}{3}\mu \frac{\partial u_i}{\partial x_i}\delta_{ij}, \tag{4}$$

where: μ is dynamic viscosity of two-phase medium. Density and Newtonian viscosity of two-component medium under consideration are found through volume fraction of liquid in cell according to the mixture rule:

$$\rho = \rho_1 F + (1 - F)\rho_2, \tag{5}$$

$$\mu = \mu_1 F + (1 - F)\mu_2, \tag{6}$$

where: ρ_1, μ_1 – density and viscosity of liquid, ρ_2, μ_2 – density and viscosity of gas. The obtained values of density ρ and viscosity μ are included in equations of motion and determine physical properties of two-phase medium.

To simulate destruction of droplets, special attention must be paid to surface tension, in this case, the CSF algorithm [19] was used, which involves introducing into equations of motion an additional body force F_s, value of which is determined from relation:

$$F_s = \sigma k \nabla F, \tag{7}$$

where: σ is surface tension coefficient, k is curvature of free surface, which is defined as the divergence of normal vector:

$$k = \nabla(\frac{n}{|n|}). \tag{8}$$

The normal to free surface is calculated, in turn, as the gradient of volume fraction of liquid phase in cell:

$$n = \nabla F. \tag{9}$$

Since turbulent flows are observed during secondary destruction, the LES model was used [20].

$$\tau_{ij} - \frac{1}{3}\tau_{kk}\delta_{ij} = -2\mu_t S_{ij}, \tag{10}$$

$$S_{ij} = \frac{1}{2}\left(\frac{\partial u_i}{\partial x_j} + \frac{\partial u_j}{\partial x_i}\right), \tag{11}$$

where: τ_{ij} is subgrid stress tensor, S_{ij} is strain rate tensor, μ_t is subgrid viscosity. In this work, we used subgrid viscosity model proposed by Smagorinsky:

$$\mu_t = \rho L_s^2 \left| S \right|, \tag{12}$$

where: L_s is length of subgrid scale mixing:

$$L_s = \min\left(\mathrm{kd}, \mathrm{C_s} \mathrm{V}^{1/3}\right), \tag{13}$$

$$|S| \equiv \sqrt{2 S_{ij} S_{ij}}, \tag{14}$$

here: k is the Karman constant, d is distance to nearest wall, V is volume of the computational cell C_s is the Smagorinsky constant. In this work, the value $C_s = 0.17$ was used.

For modeling properties of OCWF, the Herschel-Bulkley rheological model was used:

$$\mu\left(\dot{\gamma}\right) = \frac{k\dot{\gamma}^n + \tau_0}{\dot{\gamma}}. \tag{15}$$

where: $\dot{\gamma}$ is shear rate, τ_0 is yield strength of the viscoplastic fluid, n is flow index, k is fluid consistency index.

For modeling destruction of droplets, including very small ones, special attention should be paid to computational mesh. During secondary destruction of OCWF, small drops are formed, resolution of which is a rather complex process, therefore, the technology of gradient adaptation of the computational mesh is used in proposed numerical technique. According to this technology, during calculation process mesh is automatically condensed in area of large solution gradients, gradient of volume fraction of liquid was chosen as control parameter. At initial moment of time, there are 40 calculated cells per drop along its diameter. In this case, there are at least 8 cells per interface. Total number of computational nodes in optimized mesh during calculation process was close to 12 million nodes.

2. Problem formulation and numerical simulation results

To describe destruction of OCWF droplets in a gas flow, an isothermal formulation of problem was used. OCWF is a water-coal suspension consisting of 60–70% by weight of coal powder, 30–40% water and a small amount of additives. Depending on composition, OCWF can be either a Newtonian or non-Newtonian fluid. In our case, OCWF droplets have non-Newtonian

properties and are described by the Herschel–Bulkley rheology. The physical properties of fuel suspensions under consideration were taken from experimental work [21] (see Tab. 1), where ρ_l is density of OCWF, τ_0 is yield strength of viscoplastic fluid, k is consistency index, n is flow index, σ – coefficient of surface tension of OCWF, T – temperature of OCWF. Air with following properties was considered as a gas: $\rho_g = 1.7$ kg/m^3, μ_g =1.789·10^{-5} Pa·s. The computational domain is a parallelepiped with dimensions $0.026 \times 0.026 \times 0.08$ m. On one of faces of parallelepiped, an entry condition with a fixed velocity value was set, and on remaining faces of computational domain, free exit conditions were set. At initial moment of time, at a distance of 0.0015 m from entrance of computational domain, a spherical drop of OCWF with an initial diameter of $d_0 =$ 0.003 m was placed, which was affected by an air flow with a speed of
$u_g = 50$ m/s and deformed drop.

Table 1. Physical properties of OCWF fuel suspensions

T, K	ρ_l, kg/m^3	τ_0, Pa	k, Pa*s^n	n	σ, N/m	We
278	1063	47.08	0.66	1	0.247	51.6
298	1062	37.36	0.42	1	0.239	53.3
308	1061	26.57	0.39	1	0.231	55.2
318	1059	16.99	0.32	1	0.223	57.2

The secondary disintegration of an OCWF drop occurs under influence of an aerodynamic force exceeding surface tension forces. Quantitatively, ratio of these forces is determined by the Weber number. Value of the Weber number determines regime of destruction of drop.

For developing new fuel combustion technologies or burning fuel at low temperatures (e.g. in Arctic conditions), its preliminary atomization in combustion chamber is important to increase contact surface of fuel with the oxidizer. Main task in fuel atomisation and further improvement of combustion technologies is to determine induction time of destruction, shape of surface and rate of deformation of droplet at different times.

In Fig. 1 shows regimes of destruction of an OCWF drop at different temperatures, interval between pictures is $\Delta t = 500$ μs. In Fig. 1a you can see process of deformation of an OCWF drop at a temperature of 278 K, time of interaction of drop with flow is 11000 μs. At such a low temperature, drop does not collapse for a long time; a process of deformation and flattening of drop in a plane normal to gas flow velocity vector is observed. At a time of $\approx$ 8500 μs, central part of drop begins to thin out and stretch along flow, upon reaching a time of 11000 μs, complete destruction of central part of drop is observed.

When the OCWF temperature increases to 298 K, pattern of droplet deformation changes (Fig. 1b). Interaction time of the drop with flow is 6000 μs. Initially, spherical drop at time instant $\approx$ 2000 μs resembles shape of a "disk". Over time, the central part of the "disk" inflates like a "parachute"; this is clearly visible at time $\approx$ 5500 μs. This regime of destruction for a Newtonian liquid was described in detail in the work [22], authors write that this regime of destruction for Newtonian liquids exists in the range of Weber numbers from 12 to 50. In this case, when destruction of a non-Newtonian drop of OCWF at temperature 298 K, Weber number is We = 53.3.

In Fig. 1c shows pictures of destruction of a drop of OCWF at a temperature of 308 K. The drop is destroyed according to a scenario close to previous case (see Fig. 1 b). However, if in case of Fig. 1b, destruction of the "parachute" is observed at $\approx$ 5500 μs, but in this case destruction

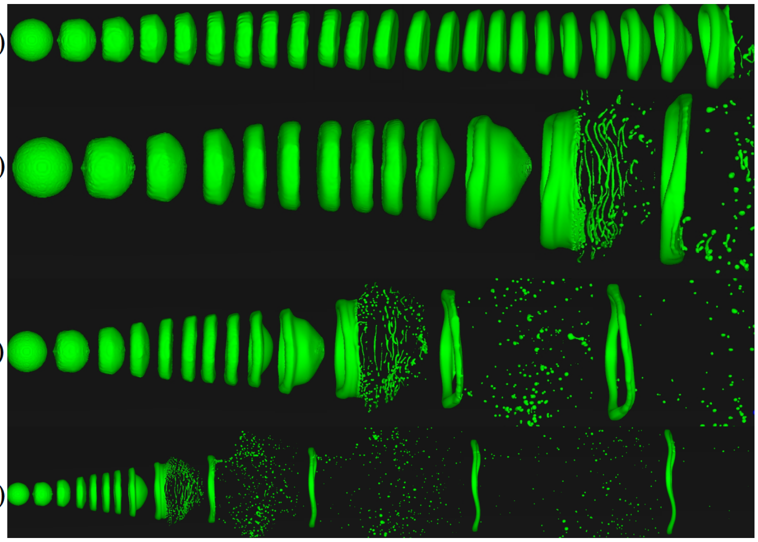

Fig. 1. Regimes of destruction of a drop of OCWF at different temperatures. Interval between frames Δt = 500 μs. a) t = 278 K, period 0 – 11000 μs; b) t = 298 K, period 0 – 6000 μs; c) t = 308 K, period 0 – 6000 μs; d) t = 318 K, period 0 – 6000 μs

occurs earlier, at $\approx$ 5000 μs. As can be seen, even with such a small increase in temperature of the OCWF drop from 298 K to 308 K, process of destruction of drop increases in time. Change in the surface shape of an OCWF droplet at a temperature of 318 K is shown in Fig. 1d. The interaction time of a drop with a flow is 6000 μs. In this case, tendency for destruction time to depend on the initial temperature of drop remains unchanged. Destruction of the "parachute" occurs at a time equal to $\approx$ 4000 μs. Further, shell of central part of OCWF drop is destroyed with formation of small drops; at moment of time $\approx$ 5000 μs, only a ring remains from initial drop, which subsequently becomes thinner and destroyed.

In course of mathematical modeling, formation of a ring and its further movement along flow was obtained for following OCWF temperatures of 298 – 318 K. After the "parachute" is destroyed, only a ring remains from initially spherical drop, which over time increases in diameter and becomes thinner. For the case of an OCWF droplet with a low temperature of 278 K, we observe formation of a ring, but it thins out so slowly that the computational region was not enough to record complete destruction of droplet. However, for this study this is not important, because we are studying moment of induction of destruction, and not the late stage of interaction of drop with the flow.

The most important indicator of droplet destruction is not only dynamics of deformation, presented in Fig. 1, but also induction time of destruction of the OCWF droplet. Fig. 2 shows pictures of destruction of a drop at a temperature of 278 K at various times. As can be seen, at the moment of time 10377 μs the central part of drop has already thinned out, but remains intact, and at moment of time 10465 μs a violation of integrity of shell is already observed, it follows that the OCWF droplet at a temperature 278 K begins to collapse at a time equal to $t_1 \approx 10421$ μs. Based on Fig. 1a, Fig. 2, drop was deformed for a long time, and after reaching destruction induction time, central part of drop quickly collapsed.

In Fig. 3 shows dynamics of destruction of a drop of OCWF at a temperature of 298 K in frontal projection. This type of destruction differs from previous case in that there is a gradual destruction of central part of the drop with a simultaneous thinning of edge of drop - appearance of a ring that increases until it collapses. Induction time of destruction in this case is $t_2 \approx 4955$ μs. Fig. 3 clearly shows that drop begins to collapse from central part. At moment of time ≈ 5006 μs the "parachute" has become so thin that streams break off from drop, which increase and break up into small drops. At time ≈ 5560 μs, complete destruction of central part of drop is observed, liquid ring has increased in size, but has not yet become thin enough to collapse.

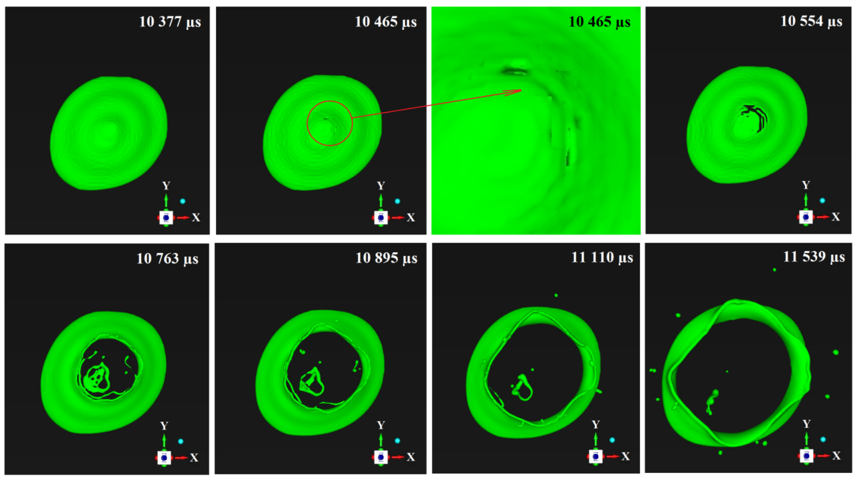

Fig. 2. Frontal projection of destruction of an OCWF drop at t = 278 K

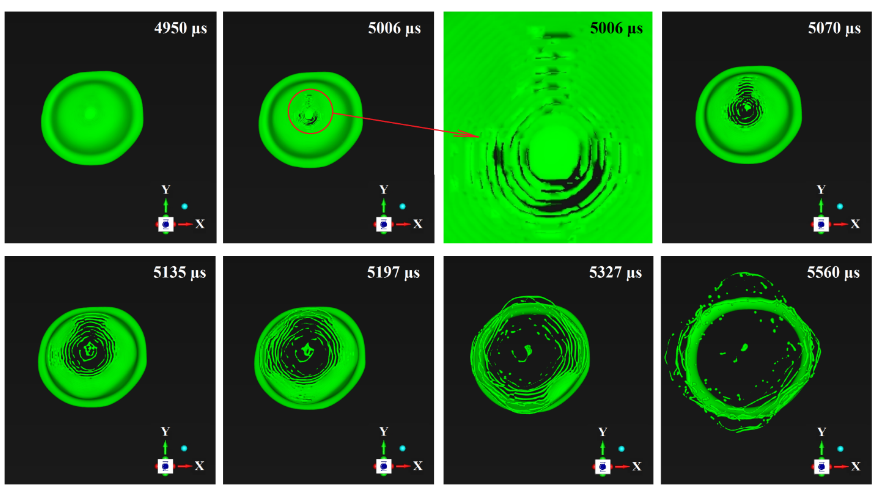

Fig. 3. Frontal projection of destruction of an OCWF drop at t = 298 K

Fig. 4 shows moments of destruction of an OCWF drop at a temperature of 308 K. Induction time of destruction in this case is $t_3 \approx 4463$ μs. If we compare results obtained in Fig. 4 with results presented in Fig. 3, we see that with increasing temperature destruction process begins to proceed faster. Thus, at a temperature of 298 K (Fig. 3), a drop of OCWF began to collapse at time instant ≈ 4955 μs. And at a temperature of 308 K (Fig. 4) at same point in time, we observe that the central part of the drop has already been completely destroyed and only a liquid ring remains.

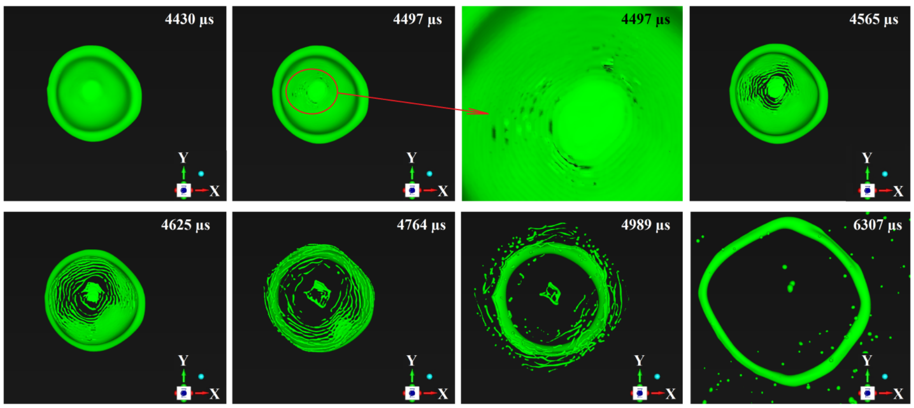

Fig. 4. Frontal projection of destruction of an OCWF drop at t = 308 K

The scenarios for destruction of an OCWF drop at temperatures of 298–318 K are very similar: gradual transverse stretching of the drop along midsection until drop resembles shape of a "disk", further thinning of central part of drop and its inflation in a "parachute" type, destruction of "parachute" into small drops and as a result, a ring remains from original drop, which becomes thinner and collapses. In this case, destruction begins at time $t_4 \approx 3598$ μs, this can be seen from Fig. 5.

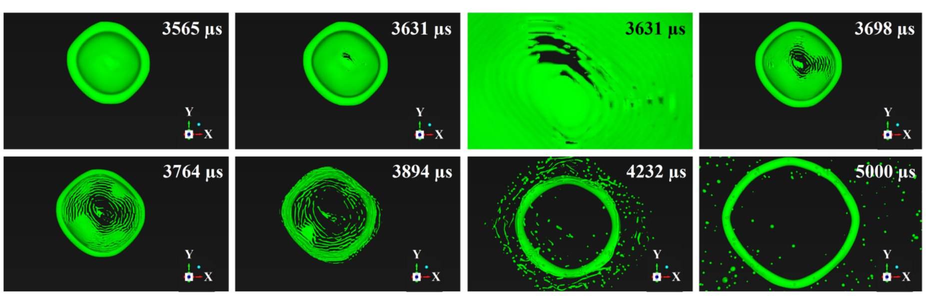

Fig. 5. Frontal projection of destruction of an OCWF drop at t = 318 K

For quantitative assessments of destruction of droplet surface shape, dependence of ratio of maximum value of droplet midsection to initial size d_0 is used, where d_{max} is maximum size of droplet shape during the deformation process, at a moment in time. This dependence is also called rate of transverse deformation of the drop (Fig. 6).

Based on results (Fig. 6), as temperature of the OCWF drop increases, ratio of maximum deformation of drop to initial size increases. Also, for the first time, estimates were made of the influence of temperature of an OCWF drop on induction time of destruction and rate of deformation of drop at moment of destruction. Thus, with increasing temperature,destruction time of an OCWF droplet decreases, and ratio of maximum deformation of droplet to initial size increases. Quantitative calculation indicators, such as the induction time of destruction and ratio of maximum deformation of drop to initial size at moment of destruction are presented in Tab. 2.

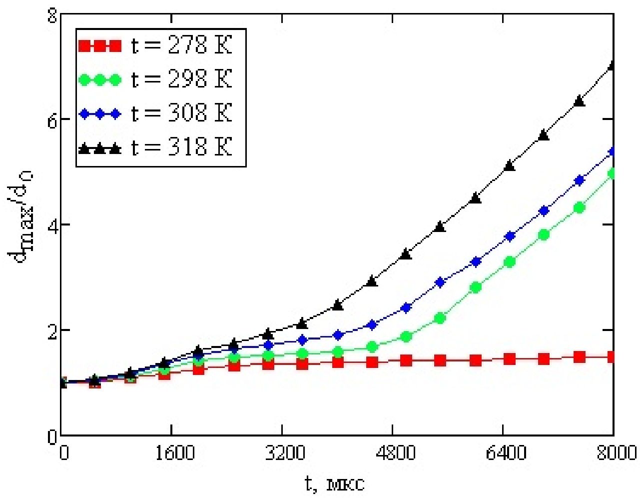

Fig. 6. Rate of transverse deformation of an OCWF drop at different fuel temperatures

Table 2. Quantitative results of destruction of a drop of OCWF

OCWF temperature, T, K	Induction time of destruction, t, μs	d_{max}/d_0
278	10421	1.798
298	4955	1.874
308	4463	2.069
318	3598	2.185

Conclusion

A computational study of secondary destruction of a drop of organic-coal fuel in a gas flow was carried out in order to improve its combustion technologies. Droplets with different initial temperatures from 278 to 318 K were studied.

The results of numerical modeling have yielded images of destruction of OCWF droplets. These images demonstrate that fuel drops, which have non-Newtonian properties and are described by the Herschel–Bulkley rheology, deform according to the "parachute" scenario within the studied temperature range. At the same time, for a temperature close to freezing and equal to 278 K, the drop is deformed for a long time before collapsing. This is due to fact that at such low temperatures fuel has a higher yield strength, as well as a higher surface tension coefficient. At the initial temperature of the OCWF drop equal to 318 K, the drop is destroyed much more intensely. Induction time of destruction is reduced by approximately 3 times (compared to a temperature of 278 K), which has a beneficial effect on mixing of OCWF with air.

Dependences of induction time of destruction and rate of transverse deformation of drop on initial temperature of the OCWF drop obtained in work will be useful for improving technology of combustion of OCWF, including in regions of the Far North.

The reported study was carried out with the support of the "Krasnoyarsk Regional Fund for Support of Scientific and Scientific-Technical Activities" within the framework of the scientific project "Study of the characteristics of secondary crushing of coal water slurries containing petrochemicals in order to improve technologies for its combustion in Arctic conditions" no. 20231113-06407.

References

[1] A.Kijo-Kleczkowska, Combustion of coal-water suspensions, *Fuel*, **90**(2011), 865–877.

[2] BP, BP Statistical Review of World Energy, *London: BP* , **90**(2015), 48.

[3] G.S.Khodakov, E.G.Gorlov, Suspension coal fuel, *Chemistry of solid fuel*, **6**(2005), 15–32 (in Russian).

[4] V.I.Murko, V.I.Fedyaev, et al., Investigation of the spraying mechanism and combustion of the suspended coal fuel, *Thermal Science*, **19**(2015), 243–251.
DOI: 10.2298/TSCI120618095M

[5] A.P.Burdukov, A.A.Emel'yanov, V.I.Popov, S.N.Tarasenko, An investigation of the rheology and dynamics of combustion of composite coal-water slurries, *Thermal Engineering.*, **44**(1997), 492–497.

[6] Z.Gao, S.Zhu, M.Zheng, Z.Wu, H.Lu, W.Liu, Effects of fractal surface on rheological behavior and combustion kinetics of modified brown coal water slurries, *International Journal of Coal. Science and Technology*, **2**(2015), 211–222. DOI: 10.1007/s40789-015-0075-0

[7] S.M.Tavangar, H.Hashemabadi, A.Saberimoghadam, CFD simulation for secondary breakup of coal-water slurry drops using OpenFOAM, *Fuel Processing Technology*, **132**(2015), 153–163. DOI: 10.1016/j.fuproc.2014.12.037

[8] S.C. Yao, Burning of suspended coal-water slurry droplet with oil as combustion additive, *Combustion and Flame*, **66**(1986), 87–89.

[9] N.I.Fedorova, Yu.F.Patrakov, V.G.Surkov, A.K.Golovko, Analysis of the combustion character of composite fuels obtained by the cavitation method, *Bulletin of the Kuzbass State Technical University*, **4**(2007), 38–41 (in Russian).

[10] K.Svoboda, et al., Fluidized bed gasification of coal–oil and coal–water–oil slurries by oxygen–steam and oxygen–CO2 mixtures, *Fuel Processing Technology*, **95**(2012), 16–26.
DOI: 10.1016/j.fuproc.2011.11.001

[11] M.Kurmangaliev, V.Nekrasov, Breakup of water-coal slurry drops in air flows, *Fluid Mech. Sov. Res.*, **4**(1975).

[12] T.Yu., et al., Secondary atomization of coal water fuels for gas turbine applications, *MIT Energy Lab Report.*, **88**(1988).

[13] H.Zhao, et al., Secondary breakup of coal water slurry drops, *Phys. Fluids*, **23**(2011), 113101–113101. DOI: 10.1063/1.3659495

[14] H.Zhao, et al., Breakup and atomization of a round coal water slurry jet by an annular air jet, *Chemical Engineering Science*, **78**(2012), 63–74. DOI: 10.1016/j.ces.2012.05.007

[15] H.Zhao, et al., Influence of rheological properties on air-blast atomization of coal water slurry, *J. Non-Newtonian Fluid Mech.*, **211**(2014), 1–15. DOI: 10.1016/j.jnnfm.2014.06.007

[16] A.A.Shebeleva, A.V.Minakov, M.Yu.Chernetskii, P.A.Strizhack, Deformation of a droplet of an organic water–coal fuel in a gas flow, *J. Appl. Mech. Tech. Phys.*, **59**(2018), no. 4, 653–661. DOI: 10.1134/S0021894418040119

[17] A.V.Minakov, A.A.Shebeleva, M.Y.Chernetskiy, P.A.Strizhak, R.S.Volkov, Study of the weber number impact on secondary breakup of droplets of coal water slurries containing petrochemicals, *Fuel.*, **254**(2019), 115606–115606. DOI: 10.1016/j.fuel.2019.06.014

[18] C.W.Hirt, B.D.Nichols, Volume of fluid (VOF) method for the dynamics of free boundaries, *Journal of computational physics*, **39**(1981), 201–226.

[19] J.U.Brackbill, D.B.Kothe, C.A.Zemach, Continuum method for modelling surface tension, *J. Comput. Phys.*, **100**(1992), 335–354.

[20] J.Smagorinsky, General Circulation Experiments with the Primitive Equations, I. The Basic Experiment, *Month. Wea. Rev.*, **91**(1963), 99–164.

[21] G.Lei, L.Junguo, Study on the Influence of Pulping Process on Rheological Properties of Coal Water Slurry, *IOP Conf. Series: Earth and Environmental Science*, **384**(2019), 1–7. DOI: 10.1088/1755-1315/384/1/012107

[22] S.V.Bukhman, Experimental study of droplet disintegration, *Bulletin of the Academy of Sciences of the Kazakh SSR*, **1**(1954), 38–43 (in Russian).

Вторичное разрушение капли органоводоугольного топлива различной температуры в потоке газа

Анна А. Шебелева
Александр В. Шебелев
Андрей В. Минаков
Анастасия К. Округина
Сибирский федеральный университет
Красноярск, Российская Федерация

Аннотация. Проведено расчетное исследование вторичного разрушения капли органоводоугольного топлива (ОВУТ) в потоке газа. Впервые изучалось влияние температуры капли ОВУТ, обладающей неньютоновскими свойствами, на деформацию и ее дальнейшее разрушение. Расчетное исследование проводилось с помощью численной методики, основанной на ВОФ-методе, для учета турбулентности использовалась ЛЕС-модель, для описания поведения межфазной границы на основных турбулентных масштабах применялась технология адаптированных динамических сеток, которая позволила разрешить вторичные капли жидкости размером до 20 мкм. В ходе работы была исследована форма поверхности капли ОВУТ в процессе разрушения, а также структура потока вблизи и в следе капли. В результате расчетов были получены зависимости темпа поперечной деформации миделя капли ОВУТ для различных температур, судя по результатам, с увеличением температуры время разрушения капли ОВУТ уменьшается, что благоприятно сказывается на перемешивании ОВУТ с воздухом.

Ключевые слова: дифференциальные уравнения, задача Коши, расщепление, устойчивость, сходимость.

Journal of Siberian Federal University. Mathematics & Physics 2024, 17(5), 665–678

EDN: VBJGHW
УДК 532.5

Axisymmetric Ideal Fluid Flows Effectively not Being Tied to Vortex Zones

Isaac I. Vainshtein*
Siberian Federal University
Krasnoyarsk, Russian Federation

Received 10.06.2024, received in revised form 05.07.2024, accepted 26.08.2024

Abstract. The paper formulates a model of axisymmetric flow of an ideal fluid with n effectively inviscid vortex zones, generalizing the well-known model of M. A. Lavrentiev on the gluing of vortex and potential flows in a plane case. The possibility is shown within the framework of such a model of the existence in space of a liquid sphere streamlined around by a potential axisymmetric flow, consisting of n spherical layers of axisymmetric vortex flows. This model example generalizes the spherical Hill vortex with one vortex zone, known in hydrodynamics. Such a vortex flow with n spherical layers is also possible in a sphere, and, unlike a flow in space, such a flow is not unique. The problem of an axisymmetric vortex flow in a limited region is considered; its formulation generalizes the plane flow of an ideal fluid in a field of Coriolis forces.

Keywords: ideal fluid, vortex flows, spherical Hill vortex

Citation: I.I. Vainshtein, Axisymmetric Ideal Fluid Flows Effectively not Being Tied to Vortex Zones, J. Sib. Fed. Univ. Math. Phys., 2024, 17(5), 665–678. EDN: VBJGHW.

Introduction. Setting of the problem

A large number of works and monographs are devoted to the study of vortex flows. The topic of vortex flows is presented in every hydrodynamics course. The monographs by M. A. Gol'dshtik "Vortex Flows" [1], M. A. Lavrentiev, B. V. Shabat "Problems of Hydrodynamics and Their Mathematical Models" [2] can be considered fundamental in this research area. The monographs indicate various examples of vortex flows in nature and technology, present a study of problems of signifit scientific and practical interest, and formulate various mathematical problems for research.

The paper examines one of them, related to the existence and non-uniqueness of axisymmetric flows according to the scheme of M. A. Lavrentiev [1, 2] with n effectively inviscid vortex zones in an unbounded and limited region.

The stationary vortex flow of an ideal incompressible fluid in the plane case is described by the equation

$$\Delta\Psi = \frac{\partial\Psi(x,y)}{\partial x^2} + \frac{\partial\Psi(x,y)}{\partial y^2} = F(\Psi),\ v_x = \frac{\partial\Psi}{\partial y},\ v_y = -\frac{\partial\Psi}{\partial x}, \tag{1}$$

$$L\Psi(z,r) = \frac{\partial^2\Psi(z,r)}{\partial z^2} + \frac{\partial^2\Psi(z,r)}{\partial r^2} - \frac{1}{r}\frac{\partial\Psi(z,r)}{\partial r} = H'(\Psi)r^2 - \Gamma'(\Psi)\Gamma(\Psi), \tag{2}$$

*isvain@mail.ru

$v_r = -\dfrac{1}{r}\dfrac{\partial \Psi}{\partial z},\ v_z = \dfrac{1}{r}\dfrac{\partial \Psi}{\partial r}$ in axisymmetric. Functions $F(\Psi),\ H'(\Psi),\ \Gamma(\Psi)$ are arbitrary functions of the flow function Ψ[1]. Various approaches to defining the functions $F(\Psi),\ H(\Psi),\ \Gamma(\Psi)$ when solving specific problems are also available in [1].

The right-hand sides of equations (1), (2) determine the value of vorticity $\omega(x, y),\ \omega(z, r)$. When the vorticity is zero, the flow is potential.

Thus, equations (1), (2) of the motion of an ideal fluid in terms of the flow function make it possible to study the motion of an ideal fluid with potential and vortex zones. With the natural requirement of continuity of the velocity field, one should require the continuity of the first partial derivatives of the flow function when passing through the common boundary of these zones.

It is important to note that equation (2) in the appropriate notation is called the Grad-Shafranov equation [3] in plasma theory, on the basis of which tokamaks are calculated and built.

The paper considers flows with effectively inviscid vortex zones, where it is assumed that the flow of an ideal fluid is the limiting flow of a viscous fluid when the viscosity tends to zero. In this case, the vorticity in the plane case is equal to a constant, in the axisymmetric case $\omega(z, r) = \omega_0 r$, ω_0 is a constant $[1, 2, 4]$. Respectively

$$\Delta\Psi(x, y) = \omega_0, \quad L\Psi(z, r) = \omega(z, r)r = \omega_0 r^2. \tag{3}$$

In this case, the M. A. Lavrentiev scheme of plane flows with n vortex zones $[1, 2, 5]$ for axisymmetric flows with n effectively inviscid vortex zones in unbounded and bounded regions can be formulated as follows: given a flow region D with a boundary Γ, numbers $\omega_i,\ i = 1, \ldots, n$. The value of the flow function $\Psi(z, r)$ on the boundary Γ of the region D or its behavior at infinity is specified. It is required to construct disjoint flow zones $D_i,\ \bigcup D_i = D$ and find in the region D a continuously differentiable flow function $\Psi(z, r)$, which in each zone D_i satisfies the equation $L\Psi = \omega_i r^2$. At all points of the boundaries Γ_i of zones B_i not belonging to the boundary Γ of area D, it is equal to zero. The possibility of the existence of zones in which the values of ω_i coincide or $\omega_i = 0$ cannot be excluded. In the latter case, the flow in the zone D_i is potential.

Note that, taking into account corrections associated with viscosity, M. A. Lavrentyev, using a plane flow model with three flow zones in a deep trench (two vortex zones with constant vorticities $\pm\omega$, and in the third — potential flow), substantiated the unacceptability burial of radioactive residues in ocean depressions $[1, 2]$.

The formulated problem with n vortex zones is nonlinear, and here an important role is played by the consideration of model problems, the results of which can be used in the formulation and solution of general problems. This will be seen when solving problem (31).

Let us formulate a simple property related to the geometry of zones D_i and the signs of ω_i.

Property 1. *If the boundaries of the zones D_i, D_j are zero streamlines and $\omega_i\omega_j > 0$ then the two zones have no common point which can be touched with circles both from the region D_i and the region D_j.*

Let there be such a point M^*. Since the flow function $\Psi(z, r)$ vanishes at the boundaries of the zones $D_i,\ D_j$, then in the case $\omega_i > 0,\ \omega_j > 0$ the function $\Psi(z, r)$ at this point attains its maximal value in the zones $D_i,\ D_j$, for $\omega_i < 0,\ \omega_j < 0$ smallest. In such a situation, the derivatives of the solution at the point M^* along the external normals from the zones $D_i,\ D_j$ are of the same sign [6], which contradicts the continuous differentiability of the solution when passing through the common boundary of the zones.

Using the known relation

$$L(r^2U(z,r)) = r^2L^*U(z,r), \quad L^*U(z,r) = \frac{\partial^2 U(z,r)}{\partial z^2} + \frac{\partial^2 U(z,r)}{\partial r^2} + \frac{3}{r}\frac{\partial U(z,r)}{\partial r},$$

to obtain solutions to the equation $L\Psi = \omega_0 r^2$, in (3), it is convenient to pass to the equation $L^*U = \omega_0$, after replacing $\Psi(z,r) = r^2U(z,r)$.

In the equation $L^*U = \omega_0$ it is already possible to look for a solution depending only on R ($R^2 = r^2 + z^2$), $U(z,r) = U(R)$. In this case

$$L^*U(R) = \frac{\partial^2 U(R)}{\partial R^2} + \frac{4}{R}\frac{\partial U(R)}{\partial R} = \omega_0.$$

Its solution is the function

$$U(R) = \frac{\omega_0}{10}R^2 + \frac{c}{R^3} + d, \ R \neq 0, \tag{4}$$

c, d — arbitrary constants. Note that $\left(\frac{\partial^2}{\partial R^2} + \frac{4}{R}\frac{\partial}{\partial R}\right)\frac{1}{R^3} = 0.$

After returning to the function $\Psi(z,r) = r^2\left(\frac{\omega_0}{10}R^2 + \frac{c}{R^3} + d\right)$ we have a solution to the equation $L\ Psi(z,r) = \omega_0 r^2$.

For further purposes, let us formulate what can be verified by direct differentiation:

Property 2. *Let* $\Psi_i = r^2\left(\frac{\omega_i}{10}R^2 + \frac{c_i}{R^3} + d_i\right)$. *If the constants* $c_i, d_i,\ c_j, d_j$ *are such that the functions* $\Psi_i,\ \Psi_j$ *vanish for* $R = a$, *then the condition for their continuous differentiability for* $R = a$ *is written in the form*

$$\frac{1}{10}\left(2\omega_i a - \frac{c_i}{a^4}\right) = \frac{1}{10}\left(2\omega_j a - \frac{c_j}{a^4}\right).$$

1. Hill vortex with n vortex spherical layers

Let us consider the possibility of the existence in the entire space of an axisymmetric flow with n vortex zones with a given geometry of the vortex zones: ($D_1 : R \leqslant a_1$, $D_i : a_{i-1} \leqslant R \leqslant a_i$, $a_1 > 0,\ a_{i-1} < a_i,\ i = 2, \ldots, n$). In the zone ($D_{n+1} : R > a_n,\ \omega_{n+1} = 0$) the flow is potential.

For a given flow case, the problem can be written in analytical form

$$L\Psi(z,r) = \begin{cases} \omega_1 r^2 & \text{if } R < a_1, \\ \omega_i r^2 & \text{if } a_{i-1} < R < a_i, i = 2, \ldots, n, \\ 0 & \text{if } R > a_n, \end{cases} \tag{5}$$

given that

$$\Psi|_{R=a_i} = 0,\ i = 1, \ldots, n, \quad \lim_{R\to\infty}\frac{\Psi}{r^2} = A > 0. \tag{6}$$

Given such a geometry of zones, according to Property 1, the signs of numbers ω_i must alternate if none of them is zero,

In accordance with (4), we look for a solution to problem (5), (6) in the form

$$\Psi(z,r) = \begin{cases} \frac{r^2}{10}\omega_1(R^2 - a_1^2) & \text{if } 0 \leqslant R \leqslant a_1, \\ \frac{r^2}{10}(\omega_i R^2 + \frac{c_i}{R^3} + d_i) & \text{if } a_{i-1} \leqslant R \leqslant a_i, i = 2, \ldots, n, \\ Ar^2(1 - \frac{a_n^3}{R^3}) & \text{if } R \geqslant a_n. \end{cases}$$

Satisfying the boundary conditions (6) and the continuous differentiability of the solution when passing through the boundaries of the zones, in accordance with Property 2, we obtain the system

$$\omega_i a_{i-1}^2 + \frac{c_i}{a_{i-1}^3} + d_i = 0, \quad \omega_i a_i^2 + \frac{c_i}{a_i^3} + d_i = 0, \ i = 2, \ldots, n, \tag{7}$$

$$2\omega_1 a_1 = 2\omega_2 a_1 - \frac{3c_2}{a_1^4}, \quad 2\omega_i a_i - \frac{3c_i}{a_i^4} = 2\omega_{i+1} a_i - \frac{3c_{i+1}}{a_i^4}, \ i = 2, \ldots, n-1, \tag{8}$$

$$2\omega_n a_n - \frac{3c_n}{a_n^4} = \frac{30A}{a_n}. \tag{9}$$

From (7–9)

$$\omega_i (a_{i-1}^2 - a_i^2) + c_i \left(\frac{1}{a_{i-1}^3} - \frac{1}{a_i^3}\right) = 0, \ i = 2, \ldots, n-1, \tag{10}$$

$$c_2 = \frac{2(\omega_2 - \omega_1)}{3} a_1^5, \quad c_{i+1} = \frac{2}{3}(\omega_{i+1} - \omega_i) a_i^5 + c_i, \quad c_1 = 0, \ i = 2, \ldots, n-1, \tag{11}$$

$$c_n = \frac{2\omega_n}{3} a_n^5 - 10 A a_n^3. \tag{12}$$

From (11)

$$\sum_{j=2}^{i} c_j = \frac{2}{3} \sum_{j=2}^{i} (\omega_j - \omega_{j-1}) a_{j-1}^5 + \sum_{j=2}^{i} c_{j-1}, \quad c_i = \frac{2}{3} \sum_{j=2}^{i} (\omega_j - \omega_{j-1}) a_{j-1}^5, \ i = 2, \ldots, n. \tag{13}$$

Let us prove a property of system (10), (11), which will be used further.

Property 3. *If the signs ω_i, $i = 1, \ldots, n$, alternate, then $a_{i-1} = t_{i-1} a_i$, $i = 2, \ldots, n$ $0 < t_{i-1} < 1$ is a root of the equation*

$$t^4 + t^3 + t^2 + \gamma_{i-1} t + \gamma_{i-1} = 0, \ \left(\gamma_{i-1} = \frac{3\omega_i}{2(\bar{\omega}_{i-1} - \omega_i)}\right), \tag{14}$$

$$\bar{\omega}_i = (1 - t_{i-1}^5)\omega_i + t_{i-1}^5 \bar{\omega}_{i-1}, \ \bar{\omega}_1 = \omega_1, \ c_i = \frac{2(\omega_i - \bar{\omega}_{i-1})}{3} t_{i-1}^5 a_i^5, \ i = 2, \ldots, n, \tag{15}$$

$$sign(\bar{\omega}_i) = sign(\omega_i), \ i = 1, \ldots, n. \tag{16}$$

We assume $i = 2$. Considering $\bar{\omega}_1 = \omega_1, \ c_2 = \dfrac{2(\omega_2 - \bar{\omega}_1)}{3} a_1^5$, from (10)

$$\omega_2 (a_1^2 - a_2^2) + \frac{2(\omega_2 - \bar{\omega}_1)}{3} a_1^5 \left(\frac{1}{a_1^3} - \frac{1}{a_2^3}\right) = 0.$$

Hence $a_1 = a_2$, or

$$\omega_2 (a_1 + a_2) + \frac{2(\bar{\omega}_1 - \omega_2)}{3} a_1^2 \frac{a_2^2 + a_2 a_1 + a_1^2}{a_2^3} = 0. \tag{17}$$

d Equation (17) is homogeneous. Denoting $t_1 = \dfrac{a_1}{a_2} < 1, \ \gamma_1 = \dfrac{3\omega_2}{2(\bar{\omega}_1 - \omega_2)}, \ \omega_1 \neq \omega_2$, we obtain an equation for finding the value t_1

$$t^4 + t^3 + t^2 + \gamma_1 t + \gamma_1 = 0. \tag{18}$$

For the existence of a root $0 < t < 1$ it is necessary $\gamma_1 < 0$. From the resulting equation

$$\gamma_1(t) = -\left(t^3 + t - 1 + \frac{1}{t+1}\right), \quad 0 \leqslant t \leqslant 1, \quad \gamma_1(0) = 0, \quad \gamma_1(1) = -\frac{3}{2} < 0,$$

$$\gamma_1'(t) = -(3t^2 + 1 - \frac{1}{(t+1)^2}).$$

For $t > 0$, $\gamma_1'(t) < 0$, the function $\gamma_1(t)$ decreases monotonically as $t \geqslant 0$. Hence, for

$$-\frac{3}{2} < \frac{3\omega_2}{2(\bar{\omega}_1 - \omega_2)} < 0 \tag{19}$$

equation (18) has a single root t_1 on the interval (0,1). Note that inequality (19) is satisfied, if ω_1, ω_2 have different signs. We got $a_1 = t_1 a_2$. For $\omega_2 = \omega_1$, equation (17) implies $\omega_2 = 0$, and hence $\omega_1 = 0$, or $a_2 = a_1$. Zones D_1, D_2 are combined into one — the number of zones with such geometry should be reduced by one when setting the problem.

For what follows we set $i = 3$. From relation (13) it follows

$$c_3 = \frac{2}{3}(\omega_3 - ((1-t_1^5)\omega_2 + t_1^5\bar{\omega}_1))a_2^5 = \frac{2}{3}(\omega_3 - \bar{\omega}_2)a_2^5.$$

From (17), similarly to the case $i = 2$, we obtain equation (14) with $\gamma_2 = \dfrac{3\omega_3}{2(\bar{\omega}_2 - \omega_3)}$.

Let us show that $sign(\bar{\omega}_2) = sign(\omega_2)$. Let's write it down

$$sign(\bar{\omega}_2) = sign(\lambda(t_1)(1-t_1^5) + t_1^5) sign(\bar{\omega}_1), \quad \lambda(t_1) = \frac{\omega_2}{\bar{\omega}_1} = \frac{2\gamma_1}{3+2\gamma_1}. \tag{20}$$

From equation (14) with $\gamma_{i-1} = \gamma_2$ we express γ_2 and after substitution into (20)

$$\lambda(t_1)(1-t_1^5) + t_1^5 = \frac{2(t_1^4 + t_1^3 + t_1^2)}{2(t_1^4 + t_1^3 + t_1^2) - 3t_1 - 3}(1-t_1^5) + t_1^5 = -t_1^2 \frac{3t_1^3 + 6t_1^2 + 4t_1 + 2}{2t_1^3 + 4t_1^2 + 6t_1 + 3} < 0.$$

We got $sign(\bar{\omega}_2) = -sign(\bar{\omega}_1) = -sign(\omega_1) = sign(\omega_2)$. Since ω_1, ω_2 by assumption have different signs. This implies that inequality (19) holds for ω_3, ω_2 of different signs. Then $a_2 = t_2 a_3$.

Increasing i successively by one, similar to the previous one, we obtain $a_{i-1} = t_{i-1}a_i$ and $c_i = \dfrac{2(\omega_i - \bar{\omega}_{i-1})}{3} a_{i-1}^5 = \dfrac{2(\omega_i - \bar{\omega}_{i-1})}{3} t_{i-1}^5 a_i^5$, $sign(\bar{\omega}_i) = sign(\omega_i)$.

Let us return to the problem under consideration (5), (6). Let in some zone D_i, $\omega_i = 0$, and in the zone D_{i-1}, $\omega_{i-1} \neq 0$, $i = 2, 3, \ldots, n$, The function $\Psi(z,r)$ and its partial derivatives in the zone D_i are identically equal to zero, which contradicts the inequality of the normal derivative from the zone D_{i-1} to zero at points $R = a_{i-1}$ of the common boundary of the zones D_{i-1}, D_i, since the function $\Psi(z,r)$ in the zone D_{i-1} at boundary points $R = a_{i-1}$ takes either the largest or smallest value, depending on the sign of ω_{i-1}[6]. Further continuing these arguments, successively decreasing the index i, and then successively increasing it, we arrive at all $\omega_i = 0$, $i = 1.2, \ldots, n$.

Thus, a flow with the considered geometry of vortex zones cannot have a single internal zone with potential flow, and the alternation of signs of ω_i in zones D_i is a necessary condition for the existence of a solution to the problem under consideration.

Let the signs of ω_i alternate in the statement of the problem. Substituting $c_n = \dfrac{2(\omega_n - \bar{\omega}_{n-1})}{3} t_{n-1}^5 a_i^5$ (Property 3) into (12), we obtain the equation for finding a_n

$$\bar{\omega}_n a_n^2 = 15A, \quad \bar{\omega}_n = (1 - t_{n-1}^5)\omega_n + t_{n-1}^5 \bar{\omega}_{n-1}.$$

Requiring $\omega_n > 0$, in the problem statement by Property 3, we obtain $sign(\bar{\omega}_n) = sign(\omega_n) > 0$. Then

$$a_n = \sqrt{\frac{15A}{(1-t_{n-1}^5)\omega_n + t_{n-1}^5\bar{\omega}_{n-1}}}.$$

Next, a_i are determined inversely through a_n, $a_{i-1} = t_{i-1}a_i,\ i = n, n-1, \dots, 2$.

Note that if $\omega_n > 0$, is required, ω_1 must be less than zero when n is even and $\omega_1 > 0$ when n is odd.

Thus, we have obtained that in space, within the framework of an ideal fluid, it is possible to move a liquid sphere of radius a_n, streamlined around by a potential flow, inside which there are n vortex zones with vorticities $\omega_i r$, with alternating signs ω_i, at $\omega_n > 0$.

Let us write down the solution to problem (5), (6) (the signs of ω_i alternate, $\omega_n > 0$).

$$\Psi(z,r) = \begin{cases} \dfrac{r^2}{10}\omega_1\big(R^2 - a_1^2\big) & \text{if } 0 \leqslant R \leqslant a_1, \\ \dfrac{r^2}{10}\omega_i\big(R^2 - a_i^2\big) + \dfrac{2(\omega_i - \bar{\omega}_{i-1})}{3} t_{i-1}^5 a_i^5 \left(1 - \left(\frac{a_1}{R}\right)^3\right) & \text{if } a_{i-1} \leqslant R \leqslant a_i,\ i = 2, \dots, n, \\ Ar^2\left(1 - \dfrac{a_n^3}{R^3}\right) & \text{if } R \geqslant a_n. \end{cases}$$

For $n = 1$ (one vortex zone with $\omega > 0$) we have the spherical Hill vortex, known in hydrodynamics [7], in plasma theory after "spherical plasmoid" [8]

$$\Psi(z,r) = \begin{cases} \omega r^2(R_0^2 - R^2) & \text{if } 0 \leqslant R \leqslant R_0, \\ Ar^2\left(1 - \dfrac{R_0^3}{R^3}\right) & \text{if } R \geqslant R_0, \end{cases}$$

$R_0,\ \omega,\ A$ are related by the relation $\omega = \dfrac{15A}{R_0^2}$. The Hill vortex represents a liquid sphere moving in the direction of the OZ axis in a potential flow around it with a speed of $\frac{A}{2}$ at infinity, inside which there is a vortex motion with a vorticity of ωr. It was shown in [9] that in the vicinity of the spherical Hill vortex there is no other axisymmetric vortex with one vortex zone, which differs little from it.

Note that the resulting solution to problem (5), (6) describes a natural axisymmetric generalization of the Hill vortex with n vortex zones. This structure of the vortex flow can be called a composite spherical Hill vortex.

Let us write the flow function for a composite Hill vortex with two vortex zones ($\omega_1 < 0,\ \omega_2 > 0$)

$$\Psi(z,r) = \begin{cases} \dfrac{\omega_1}{10} r^2(R^2 - a_1^2) & \text{if } R \leqslant a_1, \\ \dfrac{r^2}{10}\omega_2(R^2 - a_2^2) + \dfrac{3(\omega_2 - \omega_1)}{2} a_1^5 \left(1 - \dfrac{a_2^3}{R^3}\right) & \text{if } a_1 \leqslant R \leqslant a_2, \\ Ar^2\left(1 - \dfrac{a_2^3}{R^3}\right) & \text{if } R \geqslant a_2, \end{cases}$$

$$a_2 = \sqrt{\frac{15A}{((1 - t_1^5)\omega_2 + t_1^5\omega_1)}},\ a_1 = a_2 t_1 = \sqrt{\frac{15A}{((1 - t_1^5)\omega_2 + t_1^5\omega_1)}}\, t_1. \tag{21}$$

It is important to note that we wrote the general problem of axisymmetric flow in space with n vortex zones in analytical form for a specific particular case of the geometry of vortex zones in the form of spherical layers, assigning each zone its own vorticity from a given set of vorticities $\omega_i r$. Since the existence of such a solution requires only that the vorticities alternate signs in adjacent zones (the numerical values of ω_i determine the radii of the layers) and $\omega_n > 0$, then the specified ω_i must have $\dfrac{n}{2}$ positive and $\dfrac{n}{2}$ negative ω_i, if n is even, and $\dfrac{n+1}{2}$ positive, $\dfrac{n-1}{2}$ negative ω_i, if n is odd.

Thus, given a set of vorticities with the properties specified above, there is the possibility of the existence of $\left(\frac{n}{2}\right)!\left(\frac{n}{2}\right)!$ in space if n is even and $\left(\frac{n-1}{2}\right)!\left(\frac{n+1}{2}\right)!$ if n is odd, composite Hill vortices with n vortex zones in the form of spherical layers.

Let us note an interesting fact that, along with the composite Hill vortex with two vortex zones at $\omega_1 < 0,\ \omega_2 > 0$ of radius a_2 (21), there is a Hill vortex with the same radius a_2, but with one vortex zone with vorticity $\omega(z,r) = \big((1-t_1^5)\omega_2 + t_1^5\omega_1\big)r$ with the same value A.

Let's consider the inverse problem. Given a Hill vortex with a given value A and one vortex zone of radius R_0. It is required to find a composite Hill vortex with two vortex zones with the same values $R_0,\ A$.

In accordance with (21), we arrive at the problem of finding the numbers $\omega_1 < 0,\ \omega_2 > 0$ satisfying the relation

$$(1-t^5)\omega_2 + t^5\omega_1 = \omega = \frac{15A}{R_0^2},\ 0 < t < 1,$$

where t is an implicit function of $\omega_1,\ \omega_2$, given by equation (18) with $\gamma_1 = \dfrac{3\omega_2}{2(\omega_1-\omega_2)}$.

From $\gamma_1 = \dfrac{3\omega_2}{2(\omega_1-\omega_2)}$ we write $\omega_2 = \dfrac{2\gamma}{3+2\gamma_1}\omega_1$, and then from $(1-t^5)\omega_2 + t_1^5\omega_1 = \omega$, we get

$$\omega_1 = \frac{3+2\gamma_1}{2\gamma_1+3t^5}\omega,\quad \omega_2 = \frac{2\gamma_1}{2\gamma_1+3t^5}\omega,\quad \omega = \frac{15A}{R_0^2}. \tag{22}$$

From equation (18) we find $\gamma_1 = -\dfrac{t^4+t^3+t^2}{t+1}$, and after substitution into (22), we find

$$\omega_2 = \frac{-2(t^2+t+1)}{(t-1)(3t^3+6t^2+4t+2)}\omega > 0,\quad \omega_1 = -\frac{2t^3+4t^2+6t+3}{(3t^3+6t^2+4t+2)t^2}\omega < 0,\ 0 < t < 1.$$

Next, setting $t,\ 0 < t < 1$, arbitrarily, we find $\omega_1,\ \omega_2$, and then using formulas (21) for $t_1 = t$ the values $a_1,\ a_2$. By construction $a_2 = R_0$. Note that due to the arbitrariness of the value of $t,\ 0 < t < 1$, the inverse problem under consideration has an infinite number of solutions.

2. Flow in a sphere with vortex spherical layers

Let us consider the possibility of axisymmetric flow in a sphere of radius R_0 with a given geometry of n vortex zones in the form of spherical layers ($D_1 : R \leqslant a_1,\ D_i : a_{i-1} \leqslant R \leqslant a_i$, $i = 2,\dots,n$) and with one selected zone ($D_{n+1} : a_n \leqslant R \leqslant R_0$), adjacent to the boundary $R = R_0$, only in which vorticity can become zero, i.e. the flow may be potential. This flow design for $\omega_{n+1} = 0$ is an analogue of a composite Hill vortex in a sphere.

Just as in point 1. the problem can be written in analytical form

$$L\Psi(z,r) = \begin{cases} \omega_1 r^2 & \text{if } R < a_1,\\ \omega_i r^2 & \text{if } a_{i-1} < R < a_i,\ i = 2,\dots,n,\\ \omega_{n+1} r^2 & \text{if } a_n < R < R_0,\end{cases}$$

given that

$$\Psi|_{R=a_i} = 0,\ i = 1,\dots,n,\quad \Psi|_{R=R_0} = A > 0. \tag{23}$$

In accordance with (4), we look for a solution to the problem in the form

$$\Psi(z,r) = \begin{cases} \dfrac{r^2}{10}\omega_1(R^2 - a_1^2), \quad 0 \leqslant R \leqslant a_1, \\ \dfrac{r^2}{10}(\omega_i R^2 + \dfrac{c_i}{R^3} + d_i), \quad a_{i-1} \leqslant R \leqslant a_i,\ i = 2, \dots, n, \\ \dfrac{r^2}{10}\left(\omega_{n+1}(R^2 - a_n^2) + \dfrac{(10A - \omega_{n+1}(R_0^2 - a_n^2))R_0^3}{(R_0^3 - a_n^3)}\left(1 - \dfrac{a_n^3}{R^3}\right)\right), \quad a_n \leqslant R \leqslant R_0. \end{cases}$$

Here, the boundary conditions are satisfied in the zone D_1 with $R = a_1$, in the zone D_n with $R = a_n$, in the zone D_{n+1} with $R = a_n,\ R = R_0$. Satisfying the remaining boundary conditions (23) and the continuous differentiability of the solution when passing through the boundaries of the zones, we obtain system (10–12), in which equation (12) should be replaced by the equation

$$\frac{1}{10}\left(2\omega_n a_n - \frac{3c_n}{a_n^4}\right) = \frac{1}{10}\left(2\omega_{n+1}a_n + \frac{3R_0^3(10A - \omega_{n+1}(R_0^2 - a_n^2))}{(R_0^3 - a_n^3)a_n}\right). \tag{24}$$

In accordance with Property 3, the signs of ω_i must alternate and $a_{n-1} = t_{n-1}a_n,\ c_n = \dfrac{2(\omega_n - \bar{\omega}_{n-1})}{3}t_{n-1}^5 a_n^5$. Taking this into account, from (24) the equation for determining the value of a_n follows

$$a_n^5 - R_0^3 a_n^2\left(1 - \frac{3\omega_{n+1}}{2(\bar{\omega}_n - \omega_{n+1})}\right) + \frac{3R_0^3(10A - \omega_{n+1}R_0^2)}{2(\bar{\omega}_n - \omega_{n+1})} = 0. \tag{25}$$

We set $\omega_n > 0,\ \omega_{n+1} \leqslant 0$. Then $\bar{\omega}_n > 0$ and $\dfrac{3R_0^3(10A - \omega_{n+1}R_0^2)}{2(\bar{\omega}_n - \omega_{n+1})} > 0$. Consider the function

$$f(a_n) = a_n^5 - R_0^3 a_n^2\left(1 - \frac{3\omega_{n+1}}{2(\bar{\omega}_n - \omega_{n+1})}\right) + \frac{3R_0^3(10A - \omega_{n+1}R_0^2)}{2(\bar{\omega}_n - \omega_{n+1})}.$$

We have $f(0) > 0,\ f(R_0) > 0$. At point $a_n^* = \left(\dfrac{2}{5}\left(1 - \dfrac{3\omega_{n+1}}{2(\bar{\omega}_n - \omega_{n+1})}\right)\right)^{\frac{1}{3}} R_0,\ f'(a_n^*) = 0$. It is checked that if $\omega_n,\ \omega_{n+1}$ have different signs, then $0 < \left(\dfrac{2}{5}\left(1 - \dfrac{3\omega_{n+1}}{2(\bar{\omega}_n - \omega_{n+1})}\right)\right)^{\frac{1}{3}} R_0 < R_0$ and $f''(a_n^*) > 0$. So at point a_n^* the function $f(a_n)$ has a minimum.

Demanding $f(a_n^*) \leqslant 0$, we obtain the condition under which equation (25) on the interval $0 < a_n < R_0$ has a root (in the case of a strict inequality, there are two roots)

$$\frac{10A}{R_0^2} \leqslant \frac{2(\bar{\omega_n} - \omega_{n+1})}{3}\left(\frac{3}{5}\left(\frac{2}{5}\right)^{\frac{2}{3}}(1 - \gamma_n)^{\frac{5}{3}} + \gamma_n\right),\ \gamma_n = \frac{3\omega_{n+1}}{2(\bar{\omega}_n - \omega_{n+1})}. \tag{26}$$

From Property 3. it follows $-\dfrac{3}{2} < \gamma_n < 0$.

On the interval $(-\frac{3}{2}, 0)$ the function $F(\gamma_n) = \dfrac{3}{5}\left(\dfrac{2}{5}\right)^{\frac{2}{3}}(1-\gamma_n)^{\frac{5}{3}} + \gamma_n$ is positive, monotonically increasing and $0 < F(\gamma_n) < \dfrac{3}{5}\left(\dfrac{2}{5}\right)^{\frac{2}{5}},\ F\left(-\dfrac{3}{2}\right) = 0,\ F(0) = \dfrac{3}{5}\left(\dfrac{2}{5}\right)^{\frac{2}{5}}$. Taking into account that $\bar{\omega}_n - \omega_{n+1} > 0$, we found that the right part of the inequality in (26) is greater than zero.

Note that the right-hand side of condition (26) does not depend on A and R_0, therefore condition (26) is satisfied. In the case of strict inequality in condition (26), there are two solutions. If condition (26) is not met, there is no solution.

Let us write down condition (26) when in the zone B_{n+1}, adjacent to the boundary of the ball $R = R_0$, the flow is potential ($\omega_{n+1} = 0$)

$$\frac{A}{\bar{\omega}_n R_0^2} \leqslant \frac{1}{25}\Big(\frac{2}{5}\Big)^{\frac{2}{3}}.$$

Let us write down the solutions to the problem ($\omega_n > 0,\ \omega_{n+1} \leqslant 0$, signs of $\omega_i,\ i \leqslant n$ alternate)

$$\Psi(z,r) = \begin{cases} \dfrac{r^2}{10}\omega_1(R^2 - a_1^2), \quad 0 \leqslant R \leqslant a_1, \\ \dfrac{r^2}{10}\omega_i(R^2 - a_i^2) + \dfrac{2(\omega_i - \bar{\omega}_{i-1})}{3} t_{i-1}^5 a_i^5 \Big(1 - \big(\frac{a_1}{R}\big)^3\Big), \quad a_{i-1} \leqslant R \leqslant a_i, i = 2, \dots, n, \\ \dfrac{r^2}{10}\omega_{n+1}(R^2 - a_n^2) + \dfrac{(10A - \omega_{n+1}(R_0^2 - a_n^2))R_0^3}{(R_0^3 - a_n^3)}\Big(1 - \dfrac{a_n^3}{R^3}\Big), \quad a_n \leqslant R \leqslant R_0, \end{cases}$$

$a_{i-1} = t_{i-1}^5 a_n$, t_{i-1} — root of equation (14), corresponding to the $i-1$ zone, a_n — root of equation (25).

Let us note an interesting fact: if a flow with a given number of vortex zones in space exists, for example, a composite spherical Hill vortex, and in it the geometry of the layers is determined uniquely, then a similar flow in the sphere does not always exist, and if it does exist, then two different geometries are possible spherical layers.

Let us consider the possibility of the existence of two zones at $\omega_1 \leqslant 0,\ \omega_2 > 0$. We will need this model example later. For this case, equation (25) for finding the value a_1 takes the form

$$f(a_1) = a_1^5 - R_0^3 a_1^2\Big(1 - \frac{3\omega_2}{2(\omega_1 - \omega_2)}\Big) + \frac{3R_0^3(10A - \omega_2 R_0^2)}{2(\omega_1 - \omega_2)} = 0 \tag{27}$$

We have $f(0) = \dfrac{3R_0^3(10A - \omega_2 R_0^2)}{2(\omega_1 - \omega_2)}$, $f(R_0) = \dfrac{15R_0^3 A}{(\omega_1 - \omega_2)} < 0$. At point $a_1^* = \Big(\dfrac{2}{5}\Big(1 - \dfrac{3\omega_2}{2(\omega_1 - \omega_2)}\Big)\Big)^{\frac{1}{3}} R_0$ its only extremum is the minimum, since $f''(a_1^*) = \dfrac{6\omega_1 - 15\omega_2}{\omega_1 - \omega_2} > 0$. And only for $f(0) > 0$ does equation (27) have a root on the interval $(0, R_0)$, and this root is unique. The condition $f(0) > 0$ is satisfied for $\omega_2 > \dfrac{10A}{R_0^2}$. For $\omega_1 = 0$ in each meridian plane in the zone $R \leqslant a_1^*$ the flow function $\Psi(z,r)$ is identically equal to zero.

We found that in a sphere with $\omega_2 > \dfrac{10A}{R_0^2}$ it is possible for two vortex zones with $\omega_1 \leqslant 0$, $\omega_2 > 0$, and zones with the considered geometry are calculated uniquely.

It is obvious that problem (5), (6) for $\omega_n > 0,\ \omega_{n+1} = 0$ is a generalization of the problem of M. A. Gol'dshchik [1, 10] in M. A. Lavrentiev scheme of plane flow of an ideal fluid in the model case of an axisymmetric flow with $n+1$ vortex zones.

For $\omega_1 \leqslant 0,\ \omega_2 > 0$ its formulation is an extension of the problem of plane motion of an ideal fluid in the field of Coriolis forces [1, 11] to the axisymmetric case, as well as on the model principle.

3. Vortex flows in an arbitrary limited axisymmetric region

Let D be an arbitrary bounded region adjacent to the axis $r = 0$ in variables $z, r,\ r \geqslant 0$. Its boundary Γ consists of a smooth curve σ in the upper half-plane $r > 0$ and the segment $[\alpha, \beta]$ of the axis $z = 0$, $\alpha < 0, \beta > 0$. The curve σ adjoins the points α, β at angles different from zero and π respectively. Let us write the boundary condition for the flow function

$$\Psi|_\Gamma = \varphi(s) r^2 \geqslant 0. \tag{28}$$

Since the flow region and boundary function are arbitrary, assumptions about the geometry of vortex zones, as was done for flow in a sphere or in all space, are problematic. In this regard, at the first stage a difficult problem arises in the analytical formulation of the problem. It is natural to begin the study for a flow with two vortex zones.

For the analytical formulation of the problem in this case, the formulation of two dual problems by M. A. Gol'dshtik [1, 11] is well suited. This has already been discussed when constructing flows in a sphere. Thus, in a flat bounded domain D, it is required to find continuously differentiable solutions to problems ($\omega_1 > 0$, $\varphi(s) \geqslant 0$)

$$\Delta\Psi(x, y) = \begin{cases} \omega_1 & \text{if } \Psi < 0, \\ 0 & \text{if } \Psi > 0, \end{cases} \quad \Delta\Psi(x, y) = \begin{cases} \omega_1 & \text{if } \Psi > 0, \\ 0 & \text{if } \Psi \leqslant 0, \end{cases} \quad \Psi|_S = \varphi(s) \geqslant 0. \tag{29}$$

They define flows with two zones, vortex and potential.

In accordance with these problems, to obtain a flow with two vortex zones in the axisymmetric case, we come to two also dual problems, written in analytical form ($\omega_1 > 0, \omega_2 \leqslant 0$)

$$L\Psi(x, y) = \begin{cases} \omega_1 r^2 & \text{if } \Psi < 0, \\ \omega_2 r^2 & \text{if } \Psi > 0, \end{cases} \quad \Psi|_\Gamma = \varphi(s) r^2 \geqslant 0, \tag{30}$$

$$L\Psi(x, y) = \begin{cases} \omega_1 r^2 & \text{if } \Psi > 0, \\ \omega_2 r^2 & \text{if } \Psi < 0, \end{cases} \quad \Psi|_\Gamma = \varphi(s) r^2 \geqslant 0. \tag{31}$$

Let's consider problem (30). A function $\Psi_0(z, r)$ satisfying the equation $L\Psi_0(z, r) = \omega_2 r^2$ and boundary condition (30) in the domain D is positive in the domain D, and therefore is trivial solution to this problem. At $\omega_2 = 0$ the flow is potential in the entire region D, at $\omega_2 < 0$ the entire region D is a vortex zone. In [12], the existence of a nontrivial solution was proven.

Let us observe that the possibility of the existence of a second nontrivial solution with two vortex zones, which exists in a model problem in a sphere, is a difficult, independent mathematical problem. For the plane case with $\omega_2 = 0$, the existence of a nontrivial solution (flow with a vortex and potential zone) was proven in [10, 13, 14], and the existence of a second nontrivial solution in [5, 15]. For $\omega_2 \neq 0$ the existence of a nontrivial solution was proven in [16].

Let's consider problem (31). Note that its solution cannot take negative values in the region D. We assume that at some point $M^* \subset D$, $\Psi(M^*) < 0$. From the boundary condition in (31) it follows that there is a subdomain $D^* \subset D$ on the boundary of which $\Psi^* = 0$, and inside it $L\Psi(z, r) = \omega_2 r^2 \leqslant 0$. Hence $\Psi \geqslant 0$ in D^*. We obtain a contradiction.

From problem (31) we move on to the problem: we need to find a continuously differentiable non-negative solution to the problem

$$L\Psi(z, r) = \omega_1 r^2 \text{ if } \Psi(z, r) > 0, \ \Psi|_\Gamma = r^2 \varphi(s) \geqslant 0. \tag{32}$$

To construct a solution to the problem $L\Psi(z, r) = \omega r^2 f(z, r)$, $\Psi|_\Gamma = r^2\varphi(s)$ it is convenient to go to the variables $z = \xi$, $r = 2\sqrt{t}$, after which $L\Psi(z, r) = S\Psi = t\Psi_{tt} + \Psi_{\xi\xi} = 4\omega t f(\xi, 2\sqrt{t})$, $L^*U(z, r) = S^*U = tU_{tt} + U_{\xi\xi} + 2U_t = \omega f(\xi, 2\sqrt{t})$. In the variables ξ, t we obtained the equations ($S(tU) = tS^*U$) degenerate on the boundary of the region at $t = 0$, which are well studied in [17–19]. For example, for the equation $S\Psi = 0$ the usual formulation of the Dirichlet problem is correct, for the equation $S^*U = 0$ for the considered domain D the modified formulation is correct — the solution is specified only on the curve σ and the solution is sought in class of functions bounded at $r \to 0$ [17]. Note that in the case under consideration such a solution is continuous up to $r = 0$ and extreme values are reached at σ[19].

For the operator L^* there is a fundamental solution[20]

$$E(z, r, z_1, r_1) = \frac{4}{\pi} \int_0^{\pi} [(z - z_1)^2 + r^2 + r_1^2 - 2rr_1 \cos \beta]^{-\frac{3}{2}} \sin^2 \beta d\beta,$$

which has a logarithmic singularity for $r,\ r_1 > 0$

$$E(z, r, z_1, r_1) = -\frac{2}{\pi}(rr_1)^{-\frac{3}{2}} \ln((z - z_1)^2 + (r - r_1)^2) + \Phi(z, r, z_1, r_1),$$

$\Phi(z, r, z_1, r_1)$ is a regular function.

Using Green's formula [18, 19] with $v = W,\ u = rG(z, z_1, r, r_1)$

$$\iint\limits_D (uSv - vS^*u) d\xi_1 dt_1 = \oint\limits_\Gamma (vu_{\xi_1} - v_{\xi_1} u) dt_1 - (t_1 v u_{t_1} - t_1 v_{t_1} u - vu) d\xi_1,$$

we obtain a representation of the solution to the problem $LW(z, r) = \omega r^2 f(z, r),\ W|_\Gamma = 0$ in the form

$$W(z, r) = -\frac{\omega}{8} r^2 \iint\limits_D r_1^3 f(z_1, r_1) G(z, z_1, r, r_1) dz_1 dr_1. \tag{33}$$

Here $G(z, z_1, r, r_1)$ is the Green's function for the problem $L^*U = \omega f(z, r),\ U|_\sigma = \varphi(s)$ (the solution is bounded for $r \to 0$), which is standardly constructed using the fundamental solution $E(z, r, z_1, r_1)$. $G(z, z_1, r, r_1) = E(z, r, z_1, r_1) - G_1(z, z_1, r, r_1)$, where $G_1(z, z_1, r, r_1)$ in variables $\xi_1 \neq \xi,\ t_1 \neq t$ solution of problem $S^*G_1 = 0,\ G|_\sigma = -E|_\sigma$ bounded at $t_1 \to 0$. From the above extremum principle for the equation $S^*U = 0$ it follows that for $z \neq z_1, r \neq r_1$ the Green's function $G(z, z_1, r, r_1) > 0$ in $D \bigcup (\alpha, \beta)$,

It is important to note that function (33) has all the properties of a logarithmic potential in the D domain, since the Green's function by construction has a logarithmic singularity inside the D domain.

Let's return to problem (32).

To prove the existence of a solution to this problem that goes to zero at points in the region D, consider the sequence of problems

$$L\Psi_n(z, r) = \omega_1 r^2 th(n\Psi_n(z, r)), \quad \Psi_n|_\Gamma = r^2 \varphi(s) \geqslant 0. \tag{34}$$

Just as before, it is easy to show that $\Psi_n \geqslant 0$.

Problem (34) is equivalent to the integral equation

$$\Psi_n(z, r) = -\frac{\omega_1}{8} r^2 \iint\limits_D r_1^3 th(n\Psi_n(z_1, r_1)) G(z, z, r, r_1) dz_1 dr_1 + \Psi_0(z, r). \tag{35}$$

Similarly [1, 11, 12], taking into account the properties of the integral (33) with the introduced Green's function as a logarithmic potential, using Schauder's theorem, we establish the existence for each $n > 0$ of a solution $\Psi_n \geqslant 0$ continuous in $\overline{D}$ of the integral equation (35), and by

Arzel's theorem, the compactness of the sequence of solutions $\Psi_n(z,r)$ in the space of functions continuously differentiable in the domain D. Note that the solution to problem (34) is unique, which follows from $\dfrac{\partial th(n\Psi_n)}{\partial \Psi_n} = \dfrac{n}{ch^2(n\Psi_n)} > 0$. Let the subsequence $\Psi_{n_k}(z,r)$ converge to a continuously differentiable function $\Psi(z,r) \geqslant 0$.

Further, repeating the proof from [1, 11, 12], it is established that the limit function is a solution to problem (34)

Here it is taken into account that for the right side of the equation in (34)

$$\lim_{n_k\to\infty} th(n_k\Psi_{n_k}(z,r)) = 1 \quad \text{if} \quad \Psi(z,r) > 0.$$

Let us obtain the condition under which the resulting solution goes to zero in the region D. Under the assumption that $\Psi(z,r) > 0$ at all points of the region D, it follows from equation (35)

$$\Psi(z,r) = \Psi_0(z,r) - \frac{\omega_1}{8} r^2 \iint\limits_D r_1^3 G(z,r,z_1,r_1)dz_1 r_1. \tag{36}$$

Let D_0 be a semicircle ($r \geqslant 0$) of the largest radius R_0 that can be inscribed in the region D (we can assume that its center is at the origin of coordinates $z = 0, r = 0$) and $C = \max(\varphi(s)r^2)$.

For the model case $D = D_0,\ r^2\varphi(s) = Cr^2$ in the second paragraph, if we go to the notation of problem (31), redesignating ω_2 by ω_1, ω_1 on ω_2, it is found that if the inequality $\omega_1 > \dfrac{10C}{R_0^2}$ is satisfied, the problem (31) under consideration has a solution $\Psi_{D_0}(z,r)$, which in the semicircle $D_a \subset D_0,\ r^2 + z^2 \leqslant a^2,\ r \geqslant 0,\ a < R_0$ is identically equal to zero, and in $D_0 \setminus D_a$ is greater than zero. The value a is the root of equation (27) at $A = C,\ \omega_1 = 0$.

The function $\Psi_{D_0}(z,r)$ for this case can be written as

$$\Psi_{D_0}(z,r) = C - \frac{\omega_1}{8} r^2 \iint\limits_{D_0\setminus D_a} r_1^3 G_{R_0}(z,r,z_1,r_1)dz_1 r_1.$$

$G_{R_0}(z,r,z_1,r_1)$, the Green's function introduced in the work for the region D_0.

Let us represent the function $\Psi(z,r)$ (36) in D_a in the form

$$\begin{aligned}\Psi(z,r) = (\Psi_0(z,r) - C) + \Bigg(C - \frac{\omega_1}{8} r^2 \iint\limits_{D_0\setminus D_a} r_1^3 G_{R_0}(z,r,z_1,r_1)dz_1 r_1\Bigg) + \\ + \frac{\omega_1}{8} r^2 \iint\limits_{D_0\setminus D_a} r_1^3 \big(G_{R_0}(z,r,z_1,r_1) - G(z,r,z_1,r_1)\big)dz_1 dr_1 - \\ - \frac{\omega_1}{8} r^2 \iint\limits_{D\setminus D_0} r_1^3 G(z,r,z_1,r_1)dz_1 dr_1 - \frac{\omega_1}{8} r^2 \iint\limits_{D_a} r_1^3 G(z,r,z_1,r_1)dz_1 dr_1.\end{aligned} \tag{37}$$

In the circle D_a, the expression in the second bracket of equality (37) is equal to zero, the remaining terms on the right side are negative. So, the function $\Psi(z,r)$ is negative in $D_a \subset D$, which contradicts the assumption that it is positive in the entire domain D. We found that for $\omega_1 > \dfrac{10C}{R_0^2}$ the function $\Psi(z,r)$ goes to zero in the domain $D_a \in D$.

Further, similarly to works [1, 11, 12], it is possible to prove that the problem (31) under consideration has a unique solution and under the condition that the boundary set σ on which the boundary function $\varphi(s)$ is nonzero is connected , the set on which the solution is positive is a region.

Thus, it was established that with $\omega_1 > \dfrac{10C}{R_0^2}$ and with the above requirement on the boundary function $\varphi(s)$, in the region D a flow is possible, which in some region vortex with vorticity $\omega_1 r$, and in addition to it the flow function $\Psi(z, r)$ equals zero - the fluid is motionless.

Note that in the work the problem of the possibility of the existence of vortex axisymmetric flows in a limited area was considered with only two vortex zones. Therefore, it is natural to continue the study of the existence of flows with n $(n > 2)$ vortex zones with questions of their non-uniqueness, which occurs with model flows in a sphere.

References

[1] M.A.Gol'dshtik, Vortex flows, Novosibirsk, Science, 1981.

[2] M.A.Lavrentyev, B.V.Shabat, Problems of hydrodynamics and their mathematical models, Moscow, Science, 1973.

[3] K.V.Braginsky, V.V.Savelyev, Magnetic traps for plasma confinement, *Mathematical modeling*, **11**(1999), no. 5, 3–36.

[4] G.K.Bathelor, A proposal conserning laminar wakes behind bluff bodies at large Reynolds humbers, *J. Fluid Mech.*, **1**(1956), no. 4, 388–398.

[5] I.I.Vainshtein, Solution of two dual problems on gluing vortex and potential flows using the variational method of M.A.Gol'dshtik, *J. Sib. Fed. Univ. Math. Phys.*, (2011), no. 4(3),320–331.

[6] R.Kurant, Partial differential equations, Moscow, World Soc., 1964.

[7] M.Thompson, Theoretical hydrodynamics, Moscow, World, 1964.

[8] V.D.Shafranov, On Magnetohydrodynamical Equilibrium Configurations, *Journal of Experimental and Theoretical Phisics*, (1958), no. 3.

[9] I.I.Vainshtein, On a boundary value problem of vortex and potential flows of an ideal fluid in the axisymmetric case, *Differential equations*, **6**(1970), no. 1, 109–122.

[10] M.A.Gol'dshtik, Mathematical model of separated flows of incompressible fluid, *Reports of the USSR Academy of Sciences*, **147**(1962), no. 6, 1310–1313.

[11] I.I.Vainshtein, M.A.Gol'dshtik, On the motion of an ideal fluid in the field of Coriolis forces, *Reports of the USSR Academy of Sciences*, **173**(1967), no. 6, 1277–1280.

[12] I.I.Vainshtein, I.M.Fedotova, Goldshtik problem on gluing vortex flows of an ideal fluid in the axisymmetric case, *Bulletin of the Siberian State University named after Academician M. F. Reshetnev*, **3**(1914), no. 55, 48–54.

[13] S.N.Antontsev, V.D.Lelyukh, Some problems of coupling vortex and potential subsonic flows, *Dynamics of a continuous medium*, (1969), no. 1, 134–153.

[14] P.I.Plotnikov, On the solvability of one class of problems on gluing potential and vortex flows, *Dynamics of a continuous medium*, (1969), no. 3, 61–69.

[15] D.K.Potapov, On the number of solutions for one class of elliptic type equations with a spectral parameter and discontinuous nonlinearity, *Far Eastern Mathematical Journal*, **12**(2012), no. 1, 86–88.

[16] I.I.Vainshtein, V.K.Yurovsky, On a problem of conjugation of vortex flows of an ideal fluid, *Journal of Applied Mechanics and Technical Physics*, (1976), no. 5, 98–100.

[17] M.V.Keldysh, On some cases of degeneration of equations of elliptic type on the boundary of a domain, *Report of the USSR Academy of Sciences*, **77**(1951), no. 2, 181–183.

[18] S.A.Tersenov, On the theory of equations of elliptic type that degenerate on the boundary of the domain, *Sib. math. journal*, **3**(1973), no. 6, 1120–1143.

[19] I.L.Karol, On the theory of boundary value problems for equations of mixed elliptic-hyperbolic type, *Mathematical collection*, **38**(1956), no. 80, 261–282.

[20] A.Weinshtein, Jeneral Axially Simmetric Patenial teory, *Bulletin of the Amer. Math.Sosiety*, **59**(1953), no. 1.

Осесимметрические потоки идеальной жидкости с эффективно невязкими вихревыми зонами

Исаак И. Вайнштейн
Сибирский федеральный университет
Красноярск, Российская Федерация

Аннотация. В работе сформулирована модель осесимметрического течения идеальной жидкости с n эффективно невязкими вихревыми зонами, обобщающая известную модель М. А. Лаврентьева о склейке вихревых и потенциальных течений в плоском случае. Показана возможность в рамках такой модели существования в пространстве жидкой сферы, обтекаемой потенциальным осесимметрическим потоком, состоящей из n шаровых слоев осесимметрических вихревых течений. Этот модельный пример обобщает известный в гидродинамике сферический вихрь Хилла с одной вихревой зоной. Такое вихревое течение с n шаровыми слоями также возможно и в сфере, причем в отличие от течения в пространстве, такое течение неединственно. Рассмотрена задача об осесимметрическом вихревом течении в ограниченной области, по постановке обобщающая плоское течение идеальной жидкости в поле кориолисовых сил.

Ключевые слова: идеальная жидкость, вихревые течения, сферический вихрь Хилла.

Journal of Siberian Federal University. Mathematics & Physics 2024, 17(5), 679–683

EDN: WYJIOS
УДК 510.665; 510.643

Interval Multi-agent Logic with Reliability Operator

Vladimir R. Kiyatkin*
Vladimir V. Rybakov†
Siberian Federal University
Krasnoyarsk, Russian Federation

Received 10.04.2024, received in revised form 19.05.2024, accepted 24.07.2024

Abstract. We study intransitive temporal multi-agent logic with agents' multi-valuations for formulas letters and relational models representing reliable states. This logic is defined in a semantic as a set of formulas which are true at linear models with multi-valued variables. We propose a background for such approach and a technique for computation truth values of formulas. Main results concerns solvability problem, we prove that the resulting logic is decidable.

Keywords: modal logic, temporal logic, common knowledge, deciding algorithms, multi-agent logic.

Citation: V.R. Kiyatkin, V.V. Rybakov, Interval Multi-agent Logic with Reliability Operator, J. Sib. Fed. Univ. Math. Phys., 2024, 17(5), 679–683. EDN: WYJIOS.

Introduction

Mathematical logics widely applied in research concerning computer science and information sciences overall. We can observe the both side interaction. Tasks and problems in computer science generate new areas in mathematical logic and induce creation new technique and tools in mathematical logic itself. Conception of knowledge, which arose in the analysis of distributed systems, leaded to development multi-agent and multi-valued logical systems. More details about this can be found in the works of Halpern, Vardy (Reasoning About Knowledge [1]), Rybakov (Refined common knowledge logics or logics of common information, [2]).

It concern also from the certain point of view approaches to omniscience, monotonicity, justified knowledge, etc (cf. for example Artemov (Evidence-Based Common Knowledge [3]), S. Artemov (Evidence-Based Common Knowledge, (Technical Report TR-2004018) [4]), S. Artemov (Explicit Generic Common Knowledge, [5]), S. Artemov (Justification awareness, [5]). And it also was implemented in research concerning uncertainty and plausibility (cf. V. Rybakov Temporal Multi-Agent's Logic, Knowledge, Uncertainty, and Plausibility [6] Agents and Multi-Agent Systems: Technologies and Applications, LNCS, 2021, 2005–2014. Later some works were done towards consolidation such technique and to improve hybrid cooperation of the agents [7–9]. Also technique for formalization of knowledge was enriched by research in description logics (cf. Balder and Staler, [10]), first-order logic was also implemented (cf. F. Selaginella, A. Lombroso [11]). Various semantic technique was used (cf. Horrors, Settler, — A Description Logic with Transitive and Inverse Roles and Role Hierarchies [12]; Horrors, Geese, Karamu, Waller, — Using Semantic Technology to Tame the Data Variety Challenge, [13]).

Nowadays research concerning knowledge was combined with implementation of temporal logic (cf. Rybakov [14–17]). An automata-theoretic approach to multi-agent planning was evolved at Footbridge, [18].

*kiyatkinvr@mail.ru
†Vladimir_Rybakov@mail.ru https://orcid.org/0000-0002-6654-9712

In this our short paper we study intransitive temporal multi-agent logic with agents' multi-valuations for formulas letters. Common knowledge in [1] was modelled at Triple models. This brought interesting strong results, correlating well with observed examples and intuition. Here we wish to develop this approach towards modelling knowledge with Triple frames which are linear time models and treating reliable states of models. Here time is intransitive and it acts to only finite intervals. Main results concerns solvability problem, we prove that the resulting logic is decidable, prove existence of sone deciding algorithm.

1. Notation, Preliminary facts

Formulas of our logic $\mathcal{L}(\mathcal{M}_{\mathbb{N}})$ will be introduced as the set of special formulas, which are true at states of certain special relational Kripke-like models.

Alphabet for the language of our logic $\mathcal{L}(M_{\mathbb{N}})$ is defined in a standard way and consists of denumerable set of propositional letters (variables), parenthesises, logical Boolean operators, modal operators $\Box$, $\Diamond$, logical reliability operator $\mathcal{S}$ and also special time operator $\mathcal{N}$.

We remind, that every modal operation $\Box$ can be defined by means of modal operation $\Diamond$ as follows $\Box = \neg\Diamond\neg$. Now we give inductive definition of the formulas in the language of our logic $\mathcal{L}(\mathcal{M}_{\mathbb{N}})$.

1. Any propositional variable $p \in Prop$ is formula.
2. If α is formula, then $\neg\alpha$ is formula also.
3. If α and β are formulas, then $(\alpha \wedge \beta)$, $(\alpha \vee \beta)$ and $(\alpha \to \beta\beta)$ are formulas as well.
4. If α is formula, then $\Box\,\alpha$ is a formula also.
5. If α is formula, then $\Diamond\,\alpha$ is a formula also.
6. If α is formula, then $\mathcal{S}\alpha$ is formula as well.
7. If α is formula, then $\mathcal{N}\alpha$ is formula also.

There is no other formulas in the language of logic $\mathcal{L}(\mathcal{M}_{\mathbb{N}})$.

No we turn to describe relational models for our logic. We take as the basic set of the model $\mathcal{M}_{\mathbb{N}}$ the set $\mathbb{N}$ of all natural numbers. Here we suppose $\mathbb{N} = \bigcup_{j=1}^{\infty} Int_j$, where Int_j are not intersecting intervals on $\mathbb{N}$ possibly of different length. Each interval Int_j can have inside some intervals $Int_{j1}, Int_{j2}, \ldots, Int_{js}$ of "reliable states" inside. Denote $C(Int_j) = \bigcup_{t=1}^{s} Int_{jt}$. Binary relation $\preccurlyeq$ coincides with the standard linear order $\leqslant$ only inside but not outside every interval Int_j.

$Next$ is the binary relation inside every interval Int_j such that if $a \in Int_j$ and $aNextb$, then b is the first number of the interval Int_{j+1} (first following after Int_j, that is $a + 1 = b$ holds). We keep it to connect subsequently following intervals. We can write $Next(a) = b$. That makes connection between neighboring intervals. Linear multi-agent model is the model of the form:

$$\mathcal{M}_{\mathbb{N}} = \langle \mathbb{N}, \preccurlyeq, Next, V_1, \ldots, V_k \rangle\,,$$

where valuations $V_i,\ i \in [1,\ k]$ of every propositional variable p are some subsets $V_i(p)$ from $\mathbb{N}$.

Now we precisely define the truth values of formulas in our model.

For any a, b, $c \in \mathcal{M}$ the truth relations are as follows:

$$\forall p \in Prop: \ a \Vdash_{V_i} p \iff a \in V_i(p),$$
$$a \Vdash_{V_i} \neg\alpha \iff a \nVdash_{V_i} \alpha,$$
$$a \Vdash_{V_i} (\alpha \wedge \beta) \iff a \Vdash_{V_i} \alpha \quad \text{and} \quad a \Vdash_{V_i} \beta,$$
$$a \Vdash_{V_i} \Box\,\alpha \iff \forall\, b\,[(a \preccurlyeq b) \Rightarrow (b \Vdash_{V_i} \alpha)]\,,$$
$$a \Vdash_{V_i} \Diamond\,\alpha \iff \exists\, b\,[(a \preccurlyeq b) \wedge (b \Vdash_{V_i} \alpha)]\,.$$
$$a \Vdash_{V_i} \mathcal{S}\,\alpha \iff (\,a \in Int_j \Rightarrow (\exists\, b \in C(Int_j)\,[(a \preccurlyeq b) \Rightarrow b \Vdash_{V_i} \alpha])),$$
$$a \Vdash_{V_i} \mathcal{N}\,\alpha \iff \forall\, b\,[(a\,Next\,b) \Rightarrow b \Vdash_{V_i} \alpha]\,.$$

Formula α is said to be refutable in the logic , if there exist a state $a \in \mathcal{M}_{\mathbb{N}}$ such as $a \nVdash_{V_i} \alpha$. Formula α is said to be true in model $\mathcal{M}_{\mathbb{N}}$ if it is true at any state a from $\mathbb{N}$.

The set of all formulas, which are true in all our models is said to be the logic $\mathcal{L}(\mathcal{M}_{\mathbb{N}})$ generated by model $\mathcal{M}_{\mathbb{N}}$.

2. Decidability of logic $\mathcal{L}(\mathcal{M}_{\mathbb{N}})$

To solve the problem of decidability of logic $\mathcal{L}(\mathcal{M}_{\mathbb{N}})$ we shell transform models $\mathcal{M}_{\mathbb{N}}$ to get special finite like models, named $\mathcal{M}_C$, which, in a sense, are equivalent to $\mathcal{M}_{\mathbb{N}}$. That means that formula α belongs to the logic $\mathcal{L}(\mathcal{M}_{\mathbb{N}})$ if and if only it is true at any state from any model $\mathcal{M}_C$. The details will be given later.

Now we begin to subsequently describe undertaken transformation. First step.

1. For any state $a \in \mathcal{M}_{\mathbb{N}}$ and for valuation $V_i \quad i \in [1,\ k]$ we define the following theory:

$$Sub_i(a) = \{\beta \in Sub(\alpha) \mid b \Vdash_{V_i} \beta\}.$$

Evidently, there exist at most $2^{\|Sub(\alpha)\|}$ such different theories.

2. The set of theories:

$$T(a) = \{Sub_1(a), Sub_2(a), \ldots, Sub_k(a)\}$$

corresponds to every state $a \in \mathcal{M}_{\mathbb{N}}$.

There exists only
$$d = 2^{\|Sub(\alpha)\|} \times \cdots \times 2^{\|Sub(\alpha)\|} = 2^{k\cdot\|Sub(\alpha)\|}$$
such different sets of theories.

3. We shell obtain model $\mathcal{M}_C$ from $\mathcal{M}_{\mathbb{N}}$ with the help of the procedure of *rarefaction.*

Consider one arbitrary interval Int_j.

The set of all states in interval Int_j we denote $\mathcal{A}(Int_j)$, the set of all of reliable states in Int_j— $\mathcal{C}(Int_j)$ and the set of all not reliable states — $\mathcal{B}(Int_j)$. The character of the reliable states differs from the character of the other states, that is why we apply such rarefaction procedure for $\mathcal{B}(Int_j)$ and $\mathcal{C}(Int_j)$ separately.

Let us represent $\mathcal{B}(Int_j) = B_1 \cup B_2 \cup, \ldots, \cup B_s$, where the any set $B_i,\ i \in [1,\ s]$ consists of the states b only, which have the same set $T(b)$ of theories.

First of all, we remove from Int_j all the states from B_1, except one the largest state b. We name that state *representative* of B_1, and denote $\bar{b}$. That is procedure of *rarefaction of states.*

Then we rarify in such manner all $B_2,\ B_3, \ldots, B_s$ from $\mathcal{B}(Int_j)$.

After such transformations of the interval Int_j there leaved fixed only (some) s non-reliable states with pairwise different set of theories.

Further, we represent reliable states as follows – $\mathcal{C}(Int_j) = C_1 \cup C_2 \cup, \dots, \cup C_r$, where the set $C_j,\ j \in [1,\ r]$ of states c, which have the same set $T(c)$ of theories. Then we apply procedure of rarefaction to every set $C_1,\ C_2, \dots, C_r$ of reliable states as before we did for non-reliable states.

After such transformation of the interval Int_j inside it there were be leaved fixed only a finite (computable bounded size) reliable states with pairwise different sets of theories. So we obtain totally rarified interval with reliable and non-reliable states.

We denote this interval $\overline{Int_j}$.

If in the all our model we will replace the intervals Int_j by intervals $\overline{Int_j}$, and else will leave in any intervals the smallest and biggest states (re-deifying Next relation appropriately, to keep connection), then the states of intervals $\overline{Int_j}$ will have the same truth values of formulas as in the initial models (may be shown by usual induction by temporal and modal length o formulas).

To complete our result, we only need to clarify now many intervals $\overline{Int_j}$ subsequently maybe be chosen and inserted to support truth values of the formulas.

Theorem 1. *For any formula α with temporal degree t and any given modal degree this formula maybe be disproved at a model $\mathcal{M}_C = \langle \overline{N}, \preccurlyeq, Next, V_1, \dots, V_k \rangle$, iff α may be disproved in the model obtained from intervals $\overline{Int_j}$ (described earlier above) by subsequent concatenation of at most $t+1$ finite intervals So we get the logic in decidable.*

Proof. Straightforward through induction by t using the described above construction. □

Conclusion

In this paper we considered problem of decidability of a logic with models including reliable states. We investigated temporal modal logic $\mathcal{L}(\mathcal{M}_{\mathbb{N}})$ for description of reliability information. We considered intervals of stable truth values of formulas and their interaction. The techniques is constructed and by it we wind an algorithm which may recognize decidability that logic.

This work is supported by the Krasnoyarsk Mathematical Center and financed by the Ministry of Science and Higher Education of the Russian Federation (Agreement No. 075-02-2024-1429).

References

[1] R.Fagin, J.Y.Halpern, Yoram Moses and Moshe Vardi), MIT, 1995.

[2] V.V.Rybakov, Refined common knowledge logics or logics of common information, *Archive for Mathematical Logic*, **42**(2003), 179–200. DOI:1 0.1007/s001530100134

[3] S.Artemov, Evidence-Based Common Knowledge, Technical Report TR-2004018 CUNY Ph.D. Program in Computer Science (revised version), 2006.

[4] S.Artemov, Explicit Generic Common Knowledge, Lect/ Notes in CS, LFCS 2013: Logical Foundations of Computer Science, 2013, 16–28.

[5] S.Artemov, Justification awareness, *Journal of Logic and Computation*, **30**(2020), no. 8, 1431–1446.

[6] V.Rybakov, Temporal Multi-Agent's Logic, Knowledge, Uncertainty, and Plausibility. – Agents and Multi-Agent Systems: Technologies and Applications, LNCS, 2021, 2005 - 2014.

[7] S.Babenyshev, V.Rybakov, Decidability of Hybrid Logic with Local Common Knowledge Based on Linear Temporal Logic LTL, CiE 2008: Lecture Notes in Computer Science, vol. 5028, 2008, 32-41. DOI: 10.1007/978-3-540-69407-6_4

[8] S.Babenyshev, V.Rybakov, Logic of Discovery and Knowledge: Decision Algorithm, KES (2), Lecture Notes in Computer Science, vol. 5178, 2008, 711–718.
DOI: 10.1007/978-3-540-85565-1_88

[9] S.Babenyshev, V.Rybakov, Describing Evolutions of Multi-Agent Systems, KES (1), Lecture Notes in Computer Science, vol. 5711, 2009, 38–45.
DOI: 10.1007/978-3-642-04595-0_5

[10] F.Baader, ,Sattler Expressive Number Restrictions in Description Logics, *J. Log. Comput.*, **9**(1999), no.3, 319–350.

[11] F.Belardinelli, A.Lomuscio, Interactions between Knowledge and Time in a First-Order Logic for Multi-Agent Systems: Completeness Results, *Journal of Artificial Intelligence Research*, **45**(2012), 1–45.

[12] I.Horrocks, U.Sattler, A Description Logic with Transitive and Inverse Roles and Role Hierarchies, Description Logics, 1998.

[13] I.Horrocks, M.Giese, E.Kharlamov, A.Waaler, Using Semantic Technology to Tame the Data Variety Challenge, *IEEE Internet Computing*, **20**(2016), no. 6, 62–66.
DOI: 10.1109/MIC.2016.121

[14] V.V.Rybakov, Non-transitive linear temporal logic and logical knowledge operations, *J. Logic and Computation*, Oxford University Press, **26**(2016), no. 3, 945–958.
DOI: 10.1093/logcom/exv016

[15] V.V.Rybakov, Temporal logic with overlap temporal relations generated by time states themselves, *Siberian Mathematical Reports*, **17**(2020), 923–932.

[16] V.V.Rybakov, Multi-agent temporal nontransitive linear logics and the admissibility problem, *Algebra and Logic*, **59**(2020), 87–100. DOI: 10.33048/alglog.2020.59.108

[17] V.V.Rybakov, Branching Time Logics with Multiagent Temporal Accessibility Relations, *Siberian Mathematical Journal*, **62**(2021), no. 3, 503–510. DOI: 10.33048/smzh.2021.62.313

[18] M.Wooldridge, An Automata-theoretic approach to multi-agent planning, Proceedings of the First European Workshop on Multi-agent Systems (EUMAS), December 2003, Oxford University.

Интервальная многоагентная логика с оператором надёжности

Владимир Р. Кияткин
Владимир В. Рыбаков
Сибирский федеральный университет
Красноярск, Российская Федерация

Аннотация. В предлагаемой статье мы изучаем нетранзитивную временную многоагентную логику с мультиозначиванием агентов и реляционные модели, представляющие надёжные состояния. Эти логики определяются семантически, как множества формул, истинных на линейных моделях с мультиозначиванием. В работе мы предложили основу для такого подхода и разработали технику для вычисления истинностных значений формул. Основной результат касается проблемы разрешимости. Доказано, что рассматриваемая логика разрешима.

Ключевые слова: модальные логики, модели Крипке, многоагентные логики, проблема разрешимости.

Journal of Siberian Federal University. Mathematics & Physics 2024, 17(5), 684–688

EDN: YYANLK
УДК 512.54

To the Question of the Closure of the Carpet

Elizaveta N. Troyanskaya*
Siberian Federal University
Krasnoyarsk, Russian Federation

Received 10.03.2024, received in revised form 15.04.2024, accepted 17.05.2024

Abstract. For a root system Φ, the set $\mathfrak{A} = \{\mathfrak{A}_r \mid r \in \Phi\}$ of additive subgroups $\mathfrak{A}_r$ over commutative ring K is called a carpet of type Φ if commuting two root elements $x_r(t), t \in \mathfrak{A}_r$ and $x_s(u), u \in \mathfrak{A}_s$, gives a result where each factor lies in the subgroup $\Phi(\mathfrak{A})$ generated by the root elements $x_r(t), t \in \mathfrak{A}_r, r \in \Phi$. The subgroup $\Phi(\mathfrak{A})$ is called a carpet subgroup. It defines a new set of additive subgroups $\overline{\mathfrak{A}} = \{\overline{\mathfrak{A}}_r \mid r \in \Phi\}$, the name of the closure of the carpet $\mathfrak{A}$, which is set by equation $\overline{\mathfrak{A}}_r = \{t \in K \mid x_r(t) \in \Phi(\mathfrak{A})\}$. Ya. Nuzhin wrote down the following question in the Kourovka notebook. *Is the closure $\overline{\mathfrak{A}}$ of a carpet $\mathfrak{A}$ a carpet too? (question 19.61).* The article provides a partial answer to this question. It is proved that the closure of a carpet of type Φ over commutative ring of odd characteristic p is a carpet if 3 does not divide p when Φ of type G_2.

Keywords: commutative ring, Chevalley group, carpet of additive subgroups, K-character.

Citation: E.N. Troyanskaya, To the Question of the Closure of the Carpet, J. Sib. Fed. Univ. Math. Phys., 2024, 17(5), 684–688. EDN: YYANLK.

1. Introduction

Let Φ be an indecomposable root system of rank $l, \Phi(K)$ be an elementary Chevalley group of type Φ over a commutative ring K. The group $\Phi(K)$ is generated by its root subgroups

$$x_r(K) = \{x_r(t) \mid t \in K\}, \ r \in \Phi.$$

The subgroups $x_r(K)$ are abelian and for each $r \in \Phi$ and any $t, u \in K$ the following relations hold

$$x_r(t)x_r(u) = x_r(t+u). \tag{1}$$

A set of additive subgroups $\mathfrak{A} = \{\mathfrak{A}_r \mid r \in \Phi\}$ is called a *carpet* of type Φ over the ring K if

$$C_{ij,rs}\mathfrak{A}_r^i\mathfrak{A}_s^j \subseteq \mathfrak{A}_{ir+js}, \ \text{at} \ r, s, ir+js \in \Phi, \ i>0, \ j>0, \tag{2}$$

where $\mathfrak{A}_r^i = \{a^i \mid a \in \mathfrak{A}_r\}$, and the constants $C_{ij,rs} = \pm1, \pm2, \pm3$ are defined by the Chevalley commutator formula

$$[x_s(u), x_r(t)] = \prod_{i,j>0} x_{ir+js}(C_{ij,rs}(-t)^i u^j), \quad r, s, ir+js \in \Phi. \tag{3}$$

This definition of a carpet was introduced by V. M. Levchuk in the article [1]. Each carpet $\mathfrak{A}$ defines a *carpet subgroup*

$$\Phi(\mathfrak{A}) = \langle x_r(\mathfrak{A}_r) \mid r \in \Phi \rangle,$$

*troyanskaya.elizaveta@yandex.ru

where $\langle M\rangle$ denotes the subgroup generated by the set M from any subgroup. We call the *closure* of the carpet $\mathfrak{A}$ the set $\overline{\mathfrak{A}} = \{\overline{\mathfrak{A}}_r \mid r \in \Phi\}$ that is defined by

$$\overline{\mathfrak{A}}_r = \{t \in K \mid x_r(t) \in \Phi(\mathfrak{A})\},\ r \in \Phi.$$

A carpet $\mathfrak{A}$ is called *closed* if $\Phi(\mathfrak{A}) \cap x_r(K) = x_r(\mathfrak{A}_r), r \in \Phi$. In our notation this is equivalent to the equality $\overline{\mathfrak{A}}_r = \{\mathfrak{A}_r\}$ for all $r \in \Phi$, shortly $\overline{\mathfrak{A}} = \mathfrak{A}$. Examples of non-closed carpets for commutative rings of sufficiently wide classes are given in the articles [2] and [3].

This article received the following question from Ya. Nuzhin from the Kourovka notebook.

A) *Is the closure $\overline{\mathfrak{A}}$ of the carpet $\mathfrak{A}$ a carpet too?* [4, question 19.61]

From the conditions of carpet (2) a statement follows. If $t \in \mathfrak{A}_r, u \in \mathfrak{A}_s$, then each factor from the right side of the formula (3) lies in the carpet subgroup $\Phi(\mathfrak{A})$. On the other hand, for the arbitrary subgroup M of the Chevalley group $\Phi(K)$ the set $\mathfrak{M} = \{\mathfrak{M}_r \mid r \in \Phi\}$, defined by the

$$\mathfrak{M}_r = \{t \in K \mid x_r(t) \in M\},\ r \in \Phi$$

is not always a carpet [5, page 528]. However, for the types A_l, D_l and E_l, the set $\mathfrak{M}$ defined by the subgroup M is a carpet, as for this type formula (3) has the form $[x_r(t), x_s(u)] = x_{r+s}(\pm tu)$. Therefore, for types A_l, D_l and E_l closure of the carper is always a carpet. Thus, the question A) is relevant only for $\Phi = B_l, C_l, F_4, G_2$. The main result of the article is

Theorem 1. *The closure $\overline{\mathfrak{A}}$ of a carpet $\mathfrak{A}$ of type Φ over a ring of odd characteristic p is a carpet if 3 does not divide p when Φ of type G_2.*

2. Preliminary results

The Chevalley group $\Phi(K)$ is increased to the extended group $\hat{\Phi}(K)$ by all diagonal elements $h(\chi)$, where χ is the K-character of the integer root lattice $\mathbb{Z}\Phi$, that is, a homomorphism of the additive group $\mathbb{Z}\Phi$ into the multiplicative group K^* of the field K. Of course, the following equalities hold

$$\chi(a + b) = \chi(a)\chi(b), \quad a, b \in \Phi,$$
$$\chi(-a) = \chi(a)^{-1}, \quad a \in \Phi,$$

which will be used frequently.

Lemma 1. [6, Sec. 7.1] *Any K-character χ is uniquely determined by values on the fundamental roots and for any $r \in \Phi, t \in K$*

$$h(\chi)x_r(t)h^{-1}(\chi) = x_r(\chi(r)t). \tag{4}$$

The next lemma follows from the definition of a carpet and a carpet subgroup.

Lemma 2. *Let $\mathfrak{M} = \{\mathfrak{M}_r \mid r \in \Phi\}$ — a set of additive subgroups of the ring K, the subgroup M of the Chevalley group $\Phi(K)$ is generated by the subgroups $x_r(\mathfrak{M}_r)$, $r \in \Phi$, and $M \cap x_r(K) = x_r(\mathfrak{M}_r)$. A set $\mathfrak{M}$ is a carpet if and only if for any $r, s \in \Phi$ with the condition that $r + s \in \Phi$, each factor from the right side of the commutator formula for elements $x_r(t)$ and $x_s(t)$, where $t \in \mathfrak{M}_r,\ u \in \mathfrak{M}_s$, lies to M.*

The article by Ya. Nuzhin gives examples of a subgroup M of the Chevalley group $\Phi(K)$ of types B_2, G_2 such that the set $\mathfrak{M}$ defined as in Lemma 2, is not a carpet [5, examples 1-2].

Lemma 3. *Each diagonal element $h(\chi)$ normalizes any subgroup of the Chevalley group that is generated by the root elements if for all $r \in \Phi$ the value $\chi(r)$ lies in the simple subring generated by 1.*

3. Proof of the Theorem 1

Any two roots r, s with the condition that $r+s$ is a root lie in a root system of type A_2, B_2 or G_2. Therefore, by Lemma 2, it is enough to prove Theorem 1 for these types of rank 2. As already noted in the introduction, for the type A_2 the closure of any carpet is a carpet. That means that only the types B_2 and G_2 remain.

Let $r, s, r+s$ be the roots of the root system Φ of type B_2 or G_2, $\mathfrak{A} = \{\mathfrak{A}_r \mid r \in \Phi\}$ is a carpet of type Φ, $\overline{\mathfrak{A}} = \{\overline{\mathfrak{A}}_r \mid r \in \Phi\}$ the closure of a carpet,

$$M = < x_r(\overline{\mathfrak{A}}_r) \mid r \in \Phi > .$$

By Lemma 2, to prove Theorem 1 it is enough to establish the following statement.

B) For any $t \in \overline{\mathfrak{A}}_r, u \in \overline{\mathfrak{A}}_s$ each factor from the right side of the commutator formula for elements $x_r(t)$ and $x_s(u)$ lies in M.

It is clear that we will be interested only in those cases for which there are two or more factors on the right side of the commutator formula (3).

Let Φ be of type B_2. In this case, there are two types of commutator formula (3) with more than one factor on the right side, these are the following formulas

$$[x_a(t), x_b(u)] = x_{a+b}(\varepsilon_1 tu) x_{2a+b}(\varepsilon_2 t^2 u), \tag{5}$$

$$[x_b(u), x_a(t)] = x_{a+b}(\varepsilon_3 tu) x_{2a+b}(\varepsilon_4 t^2 u), \tag{6}$$

where $\varepsilon_i = \pm 1$, $i = 1, 2, 3, 4$. The right sides of these two formulas differ only in sign, so it is enough to consider only one of them, for example, the first.

Let $\chi(a) = \chi(b) = -1$. According to Lemma 3, $h(\chi)$ normalizes M and by Lemma 1

$$h(\chi)[x_a(t), x_b(u)]h^{-1}(\chi) = x_{a+b}(\varepsilon_1 tu) x_{2a+b}(-\varepsilon_2 t^2 u). \tag{7}$$

Multiplying the right sides (5) and (7), we obtain the inclusion $x_{a+b}(\varepsilon_1 2tu) \in M$. Since the characteristic is odd, then $x_{a+b}(\pm tu) \in M$. Multiplying it to the (5), we get $x_{2a+b}(\varepsilon_2 t^2 u)$. Thus, statement B) is established.

Let Φ be of type G_2. Chevalley commutator formulas having more than one factor on the right side are represented by four cases

$$[x_a(t), x_b(u)] = x_{a+b}(\varepsilon_1 tu) x_{2a+b}(\varepsilon_2 t^2 u) x_{3a+b}(\varepsilon_3 t^3 u) x_{3a+2b}(\varepsilon_4 t^3 u^2), \tag{8}$$

$$[x_b(u), x_a(t)] = x_{a+b}(\varepsilon_1 tu) x_{2a+b}(\varepsilon_2 t^2 u) x_{3a+b}(\varepsilon_3 t^3 u) x_{3a+2b}(\varepsilon_4 2t^3 u^2), \tag{9}$$

$$[x_a(t), x_{a+b}(u)] = x_{2a+b}(\varepsilon_1 2tu) x_{3a+2b}(\varepsilon_2 3tu^2) x_{3a+b}(\varepsilon_3 3t^2 u), \tag{10}$$

$$[x_{a+b}(u), x_a(t)] = x_{2a+b}(\varepsilon_1 2tu) x_{3a+2b}(\varepsilon_2 3tu^2) x_{3a+b}(\varepsilon_3 3t^2 u), \tag{11}$$

where $\varepsilon_i = \pm 1$. Formulas (8) and (9) have different factors on the right side. The right sides of (10), (11) differ only in sign, so it is enough to consider only (10).

Let it begin with the formula (8). Let $\chi(a) = -1, \chi(b) = 1$. By Lemma 1

$$h(\chi)[x_a(t), x_b(u)]h^{-1}(\chi) = x_{a+b}(-\varepsilon_1 tu) x_{2a+b}(\varepsilon_2 t^2 u) x_{3a+b}(-\varepsilon_3 t^3 u) x_{3a+2b}(-\varepsilon_4 t^3 u^2). \tag{12}$$

Multiplying the right sides (8) and (12), we have $x_{2a+b}(\varepsilon_2 2t^2u) \in M$. Since the characteristic is odd, then $x_{2a+b}(-\varepsilon_2 t^2u) \in M$. Multiplying the right side (12) by it, we obtain the product

$$x_{a+b}(-\varepsilon_1 tu)x_{3a+b}(-\varepsilon_3 t^3u)x_{3a+2b}(-\varepsilon_4 t^3u^2). \tag{13}$$

Let $\chi(a) = -1, \chi(b) = -1$. Then

$$h(\chi)[x_{a+b}(\varepsilon_1 tu)x_{3a+b}(\varepsilon_3 t^3u)x_{3a+2b}(\varepsilon_4 t^3u^2)]h^{-1}(\chi) = x_{a+b}(\varepsilon_1 tu)x_{3a+b}(\varepsilon_3 t^3u)x_{3a+2b}(-\varepsilon_4 t^3u^2). \tag{14}$$

Multiplying the right sides (13) and (14), we obtain $x_{3a+2b}(-2t^3u^2) \in M$, and therefore

$$x_{a+b}(-\varepsilon_1 tu)x_{3a+b}(-\varepsilon_3 t^3u).$$

This product cannot be split using the sets $\chi(r) = \pm 1$. Let us choose other values of $\chi(r)$ from the multiplicative groups of the field. Since the characteristic $p > 3$ is odd, the number 2 is different from ± 1 and invertible in the field K. We use this fact to choose $\chi(r)$. Let $\chi(a) = 2, \chi(b) = -2$, then

$$h(\chi)[x_{a+b}(\varepsilon_1 tu), x_{3a+b}(\varepsilon_2 t^3u)]h^{-1}(\chi) = x_{a+b}(-4\varepsilon_1 tu)x_{3a+b}(-16\varepsilon_2 t^3u). \tag{15}$$

Let $k \leqslant p$ be the inverse element for -4 in the ring, then we raise $x_{a+b}(-4\varepsilon_1 tu)x_{3a+b}(-16\varepsilon_2 t^3u)$ to the power k and get $x_{a+b}(\varepsilon_1 tu)x_{3a+b}(4\varepsilon_3 t^3u)$. Adding this result to the product $x_{a+b}(-\varepsilon_1 tu)x_{3a+b}(-\varepsilon_3 t^3u)$, we obtain $x_{3a+b}(3\varepsilon_3 t^3u) \in M$. Since the characteristic of the ring K is not divisible by 3 , then $x_{3a+b}(\varepsilon_3 t^3u) \in M$. So, we managed to split the factors of the formula (8). Formula (9) differs in the multiplier coefficient $x_{3a+2b}(\varepsilon_4 2t^3u^2)$, which, as above, splits off from the product at the second step and does not play a role in the proof. Thus, statement B) holds for (8), (9).

Carry out a similar procedure for the formula (10). Let $\chi(a) = 1, \chi(b) = -1$. By Lemma 1

$$h(\chi)[x_a(t), x_{a+b}(u)]h^{-1}(\chi) = x_{2a+b}(-2\varepsilon_1 tu)x_{3a+2b}(3\varepsilon_2 t^2u)x_{3a+b}(-3\varepsilon_3 t^2u). \tag{16}$$

Let $\chi(a) = -1, \chi(b) = 1$. By Lemma 1

$$h(\chi)[x_a(t), x_{a+b}(u)]h^{-1}(\chi) = x_{2a+b}(2\varepsilon_1 tu)x_{3a+2b}(-3\varepsilon_2 t^2u)x_{3a+b}(-3\varepsilon_3 t^2u). \tag{17}$$

Multiplying the right sides (10) and (16), we have $x_{3a+2b}(6\varepsilon_2 t^2u)$. Multiplying the right sides (10) and (17), we have $x_{2a+b}(4\varepsilon_1 tu)$. Since the numbers 6 and 4 are coprime with the characteristic of the ring K, then the elements $x_{2a+b}(\varepsilon_1 tu), x_{3a+2b}(\varepsilon_2 t^2u)$ lie in M. Consequently, the factors of Chevalley's formula (10) are able to be split. The theorem has been proven.

The author expresses deep gratitude to his scientific supervisor Ya. Nuzhin for setting the problem, constant attention to the work and support at all stages of its implementation.

This work is supported by the Krasnoyarsk Mathematical Center and financed by the Ministry of Science and Higher Education of the Russian Federation (Agreement No. 075-02-2024-1429).

References

[1] V.M.Levchuk, Parabolic subgroups of certain ABA-groups, *Mathematical Notes*, **31**(1982), no. 4, 259–267. DOI: 10.1007/BF01138934

[2] V.A.Koibaev, Elementary nets in linear groups, *Trudy Inst. Mat. i Mekh. UrO RAN*, **17**(2011), no. 4, 134–141 (in Russian).

[3] S.K.Kuklina, A.O.Likhacheva, Ya.N.Nuzhin, On closeness of carpets of Lie type over commutative rings, *Trudy Inst. Mat. i Mekh. UrO RAN*, **21**(2015), no. 3, 192–196 (in Russian).

[4] Kourovskaya notebook. Unsolved questions in group theory, 19th ed., Novosibirsk, IM SB RAS Publishing House, 2018.

[5] Ya.N.Nuzhin, Factorization of carpet subgroups of the Chevalley groups over commutative rings, *J. Sib. Fed. Univ. Math. Phys.*, **4**(2011), no. 4, 527–535 (in Russian).

[6] R.Carter, Simple groups of lie type, Wiley and Sons, London–New York–Sydney– Toronto, 1972.

К вопросу о замыкании ковра

Елизавета Н. Троянская
Сибирский федеральный университет
Красноярск, Российская Федерация

Аннотация. Для системы корней Φ набор $\mathfrak{A} = \{\mathfrak{A}_r \mid r \in \Phi\}$ аддитивных подгрупп $\mathfrak{A}_r$ коммутативного кольца K называется ковром типа Φ, если при коммутировании двух корневых элементов $x_r(t), t \in \mathfrak{A}_r$ и $x_s(u), u \in \mathfrak{A}_s$, каждый сомножитель из правой части коммутативной формулы Шевалле лежит в подгруппе $\Phi(\mathfrak{A})$, порожденной корневыми элементами $x_r(t), t \in \mathfrak{A}_r, r \in \Phi$. Подгруппа $\Phi(\mathfrak{A})$ называется ковровой подгруппой. Она определяет новый набор аддитивных подгрупп $\overline{\mathfrak{A}} = \{\overline{\mathfrak{A}}_r \mid r \in \Phi\}$, называемый замыканием ковра $\mathfrak{A}$, который задается равенствами $\overline{\mathfrak{A}}_r = \{t \in K \mid x_r(t) \in \Phi(\mathfrak{A})\}$. Я.Н. Нужин записал в Коуровской тетради следующий вопрос. *Является ли замыкание $\overline{\mathfrak{A}}$ ковра $\mathfrak{A}$ ковром? (вопрос 19.61).* В статье доказано, что замыкание ковра типа Φ над коммутативным кольцом нечетной характеристики p является ковром, если 3 не делит p, когда Φ типа G_2.

Ключевые слова: коммутативное кольцо, группа Шевалле, ковер аддитивных подгрупп, K-характер.